

Battery aging in full electric ships

S. ten Cate Hoedemaker

An assessment of the relationship between battery size, charging strategy and battery lifetime

SDPO.17.031.m



Battery aging in full electric ships

by

S. ten Cate Hoedemaker

to obtain the degree of Master of Science
at the Delft University of Technology,
to be defended publicly on Tuesday September 12, 2017 at 10:00 AM.

Student number: 1533959
Project duration: November 28, 2016 – September 12, 2017
Thesis committee: Rear Admiral Ir. K. Visser, TU Delft, 3ME, SDPO
Ir. I. Georgescu, TU Delft, 3ME, SDPO
Ir. P. Rampen, Damen Shipyards Gorinchem
Dr. E.M. Kelder, Tu Delft, TNW, RST

An electronic version of this thesis is available at <http://repository.tudelft.nl/>.

Preface

Throughout the first year of my master's studies I have tried to include batteries in all courses and projects that allowed me. For my second year I could not have wished for a better opportunity continuing my search for knowledge on batteries. First an internship where I gathered as much information on marine battery systems as possible, followed by my thesis on battery aging in full electric ships. I want to thank everyone at Damen Shipyards that made this possible for me. Special thanks go to Peter for giving me exactly the right amount of supervision, Erik-jan for his shared enthusiasm for batteries, Robert for the information on tugs and Gocke for the information on ferries, including the nice picture on the front. From TU Delft I want to thank Klaas Visser for showing so much interest and support in my research and Ioana Georgescu for guiding me and teaching me how to approach the problem in a scientific way. I want to thank all my friends for the great time I've had in Delft. Special thanks go to Claudia, for removing the spelling mistakes in this report. Although I always make fun of your Spanish accent, I do think your knowledge of the English language is better than mine. At last I want to thank my parents for their endless support and who never, in all my years of studying, have stopped believing that one day I will finally finish.

*S. ten Cate Hoedemaker
Delft, August 2017*

Abstract

One of the main challenges in designing fully battery powered ships is to predict how long the battery will last. The degradation of capacity and power of the battery is called aging. This thesis has two main goals; to investigate the predictability of battery aging and to translate this into a method for the optimization of battery size and operational strategy for fully battery powered ships.

First the considerations to select a battery for a specific application are described to assess the challenges in this process. This results in the decision to only include lithium-ion batteries. A comprehensive research is performed on battery aging studies to analyze the aging behaviour of different batteries under variable conditions. The measurements from the battery aging tests and a selection of aging models are evaluated to investigate the predictability of aging, which results in the conclusion that it is possible to predict the aging of batteries.

A new model is developed based on the conclusions of the aging research and evaluation of existing models. The model is designed to predict the aging rate and thermal behaviour of batteries based on the operational profile of a ship. This model is used to perform a general analysis of the aging behaviour at different operational conditions. The results of this general analysis are translated into two optimization methods which are applied to case studies of a harbour tug and a ferry. For the harbour tug this results in a battery of 5.5 MWh that lasts 10 years. For the ferry this results in a battery of 1 MWh that lasts 5 years.

This research provides a vision on the considerations for the optimization of battery size and operational strategy for battery powered ships. However, each type of battery ages differently, which makes it difficult to make general assumptions. If the proposed model and optimization methods are used for the design of a battery system for a specific ship, it is recommended to fit the model to the selected batteries by performing aging tests and an analysis of the thermal behaviour.

Contents

1	Introduction	1
1.1	Motivation	1
1.2	Problem description	2
1.3	Methodology	3
1.4	Terminology	4
2	Battery selection	5
2.1	Selection criteria	5
2.1.1	Capacity	6
2.1.2	Power	6
2.1.3	Longevity	7
2.1.4	Costs	7
2.1.5	Safety	7
2.1.6	Dimensions	7
2.2	Battery types	7
2.2.1	Chemistry	8
2.2.2	Cell design	9
2.3	Battery costs	10
2.3.1	Cell/system costs	10
2.3.2	Battery price development	12
2.3.3	Lifetime costs	13
2.4	Selecting a battery	13
2.4.1	Operational requirements	13
2.4.2	CAPEX/OPEX	13
2.4.3	System integration	14
3	Battery aging	15
3.1	Aging mechanisms	16
3.1.1	Loss of free lithium	16
3.1.2	Surface layer formation	16
3.1.3	Electrode disintegration	17
3.1.4	Material deterioration	17
3.1.5	Contact deterioration	17
3.2	Aging causes	17
3.2.1	Temperature	18
3.2.2	State of charge	18
3.2.3	Depth of discharge	18
3.2.4	C-rates	19
3.2.5	Other causes	19
3.3	Aging test methodology	19
3.3.1	Evaluation	20
3.4	Calendar aging	20
3.4.1	Temperature	21
3.4.2	State of charge	24
3.4.3	Storage time	27
3.4.4	Conclusions calendar aging	28

3.5	Cycle aging	29
3.5.1	Depth of discharge	29
3.5.2	C-rate	31
3.5.3	Average SOC	32
3.5.4	Conclusions cycle aging	33
4	Proposed aging model	35
4.1	Approach	35
4.1.1	Goals	35
4.1.2	Method	36
4.2	Aging calculations	36
4.2.1	Temperature	36
4.2.2	SOC	37
4.2.3	DOD	38
4.2.4	C-rates	39
4.3	Integrated model	39
4.3.1	Overview	39
4.3.2	Calendar aging	41
4.3.3	Cycle aging	41
4.3.4	Thermal model	41
4.3.5	Time step size	42
4.4	Validation	43
4.4.1	Variation	43
4.4.2	Versatility	43
4.4.3	Proposed model vs. other models	46
4.5	Verification	47
4.5.1	Parameters	48
4.5.2	Errors at specific conditions	49
4.5.3	Statistical distribution of errors	50
5	Battery size and strategy optimization	53
5.1	System boundaries	53
5.1.1	Charging	53
5.1.2	Discharging	53
5.1.3	Optimality	53
5.2	General analysis	54
5.2.1	DOD	54
5.2.2	Average SOC	55
5.2.3	Effect of different Woehler curve	56
5.2.4	Charge strategy	57
5.2.5	Thermal management	58
5.2.6	Conclusions	59
5.3	Optimization method 1	59
5.3.1	Optimization steps	59
5.3.2	Case study: Harbour tug	60
5.3.3	Case study: Ferry	64
5.4	Optimization method 2	67
5.4.1	Optimization steps	67
5.4.2	Case study: Harbour tug	69
5.4.3	Case study: Ferry	70
5.5	Evaluation optimization methods	70
6	Conclusions and recommendations	71
6.1	Conclusions	71
6.1.1	Battery selection	71
6.1.2	Battery aging	71
6.1.3	Aging model	72
6.1.4	Optimal battery size and strategy	72

6.2	Recommendations	74
6.2.1	Aging research	74
6.2.2	Battery aging model	75
6.2.3	Electric ships	76
A	Background information	77
A.1	Electric ships	77
A.1.1	Ampere	77
A.1.2	BB Green	78
A.1.3	Ar vag tredan	79
A.2	Environmental impact	80
A.2.1	Production of batteries	80
A.2.2	Energy source	80
A.2.3	Recycling	81
A.3	System boundaries	82
A.3.1	Charging	82
A.3.2	Discharging	82
B	Aging test methodologies	85
B.1	Calendar aging	85
B.1.1	Keil et al.	85
B.1.2	MOBICUS	85
B.1.3	Safari et al.	85
B.1.4	Schmalstieg et al.	86
B.1.5	SIMCAL	86
B.2	Cycle aging	86
B.2.1	Deshpande et al.	86
B.2.2	Liu et al.	86
B.2.3	Omar et al.	86
B.2.4	Peterson et al.	87
B.2.5	Saxena et al.	87
B.2.6	Watanabe et al.	87
B.2.7	Wang et al.	87
B.2.8	Wong et al.	87
B.3	Calendar and cycle aging	88
B.3.1	Ecker et al.	88
B.3.2	Sarasketa et al.	88
C	Aging models	89
C.1	Li et al.	89
C.2	Omar et al.	90
C.3	Saxena et al.	93
C.4	Schmalstieg et al.	93
C.5	Ecker et al.	94
C.6	Magnor et al.	95
C.7	Sarasketa-Zabala et al.	95
C.8	Wang et al.	97
D	Simulink® model	99
D.1	Simulink®	99
D.1.1	Main screen.	99
D.1.2	Operational profile	99
D.1.3	Thermal model	100
D.1.4	Cycle analysis	102
D.1.5	Calendar aging	103
D.1.6	Cycle aging	104
D.1.7	Results	105

E Validation	107
F Results	117
F.1 Behavioural analysis117
F.2 Variable Woehler curves130
F.3 Variable ambient temperature132
F.4 Mean SOC134
F.5 Case study: Tug134
F.6 Case study: Ferry136
Bibliography	139
List of Figures	145
List of Tables	149
List of Abbreviations	151

Introduction

In all transportation modes a shift is happening in the propulsive system; from burning fossil fuels to using the power of electricity. The market for electric vehicles keeps growing and most of the respected car companies have at least one full electric model. The first fully battery powered airplane made a journey around the world. There is also a fully battery powered ferry, carrying up to 360 passengers and 120 cars, crossing the fjords in Norway daily. However, this is not the first battery powered ship. In 1838, a German named Moritz Von Jacobi, built an 8 meter long boat only powered by batteries. It sailed in St. Petersburg, Russia, on a 7.5 km route at a speed of 2.5 km/h.[43] Battery powered boats remained popular until approximately the 1920s, when internal combustion engines became safer, cheaper, could reach higher speeds and had a longer range. Now, with the current knowledge of the impact of internal combustion engines on the environment, the need for a less polluting propulsion system is as high as ever. With the car industry leading the way, the shipbuilding industry is following at a very slow speed.

1.1. Motivation

The original source of motivation for this thesis is the will to contribute to the development of full electric ships. In this case full electric means that the ship is only powered by energy from electricity which is stored on board of the ship by using batteries. Research has already been done on how batteries can be used to power a ship and the first fully battery powered ships have already been built, see appendix A.1.1. Therefore the goal of this thesis is to increase the knowledge on fully battery powered ships in general and not only on a case to case basis. To reach this goal the first objective is to determine the challenges of using batteries to power a ship that needs to be solved. Luckily, there are plenty of problems to solve for batteries. The first challenges that come to mind when investigating the use of batteries to power a ship are the low energy density, high costs and low safety. These are all problems that need to be solved from the side of electrochemistry and battery manufacturing. For this research a problem is required that can be approached from the side of designing or operating a battery powered ship. A challenge of batteries is the degradation of capacity and power over time, a phenomenon called battery aging. For full electric ships, the fading of capacity is the limiting factor of battery life; therefore the aging of the batteries that is discussed in this research is concerning capacity loss only. Aging can be controlled by adjustments in the design or operations of the ship. Therefore, the problem that is chosen for this thesis to investigate is battery aging.

1.2. Problem description

All batteries gradually lose their capacity to store energy. This is caused by cycling the battery, or just by storing the battery without using it. Cycling of a battery is the process of charging and discharging it. A discharge, followed by a charge is known as a cycle. The process of losing energy storing capacity because of performed cycles is called cycle aging. The process of losing capacity while being in storage is called calendar aging. A lot of research has been done on the aging of batteries when performing static cycles. Static cycles are cycles at for instance a constant temperature or charge rate. However, not much is yet known about the effects of a dynamic operational profile of a ship on the aging process of batteries and how to take them into account in the design phase of a fully battery powered ship. Ships are usually designed to last for about 30 years. With batteries, this is very hard to achieve. Therefore, when designing a battery powered ship, the aim is generally at an expected battery life of 10 years. The installed battery system is usually over-sized to increase the expected life time. It is however not fully understood how much effect the over-sizing of batteries has and what the optimal size is for reaching 10 years of operational life. The general assumption is that increasing the size of the battery has a positive effect on the aging effects, but research is required to quantify this assumption. There are three major considerations when the battery size is increased. First of all, the weight and volume of the installed batteries also increases. Depending on the ratio between the weight and volume of the ship and the weight and volume of the batteries it has to be determined if the increase in size of the batteries influences the power requirements at a significant level or if the increase in weight or volume is negligible. The second problem of increasing the battery size is the costs. A larger battery requires a larger investment. The average costs for lithium-ion battery packs has decreased 77% in the last 6 years.[34] Therefore, choosing a more expensive and larger battery that will last longer, might be regretted when a smaller, better performing battery is available before the end of the expected lifetime of the first chosen battery. The third problem of changing the battery size also has to do with the expected lifetime. Usually, batteries are assumed to be at the end of their life when they reach 80% of the initial capacity. The problem with larger batteries at 80% of the initial capacity is that it leads to a larger remaining capacity at the end of their life compared to a smaller battery. For instance, a battery with a rated capacity of 100 kWh has a capacity of 80 kWh at 80%. A battery with a rated capacity of 150 kWh has a capacity of 120 kWh at 80%. Although the larger battery has a remaining capacity of 20% more than the smaller battery at the rated situation, it does get to be determined to have reached the end of its life.

All batteries suffer from aging, but every type of battery ages differently. Information on the aging of a specific battery can be given by the manufacturer, but the information is usually biased and incomplete. The understanding of the aging mechanisms and their relations to battery chemistry and structure is very important to select the right battery type for a specific application. Besides selecting the type of battery, the appropriate size of the battery cells is also of influence on the aging process and needs to be investigated. Cell selection is an important step of designing battery powered vessels and therefore is an important part of this research. Only types of lithium-ion batteries are included in this research, as explained in section 2.2. This leads to the first research question:

Can the aging of batteries be predicted based on the operational profile of a full electric ship?

Other alternatives than over-sizing of batteries to improve the life time should also be investigated during the design process. An example of an alternative solution is changing the charging strategy of the ship, this can be seen as designing the operational profile. Not all types of ships allow their operational profiles to be designed, but for some ships it is possible. The operational profiles will need to be determined taking the capabilities of the batteries into account. This will determine for example the possible speeds, required charging protocol and operational security. In other words: the functionality of the ship. The investigation of ship

types that allow their operational profiles to be designed is also a challenge for this research and leads to the second research question:

How can the combination of battery size and operational strategy for a full electric ship be optimized?

1.3. Methodology

There are four main steps taken to find the answers to the two research questions. The first step is to analyze the process of selecting a battery for a specific application. The second step is to investigate battery aging. The third step is to develop a model to predict battery aging. The fourth and final step is to use the three previous steps to investigate the process of optimizing battery size and operational strategy for full electric ships.

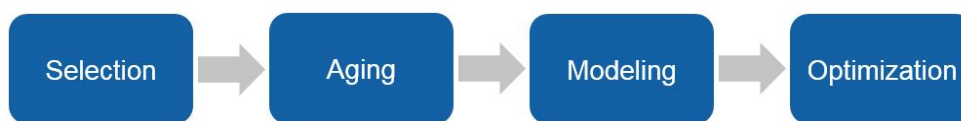


Figure 1.1: Main steps in approach of this research

The process of selecting a battery for a specific application is investigated to determine the main characteristics of batteries. The selection criteria and different battery types are evaluated. The costs for batteries are often an important point of decision and therefore it is evaluated separately.

The mechanisms and causes of battery aging are determined by studying existing literature. Battery aging studies are analyzed to qualify and quantify the aging behaviour of different types of lithium-ion batteries. All available data from aging tests is collected. The methods of performing aging tests as well as the results are compared and evaluated to determine if there are mathematical or statistical relations between operating conditions of the battery and the aging behaviour. Existing aging models are evaluated for their accuracy and complexity.

With the gained knowledge of the analyzed aging test data and aging models a new model is developed. It is validated if this proposed model describes the aging of lithium-ion batteries correctly and if it is an improvement over the existing models. Finally it is verified if the model is applicable as a general prediction model for the aging of batteries of a full electric ship.

The system boundaries of discharging and charging an electric ship are set first. Then the proposed aging model is used to perform a general analysis of aging in electric ships. Different operational conditions are simulated and evaluated. The results of the general analysis are used to develop two battery optimization methods. Two case studies are evaluated with the two different methods to determine the optimal battery size and strategy to ensure a 5 or 10 year battery life for a harbour tug and a ferry. The two methods are compared to each other and evaluated on their accuracy, ease of use and usefulness.

1.4. Terminology

There are several terms relating to batteries used repeatedly throughout this thesis. To avoid any misunderstandings these terms are explained briefly. The state of charge (SOC) is the available energy in the battery as a percentage of the full capacity. The depth of discharge (DOD) is the percentage of energy that is discharged in one cycle. The DOD is sometimes used for the SOC at which a discharge ends, but this is not the case in this thesis. A DOD of 50% can be a discharge from 100% SOC to 50% SOC, but also from 60% SOC to 10% SOC. To describe the SOC range at which a discharge takes place the term average SOC (μ SOC) is used in this thesis. The amount of cycles that is performed by a battery is defined as the number of full equivalent cycles (FEC). A full equivalent cycle is a cycle at 100% DOD. The state of health (SOH) of a battery is the percentage of the initial capacity that is available due to aging. The end of life (EOL) of the battery is a predetermined point of SOH at which the battery is considered to be unable to power the application.

2

Battery selection

Each type of battery cell has different characteristics, which are mainly determined by the composition of chemistry, structural design and size. Selecting the right battery is finding the right combination of characteristics, but in the end costs are often a main factor in the selection of batteries. This chapter discusses these subjects, to fully understand the decisions that have to be made for selecting the right cell for a specific application. The specific application in this case will be powering a ship. The characteristics of the battery determine the operational limitations of battery powered ships and therefore battery selection is an important step in this research. First the main selection criteria are discussed, followed by the different types of rechargeable batteries. Then the cost components for battery cells and systems are discussed, as well as the development of battery prices. The last section provides a guideline in the selection process for batteries.

2.1. Selection criteria

For most battery applications there are six main selection criteria. Three are based on the operational performance: capacity, power and longevity. The other three are costs, safety and dimensions (size and weight). Which factors weigh more than others in the selection process depends on the application. From a maritime point of view, the capacity and power rating of the battery relate to the range and speed of the ship. The longevity and costs will determine the installation and operational costs of the ship. The safety and dimensional characteristics of the selected battery will have an influence on the location and integration of the battery in the ship. Each selection criteria is influenced by several parts of the battery. Figure 2.1 shows a schematic representation of a rechargeable battery and the parts that are of main influence on the battery selection criteria. The parts of the battery that have the largest influence on the six selection criteria are the electrodes, electrolyte, separator, container, terminals and the vent.[68]

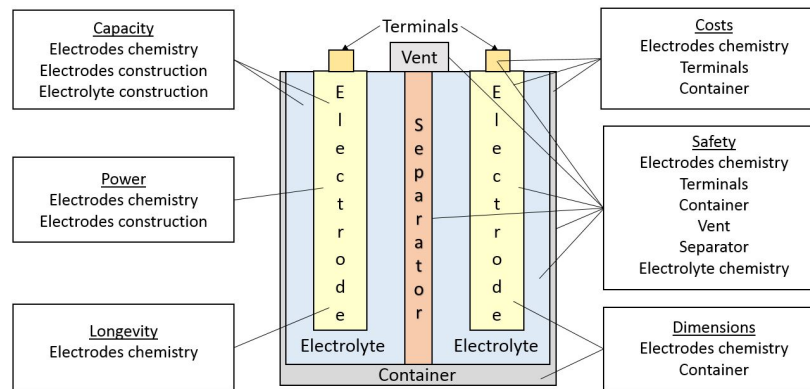


Figure 2.1: Main influences on battery selection criteria

2.1.1. Capacity

The capacity of a battery is the maximum usable energy it can store and is often measured in Watt-hours (Wh). To compare different batteries or battery materials the energy density is more commonly used. The energy density can be gravimetric (Wh/kg) or volumetric (Wh/L). The energy density of a battery can typically be between 40 Wh/kg and 250 Wh/kg. Figure 2.1 shows the three main influences on the capacity: the chemistry and construction of the electrodes and the structure of the electrolyte. The capacity is determined by the amount of energy that can be stored in the electrode, therefore, a thicker electrode or an electrode with more mass results in a higher capacity. Different materials have different energy storage characteristics. This is dependent on the molecular structure of the electrode materials. Materials that provide a better binding opportunity for lithium-ions, increase the energy storage capabilities of the electrodes. The last part of the battery that is a main influence on the capacity is the structure of the electrolyte. The electrolyte transfers lithium-ions from the anode to the cathode, enough transferring capability needs to be available to make use of the total energy storing capacity of the battery.

2.1.2. Power

The power rating of the battery is the ability to charge and discharge with high current rates and is usually measured in Watts (W). To compare different batteries on their power rating usually the power density is used. The power density is expressed in gravimetric density (W/kg) or in volumetric density (W/L). The power density of a battery lies typically between the 50 W/kg and 3000 W/kg. For a fast charging speeds, which is required for a lot of applications, a high power battery cell is required. For a high power rating the chemical reactions inside the cell need to have as little resistance as possible. A low internal resistance can be achieved by having thin electrodes resulting in a larger active surface area. This is the opposite as required for a high capacity. Therefore, always a balance has to be found for the right combination of capacity and power. A larger active surface area can also be achieved by choosing the right chemistry with this characteristic. A higher power rating is also connected to a higher charging rate. The speed of charging and discharging a battery is described by the C-rate. A C-rate of 1C stands for a full charge or discharge in 1 hour. So a 1 kWh battery discharged at 1C should deliver a current of 1 kW for 1 hour. Discharging the same 1 kWh battery at 2C should deliver a current of 2 kW for half an hour. Discharging the battery at 0.5C it should deliver a current of 0.5 kW for 2 hours. Increasing the C-rate is increasing the current and decreasing the time. Increasing the charge or discharge current also increases the internal losses and decreases the efficiency of a battery. Therefore, when a battery is charged at a relatively high C-rate of 1C it takes the battery often more than 1 hour to fully charge the battery.

2.1.3. Longevity

The longevity of a battery is determined by two different characteristics, the calendar life and the cycle life. The calendar and cycle life are determined by the aging of the battery. Calendar aging is the decrease in capacity and power over time. Cycle aging is the decrease in capacity and power due to the usage of the battery. There is one part of the battery that is most determining for the longevity of the battery and that is the chemistry of the electrodes. There are five main aging mechanisms, see section 3.1. The aging mechanisms are chemical reactions that take place with or at the electrodes. The reactivity of the electrodes is determined by the material that is used. A high reactivity is required for a good battery performance, but this also increases the aging rate. Materials are added to the electrodes to make them more resistant to aging, but this usually leads to a loss of performance. Choosing the right material for the electrodes is finding the right balance between the performances on capacity, power and longevity.

2.1.4. Costs

The costs of a battery is mainly influenced by the material for the electrodes.[23] The electrodes are made of highly complex combinations of metals and on average about one third of the price of the battery is reserved for the electrode materials. The other main contributors to the high prices of batteries are the terminals and the battery container.[41] The high costs for the battery container and terminals are mainly caused by the manufacturing processes and not by the material costs for these parts. More on the costs of batteries is explained in section 2.3.

2.1.5. Safety

As shown in figure 2.1, the safety of the battery cell depends on all parts of the cell. The constructional parts like the terminals, container and vent need to be designed for optimal safety. The separator, electrodes and electrolyte are in constant interaction with each other and need to be selected for their combined safety. The most important factors for safety are the electrode and electrolyte chemistry. All the energy of the battery is stored in the material and this must be resistant to for instance thermal runaway. Thermal runaway is the venting of hot gases and flames by a battery cell. Some battery materials have a low temperature limit where thermal runaway starts taking place, other materials are less vulnerable. Usually, more safety means less capacity.

2.1.6. Dimensions

For most applications a small and light weight battery is preferred. The dimensions are dependent on the balance between energy and power densities. The dimensions and weight for similar cell designs can be very different. This has to do with three factors. The proportion of active material mass compared to inactive material mass, the ratios of positive to negative active material masses and the surface to volume ratios of the materials used, the thickness factor.[68] Main influences on these factors are the chemistry of the electrodes and the construction of the battery container.

2.2. Battery types

Batteries can be made using many different types and combinations of materials. Each material will give the battery different characteristics concerning capacity, power, costs, safety, charging speeds and other operational aspects. The three most common types of rechargeable batteries are lead-acid, nickel-based and lithium-ion. Each of these types come in a large variation of different sub-types, all with a specific set of characteristics. Lead-acid batteries are cheap, but have a small capacity and charge very slow. Nickel-based batteries have

a slightly higher capacity than lead-acid batteries and can be charged faster. Lithium-ion batteries are more expensive, but have a much higher capacity. Table 2.1 shows an overview of the characteristics of the three different battery types. The specific characteristics of a battery can differ much depending on the combinations of materials in the sub-type. This table is only meant for a quick impression of the differences between the three different types of batteries.

Table 2.1: Overview of characteristics per battery type[12]

Battery type	Lead-acid	Nickel-based	Lithium-ion
Costs (€/kWh)	€100 - €200	€300 - €600	€250 - €1500
Energy (Wh/kg)	30 - 50	45 - 120	100 - 250
Power (W/kg)	50 - 180	150 - 1000	250 - 3000
Cycle life	200 - 300 cycles	300 - 1100 cycles	300 - 7000 cycles
Safety	Average	Good	Sub-type dependent
Temperature	-20°C - 50°C	-40°C - 70°C	-20°C - 60°C
Typical C-rates	0.1 C	0.1 - 10 C	0.3 - 10 C

2.2.1. Chemistry

There are multiple advantages as well as disadvantages of using lithium-ion compared to lead-acid and nickel. The most important aspect is the high capacity of lithium-ion batteries. Although the capacity is not even close to that of a diesel powered system, it is much higher than lead-acid or nickel-based batteries. Another reason for using lithium-ion batteries to power ships is the high power density. The higher cycle life is a big advantage for lithium-ion batteries, as well as the high acceptable C-rates. Lithium-ion batteries have a charge efficiency that is 30% more efficient than lead-acid batteries.[8] This makes the overall energy efficiency of lithium-ion batteries much higher. The last main advantage is that lithium-ion batteries are considered to be maintenance free. Lead-acid batteries require refills from time to time and nickel-based batteries suffer from the so called memory effect. This effect requires nickel-based batteries to regularly have a complete discharge.[12]

The main disadvantage to lithium-ion batteries is the high price. However, over the last 6 years the prices for lithium-ion battery systems have decreased with 77%.[34] This is a result of the increase in interest in lithium-ion batteries and the research that is being done. Less research is being performed on improving lead-acid and nickel-based batteries. Therefore, lithium-ion battery prices will continue to decrease and come closer to the level of lead-acid and nickel-based batteries in the near future. An argument that is being used for the appliance of lead-acid batteries for some specific ship types is the improvement of stability because of the large weight. The number of ship types that benefit from the large weight of lead-acid batteries is limited. Also, instead of adding more weight to a ship, another option might be to redesign the hull so weight requirements are not that high and the ship can be lighter and more energy efficient. The last argument against lithium-ion batteries is the safety. This is a serious issue but also very dependent on the specific type of lithium-ion battery that is used. The safety can be increased to an acceptable level by designing a safe battery system with integrated safety features. Taking all this into account, it is chosen to only use lithium-ion batteries in this research.

There are many different types of lithium-ion batteries. Table 2.2 shows the unweighted classification of the six most common lithium-ion battery types. In this overview a rating of 1 indicates the best option for that specific criteria, a rating of 6 indicates the least optimal option. Next to the criteria of power rating, also the criteria of fast charging is added. This is to make a distinction between the capability of delivering high power and receiving high power. The criteria for optimal dimensions is based on the capacity in this case. This is because for most marine applications the capacity is a limiting factor.

Table 2.2: Most common used lithium-ion battery chemistries rated for each selection criteria (1 = best option, 6 = worst option)

Unweighted selection criteria for most common lithium-ion battery types						
Chemistry	LCO	NCA	LMO	NMC	LFP	LTO
Structure	Layered	Layered	Spinel	Spinel	Olivine	Spinel
Capacity	3	1	4	2	5	6
Power	6	5	3	4	1	2
Fast charging	6	4	2	5	3	1
Longevity	5	4	6	3	2	1
Costs	4	5	1	2	3	6
Safety	5	6	3	4	2	1
Dimensions	3	1	4	2	5	6

2.2.2. Cell design

Next to selecting the right chemistry, the structural design of the cell also determines a large part of the characteristics of the battery. The design of the battery cell can basically vary in two different ways, cell shape and cell size.

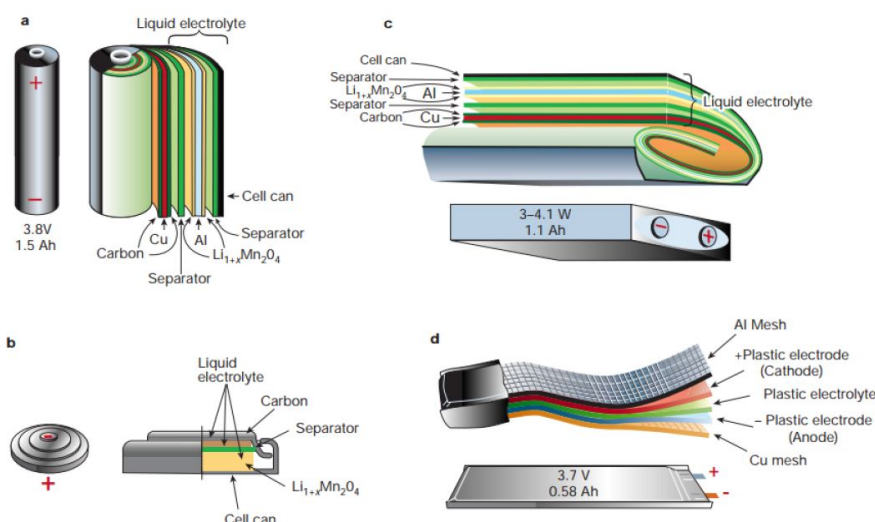


Figure 2.2: Different types of cell design, cylindrical (a), coin (b), prismatic (c) and pouch (d) [57]

There are four main types of cell design: cylindrical, coin, prismatic and pouch cells, see figure 2.2. Coin cells are not suitable for use in large battery systems because of their small size and the lack of integrated safety systems and therefore will not be included in this research. Cylindrical cells have a high energy density, are easy and cheap to manufacture and usually offer a good cycle and calendar life. The cells can be cooled easily and have a relatively high safety. The largest disadvantage is that the packing density is low, so the energy density of a battery system with cylindrical cells is much lower than the energy density of a single cell. Prismatic cells have a higher packing density, but are more difficult and expensive to manufacture, offer a lower cycle life and are difficult to cool evenly. Pouch cells are very light weight and cost effective. They are flexible in the design of battery systems and make an excellent use of space. Pouch cells are relatively sensitive to high humidity and high temperatures and it is difficult to provide them with safety features.[12]

Table 2.3: Different designs for battery cells and their main characteristics compared to each other

Cell shapes		
Cylindrical	Prismatic	Pouch
High energy density	High packing density	Light weight
Cheap	Expensive	Cost effective
Easy manufacturing	Difficult manufacturing	Flexible in design
High cycle life	Low cycle life	Mechanical less stable
Easy to cool	Difficult to cool	Vulnerable to high temperatures
High safety	Average safety	Low safety

After choosing the right chemistry and structural cell design, selecting a battery size is also important for the performance. There are two main philosophies when it comes to the right battery size for large battery systems. A battery system can exist of a large number of small cells, or of fewer but larger cells. Smaller cells are cheaper because they are being mass produced. This also makes smaller cells more easily available and a more proven technology. Another advantage of using smaller cells is that they are more easily and effectively cooled. Larger cells can have a higher energy density, because relatively less packaging material is required. Due to the increase in size, larger battery cells are also more rugged and mechanically stable. Also larger cells are capable of delivering higher power. Balancing the battery cells is also less complicated because of the smaller number of cells. If every cell has a specific probability of sudden failure, using less cells means having a smaller total risk of a failure occurring. This would make the option of having larger cells less vulnerable to failures. However, losing a larger cell, does mean that a larger part of the capacity is lost, compared to losing a smaller cell.

2.3. Battery costs

The costs of batteries can be based on the costs for a battery cell or on the costs for a battery system. The costs are usually expressed compared to the capacity of the battery, in €/Wh or €/kWh. The overall trend of both cell costs as well as system costs is that prices are decreasing. This section discusses the difference in cell costs and system costs and how much the costs are actually decreasing. Also the limits to battery costs and the effects of the decreasing costs are discussed.

2.3.1. Cell/system costs

The costs of batteries depends mainly on two factors, the choice of battery cells and of the battery system. Figure 2.3 shows an estimation of the cost components for a lithium-ion cell.[49] This is an average estimation and will vary depending on the specific cell chemistry, design and manufacturer. Material costs are by far the highest expense at an estimated 60% of the total costs. These costs can be decreased in mainly two different ways. The first method is by the economies of scale. Producing higher volumes is being applied widely to drive battery costs down, but this will only work up to a certain scale. Also the higher demand for the materials can lead to a higher price, driving the material costs up again. Another option to decrease the material costs is the use of different, cheaper materials with the same capabilities to replace current materials, or to use them as additives to decrease the overall price. This however, will translate into the overhead costs, by investing money in the research on new materials and the development of new battery types. Labor costs are only a small part of the total costs. This is due to the high level of automation in battery production facilities. Economies of scale can also decrease the costs for labor, but with the small role it is playing in the overall costs it will not likely lead to large improvements.

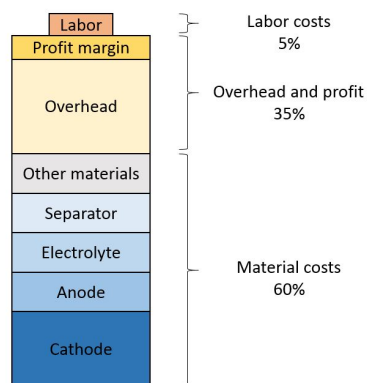


Figure 2.3: Cost components for lithium-ion battery cells [49]

When it comes to battery systems, the estimation of cost components is more difficult. This is due to the wide variation in components and the definition of a system. Depending on the application, the system can include multiple monitoring and safety systems. The main factors that influence the total costs for battery systems are safety, performance and reliability. Especially for marine battery systems, safety is a key factor. The first safety feature is the battery management system (BMS). The BMS measures the state of the cells to make sure certain limits in for instance voltage and temperature are not exceeded. In case of an internal short circuit or thermal runaway, the system must provide for protection of the other cells. System housing and internal cell support also needs to provide for an extra level of safety. Controlling the temperature of the battery cells is very important for safety as well as performance. Cooling the batteries is important to avoid them from overheating, which can lead to thermal runaway, or affecting the life expectancy of the batteries. Thermal management can be done by active or passive air-cooled or liquid-cooled systems, varying in costs, performance, size and energy requirements. Power electronics, wiring and connectors are also depending the overall costs of the system. Choosing a higher quality of components leads to a higher safety, performance and reliability.[14]

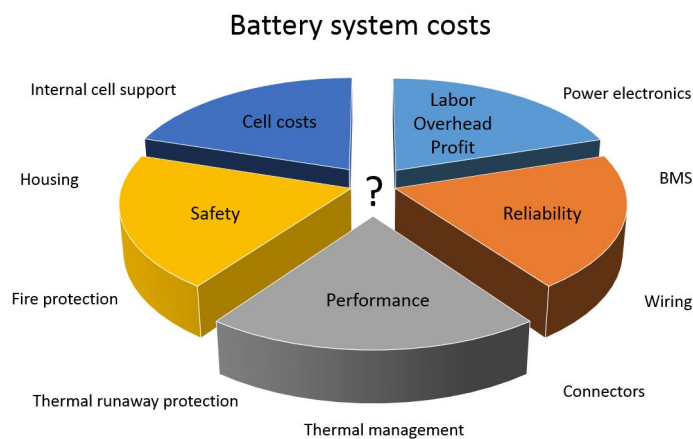


Figure 2.4: Cost determining factors for battery systems

2.3.2. Battery price development

Price estimations for batteries are varying widely. This is partially caused by the different cell chemistries and designs. Another reason is the secretive nature of battery manufacturers, both for cells and for systems. Battery costs are usually overestimated by the industry and this can be due to multiple reasons. One reason can be that manufacturers are avoiding to reveal the actual cost or that they subsidize batteries to gain market shares. With the actual prices for marine battery systems being hard to determine, research based on battery packs for electric vehicles (EV) is used to determine the trends in battery costs. The prices for these types of battery systems are much lower than for marine battery systems. The electric car manufacturing industry is much more developed than the maritime industry. Also EV systems are smaller and less energy is being stored compared to marine battery systems. Nevertheless, the overall trend of battery system costs is declining and although the maritime industry is a little behind, the same development of system costs can be expected to occur there.

In the research by B. Nykvist and M. Nilsson (2015 [42]), over 80 different estimations of battery costs, as well as future predictions, reported between 2007 and 2014 have been analyzed to determine the trend in cost development for battery packs in electric vehicles, see figure 2.5. According to their data, overall prices for battery systems decline annually with 14%, for market leaders this is 8%. For electric vehicles it is stated that a battery price of 150\$/kWh is required to achieve the same competitiveness as a car with an internal combustion engine. According to the research this level of costs can be achieved in 2025. For the maritime industry it is difficult to determine the battery costs at which can be competed with internal combustion engines because of the wide variety of ship types, sizes and operational profiles. This will have to be calculated for each case separately. At the moment, marine battery systems are estimated to be in the price range of €550 to €800 for LFP and NMC batteries. Marine battery systems with LTO cells are estimated to be in the price range of €1100 to €1500.

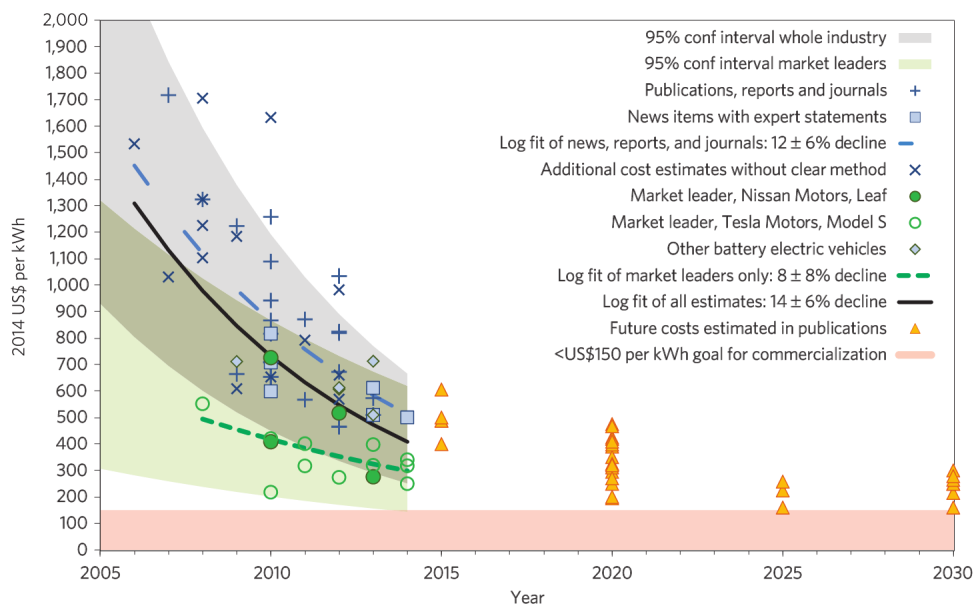


Figure 2.5: Expected battery price development (Nykvist (2015) [42])

2.3.3. Lifetime costs

The costs of installing a large battery system on a ship is estimated to be around €1000 per kWh. The costs to replace the batteries are estimated to be similar, with a reduction of the annual decrease in battery prices. The costs of removing the original battery system is expected to be accounted for by the second life destination of the batteries. To calculate the costs for batteries in a ship, also the costs of the interest on the initial investment need to be taken into account. The interest is estimated to be 5%. [56]

2.4. Selecting a battery

Determining the right battery for a specific application can be very complex, this also applies to selecting a marine battery system, because of the large varieties in requirements for marine battery systems. This section provides several steps that can be taken in the battery selection process for fully battery powered ships. The selection process can be divided in three steps, determining the operational requirements, calculating the initial and operational costs and the integration of the battery system in the ship.

2.4.1. Operational requirements

The first step in the selection process for a suitable battery system in a marine application is determining the operational requirements, based on the operational profile of the ship. The capacity of the battery needs to be sufficient for the required range and cruising speed of the ship. The speed of the ship as well as the required charging time is determined by the power rating of the battery system. Battery cells can be divided into high power cells and high energy cells. For applications with a demand for high maximum speeds or a short charging time, high power cells are more suitable. High energy cells are preferred for a longer range. Depending on the type of application, the importance of each operational aspect has to be determined. Compromises have to be made between having a long range, high cruising speed or a high maximum speed and short charging time. Putting emphasis on one, will result in giving in on the others.

2.4.2. CAPEX/OPEX

The second step in the selection process is the consideration of the ratio between the initial and the operational costs of the system, the CAPEX and the OPEX. The CAPEX are determined by the specific costs for the battery cells, as well as the total installed capacity and power. For low CAPEX the cell costs and total installed capacity and power all need to be low. The OPEX are mainly determined by the weight and the longevity of the batteries. A low weight will lower the required propulsive power and therefore the demand for energy. A higher longevity expands the lifetime of the battery, postponing the replacement of the battery system and therefore lowering the OPEX. Battery cells with a higher longevity are usually more expensive, or have a smaller energy density. The more expensive cells lead to a higher CAPEX, but also increases the costs in case the battery system has to be replaced. The lower energy density leads to a higher weight of the system, which increases the OPEX. Another option for improving the longevity of the battery is to increase the installed capacity or power, also resulting in higher CAPEX as well as higher OPEX. Figure 2.6 shows the difficulties in the relations between the requirements for a low CAPEX and OPEX. A low CAPEX interferences with a low OPEX on total installed capacity and power and on the cell price. Considering the OPEX the demand for a high longevity interferences with the demand for a low weight of the system. To select a battery for a specific application, the advantages of having low CAPEX or low OPEX should be carefully calculated

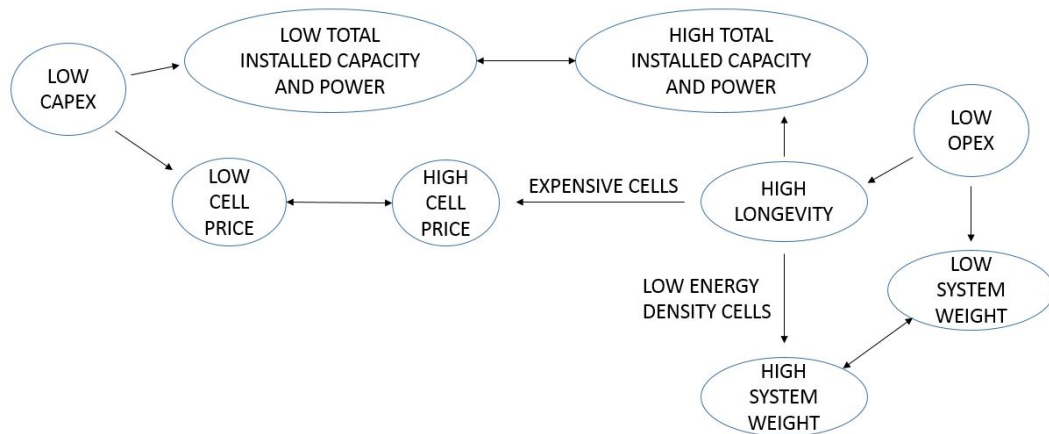


Figure 2.6: Selecting a battery cell on CAPEX and OPEX

2.4.3. System integration

The last step in the selection process is the integration of the battery system in the ship. This step concerns the physical placing of the batteries, but more relevant to the selection of a battery type is designing the features to increase the safety and performance of the system. The physical placing of the battery system is influenced by the dimensions and the weight of the system. In any case the system will be heavy and large and therefore selecting a different battery will not have a major influence on the placing from dimensional point of view. Different battery types do have different safety demands. This translates in the requirements for fire fighting systems, ventilation and thermal management. Cells with a high energy density such as NCA, might require a more elaborated fire fighting or cooling system than a safer chemistry like LTO. This decreases the overall energy density of the system and increases the costs, both CAPEX and OPEX.

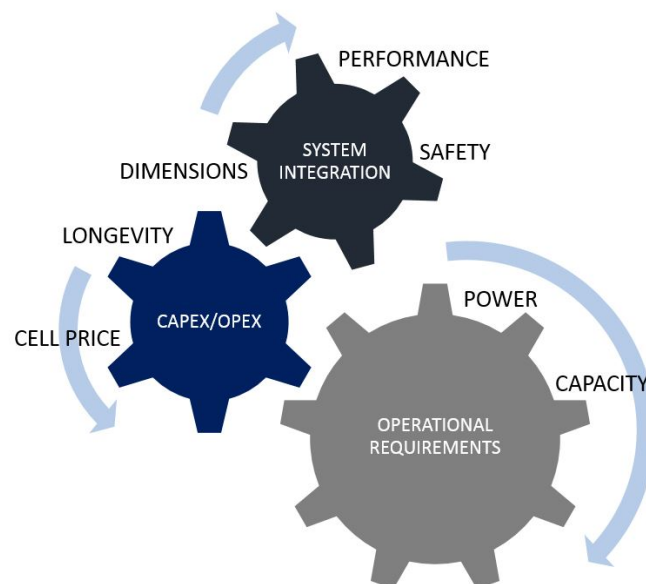


Figure 2.7: Battery selection process

3

Battery aging

Lithium-ion batteries come in many different types, but what they have in common are, obviously, the lithium-ions traveling between the anode and cathode. Figure 3.1 shows a schematic representation of a lithium-ion battery during charge and discharge. The discharging battery is in a charged state, therefore the majority of the lithium is bound with the negative electrode. During discharge, oxidation takes place and the lithium splits from the electrode material, loses an electron and becomes a lithium-ion. While the electron travels through the electrical circuit to the positive electrode, the lithium-ion is transported by the electrolyte through the separator to the positive side. At the positive electrode, reduction takes place by binding the lithium-ion with an electron to the electrode material. During charge, the opposite reactions take place and the positive electrode loses the lithium which then travels to the negative side. The ability of the battery to perform these reactions decreases because of aging. The mechanisms that cause this aging are discussed first. Then the operational conditions that enhance these mechanisms are explained. Tests can be performed on a battery to measure the rate at which aging takes places. The methodologies of different studies on aging are evaluated and the results are compared to each other and to the theoretical expectations.

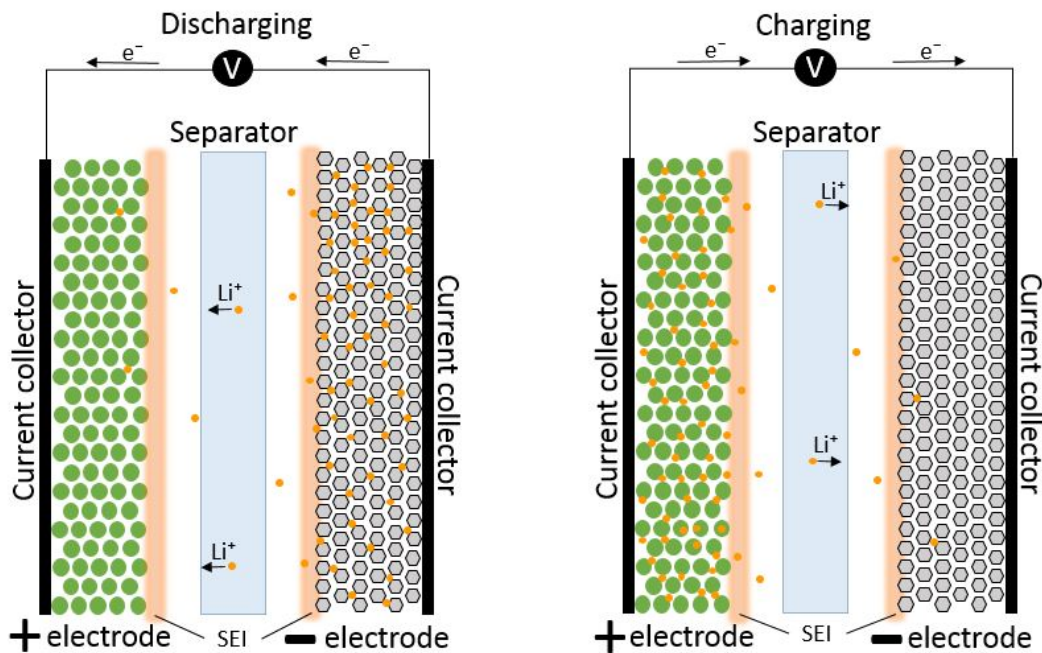


Figure 3.1: Schematic representation of a lithium-ion battery

3.1. Aging mechanisms

In Pelletier et al.(2015)[46], an overview is given of the main aging mechanisms in lithium-ion batteries. Aging can be divided into two different groups based on their consequences, capacity loss and power loss. Basically there are three main causes for capacity loss and two main causes for power loss, see figure 3.2. The main causes for capacity loss are electrode disintegration, material deterioration and loss of free lithium. The main causes for power loss are surface layer formation and contact deterioration.[28] Although for this research only capacity loss is taken into account, the reactions that cause power loss will also be discussed, because of the close relationships between the different mechanisms. The rate of aging is very much dependent on the chemistry and structure of the battery cell. Each combination of cell chemistry and structure has a different sensitivity to specific aging mechanisms.

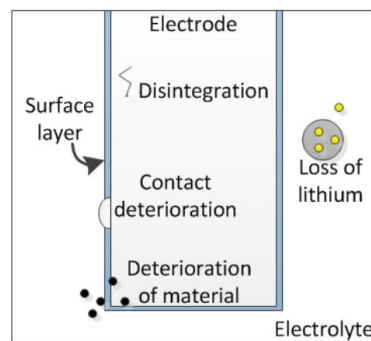


Figure 3.2: Battery half cell representing the five main aging mechanisms

3.1.1. Loss of free lithium

The electrodes and electrolyte are in constant reaction with the lithium and with each other. These chemical reactions affect the amount of free lithium that is usable for the storing of energy in the electrodes. Although the lithium is still inside the battery, it can't be transported between the electrodes anymore. With less lithium available to store energy at the electrodes, the capacity of the battery decreases.

3.1.2. Surface layer formation

In figure 3.1 there are two layers visible at the surface between the electrodes and the electrolyte. These layers are called the solid electrolyte interface (SEI). The formation of the SEI starts with the electrochemical stability window of the electrolyte and the loss of free lithium. When cell voltage reaches a level outside of the electrochemical stability window of the electrolyte, the electrolyte material reacts with the electrode, forming a layer on the surface of the electrode. According to Ploehn (2004)[48], the thickness of the SEI layer evolves linearly with the square root of time. This is especially the case at the graphite anode, which typically has a potential outside the electrolyte stability window. With the first cycle of the battery, the SEI is formed. The SEI has the characteristic that it does allow lithium-ions to move through, but not other materials such as the electrolyte. Therefore the SEI acts as a protective layer against further electrolyte decomposition. The SEI however, does increase the impedance, resulting in a loss of power.

3.1.3. Electrode disintegration

In a charged state, the negative electrode is filled with lithium (lithiated) and the positive electrode is not (delithiated). When discharged, the positive electrode is lithiated and the negative electrode is delithiated, see figure 3.1. A lithiated electrode is larger in size than a delithiated electrode because of all the added lithium. The expansion rate can be very different depending on the material, bindings and structure of the electrode material, see table 3.1. An electrode that changes in size much, will slowly disintegrate with every cycle. Cracks in the material will decrease the amount of active material available to store the lithium. Therefore, electrode material with smaller expansion rates will suffer less from capacity fade and have a longer cycle life. The high stresses induced by these volume expansions can also cause large shifts in voltage levels of the cell.[11] As a rule of thumb, a volume expansion of less than 10% will lead to a good mechanical cycle life.[64]

Table 3.1: Overview of expansion rates of common electrodes

Electrode material	Expansion when lithiated
LTO	0.1% [64]
NMC	2% [60]
LFP	5% [64]
LCO	9% [64]
Graphite	10% [63]
LMO	16% [27]

3.1.4. Material deterioration

Another effect of the volume changes of the electrodes is that the SEI layer cracks, exposing the electrode material to the electrolyte. At those points, side reactions take place between the electrodes and the electrolyte. One of the effects of these side reactions is that electrode material dissolves in the electrolyte. The total mass of active electrode material decreases, causing the capacity to store lithium to fade. This process stops when there is a new SEI layer formed again, but is repeated with each cycle.

3.1.5. Contact deterioration

The contact area at the electrolyte-electrode interface is an important factor for the internal resistance of the battery cell.[64] For a low resistance, and with that a high power rating, a large diffusion area is preferred. Due to the SEI formation, the area of the electrode that is in contact with the electrolyte decreases, resulting in a power loss. Another reason for the deterioration of contact area is caused by the volume expansions of the electrodes during cycling and corrosion at the electrode and current collector interface.

3.2. Aging causes

There are several operational conditions that enhance the aging mechanisms in batteries significantly. It is indicated in several studies that overcharging or over-discharging causes high stresses and increases the aging rate of the battery drastically.[45][33][4][63] Cells that are at a different state of charge at the same time and in the same system also suffer more from aging. However, the batteries in a large battery system that is designed to power a ship will have proper monitoring and safety features provided by the battery management system (BMS). The BMS balances the state of charge of the different cells and protects them from overcharging and over-discharging. Therefore, the influence of unbalanced cells, overcharging and over-discharging on aging mechanisms is outside of the scope of this research. The conditions that are investigated in this research are: temperature, state of charge, depth of discharge and C-rates.

3.2.1. Temperature

Within chemistry, the general effect of high temperatures is that chemical reactions are accelerated. This also applies to the aging mechanisms inside the battery. The electrolyte decomposes at a higher rate, (Barré et al., 2013)[5], causing an accelerated loss of active lithium, (Vetter et al., 2005)[63] and a faster SEI layer growth, (Amine et al., 2005)[3]. Low temperatures can lead to the formation of lithium plating on the anode, resulting in a lithium loss, (Barré et al., 2013)[5]. Also, lower temperatures can lead to a change in electrochemical reactions. The impedance decreases with high temperature, causing the power of the battery to increase, but also the aging rate increases. Low temperatures increase the impedance, causing an instant, but reversible power loss. Keeping the battery at a low temperature is only preferable during storage, because also the continuous aging mechanisms reduce in speed, but not when the battery is being cycled.

3.2.2. State of charge

The state of charge (SOC) of the battery affects the potentials and stresses on the electrodes. Depending on the potential of the electrode, different side reactions between electrode material and electrolyte take place. At a high SOC the graphite electrode has a low potential, outside of the electrochemical stability window of the electrolyte. This causes the electrolyte material to deteriorate (Zheng et al., 2015b)[70] and SEI layer growth on the electrodes. (Amine et al., 2005)[3] The stresses that are induced on the electrodes during high or low SOC are relative to the amount of lithium that is stored in the electrode material. The SOC also influences the internal resistance of the battery. A higher internal resistance causes higher temperatures during cycling and therefore also the aging rate.

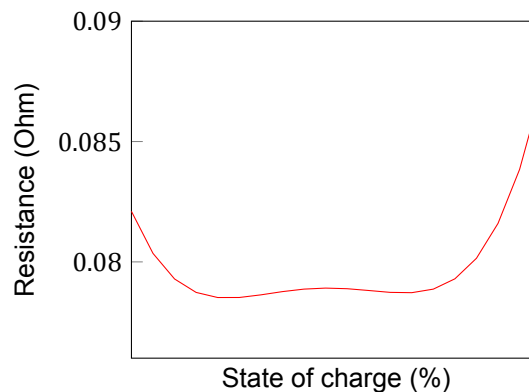


Figure 3.3: Example of a resistance curve of a lithium-ion battery[31]

3.2.3. Depth of discharge

The depth of discharge (DOD) is seen as the difference between the state of charge at the beginning of a discharge and the state of charge at the end of the discharge. A large DOD results in large volumetric changes of the electrode material. These large volumetric changes accelerate four of the five aging mechanisms: the disintegration of electrode material, by induced mechanical stresses; the reduction in contact area between electrode and current collector, by the constantly changing sizes of the material; the deterioration of electrode material, caused by the destruction of the SEI layer, exposing the electrode material to the electrolyte, causing more side reactions between them; the loss of free lithium, which increases because of the increased use of the battery. (Belt et al., 2003)[6](Vetter et al., 2005)[63]

3.2.4. C-rates

Charging and discharging at high C-rates increases the internal resistance of the battery cell. The increased resistance leads to an increase in temperature and a decrease in efficiency. Charging at high C-rates causes the electrolyte material to deteriorate and accelerates surface layer growth, (Zheng et al., 2015a)[69]. Also lithium is lost by the formation of lithium plating on the anode, (Trippe et al. 2014)[30]. Charging at high C-rates while the state of charge is at a high level can cause disintegration of the anode material, (Agubra and Ferguson, 2013)[2].

3.2.5. Other causes

The temperature, state of charge, depth of discharge and C-rates are the most investigated causes for battery aging. They are also assumed to be the leading causes. With a shipbuilding perspective there might also be other operational conditions having an influence on the aging of the batteries. The humidity and pressure in the battery space also have an affect on battery aging for instance.[13] Lithium is highly reactive with water and increased humidity levels cause an accelerated loss of active lithium and SEI layer growth. An increased humidity also increases the self-discharge rate of the battery. Too low humidity levels can cause the battery to dry out. The pressure always affects chemical reactions and therefore it is assumed that it also plays a role in aging. The first investigations on the effects of vibrations and impacts show no clear relation to capacity fade of the batteries, up to a certain level of intensity.[29][9] However, not much information is found on the quantitative effects of these conditions on battery aging and therefore more research on this is required to implement it in this study.

3.3. Aging test methodology

Battery aging can be divided into two types: calendar aging and cycle aging. Calendar aging takes place during every moment of the life of the battery, even when it is not being used. It is dependent on the state of charge (SOC) and temperature (T), and it is calculated with respect to time (t). Cycle aging takes place whenever there is a load on the battery, this can be both charging and discharging. The cycle aging effect is mainly dependent on the depth of discharge (DOD), average state of charge (μ_{SOC}) and C-rates for charging and discharging. It is calculated with respect to the amount of performed cycles or the amount of charge throughput (Ah). The calendar and cycle aging are accumulated to calculate the total capacity that is lost.

$$A_{cal} = f(SOC, T, t) \quad (3.1)$$

$$A_{cyc} = f(DOD, \mu_{SOC}, C-rate, Ah) \quad (3.2)$$

$$A_{total} = A_{cal} + A_{cyc} = f(SOC, T, t, DOD, \mu_{SOC}, C-rate, Ah) \quad (3.3)$$

The methodologies and results of 15 independent aging studies have been analyzed. The evaluated studies investigate either calendar aging, cycles aging or both. Calendar aging is tested by measuring the remaining capacity after storing the battery at a specific temperature and SOC. Cycle aging is tested by measuring the remaining capacity after cycling the battery at a specific DOD, average SOC and C-rate. Table 3.2 provides an overview of the evaluated studies. The abbreviations HE and HP for cell design stand for High Energy and High Power. The C-rate and temperature are the conditions at which the capacity measurements have taken place. The studies are evaluated on their methodology and battery type. To compare the results of the different studies with each other, it is important to know the differences in testing methodology and the type of battery that is used. Appendix B provides more information on the methodology per each single study.

Table 3.2: Overview of battery types and remaining capacity measurement conditions per test

List of studies used for analysis of battery aging						
Research	Chemistry	Cell design	Capacity	Aging type	C-rate	Temp.
MOBICUS [7]	NMC	HE	43 Ah	Calendar	0.1C	-
Safari [50]	LFP	Cylindrical	2.3 Ah	Calendar	0.04C	25°C
Keil [32]	NCA	Cylindrical	2.8 Ah	Calendar	0.7C	25°C
Keil [32]	NMC	Cylindrical	2.05 Ah	Calendar	1C	25°C
Keil [32]	LFP	Cylindrical	1.1 Ah	Calendar	1.8C	25°C
Sarasketa [51]	LFP	Cylindrical	2.3 Ah	Calendar	1C	25°C
SIMCAL [15]	NCA	Cylindrical	7 Ah	Calendar	1C	25°C
SIMCAL [15]	NMC	Pouch	12 Ah	Calendar	1C	25°C
SIMCAL [15]	NMC	Pouch	5.3 Ah	Calendar	1C	25°C
SIMCAL [15]	LFP	Cylindrical	8 Ah	Calendar	1C	25°C
SIMCAL [15]	LFP	Cylindrical	15 Ah	Calendar	1C	25°C
SIMCAL [15]	LFP	Cylindrical	2.3 Ah	Calendar	1C	25°C
Schmalstieg [55]	NMC	Cylindrical HE	2.05 Ah	Calendar	1C	35°C
Deshpande [16]	LFP	Cylindrical	2.2 Ah	Cycle	0.05C	-
Liu [38]	LFP	Cylindrical	2.2 Ah	Cycle	0.5C	-
Peterson [47]	LFP	Cylindrical	2.3 Ah	Cycle	0.5C	-
Wang [65]	LFP	Cylindrical	2.2 Ah	Cycle	0.5C	-
Watanabe [66]	NCA	Cylindrical	0.4 Ah	Cycle	1C	-
Wong [67]	NCA	Unknown	3 Ah	Cycle	1C	-
Saxena [54]	LCO	Pouch	1.5 Ah	Cycle	0.5C	25°C
Omar [44]	LFP	Cylindrical	2.3 Ah	Cycle	1C	25°C
Sarasketa [52]	LFP	Cylindrical	2.3 Ah	Cycle	1C	25°C
Schmalstieg [55]	NMC	Cylindrical HE	2.05 Ah	Cycle	1C	35°C
Ecker [17]	NMC	Pouch HP	6 Ah	Both	1C	35°C
Ecker [18]	NMC	Cylindrical HE	2.05 Ah	Both	1C	35°C

3.3.1. Evaluation

Similar test methodologies would have been convenient for comparing the results of the different aging tests with each other; however, almost none of the evaluated studies used a similar test procedure. The temperature and SOC levels at which the batteries are stored are not matching for the calendar aging. The DOD, average SOC and C-rates at which the batteries are cycled are not matching for the cycle aging. The interval at which the capacity is measured varies from 2 weeks to 10 months for calendar aging and from 50 to 200 cycles for cycle aging. The resting periods between a cycle and measurement varies from 5 minutes to 2 days. The earliest tests are ended after reaching 98% of the initial capacity, the latest test after reaching 60% of the initial capacity. Although there are a lot of differences in the test methodologies, there is enough data available to evaluate most of aging effects. This is mainly because of the large amounts of data that is produced by the studies.

3.4. Calendar aging

Calendar aging is calculated with respect to time and is dependent on the SOC and temperature of the battery cell. It is tested by first choosing the SOC and temperature levels that will be investigated and then cells are stored at those specific SOC and temperature combinations and are periodically tested for their remaining capacity. The studies that are used concern the calendar aging of LFP, NMC and NCA lithium-ion batteries. The choice for these types is purely based on the available information. More information is available than for other types of chemistry because these battery types are commonly used for powering electric vehicles. The results of 15 different tested batteries are used for the analysis of calendar aging. Tests

are performed on 7 NMC batteries, 6 LFP batteries and 2 NCA batteries. The calendar aging rate is analyzed with four different variables: temperature, SOC, storage time and type of chemistry. The aging rate in the figures is shown in the average percentage that is lost per day or per cycle at the time of measurement. The lines that show a state of health (SOH) of 80% are to indicate at what combination of aging rate and days of storage, or aging rate and number of performed cycles, the remaining capacity of the battery is 80% of the initial capacity.

3.4.1. Temperature

The data is compared at combinations of a fixed SOC at variable temperatures to analyze the effect of temperature on the aging rate. Figure 3.4 gives an overview of the minimum and maximum measured aging rates at each temperature. The combinations of this SOC level and these temperatures is used because of the high number of data points for analysis compared to other conditions. Figure 3.5 shows the aging rate at a SOC of 30% at temperatures of 30°C, 45°C and 60°C, for LFP, NCA and NMC. On the horizontal axis the number of days the battery was stored at the moment the remaining capacity was measured is shown. The vertical axis shows the average loss of capacity per day in percentage of the initial capacity. This is calculated by dividing the remaining capacity at the time of the measurement by the number of days the battery was stored.

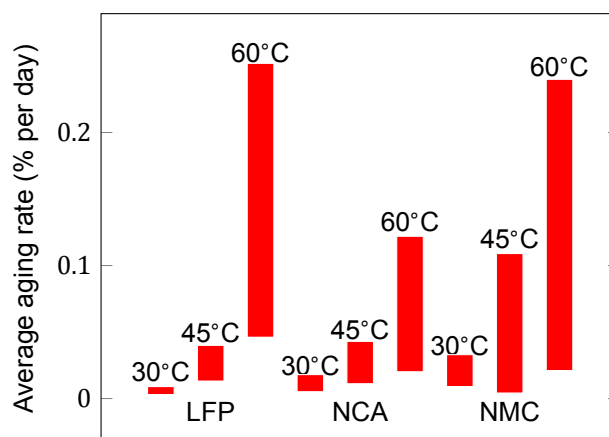


Figure 3.4: Minimum and maximum aging rate at 30% SOC

At a temperature of 30°C the following observations are made: the aging rate stays between a value of 0.003% to 0.006% per day for LFP; there is a clear decline from 0.013% to 0.005%, a decrease by almost 3 times, for NCA; the decrease is also close to a factor 3 for NMC, but then from 0.024 to 0.009. See figure 3.5 (A).

At a temperature of 45°C the following observations are made. The aging rate of LFP again stays fairly constant, but at a higher level between 0.013% and 0.027% compared to 30°C, an increase of about 4 times. For NCA the results look similar as the measurements at 30°C, but at a higher aging rate between 0.011% to 0.032%, an increase by a factor 2. The data of NMC has three very different data sets. The highest values belong to the data from the MOBICUS research project[7], this will be referred to as set 1. The set of data in the middle belongs to the 5.3 Ah battery cell from the SIMCAL project[15], this will be referred to as set 2. The set with the lowest aging rates belongs to the 12 Ah battery from the SIMCAL project[15], this will be referred to as set 3. The aging rate in set 1 varies between 0.06% and 0.11%. Set 2 varies between 0.02% and 0.04%. The aging rate of set 3 is constant around 0.004%. These are large differences for a battery of a similar chemistry at the same storage conditions. The battery cell from set 1 is a 43 Ah high energy cell. The capacity measurements are performed at a C-rate of 0.1C at an unknown temperature. The capacity of set 2 and set 3 is measured

at a C-rate of 1C and a temperature of 25°C. A lower C-rate to measure the capacity should lead to a higher measured capacity; therefore, it is unlikely that the difference comes from the method that is used to measure the capacity. One problem with comparing the 3 data sets with each other, is the storage time they have been tested at. For set 1 this is between 36 and 161 days, for set 2 between 122 and 670 days and for set 3 between 364 and 723 days. For most of the other data sets it is common for the aging rate to start at a high level and to decline with the increasing storage time. Because the measurements for these three sets are not in the same time period they are difficult to compare; however, there is a very large difference in aging rate at the parts that do overlap in time. One possible explanation for the large differences is that the used cells are constructed in a different way. It is unknown what type of cell the 43 Ah cell of set 1 is, but it is very different from the other two cells because it has a capacity of 4 to 8 times higher. Also between the cells of set 2 and 3 there is a factor 2 difference in capacity, but, because of the missing information on the actual cells it is difficult to explain the true reason of the large differences in aging rates. See figure 3.5 (B).

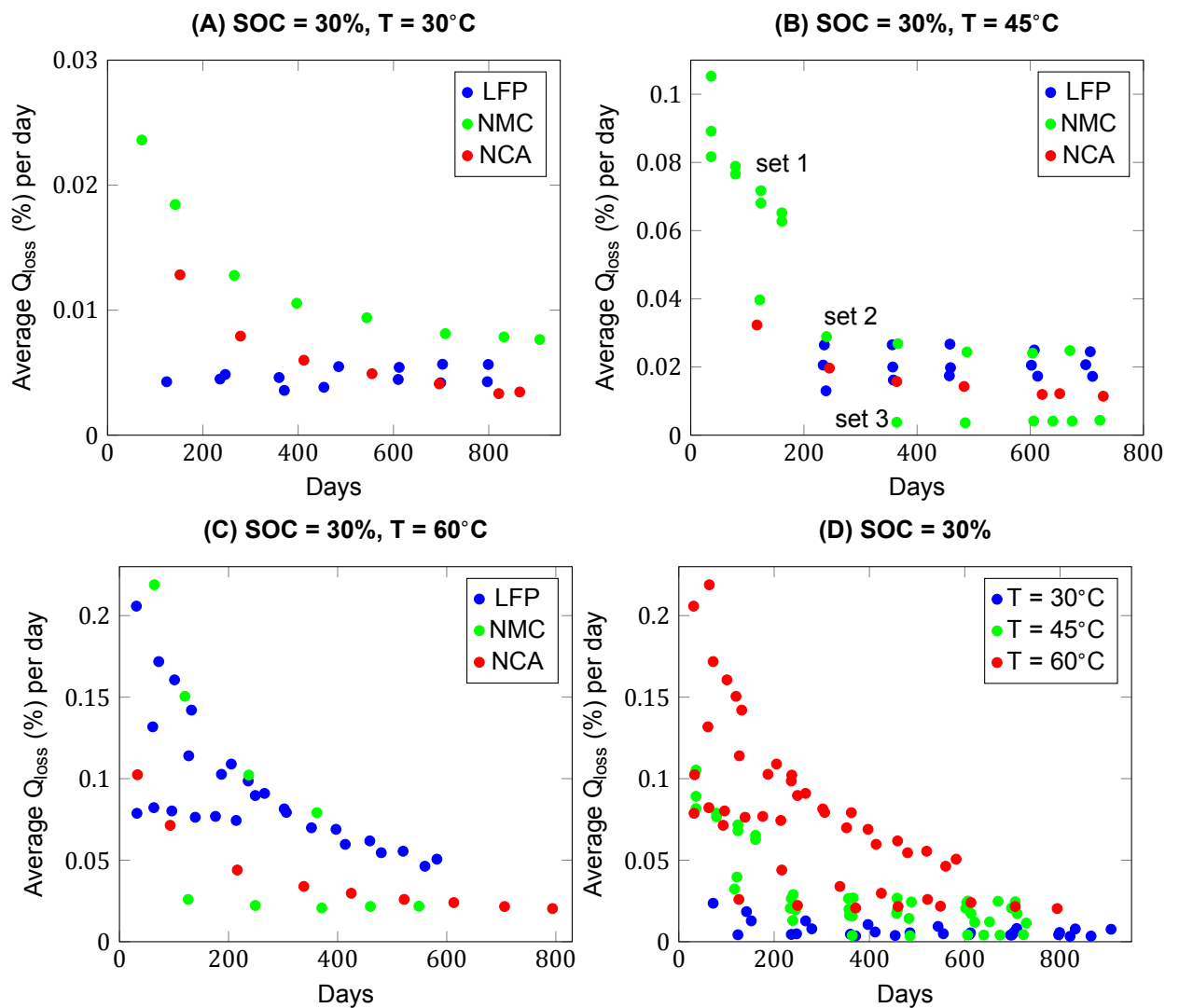


Figure 3.5: Effect of temperature on calendar aging

At a temperature of 60°C the aging rates increase significantly. The data set of LFP consist of data from three different batteries, all from the SIMCAL project research.[15] The three different curves are clearly visible. All cells are cylindrically shaped and tested with the same method, but still the variation in aging rate is very large. More information on the construction of the cells is required to explain the differences in aging rate. The data for NCA has a similar shape compared to the measurements at a temperature of 30°C and 45°C, but the aging rate varies now between 0.020% and 0.102% per day. This is an increase of 3 times compared to the aging rate at 45°C and almost 8 times compared to the aging rate at 30°C. The data set for NMC is from the same batteries as set 2 and set 3 in figure 3.5 (B). The aging rate of the two batteries develops in the same way at a temperature of 60°C compared to 45°C. See figure 3.5 (C).

All data from the different temperature sets and batteries is combined in figure 3.5 (D). The aging rate at 30°C varies between 0.003% and 0.024%. At 45°C the aging rate varies between 0.004% and 0.105%. At 60°C the aging rate varies between 0.020% and 0.219%. From 30°C to 45°C the aging rate increases with a minimum factor of 1.3, up to a maximum factor of 4.4. From 30°C to 60°C, the aging rate increases with a minimum factor of 6.7, up to a maximum factor of 9.1. This shows that the temperature of the battery cells has a high influence on the aging rate of the battery.

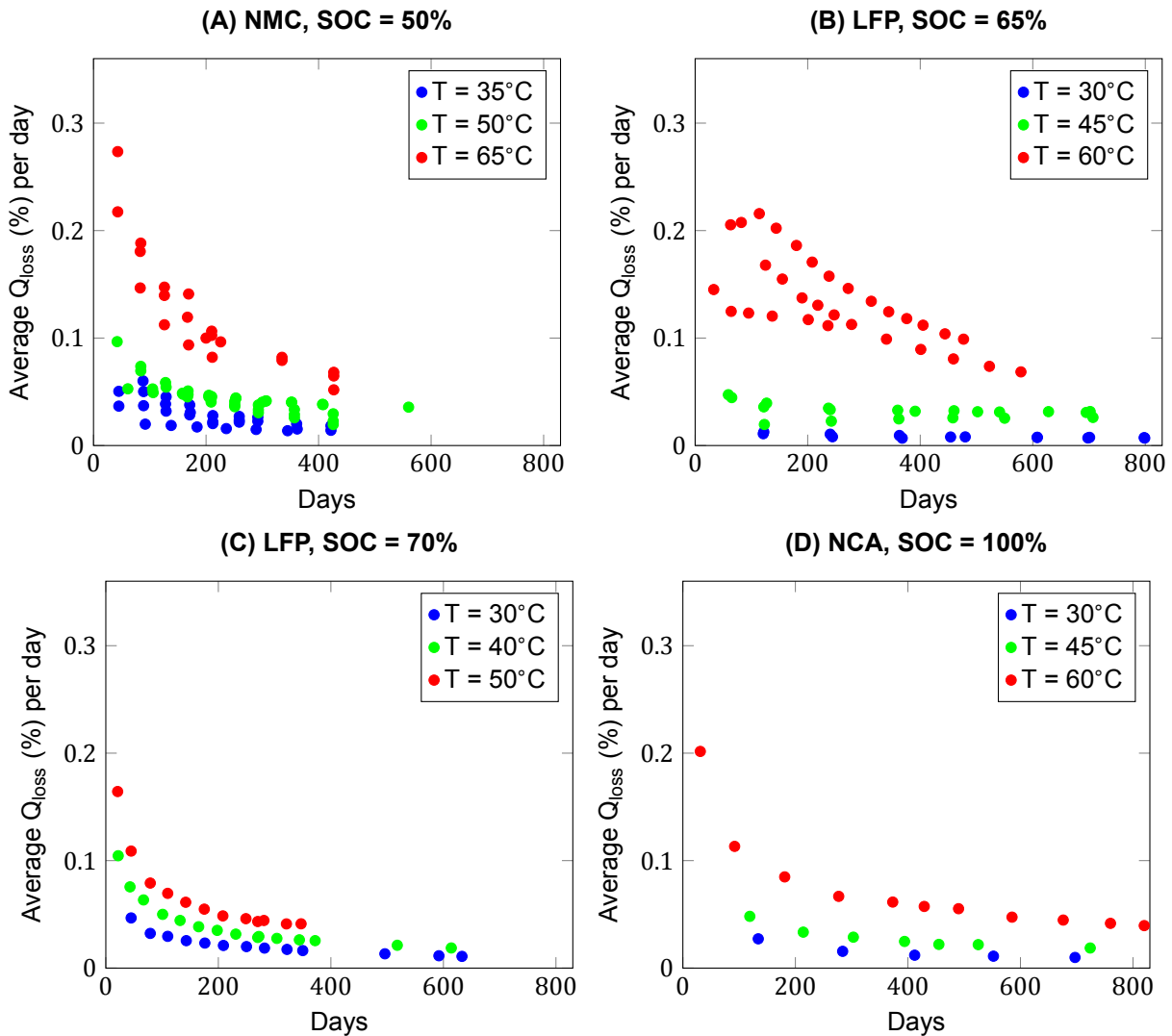


Figure 3.6: Effect of temperature on calendar aging

Four different data sets are shown of aging data from batteries of a specific chemistry, at a constant SOC and at variable temperatures in figure 3.6. All figures show the same behaviour, independent of SOC level or battery chemistry. The aging rate increases with the temperature. The differences between the maximum and minimum aging rates is the smallest at a temperature of 30°C. At temperatures between 35°C and 50 °C, it is clearly visible that the aging rates increase. Especially during the first 100 days of storage the aging rate increases rapidly with an increasing temperature. Temperatures of 60°C or higher have a very large impact on the aging rate of the batteries and should be avoided for an acceptable battery lifetime.

3.4.2. State of charge

The effect of SOC level on the aging rate is analyzed by comparing aging data at a constant temperature and variable SOC levels. Figure 3.6 shows the data of test on LFP cells at 30°C (A), LFP cells at 40°C (B), NMC cells at 50°C (C) and NCA cells at 60°C (D). These data sets are chosen because of the high number of data points and because it provides a comparison between different temperatures as well as different chemistries at variable SOC levels. Figure 3.7 shows an overview of the minimum and maximum aging rates per test condition and battery chemistry.

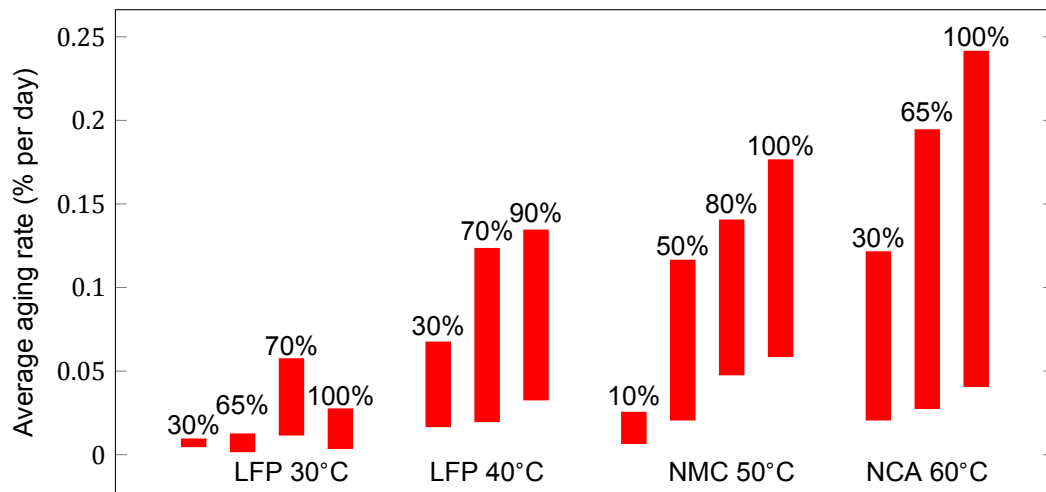


Figure 3.7: Minimum and maximum aging rate compared for variable SOC

The first observation of the minimum and maximum aging rates shown in figure 3.7, is that for most situations, a higher SOC level corresponds to a higher aging rate. There is one exception and that is the case at the tests on LFP cells at 30°C (A), where the minimum as well as the maximum aging rate is higher at 70% SOC than at 100% SOC. Figure 3.6 (A) shows even more unexpected behaviour. Some of the measured data on 65% SOC shows the lowest aging rates of the data set, lower than most measurements at 30% SOC. Then there is a set of measurements at 100% SOC that is also lower than the measurements at 30% SOC. These irregularities are easily explained by looking at the origin of the data. The data from the tests at 30%, 65% and 100% is all from the SIMCAL project[15] and concerns three different battery cells; of 2.3 Ah, 8 Ah and 15 Ah. The data points that show a low aging rate at these conditions are all from the cell of 8 Ah. This might indicate that the 8Ah cell that is used for this research was designed for a better calendar life. The data of the 2.3 Ah and 15 Ah cells shows a similar behaviour in development of the aging rate at an increasing SOC level. The measurements at the condition of 70% SOC are from the research performed by Sarasketa et al.[68] The methods that are used for measuring the remaining capacity is similar for both tests, at a C-rate of 1C and a temperature of 25°C. Therefore, this can not be the cause for the difference in aging rates.

From the data shown in figure 3.8 (B, C and D), the aging rate is developing almost linear with the increasing SOC levels. This is different compared to the influence of the temperature, where the increase of temperature caused a more dramatic increase of the aging rate. There is one more notable difference in one of the data sets. Most data sets show a decrease in aging rate developing over time. This is not the case for the measurements on the NMC batteries at 50°C at a SOC level of 10% or lower. In this case the aging rate increases with the storage time. The majority of the data at these storage conditions comes from the research performed by Ecker et al.[18] The tests are performed at a SOC level of 5% and at 10% and both show the same increasing behaviour of the aging rate. Measurements from the same research on the same type of battery cells and at 50°C, but at higher SOC levels, do not show this increasing behaviour of the aging rate. As explained in chapter 3, discharging the battery to low voltages induces large stresses on the cell and causes the battery to age. Storing the battery at a low voltage, or low SOC level, does mean that there is only a little energy stored inside the battery. Therefore, in general, the aging rate is low at storage conditions below 10% SOC. However, there is a high stress on the cell because of the low voltage. With every test cycle, these stresses cause an increase in the aging rate. Causing the aging rate to increase with time, instead of decrease with time as is the case at higher SOC levels.

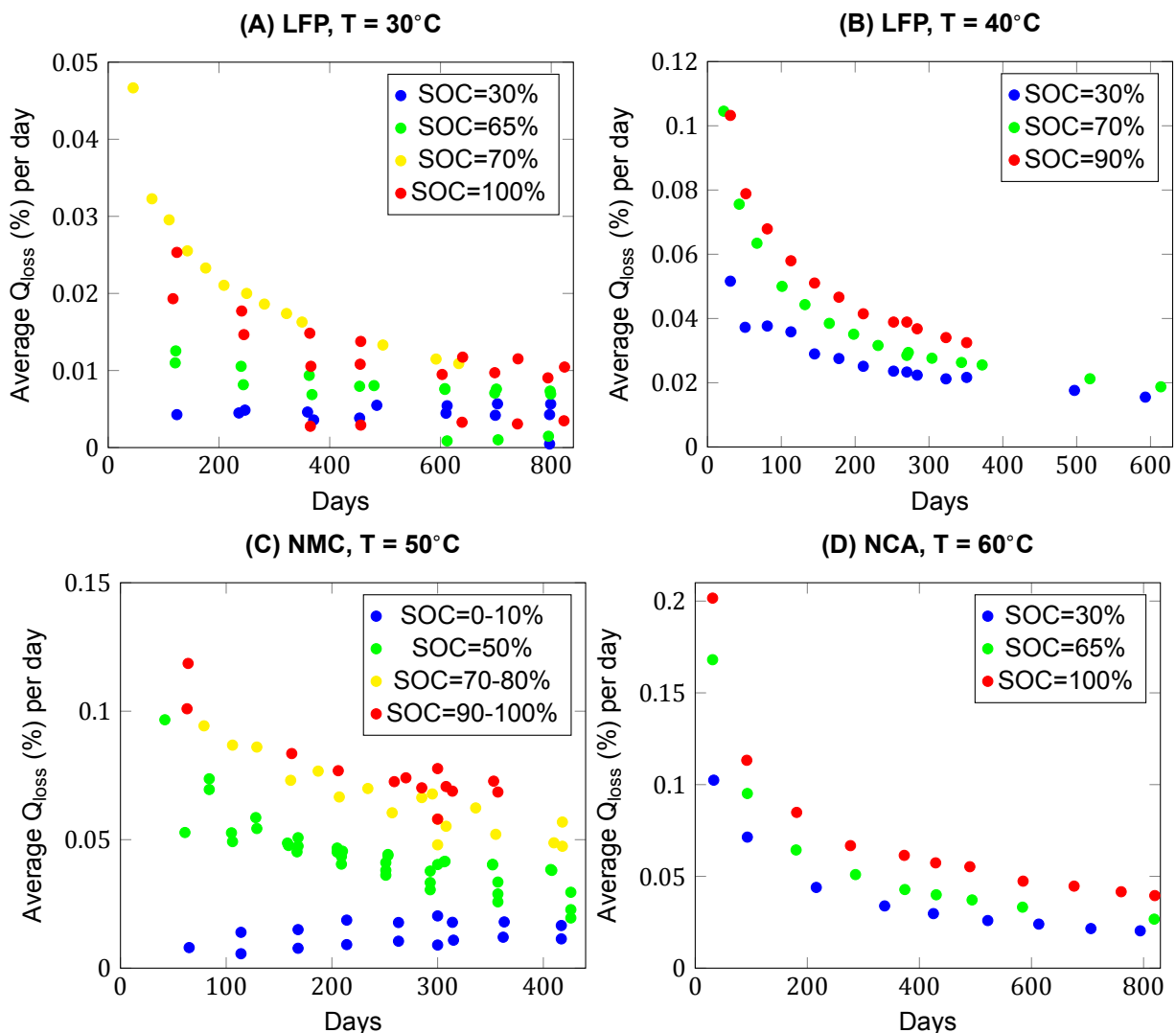


Figure 3.8: Effect of SOC on calendar aging

The aging rate changes over time. Figure 3.9 shows the effect of the SOC level at a specific moment in time for temperatures of 25°C, 40°C and 50°C, for LFP (A), NMC (B) and NCA (C) and over the full range of SOC levels. All three figures show the expected behaviour with relation to the temperature. A higher temperature causes a higher aging rate. Striking is that the tested NCA battery shows lower aging rates, although the chemistry NCA is known for having a shorter life expectancy than NMC or LFP. These data sets are from the research by Keil et al.[32] The cells that are used for this research are a 2.8 Ah NCA cell, a 2.05 Ah NMC cell and a 1.1 Ah LFP cell. Different C-rates are used for the capacity measurements. The authors suggested that the internal construction of the battery cells are similar, and therefore not the C-rates, but the charge and discharge rates in Amperes should be equal. This resulted in a C-rate of 0.7C for the measurements on the NCA cell, 1C for NMC and 1.8C for LFP. Looking at the results it can be that the reasoning for the different C-rates might not be valid. However, looking at the effect of the SOC level, there is a similar behaviour for the three different batteries. From 0% to 20% or 30% SOC the aging rate increases linearly. From 30% to 60% SOC for NMC, 20% to 55% SOC for NCA and 30% to 70% SOC for LFP, the aging rate remains constant. These levels are based on the data in figure 3.9 and are not the same for every battery of the evaluated chemistries. Above these levels the aging rate increases again. This constant value for the aging rate is explained by the voltage plateau in the discharge curve. The phases of the active materials in the battery cell do not change at this voltage plateau, only the composition of the total chemical reaction. The constant voltage level and the constant aging rate cause this part of the SOC domain of the battery to be called the sweet spot. It is the preferred operating range of the battery for an increased life expectancy. The low SOC levels causes high stresses in the battery. Although the measurements show low aging rates for these storage conditions, operating the batteries at these low SOC levels causes the batteries to age faster.

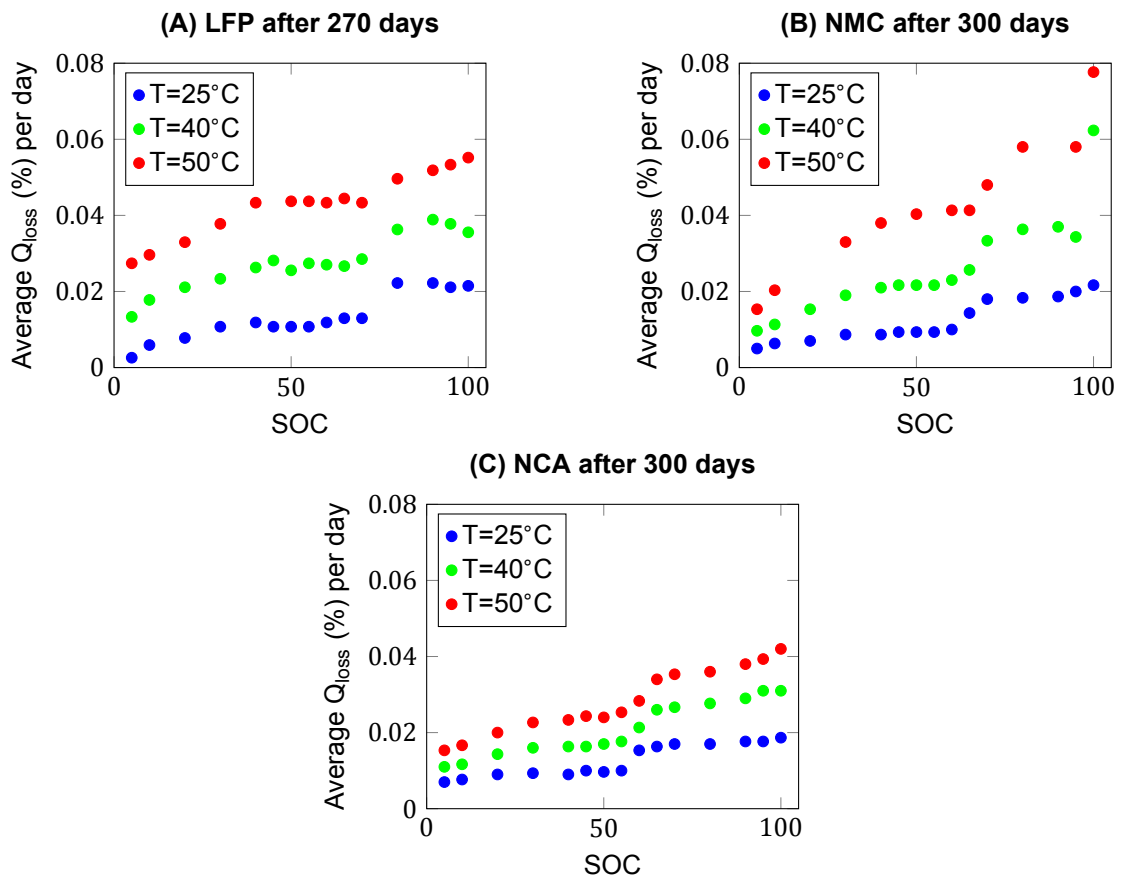


Figure 3.9: Effect of SOC on calendar aging

3.4.3. Storage time

Most of the data sets show a similar trend of a high average capacity loss per day for the first 100 to 200 days. After this initial period the data shows a more stable behaviour of the aging rate. Especially at higher temperatures and higher SOC levels this effect is very large, but also at lower temperatures and SOC levels this is the situation in most cases. The data sets of specific batteries at one temperature and one SOC level are compared to analyze this effect. Finding a general effect for the storage time is complicated, because of the wide variety in aging rates between different data sets. The behaviour of the aging rate can be represented by a power function with a negative power between 0 and -1. The general observation is that at lower temperatures and lower SOC levels the power is closer to 0. However, because all the measurements in the different data sets are performed at different time intervals, the information is incomplete. Especially the information on the aging rate in the first 100 days of storage is limited. This first period is very important for determining the actual power rate describing the behaviour of the aging rate; therefore, only the datasets with measurements that start before day 50 of storage are used to evaluate the effect of the storage time on the aging rate. The evaluated datasets are shown in figure D.17.

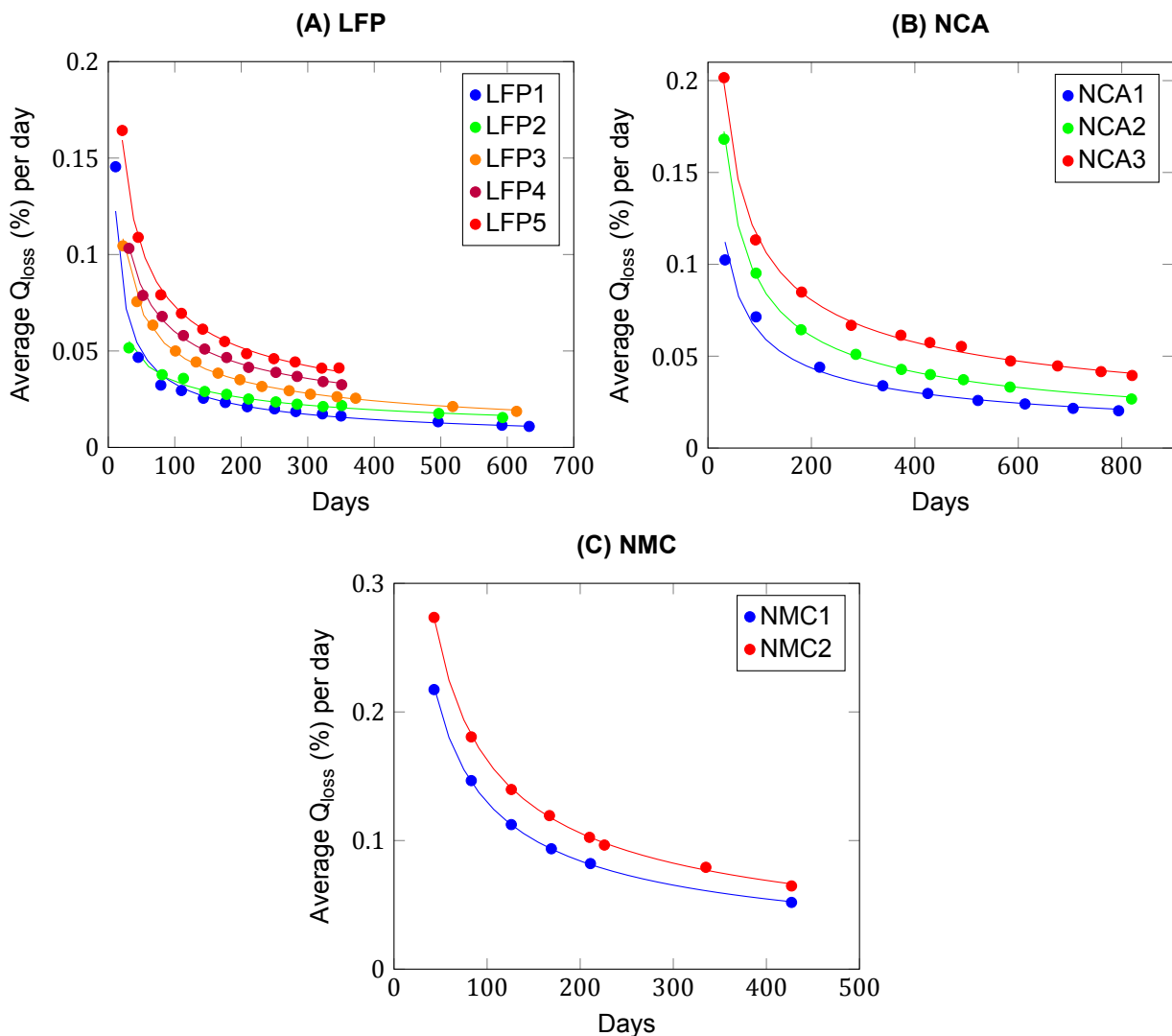


Figure 3.10: Effect of storage time on calendar aging rate

The measurements from the used datasets have been fitted with a power function by the least squares method. Table 3.3 shows the resulting fitted power functions per dataset. The data shows that the relationship between storage time and aging rate can be described by a power function. The power factors are varying between -0.4 and -0.6 for these datasets. There is not enough data to draw useful conclusions on the effects on different temperatures or SOC levels on the power factors or to construct a general rule for the effect of storage time on aging rate. However, as stated in chapter 3, and according to Ploehn (2004)[48], the thickness of the SEI layer increases linearly with the square root of time. This can be an important factor determining the relationship between time and calendar aging and would suggest a value of -0.5 for the power factor.

Table 3.3: Overview of fitting power functions per data set from figure D.17

Overview of datasets and power functions from figure D.17				
Dataset	Research	Temperature	State of charge	Power function
LFP1	Sarasketa et al.[68]	30°C	70%	$0.5102 * x^{-0.595}$
LFP2	Sarasketa et al.[68]	40°C	30%	$0.2219 * x^{-0.406}$
LFP3	Sarasketa et al.[68]	40°C	70%	$0.5351 * x^{-0.517}$
LFP4	Sarasketa et al.[68]	40°C	90%	$0.5248 * x^{-0.471}$
LFP5	Sarasketa et al.[68]	50°C	70%	$0.728 * x^{-0.499}$
NCA1	SIMCAL[15]	60°C	30%	$0.703 * x^{-0.525}$
NCA2	SIMCAL[15]	60°C	65%	$1.1714 * x^{-0.558}$
NCA3	SIMCAL[15]	60°C	100%	$1.0463 * x^{-0.484}$
NMC1	Ecker et al.[17]	65°C	50%	$2.2951 * x^{-0.624}$
NMC2	Ecker et al.[17]	65°C	50%	$2.7819 * x^{-0.617}$

3.4.4. Conclusions calendar aging

The following conclusions on calendar are drawn from the evaluated data. The temperature has the highest effect on the aging rate of the battery. The SOC level also has an effect, but this is less strong. It is shown that the aging rate increases with the temperature; therefore, lower temperatures are preferred for a long life expectancy of the battery. There is not much data available for temperatures below 25°C. What is known from other literature [12] is that temperatures below 20°C are good for storing the battery for a long period, but when being cycled, more stresses are induced because of the increased internal resistance, increasing the aging rate. Also the data from the storage tests show that a low SOC level helps keeping the aging rate low. This is particularly the case for when the battery is in storage and not when it is being cycled, just as with the temperature. It is recommended to operate the battery within the so called sweet spot between 20% and 70% SOC. These values can vary per chemistry type and battery design.

There is not enough information from similar calendar aging test on different chemistry types with equal construction and design of the battery itself. The construction and design of the battery has a large influence on the aging behaviour; therefore, it is not possible to draw any conclusions on the effect of battery chemistry on the aging rate based on the available studies. The effect of storage time on the aging rate is clearly visible as it can be fitted with a power function with a power rate related to the square root of time.

3.5. Cycle aging

Cycle aging is dependent on the depth of discharge (DOD), average SOC and the charging and discharging C-rates. It is calculated over the total Ampere-hours that went through the battery, the Ah throughput. The Ah throughput is comparable to the storage time effect for calendar aging because it indicates a certain age of the battery. Cycle aging is tested by cycling the battery repeatedly at a specific DOD and C-rate. The remaining capacity of the battery is measured after a number of cycles to calculate the aging rate. Data from 12 different studies is evaluated to analyze the effects of DOD, average SOC and C-rate on the cycle aging rate, see table 3.2. Tests are performed on 6 LFP batteries, 3 NMC batteries, 2 NCA batteries and 1 LCO battery. The Ah throughput is expressed as the number of performed full equivalent cycles.

3.5.1. Depth of discharge

Figure D.19 shows the collected data on cycle aging for a LCO (A), LFP (B), NMC (C) and NCA (D) battery cell. All tests are performed at an average SOC level of 50%, fixed C-rates and fixed temperature; except for (D), where two different temperatures have been used. The LFP cell is the least affected by aging of the 4 tested batteries. All sets of tests are analyzed in this section on the aging behaviour caused by the depth of discharge (DOD) of the performed cycles.

Figure D.19 (A) shows the data from tests on LCO cells at 50% average SOC, 0.5C and a temperature of 25°C.[54] The cycles that are performed are at a DOD of 20%, 60% and 100%. The data shows that at a DOD of 20% the aging rate is the lowest. For the first 500 cycles the cells cycled at 100% DOD show the least decrease in capacity, but after 500 cycles the aging rate increases significantly. At a DOD of 60% the aging rate remains stable after 500 cycles. In theory it is expected that at 60% DOD the aging rate would be lower than at a DOD of 100%, but this test might suggest the opposite. When comparing the aging rates of the different cells that are cycled at 20%, the results show a difference in total lost capacity of 2.08% after 350 cycles. The difference between the capacity loss of the cell with the highest aging rate at a DOD of 20% and the cell cycled at 60% is 0.7% after 350 cycles. For the cell cycled at 100% DOD this is only 0.35%. So the variation between the cells cycled at the same conditions is larger than between the cells cycled at different conditions. This difference in aging rates between the same type of cell cycled at the same conditions can be explained by small differences in the cell's construction that have occurred during the manufacturing process. It also means that for this case the difference in aging rate for cells cycled at a different DOD, might also be caused by the differences in the cell's construction and is independent of the DOD. The only plausible conclusion of this test is at a DOD of 100%, the probability of the aging rate to increase after 500 cycles is much higher than at lower DOD levels.

Figure D.19 (B) shows the data from tests on LFP cells at 50% average SOC, 1C and a temperature of 30°C.[52] The cycles are performed at a DOD of 5%, 10%, 30%, 50%, 60% and 100%. The data from these tests shows some remarkable aging behaviour. Cycling at a DOD of 5% is definitely preferable for a long cycle life. Then cycling at a DOD of 100% results in low aging rates for the first 5000 cycles, but at that point the aging rate starts increasing. The battery that is cycled at 100% DOD reaches the SOH of 80% first. However, the batteries that are cycled at 30% and 50% are not cycled enough to reach the 80% SOH point during these tests. These batteries do have the highest aging rates for the first 3000 to 4000 cycles, but because the tests did not continue long enough it is unknown how the aging rate develops with more performed cycles. The second battery to reach the 80% SOH point is cycled at 10% DOD. The battery cycled at 60% DOD is not tested long enough to reach this point, but shows relatively low aging rates for the first 6000 cycles. Extended tests should be performed to analyze the behaviour for a larger number of performed cycles at 5, 10, 30, 50 and 60% DOD to make a valid conclusion on the effect of DOD on this battery.

Figure D.19 (C) shows the data from tests on NMC cells at 50% average SOC, 1C and a temperature of 35°C.[18] The cycles are performed at a DOD of 5%, 10%, 20%, 50%, 80% and 100%. For this battery it is clear that a lower DOD results in a lower aging rate. At a DOD of 5%, 10% and 20% the aging rate follows a stable curve and the SOH of 80% is not reached within the performed tests. At 50% DOD the aging rate is significantly increased and 80% SOH is reached after a little more than 1000 cycles. The aging rates at 80% and 100% DOD do not show any stable behaviour and are very high.

Figure D.19 (D) shows the data from tests on NCA cells at 50% average SOC, 1C and at two different temperatures of 25°C and 60°C.[67] The batteries were cycled at both temperatures at a DOD of 60% and 100%. The most interesting observation from these tests is that at a DOD of 60% the effect of an increased temperature is much smaller than at a DOD of 100%. The combination of a high temperature and high DOD is amplifying the aging rate.

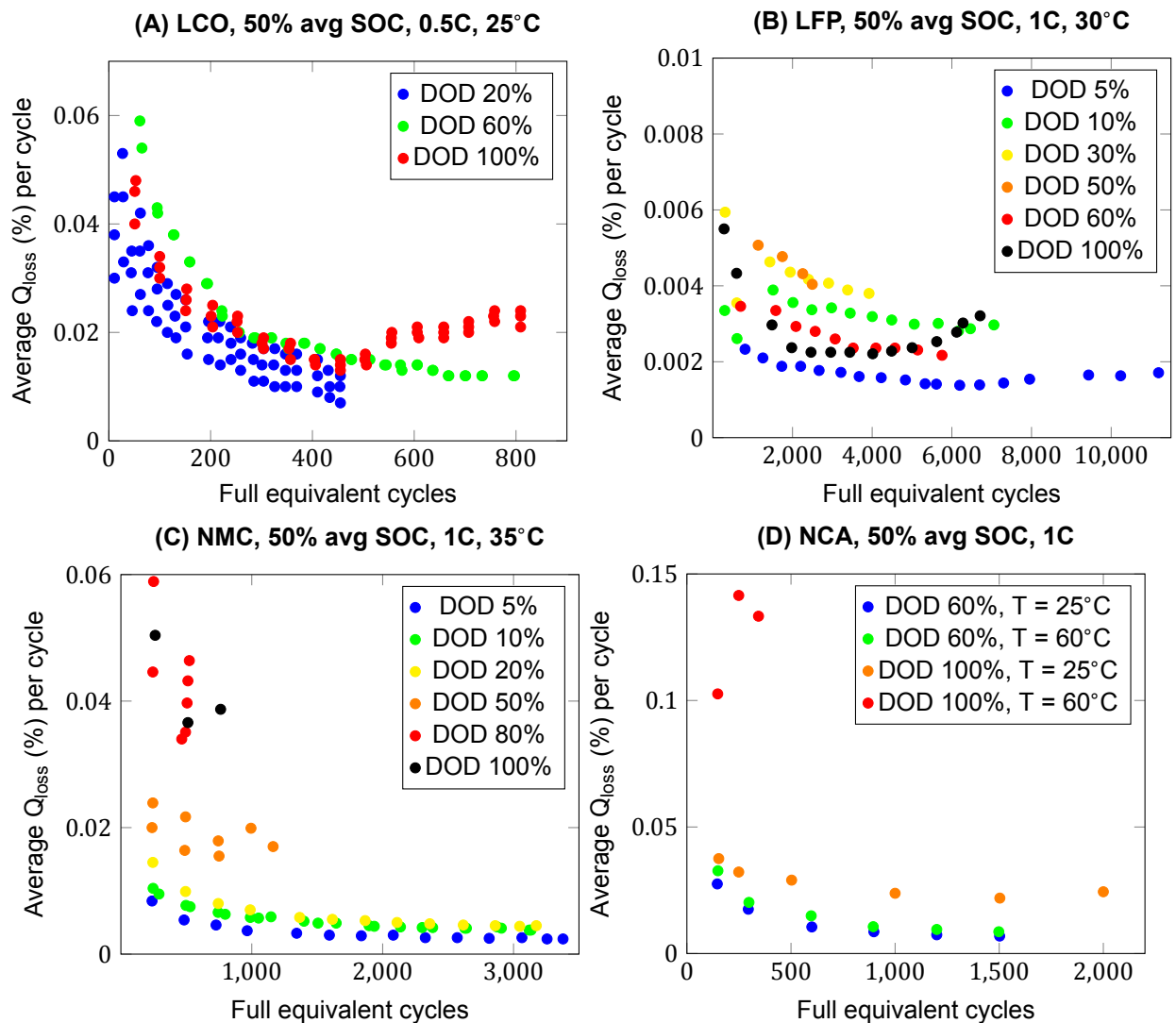


Figure 3.11: Effect of depth of discharge (DOD) on cycle aging

3.5.2. C-rate

Figure 3.12 shows the data from cycling tests performed on LCO cells at an average SOC of 50%, temperature of 25°C, at a DOD of 20%, 60% and 100%, and at C-rates of 0.5C and 2C.[54] The results from these tests show two effects of an increased C-rate. First of all, increasing the C-rate has a higher effect on the aging rate at a higher DOD. The aging rate generally increases when the C-rate increases. At the tests at 100% DOD, it is remarkable that the development of the aging rate does not show the same behaviour after 500 cycles for a C-rate of 2C as it does for a C-rate of 0.5C. Unfortunately, there is not much complete data on the effect of the C-rate on the aging rate of the battery. However, the data shown here, and theory, suggests that an increased C-rate increases the aging rate.

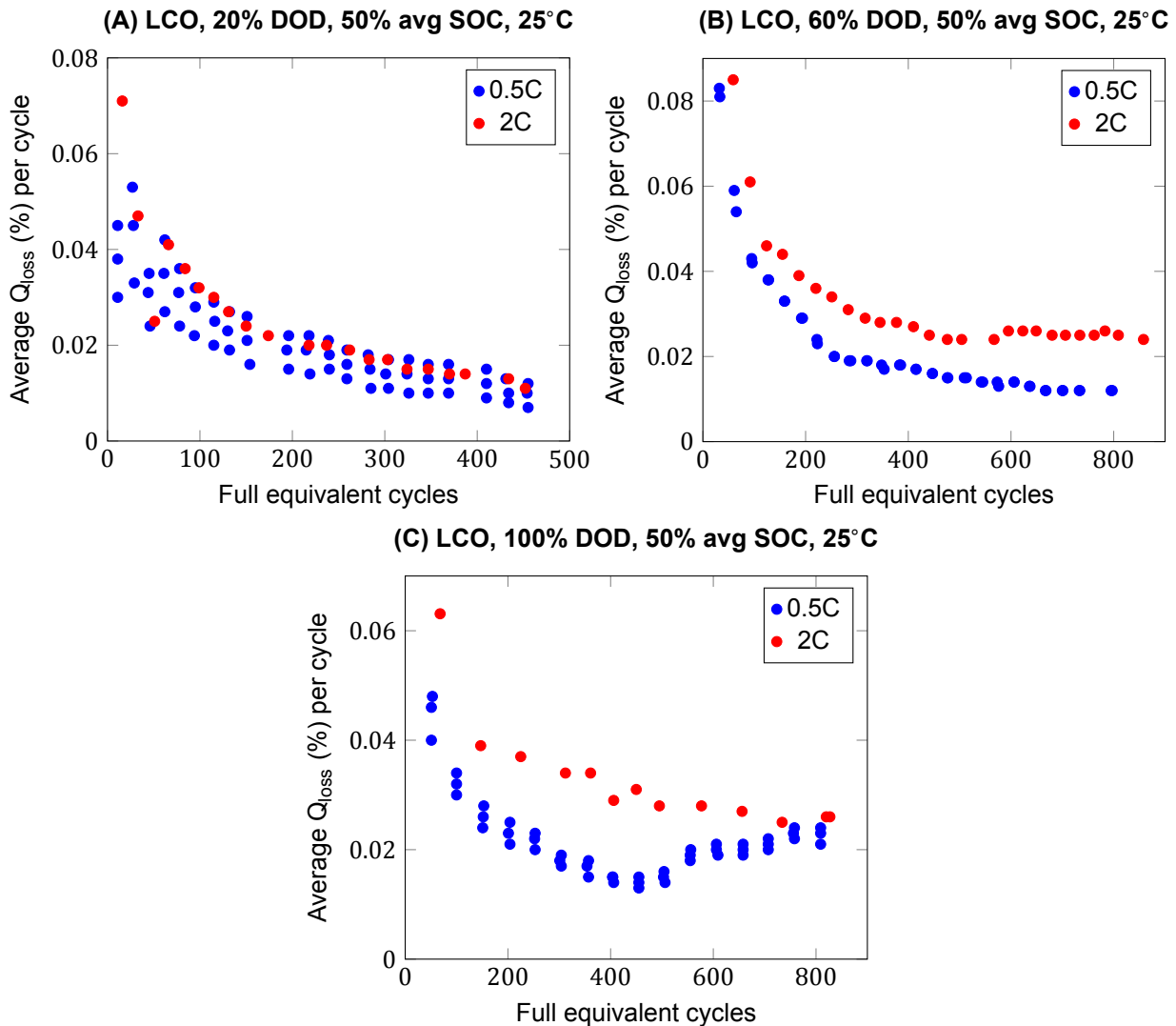


Figure 3.12: Effect of C-rate on cycle aging rate for LCO

3.5.3. Average SOC

For calendar aging it shows that the SOC level of a battery during storage has an impact on the aging rate. Therefore, the effect of average SOC levels for cycle aging is interesting to investigate as well. Figure 3.13 shows the data from tests on LCO cells at 60% DOD, 0.5C, 25°C and average SOC levels of 30%, 50% and 70%. An average SOC level of 70% shows the highest aging rates. A 50% average SOC level shows similar results, but at a slightly lower aging rate. The biggest difference is at 30% average SOC level. After 600 cycles, the cells cycled at an average SOC level of 30% show a total loss of capacity of 2.4%. At 50% average SOC this is 8.4% capacity loss and at 70% average SOC this is 9.6% capacity loss. Based on this data and for these types of batteries it clearly shows that a lower average SOC level causes less aging.

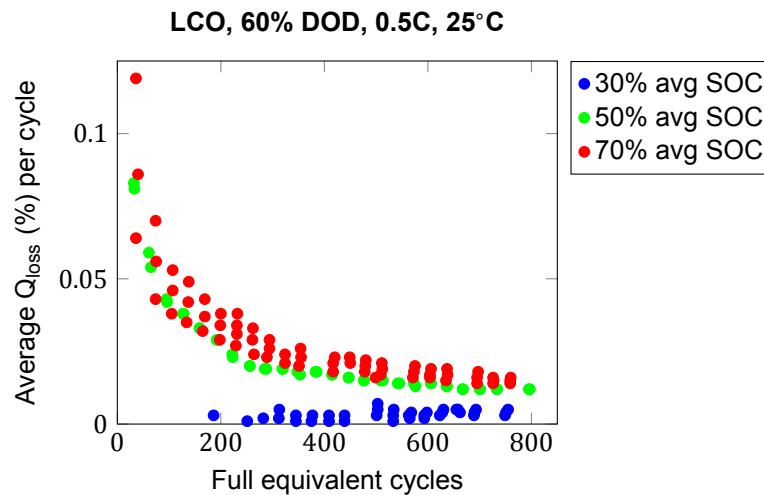


Figure 3.13: Effect of average SOC on cycle aging LCO

Figure 3.14 shows the data from cycle tests on NMC cells at 10% DOD, 1C and 35°C at six different average SOC levels.[18] This data set shows the expected behaviour for cycle aging based on the theory very clearly. Here, an average SOC of 50% provides for the lowest aging rates, followed by 25% and 75% average SOC. The average SOC levels of 10%, 90% and 95% result in the highest aging rates. This agrees with the theory that cycling a battery in the upper or lower SOC ranges cause the capacity to fade at a higher rate because of the induced stresses on the cell in these conditions.

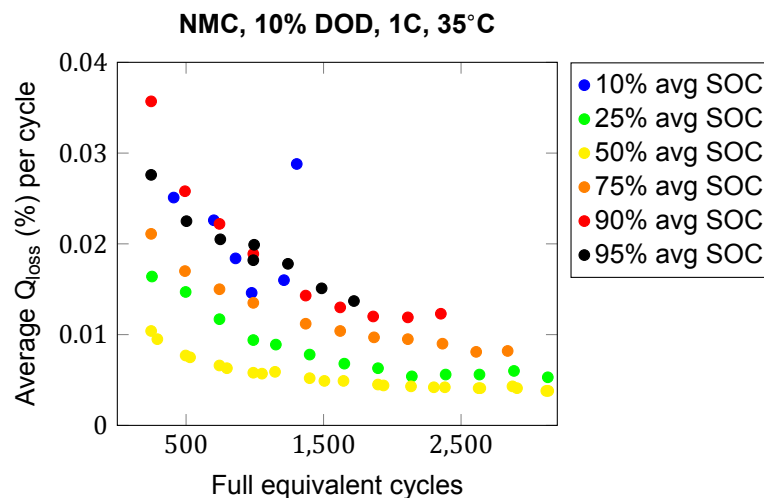


Figure 3.14: Effect of average SOC on cycle aging NMC

3.5.4. Conclusions cycle aging

The analyzed tests on cycle aging of batteries focus on very different aspects of cycle aging; therefore, not much data is available to compare between different battery types and cycle conditions. For a more substantiated conclusion on cycle aging, more tests have to be performed at similar conditions on different battery cells. However, there are some conclusions that can be drawn from the available test data.

The first conclusion is that cycle aging tests have to be performed on a specific battery cell before anything can be said about the aging of that type of battery cell. The large variations in aging behaviour of different battery types, make it very complex to draw conclusions on battery aging for multiple battery types in general. Also, batteries have to be tested for longer periods than in the performed studies to make an accurate prediction on what will happen at the end of life of the battery. As observed by Saxena et al.[54], the average SOC levels play an important role in determining the aging rate at first. After a specific period of time or amount of cycles, the DOD becomes a leading factor for the aging rate. This might indicate that for standard operational use of batteries, calendar aging is the limiting factor and not cycle aging. Also, in most tests the results are not as expected, based on the theory of battery aging. This can be explained by the variation in aging behaviour between similar cells that are tested at the same conditions. These variations are caused by differences in the cell's construction that occur during the manufacturing process.

4

Proposed aging model

The gained knowledge from the theory on battery aging, results from aging tests and evaluated aging models in chapter 3 is used to develop a model to predict battery aging in full electric ships. This model is referred to as the proposed model and its development is discussed in this chapter.

4.1. Approach

Simulink[®] is chosen to build the model in. This section describes the goals which are set for the model and the method that is used to come to the final result.

4.1.1. Goals

After studying the theory of battery aging and the results of aging tests, it is assumed there are 7 different parameters that should be included in the model. These 7 parameters are the temperature, state of charge, depth of discharge, charge C-rate, discharge C-rate, time and number of performed cycles. Using all these causes is important for making an accurate aging model. Table 4.1 shows which causes are included for each of the analyzed models. None of the studied models used all causes, more information per model is given in appendix C. Therefore the goal is to develop the proposed model including all these 7 causes.

Table 4.1: Aging parameters included in different models

Aging factors per model							
Model	Temp.	SOC	DOD	C-rate (C)	C-rate (D)	Time	Cycles
Li	✓	✗	✓	✓	✓	✗	✗
Omar	✓	✗	✓	✓	✓	✗	✗
Saxena	✗	✓	✓	✗	✗	✗	✓
Schmalstieg	✓	✓	✓	✗	✗	✓	✓
Ecker	✓	✓	✓	✗	✗	✓	✗
Magnor	✓	✓	✓	✗	✗	✓	✓
Sarasketa	✓	✓	✓	✗	✗	✓	✓
Wang	✓	✓	✗	✗	✗	✓	✓
Proposed model	✓	✓	✓	✓	✓	✓	✓

The aging behaviour is very dependent on the battery type as the results from the analysis of the battery aging tests show. The differences in aging behaviour require a model that is very versatile and can be adjusted to any kind of lithium-ion battery by just a view parameters. Even with the large differences in aging per battery, the model is required to give an acceptable

general prediction to analyze the effects of operational profiles of full electric ships on battery life. Most of the evaluated models have combined equations for multiple forms of aging. Each cause is treated separately for the proposed model so that it can be adjusted if more information becomes available on the effects of a specific aging cause.

4.1.2. Method

The development of the proposed model follows 4 steps:

1. Equations are developed to describe the effects of temperature, SOC, DOD and C-rates on the percentage of capacity lost per day.
2. The equations are combined with a thermal model and integrated into a Simulink® model.
3. The proposed model is validated for its versatility to different battery types and it is compared to other models to show the difference in accuracy.
4. It is verified if the proposed model is applicable as a general prediction method for battery aging in full electric ships.

4.2. Aging calculations

The temperature and SOC both affect calendar aging. For both causes an equation is developed based mainly on the results of the analysis of battery aging tests in chapter 3, combined with assumptions based on the theory on battery aging. The DOD and C-rates affect cycle aging. The effect of the DOD is determined by a Woehler curve, which is explained in section 4.2.3. The effect of the C-rate is calculated by an amplification factor to the DOD effect, based on the results of the analysis of battery aging tests.

4.2.1. Temperature

The majority of the aging tests that are analyzed in chapter 3 are performed at temperatures above 20°C, which is assumed to be the optimal temperature for batteries. The measurements show an exponential increase of the aging rate with the increase in temperature. In equation 4.1, the β describes this exponential behaviour and the α is used to set the aging rate at 20°C. ΔT is the difference between the actual temperature of the battery cell and the optimal temperature of 20°C. Equation 4.1 is fitted to the measurement data of each individual research to find the average values for parameter β . The aging rate shows an average increase by a factor of 1.061 per degree rise in temperature. For LFP batteries this average is 1.071, for NMC it is 1.052 and for NCA 1.057.

$$Q_T = \alpha \cdot \beta^{\Delta T} \quad (\%/day) \quad (4.1)$$

For a temperature below 20°C there is not enough measurement data available. Therefore, several assumptions are made based on the studied literature and other aging models. It is assumed that there is a difference between the effect of temperature on aging rate when the battery is in operation or not. When the battery is cycled at temperatures below 20°C it is assumed that because of the increased internal resistance the aging rate increases as well. Therefore, at these temperatures the aging rate will increase with the same exponential relation as equation 4.1. However, when the battery is not cycled it is assumed that temperatures below 20°C improve the life expectancy of the battery. Therefore the aging rate is

assumed to follow the same decline as equation 4.1 towards a temperature of 0°C. Temperatures below 0°C are not taken into account in this research because it is unlikely to reach this low temperatures inside a battery space of a ship.

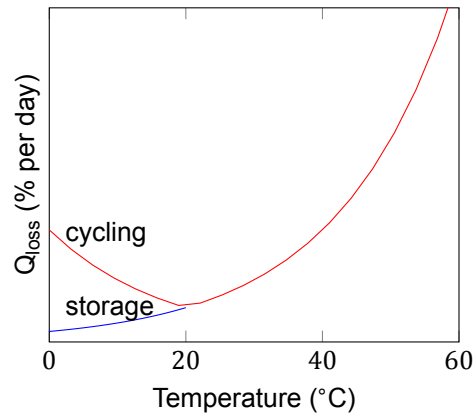


Figure 4.1: Effect of temperature on aging rate

4.2.2. SOC

For the effect of the state of charge on the aging rate is referred to the data shown in figure 3.9. The measurements at 25°C for each battery type is shown in figure 4.2. The data can be divided in two parts with an aging rate increasing linearly with the SOC. At a SOC below 65% the slope is determined by $\kappa_1 = 0.002$. Above 65% SOC it is determined by $\kappa_2 = 0.003$. The border of these parts differs for each type of battery, but the average is taken at 65% SOC. A reference (SOC_0) is required to calculate the increase or decrease in aging rate compared to the measurements at that reference SOC. Equations 4.2 and 4.3 calculate the effect of the SOC on the aging rate.

$$Q_{SOC,low} = (SOC - SOC_0) \cdot \kappa_1 \quad (\%/day) \quad SOC < 65\% \quad \kappa_1 = 0.002 \quad (4.2)$$

$$Q_{SOC,high} = (SOC - SOC_0) \cdot \kappa_2 \quad (\%/day) \quad SOC > 65\% \quad \kappa_2 = 0.003 \quad (4.3)$$

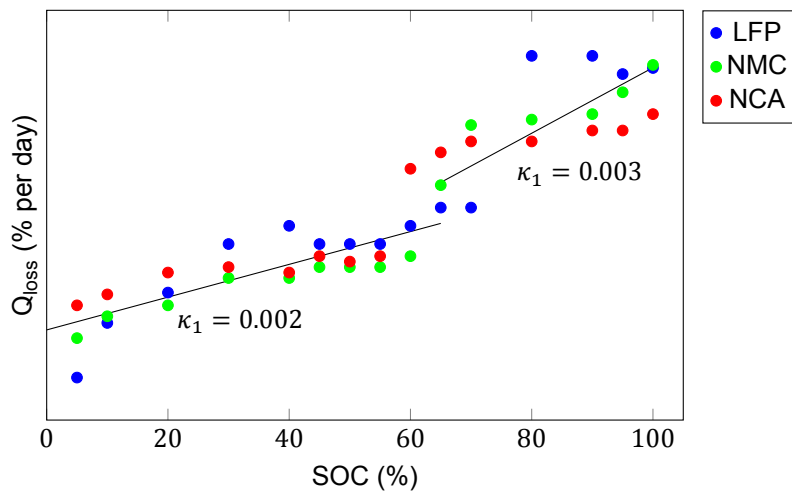


Figure 4.2: Effect of the state of charge on aging rate

A multiple order polynomial is expected to result in a higher accuracy for the effect of the SOC on the aging rate. However, there is only a limited amount of test data available for the analysis of this effect, which might result in the wrong assumptions. Because the effect of SOC on aging is less than the effect of temperature, it is assumed that the linear approach is sufficient until more research is performed on the effect of SOC.

4.2.3. DOD

In section 4.2.3 it is determined that it is too complex, if not impossible, to develop a general equation for the effect of the depth of discharge on the aging rate. The differences between battery types are too big to combine in a simple equation. Information on the aging of batteries, depending on the DOD, is usually known by the manufacturer. This information is often available in the form of a Woehler curve. A Woehler curve gives the number of full equivalent cycles a battery can make at a specific DOD until reaching the end of life capacity. Figure 4.3 is the Woehler curve of the NMC battery used for analysis in section 4.2.3. This data is based on measurements at a mean SOC of 50%, C-rate of 1C and a temperature of 35°C. The end of life capacity is determined at 80% of the initial capacity. With this knowledge it is possible to calculate the aging rate per cycle at each DOD. The Woehler curve can often be closely described by a power function, but this is not always correct. Therefore, it is assumed that a larger accuracy is provided by a linear iteration between measured points in the Woehler curve.

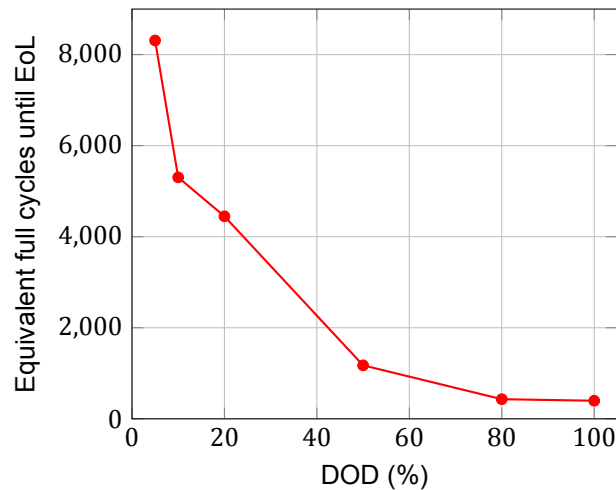


Figure 4.3: Woehler curve of aging data for NMC battery from figure D.19 (C)

Realistic operational profiles have different consecutive DOD ranges. This complicates the calculation of aging per cycle. Therefore, the cycles are divided in a discharging and a charging part, resulting in a depth of discharge (DOD) and depth of charge (DOC). The Woehler curve is used to determine the aging rate ($Q_{W,DOD}$) for a full cycle at a specific DOD. Equation 4.4 then calculates percentage of capacity that is lost for just a discharge or charge. This has as a result that the model has to perform a calculation of the aging with every single charge and discharge.

$$Q_{DOD} = Q_{DOC} = \frac{Q_{W,DOD}}{2} \quad (\%/half\ cycle) \quad (4.4)$$

4.2.4. C-rates

The amount of available test data for the effect of C-rates on the cycle aging rate was only sufficient to make an assumption combined with the theory from literature and other aging models. The relation between the C-rates and the aging rate is assumed to follow a quadratic curve. Equations 4.5 and 4.6 calculate the effect of respectively the discharge rate and charge rate on the aging rate. They are fitted to a Woehler curve from measurements at 1C when $\gamma_1 = 0.08$, $\gamma_2 = 0.0064$, $\gamma_3 = 0.15$ and $\gamma_4 = 0.0225$. $Q_{I,d}$ and $Q_{I,c}$ are dimensionless amplification factors influencing the cycle aging rate which follows from the DOD.

$$Q_{I,d} = 1 + (\gamma_1 \cdot C, rate)^2 - \gamma_2 \quad (4.5)$$

$$Q_{I,c} = 1 + (\gamma_3 \cdot C, rate)^2 - \gamma_4 \quad (4.6)$$

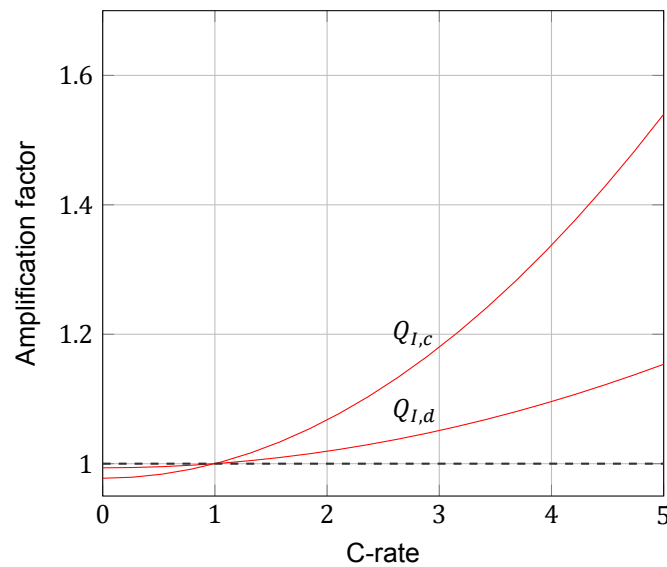


Figure 4.4: Effect of C-rate on cycle aging rate

4.3. Integrated model

A complete overview of the Simulink[®] model is available in appendix D. This section provides an overview of the main calculation steps, calendar aging, cycle aging, thermal model, parameters and time step size.

4.3.1. Overview

A complete description of the Simulink model is available in appendix D. Figure 4.5 shows the main calculation steps that are performed by the model. The input is an operational profile, with the power demand at every minute. The power profile consist of the propulsive power, auxiliary power, cooling power and charging power. From the power demand in kW, every minute the charged or discharged energy is calculated in kWh. The energy use and the total installed capacity are used to calculate the SOC of the battery. The SOC is used for the calculation of calendar aging, heat generation and to determine the change in SOC (d_SOC). The change in SOC is used to calculate the calculation of the generated heat, performed FEC, cycle aging and calendar aging. Before calculating the cycle aging, it is also determined if

the battery is charging or discharging. After every half cycle the DOD is calculated. The temperature of the battery is calculated by a heat generation part, a heat transfer part and the thermal management system. The cell temperature is used to calculate the calendar aging. The calendar and cycle aging are used for the calculation of the SOH of the battery. When the SOH reaches a value of 80%, the battery has reached the EOL and the simulation is stopped.

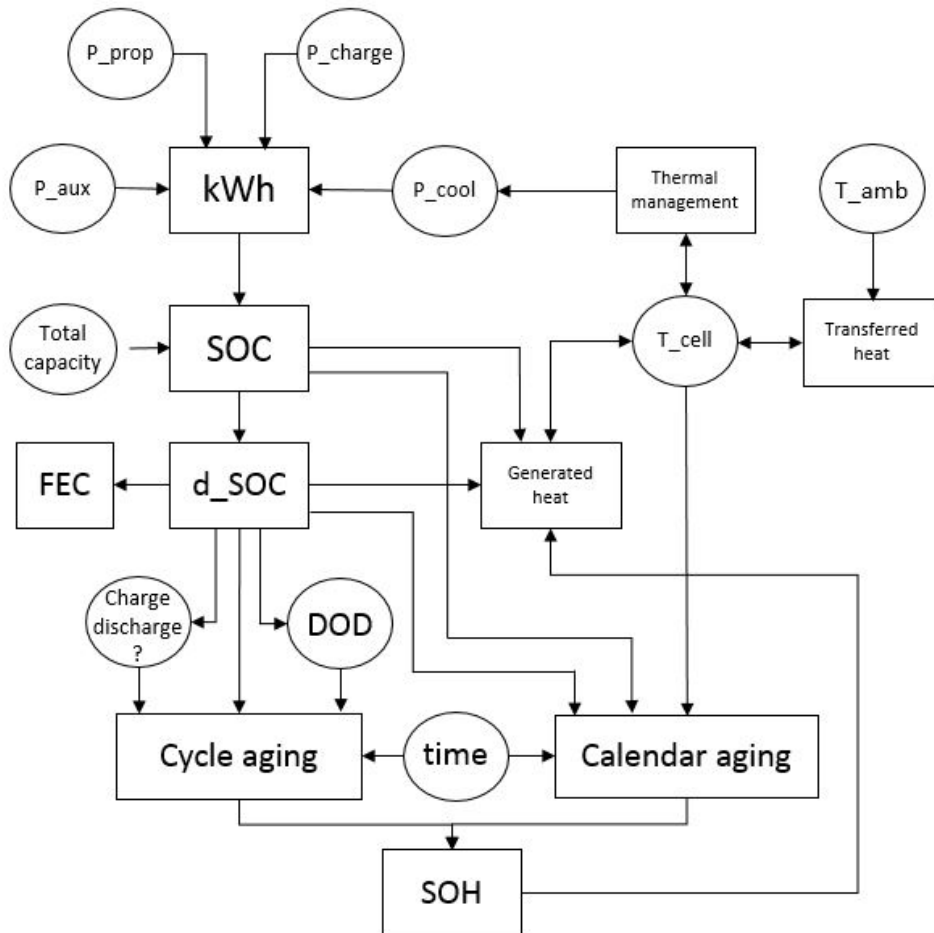


Figure 4.5: Schematic representation of calculation steps in Simulink

Before running a simulation in the model there are 3 steps that are taken. Determining the parameters, the auxiliary power demand and the main power demand. Four parameters have to be determined first: the capacity is determined in kWh, the SOC at which the battery starts with the simulation in percentage, the minimum and maximum SOC to determine the strategy for charging and discharging limits and the EOL, the SOC at which the simulation is stopped. The auxiliary power and the main power are determined by a repeated sequence. This sequence is a row of numbers representing the power demand in kW for one minute, positive for discharging and negative for charging. For the simulations in this study a sequence of 1440 numbers is used to represent the power profile for a day for both the auxiliary power and the main power demand.

4.3.2. Calendar aging

The calendar aging rate is determined by the temperature, SOC and time. Combining equations 4.1, 4.2 and 4.3 leads to equation 4.8 for a SOC below 65% and equation 4.9 above 65% SOC. Q_T is the aging rate depending at temperature at reference SOC₀ and Q_{SOC} is the aging rate depending at SOC at reference temperature T_0 . Therefore, Q_T and Q_{SOC} can be added up to calculate the total calendar aging rate.

$$Q_{cal} = (Q_T + Q_{SOC}) \cdot t^{-0.5} \quad (\%/day) \quad (4.7)$$

$$Q_{cal} = (\alpha \cdot \beta^{\Delta T} + \kappa_1 \cdot (SOC - SOC_0)) \cdot t^{-0.5} \quad (\%/day) \quad (SOC < 65\%) \quad (4.8)$$

$$Q_{cal} = (\alpha \cdot \beta^{\Delta T} + \kappa_2 \cdot (SOC - SOC_0)) \cdot t^{-0.5} \quad (\%/day) \quad (SOC \geq 65\%) \quad (4.9)$$

As observed in section 3.4.3, [17] and [51], the calendar aging rate is related to the square root of time. Therefore the summation of Q_T and Q_{SOC} is multiplied with $t^{-0.5}$, with t in days. This result in a calendar aging rate that decreases every day. This is assumed to be correct for the largest part of the life of the battery. However, at the end of life of the battery the aging rate is most likely to increase. This phenomenon is not taken into account in the proposed model because of a lack of data from aging tests including the end of life of the battery.

4.3.3. Cycle aging

The cycle aging rate is based on equations 4.4, 4.5 and 4.6. The cycle aging is different for discharging and charging and therefore these are separated. The Simulink model registers if a charge or discharge is being performed, how deep the cycle is and the time that is required to perform the cycle to calculate the C-rate. The percentage of capacity that is lost because of cycle aging is calculated by equation 4.10 for discharging and 4.11 for charging.

$$Q_{cyc,discharge} = Q_{DOD} \cdot Q_{I,d} = \frac{Q_W}{2} \cdot (1 + (\gamma_1 \cdot C,rate)^2 - \gamma_2) \quad (\%/halfcycle) \quad (4.10)$$

$$Q_{cyc,charge} = Q_{DOC} \cdot Q_{I,c} = \frac{Q_W}{2} \cdot (1 + (\gamma_3 \cdot C,rate)^2 - \gamma_4) \quad (\%/halfcycle) \quad (4.11)$$

As discussed in section 3.5.3 the mean SOC during cycling also influences the aging rate. This is partly caused by the calendar aging effect of the SOC, but close to the higher and lower SOC limits of the battery the cycle aging effect is increased as well. Therefore, the cycle aging rate is multiplied by a factor dependent on the SOC, when it reaches values below 20% or above 80%. This factor is based on the measurements from figure 3.14. This is the only available data for this aging effect, more aging test are required to improve the estimation of the effect of mean SOC on cycle aging.

4.3.4. Thermal model

The thermal part of the proposed model consists of three parts. The heat transfer between the battery cell and the ambient air, the heat generated by the battery and the heat transfer between the battery cell and the thermal management system, see figure 4.6. The transfer of heat between the battery cell, ambient air and thermal management system takes place according to the heat transfer coefficient of 0.03, which is based on the research by Brodsky (2016).[10] The powered required to heat or cool the battery is based on the power required

to change the temperature of a 50m^3 room by 1°C in 1 minute, which is 1 kW per degree Celsius per minute and is added to the total power demand on the battery.

The heat generation is based on a simplified model by Liu (2014)[37]. The C-rate determines the increase in temperature in degree Celsius per minute. This heat generation rate is then multiplied by factors according to the cell temperature, SOC and SOH, according to figure 4.6. Linear interpolation is required in case the temperature, SOC or SOH is at a state between two of the values shown in figure 4.6.

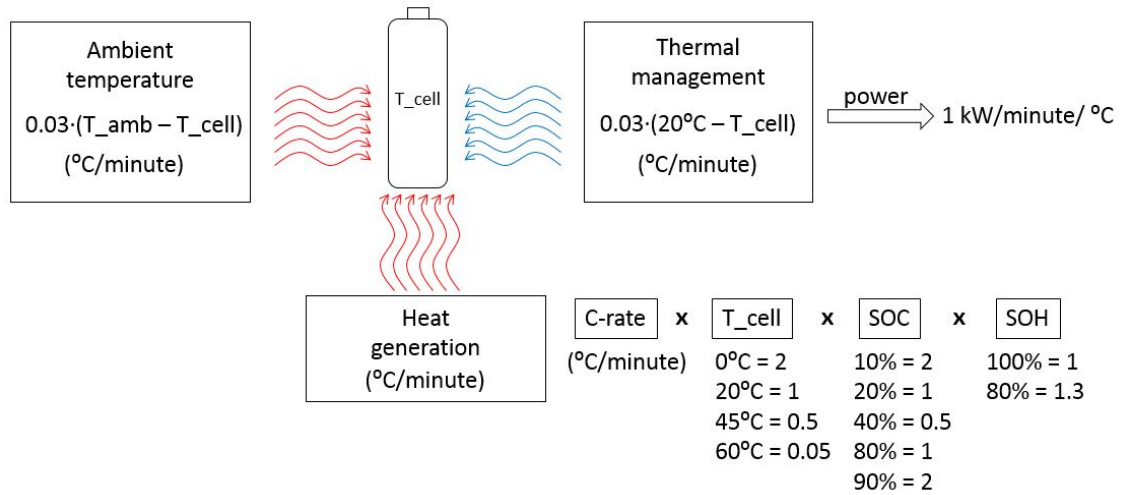


Figure 4.6: Schematic representation of thermal part in proposed aging model

4.3.5. Time step size

The optimal time step size for the model depends on the type of input and the required calculation speed. The input for the model is the power demand in kW over time. The time step has to be small enough to give an acceptable representation of the operational profile of a ship. A single trip for tugs or ferries can be done within an hour. Therefore a time step of one hour or bigger is too large. A time step of one minute is acceptable to roughly sketch the operational profile, but a more realistic profile would be with a time step of one second. The model is used to perform a simulation of 1 day of cycling and 100 days of cycling with time steps of 1 second and 1 minute. The simulated battery has a capacity of 1000 kWh and it is cycled by discharging it for 1 minute by 100 kW and then charging it for 1 minute also with 100 kW. Table 4.2 shows the results of the simulations. The simulation of 1 day of cycling is more than 22 times faster with a time step of 1 minute and the difference in SOH at the end of the simulation is only 0.0003%, which is an error of 0.18%. The simulation of 100 days of cycling is more than 57 times faster with a time step of 1 minute and the difference in SOH at the end of the simulation is only 0.23%, which is an error of 7.63%. This error is most likely caused by the fact that the thermal model is not adjusted for the time step of 1 second. Because the model will be used to model multiple years and not just days, the total simulation time will be very long and it is determined that a time step of one minute is used for the calculation in the aging model. This will allow for a larger amount of different simulations to analyze in the same amount of time with an acceptable accuracy.

Table 4.2: Simulation time and SOH for time step size of 1 second and 1 minute

1 simulated day			100 simulated days		
Time step	Simulation time	SOH	Time step	Simulation time	SOH
1 minute	3.01 seconds	99.8369%	1 minute	107.25 seconds	96.9637%
1 second	67.19 seconds	99.8372%	1 second	6190.05 seconds	96.7320%

4.4. Validation

The aging behaviour is very different per battery type, but also between two batteries of the same type there can be a large variation. The variations in battery aging tests are analyzed to determine the first goal for the accuracy of the proposed model. Then the model is validated for its versatility to different battery types. The last validation step is to compare the results from the proposed model with the results of existing models for the difference in accuracy.

4.4.1. Variation

Battery cells from the same type and same production batch show variation in aging when they are conducted to the same aging tests and procedures. Therefore, it is common to test multiple cells and use the average aging rate for further research. In [68] and [55] the average variations are given for a LFP battery (6%) and a NMC battery (4.7%). Figure 4.7 shows a 6% variation in aging for the same type of cell under similar conditions. The line represents the average aging of the battery until 80% SOH. The dashed lines mark the area of 6% variation. This variation results in a possible 1.2% absolute error at 80% SOH. For the validation of the proposed model it is assumed that an accuracy of 6% is the goal.

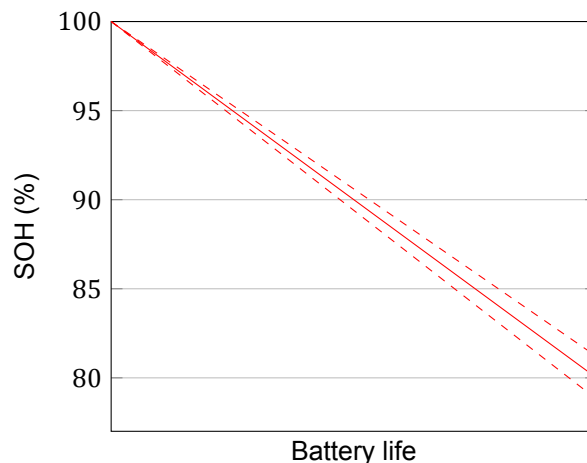


Figure 4.7: Average variation of 6% in aging for similar cell type under similar testing conditions

4.4.2. Versatility

The parameters α , β , κ_1 and κ_2 are fitted to the results of the aging tests of three different batteries. All three batteries are tested in the SIMCAL project[15]. Figure 4.8 shows the results of the tests on a 15 Ah LFP cell. Figure 4.9 shows the results of the tests on a 7 Ah NCA cell. Figure 4.10 shows the results of the tests on a 5.3 Ah NMC cell. By only adjusting the parameters the model can be fitted for the three different types of batteries.

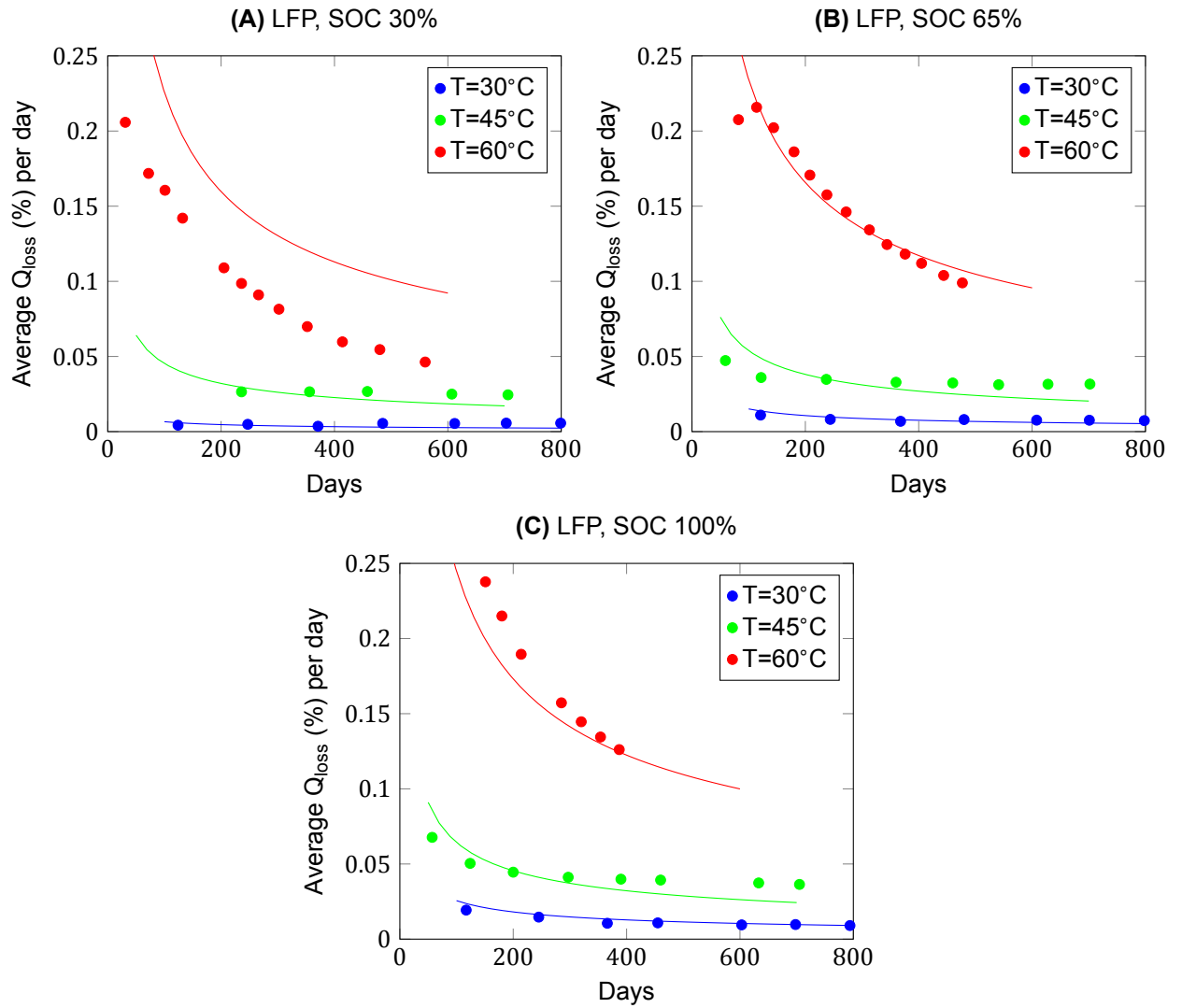


Figure 4.8: $\alpha = 0.038$, $\beta = 1.108$, $\kappa_1 = 0.002$, $\kappa_2 = 0.003$, LFP 15 Ah cell from SIMCAL aging tests [15]

For the 15 Ah LFP battery there is one condition at which the model is far of the measured aging rate. This is at a SOC of 30% and a temperature of 60°C , see figure 4.8(A). More test on the same battery are required to verify if this is correct. For now however, it is decided to not take this test condition into account to calculate the average prediction error. Without the data from 30% SOC and 60°C the model has a 4.15% average error in the prediction of the aging rate for this battery.

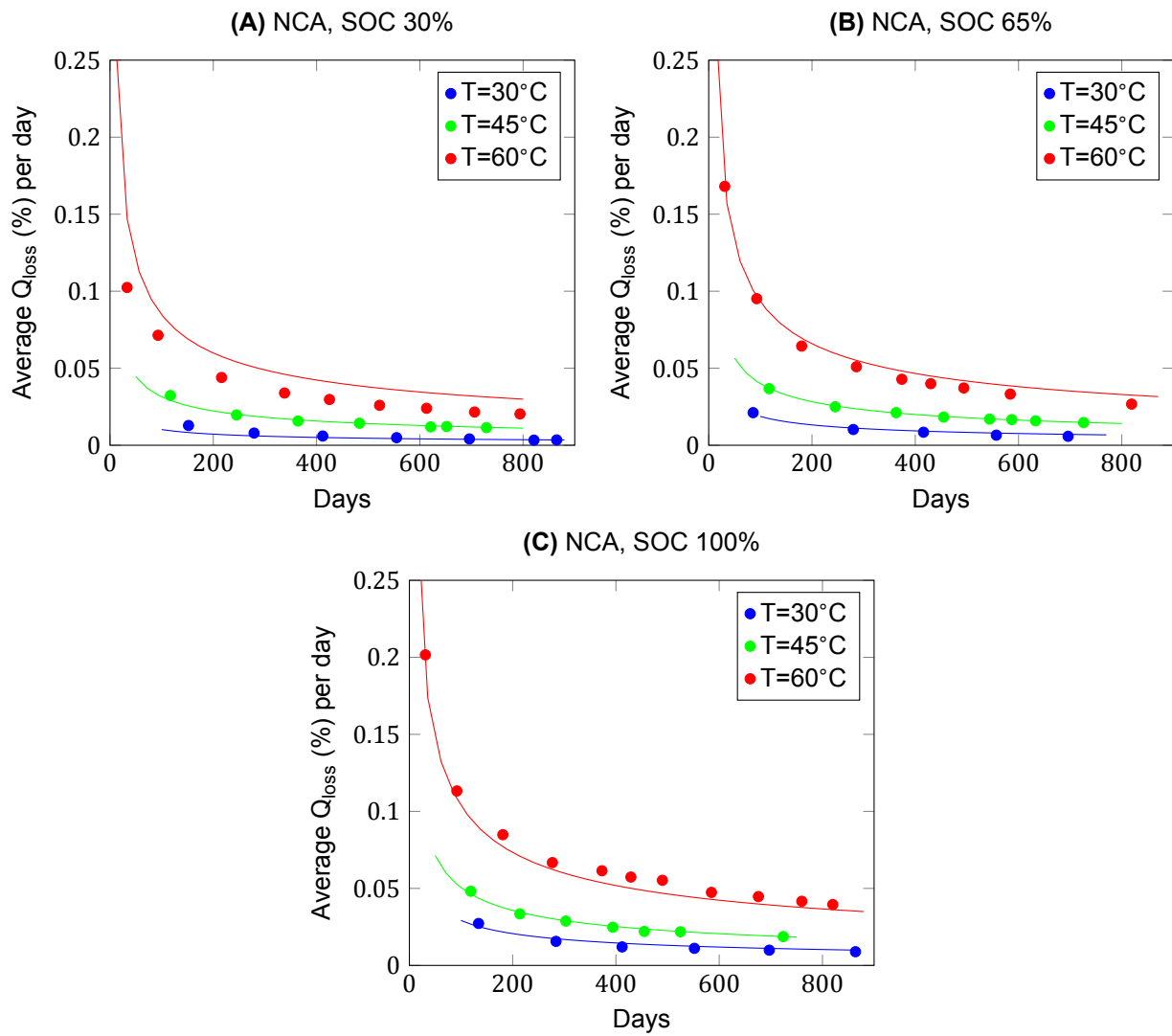


Figure 4.9: $\alpha = 0.077$, $\beta = 1.063$, $\kappa_1 = 0.002$, $\kappa_2 = 0.003$, NCA 7 Ah cell from SIMCAL aging tests [15]

The proposed model is overestimating the aging at a SOC of 30% and a temperature of 60°C for all three batteries. This might be caused by the linear equation that is used to describe the effect of SOC on the calendar aging rate. However, the model has a 4.92% average error in the prediction of the aging rate for the 7 Ah NCA battery.

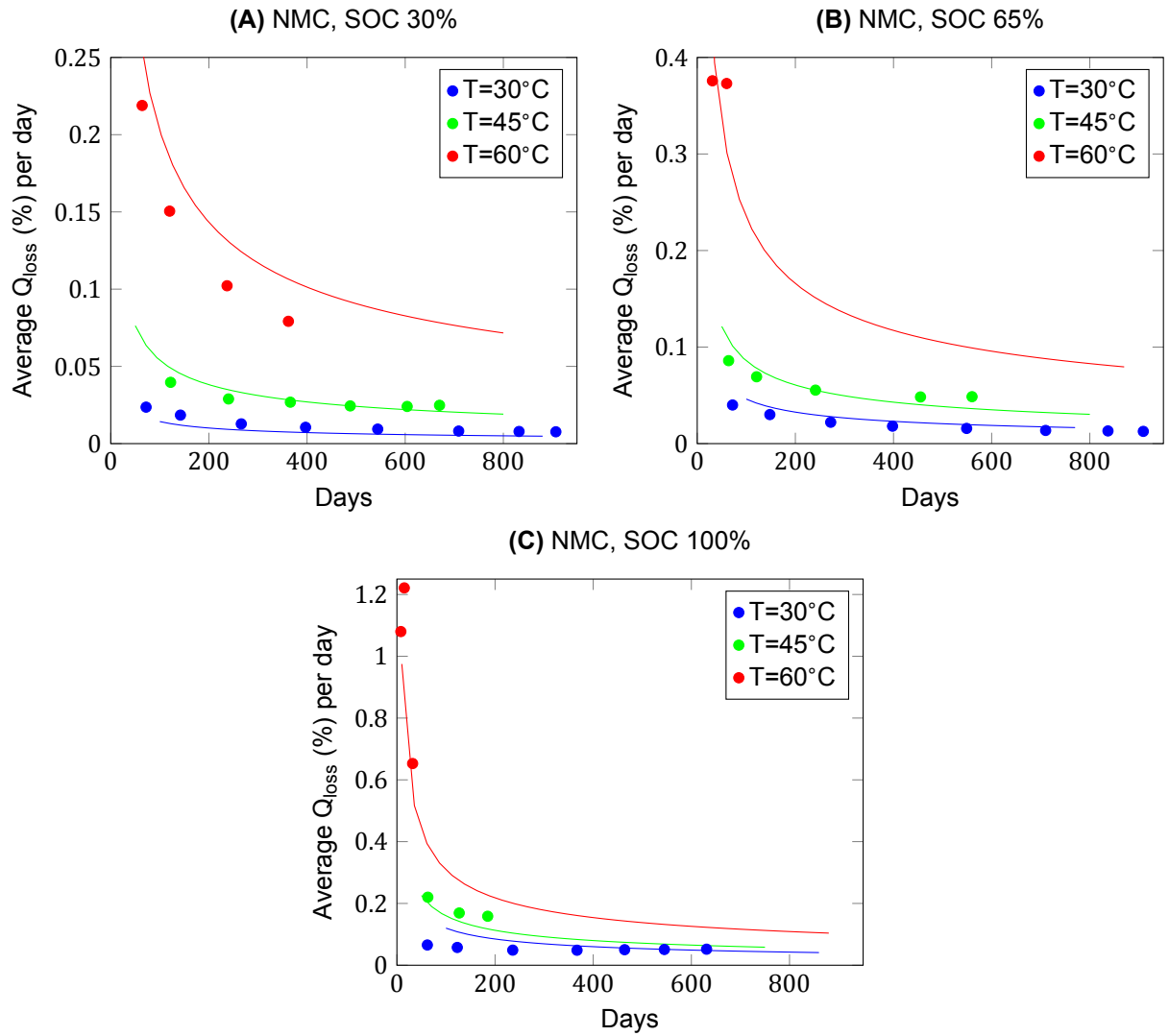


Figure 4.10: $\alpha = 0.06$, $\beta = 1.092$, $\kappa_1 = 0.0001$, $\kappa_2 = 0.0211$, NMC 5.3 Ah cell from SIMCAL aging tests [15]

The 5.3 Ah NMC battery that is tested shows very high aging rates at a high SOC, see figure 4.10. Therefore the emphasis is on adjusting the values for κ_1 and κ_2 . Even with this deviant aging behaviour it is possible to fit the model to achieve a acceptable 6.68% average error. The three test cases show that the model is very versatile to different battery types with varying aging behaviour.

4.4.3. Proposed model vs. other models

The proposed model is compared to the models by Sarasketa and Ecker, because for these two models the used aging test measurements are available as well. Five different storage conditions are simulated for the comparison to the model by Sarasketa[51]. First the α and β are estimated by the use of the least squares method in Simulink and the SOH measurements performed in [51]. This resulted in an α of 0.0585 and a β of 1.0615. The results are shown in table 4.3. Although the simulations by the proposed model does contain the highest maximum error, the averages of both the absolute error and the error are below the errors of the model by Sarasketa.

Table 4.3: Accuracy of proposed model compared to model by Sarasketa

Proposed model compared to model by Sarasketa									
				Sarasketa			Proposed model		
SOC	T	days	SOH (%)	sim (%)	abs (%)	err (%)	sim (%)	abs (%)	err (%)
30	40	593	90.8	91.54	0.74	8.04	92.76	1.96	21.30
70	30	633	93.1	91.77	-1.33	-19.28	91.87	-1.23	-17.83
70	40	614	88.5	87.76	-0.74	-6.43	87.82	-0.68	-5.91
70	50	347	85.7	86.07	0.37	2.59	85.28	-0.42	-2.94
90	40	351	88.6	89.02	0.42	3.68	88.69	0.09	0.79
				average	-0.11	-2.28	average	-0.06	-0.92

The comparison between the proposed model and the model by Ecker[17] is based on three measurements at a SOC of 50% and temperatures of 35°C, 50°C and 65 °C. The parameter α is estimated at 0.0570 and β at 1.0558. The resulting simulations are shown in table 4.4. The accuracy of the proposed model is clearly higher than for the model by Ecker. The results of the comparison between the accuracy of the proposed model and the models by Sarasketa and Ecker, show that the proposed model is very capable of achieving a high accuracy when fitted to a specific battery.

Table 4.4: Accuracy of proposed model compared to model by Ecker[17]

Proposed model compared to model by Ecker									
				Ecker			Proposed model		
SOC	T	days	SOH (%)	sim (%)	abs (%)	err (%)	sim (%)	abs (%)	err (%)
50	35	422	93.13	92.06	-1.07	-15.57	94.89	1.76	25.62
50	50	426	89.80	84.77	-5.03	-49.28	88.42	-1.38	-13.53
50	65	427	73.71	70.77	-2.94	-11.18	73.82	0.11	0.42
				average	-3.01	-25.36	average	0.16	4.17

The very high errors for the predictions by the Ecker model are unexpected because this model is developed using these particular aging test measurements. This is caused by the variation in measurement results from the aging tests. For the measurements at 35% there was an average variation of 16.5%. For the measurements at 50% there was an average variation of 23.3%. For the measurements at 65% there was an average variation of 15.8%. The Ecker model is developed with the averages of the measurements and the proposed model is fitted to these actual measurements. Therefore the accuracy is much higher for the proposed model compared to the Ecker model[17].

4.5. Verification

The model is verified to be applicable as a general prediction method for the aging of batteries in full electric ships by performing three steps. A set of parameters is determined that will predict aging with an acceptable accuracy for a large set of battery types. Then it is investigated if there are any conditions at which the predictions show a large and similar error. The third step is to determine the statistical distribution of the errors and if this is acceptable for a general prediction method.

4.5.1. Parameters

The average values for parameters β , κ_1 , κ_2 , γ_1 , γ_2 , γ_3 and γ_4 are already determined by analyzing the aging test in chapter 3, see table 4.5. Three values of α are determined for all the analyzed aging tests.

- α_1 is determined at a low temperature and medium SOC level.
- α_2 is determined at a medium temperature and medium SOC level.
- α_3 is the average of α_1 and α_2 .

Figure 4.11 shows the distribution of the average errors using the 3 different values for α compared to the related measurements. A high concentration of values for α with a small error is situated around a value of 0.07, which is chosen as the setting for α to continue with.

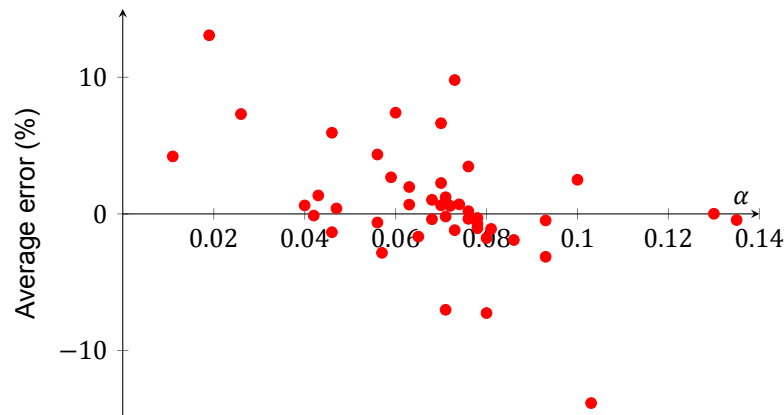


Figure 4.11: Distribution of the average errors at different values of α

Table 4.5: Parameter settings for general aging model

Parameter settings		
Parameter	Value	Description
α	0.07	Temperature effect calendar aging
β	1.061	Temperature effect calendar aging
κ_1	0.002	SOC effect calendar aging (SOC<65%)
κ_2	0.003	SOC effect calendar aging (SOC>65%)
γ_1	0.08	C-rate effect cycle aging (discharge)
γ_2	0.0064	C-rate effect cycle aging (discharge)
γ_3	0.15	C-rate effect cycle aging (charge)
γ_4	0.0225	C-rate effect cycle aging (charge)

The cycle aging behaviour of the model is decided to represent that of a typical battery for marine propulsion. Based on the information from several manufacturers of marine battery systems a general Woehler curve is chosen, see figure 4.12. [25]

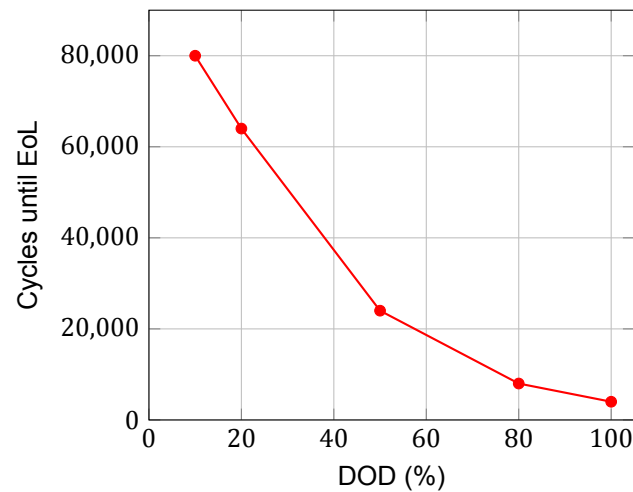


Figure 4.12: Woehler curve for general model

4.5.2. Errors at specific conditions

The errors of the prediction by the model compared to the aging measurements are evaluated for their relationship with time, SOC and temperature to see if there is a specific condition at which the model shows large errors. Figure 4.13 shows the errors at different moments in time. Although the variation of the error does increase with time, there is not a very strong relation visible and also after 1000 days there has been a very accurate prediction by the model. Unfortunately there is no data available from aging tests that lasted 5 years or longer.

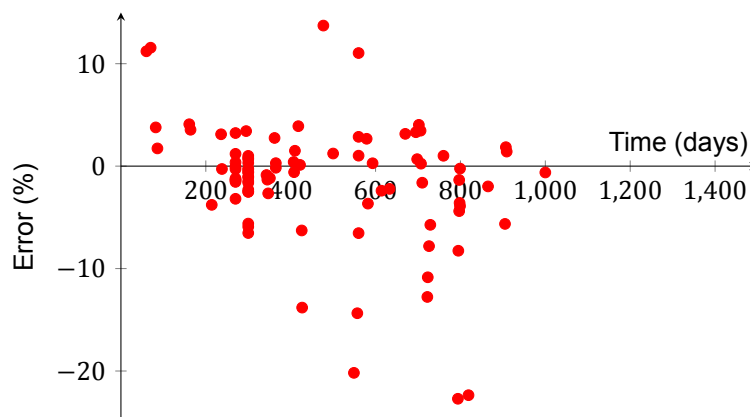


Figure 4.13: Distribution of the absolute simulation errors at different points in time

Figure 4.14 shows the distribution of the errors based on the SOC. There is a small trend visible of overestimating the aging at the lower half of the SOC range and some underestimation for the top half of the SOC range., but this occurs only for a few simulations. The highest errors are also the measurements at high temperatures, which previously has shown a larger unpredictability.

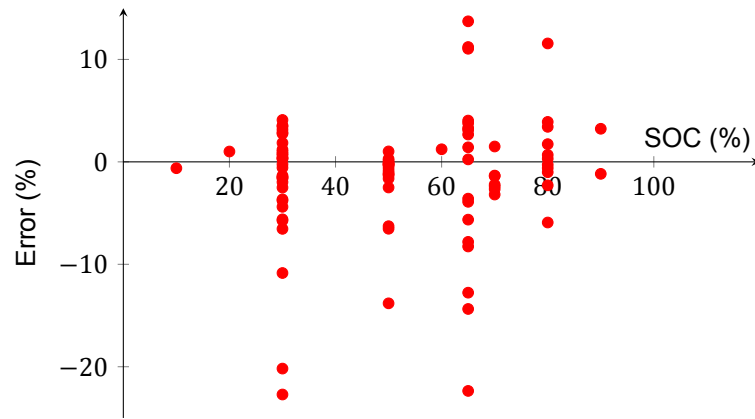


Figure 4.14: Distribution of the absolute simulation errors at different SOC levels

Figure 4.15 shows the distribution of the errors based on the temperature. The variation of the errors increases with an increasing temperature as expected. There is no clear preference for negative or positive errors based on temperature. It is assumed that the large uncertainty at high temperatures is insignificant because the model has an integrated thermal management system which keeps the temperature down. With realistic use of the battery the temperatures of 60°C will not be reached.

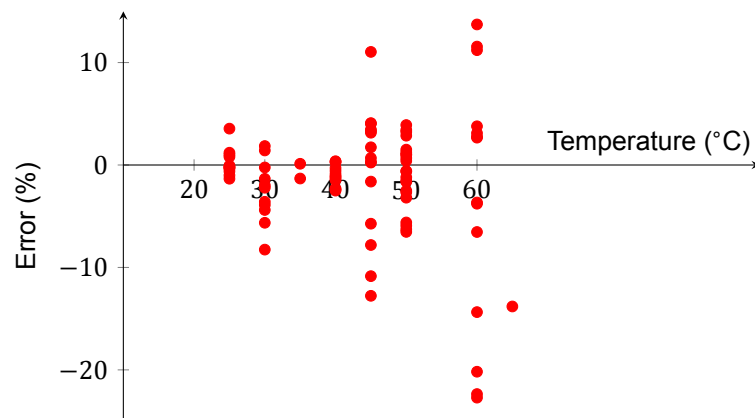


Figure 4.15: Distribution of the absolute simulation errors at different temperature levels

4.5.3. Statistical distribution of errors

Based on the comparison between measurements and simulations the distribution of the errors is shown in figure 4.16 and table 4.6. Based on the conclusion that battery aging is highly variably for different batteries and the fact that the model is capable of predicting the development of the SOH with an average error of only -1.38%, it is assumed that the model can be used as a general aging model for lithium-ion batteries. There are some cases where very high errors occur, but these occur at very high temperatures. Table 4.6 and figure 4.16 show the occurrence of errors including the measurements at 60°C and without these measurements. An error of 1% or less in almost 50% of the simulations is assumed to prove that this model describes the general lithium-ion battery aging behaviour.

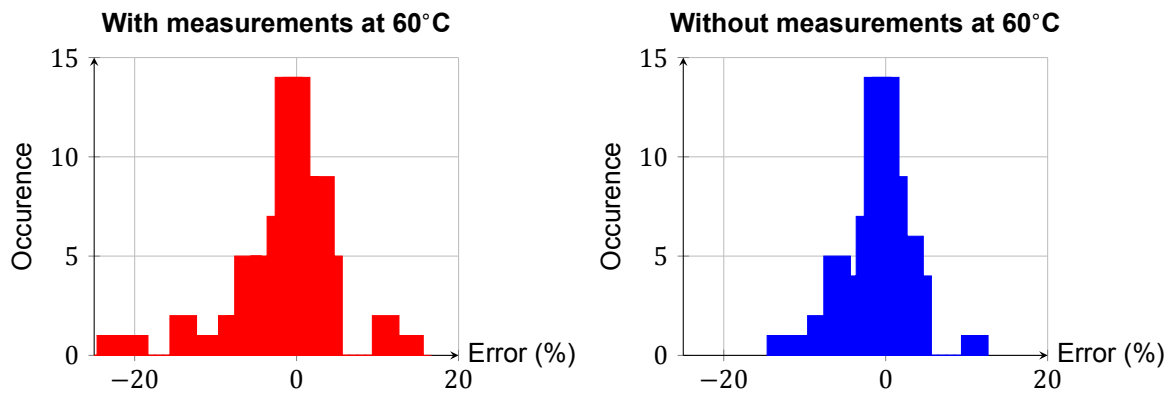


Figure 4.16: Distribution of the absolute simulation errors

The average errors in table 4.6 are the absolute error in SOH measurement. This means that if a prediction of 80% SOH is made by the model, on average the related measurement will be at 79.12% with the average error of 0.88%. The model is slightly overestimating the aging rate.

Table 4.6: Distribution of the absolute prediction errors by the model

Absolute error	Distribution with 60°C	Distribution without 60°C
≤ 1%	25.6%	49.3%
≤ 2%	48.9%	62.7%
≤ 3%	58.9%	76.0%
≤ 4%	74.4%	85.3%
≤ 5%	77.8%	85.3%
Average error	-1.38%	-0.88%

5

Battery size and strategy optimization

The optimization of battery size and operational strategy is investigated in three steps. First the system boundaries are determined. Then the model is used to perform a general analysis of the effects of different operational conditions on battery life. Two methods are developed for the battery optimization which are tested with two case studies, a harbour tug and a ferry.

5.1. System boundaries

A battery can perform two types of operations, charging and discharging. Each operation is dependent on several limiting factors, determining the boundaries of the system. These boundaries are required for defining the scope of battery optimization, but also the definition of optimal for battery size and strategy is determined.

5.1.1. Charging

The charging power of the battery in the model is limited to 1.75 MW. A power above this limit requires a separate substation on the power grid. If the operational profile of the ship allows it, charging overnight is preferred because of lower energy prices. More on the charging boundaries is found in appendix A.3.1.

5.1.2. Discharging

Discharging the battery is limited to a SOC between 80% and 20%, to take the aging losses and life expectancy into account. Efficiency of the battery is not taken into account, this is also the case for the charge efficiency. The EOL is determined to be at 80% SOH and no second life options are taken into account. More on the discharge boundaries is found in appendix A.3.2.

5.1.3. Optimality

The optimal battery size and operational strategy can be approached from two directions. The battery size can be kept constant to evaluate the effect of different strategies. In this case the combination of life expectancy in years and the performed number of FEC in that lifetime are used for optimization. The highest combination of life expectancy and FEC relates to the strategy which makes the most optimal use of the battery. The costs per year or the costs per amount of energy throughput can be used to compare different battery sizes with the same operational strategy. Where the lowest costs relate to the optimal battery size.

5.2. General analysis

The general analysis is performed to investigate the following subjects. First the effect cycling the battery at different depths of discharges is investigated. Then it is determined at which average SOC the life expectancy is the highest. It is checked if the optimal DOD changes if the model has a different Woehler curve as input. Different charge strategies are tried to evaluate their effects and the effect of the thermal management system is evaluated at varying ambient air temperatures. The most important conclusions of this general analysis are summarized in section 5.2.6.

5.2.1. DOD

The effect of battery size on aging is investigated by simulating various operations at different combinations of DOD, C-rate and operational hours per day. The model is used to simulate a DOD of 5%, 10%, 15%, 20%, 25%, 30% and 40%. The cycles are performed at 0.1C, 0.25C, 0.5C, 1C, 1.5C and 3C. The simulations are run for 12 different operational times, between 1 and 12 hours per day. The simulations are run until the EOL at a SOH of 80% is reached. In appendix F the performed full equivalent cycles (FEC), years until EOL, percentage of calendar aging and percentage of cycle aging are shown for each simulated operational condition and operational hours per day. Figure 5.1 shows the results of these simulations.

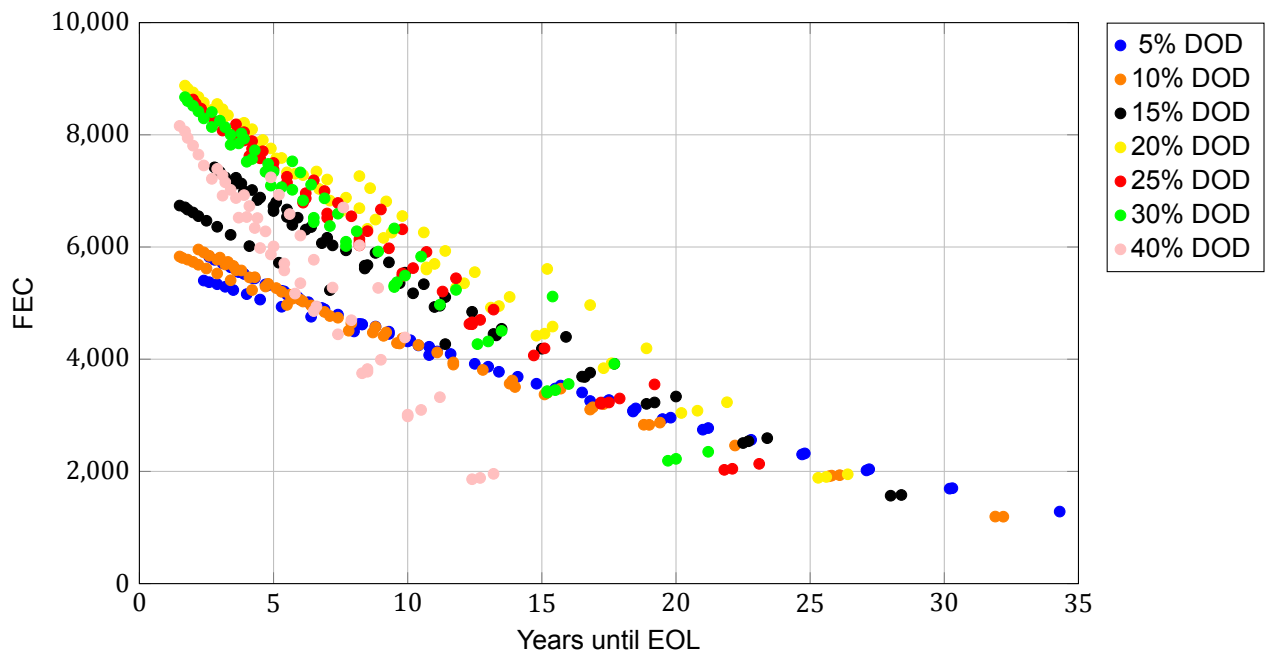


Figure 5.1: Results of general analysis simulations for performed FEC and years until EOL

Figure 5.2 shows the trend lines based on the data from figure 5.1. In most situations the battery size relating to a DOD of 20% will result in the highest combination of life expectancy and performed FEC. However, for operational strategies which result in more than 8 FEC per day, the life expectancy is becoming very similar for a DOD of 25% and 30% as well. For operational strategies which result in less than 0.3 FEC per day, the battery sizes that result in a DOD of 5% and 10% outperform the one at 20% DOD.

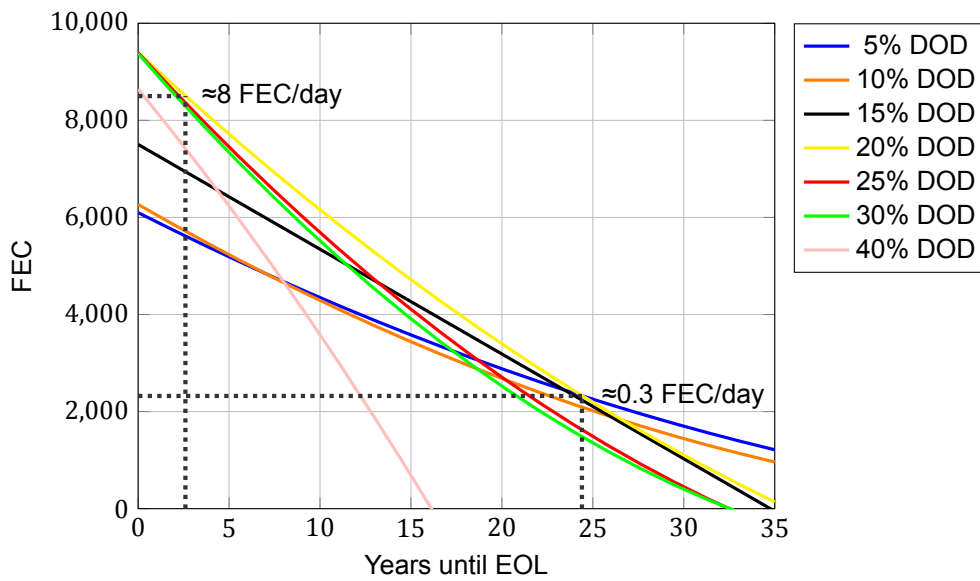


Figure 5.2: Trend lines for FEC and years until EOL

A common goal for the battery life is 10 years. Therefore the effect of DOD, C-rate and operational hours is further analyzed with the results that match a battery life of 10 years. Figure 5.3 shows the performed FEC at EOL after 10 years for each different DOD. This again shows that a DOD 20% results in the highest amount of performed FEC, followed by 25% and 30% DOD.

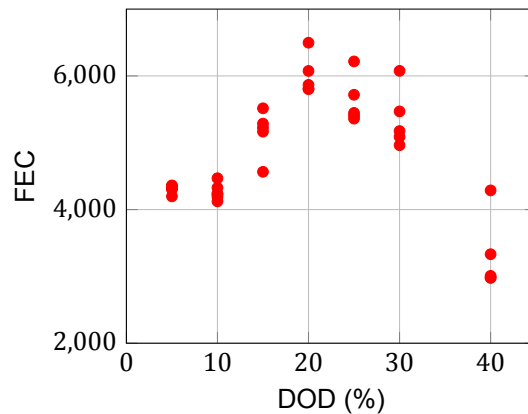


Figure 5.3: Performed FEC at EOL after 10 years for different DOD at different C-rates

5.2.2. Average SOC

As shown in section 3.5.3, the average SOC level during cycling has a strong influence on the aging of the battery. This is investigated with the aging model by running several simulations for 2, 6 and 12 operational hours per day at 20% DOD and a 1C C-rate. Figure 5.4 shows the results of these simulations for a 5 and 10 year life expectancy. The results show that an average SOC of 40% leads to the highest amount of performed FEC, when the battery is cycled at 20% DOD.

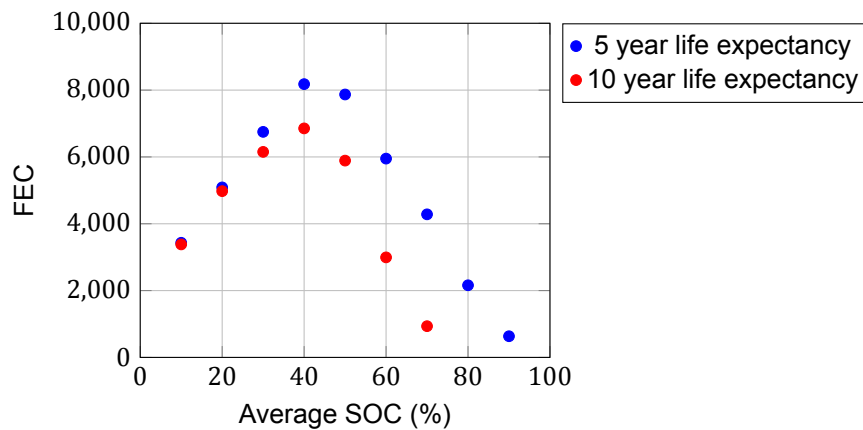


Figure 5.4: Simulation results for cycling at 20% DOD and 1C with different average SOC

5.2.3. Effect of different Woehler curve

A series of simulations with different Woehler curves as input are performed to investigate the sensitivity of the optimal DOD for batteries with other aging characteristics. Figure 5.5 shows the Woehler curves that are used for this. Woehler curve 1 is the curve used for the general behaviour analysis. Curve 2 represents a battery which is more vulnerable to cycle aging and curve 3 represents a battery which is less vulnerable to cycle aging.

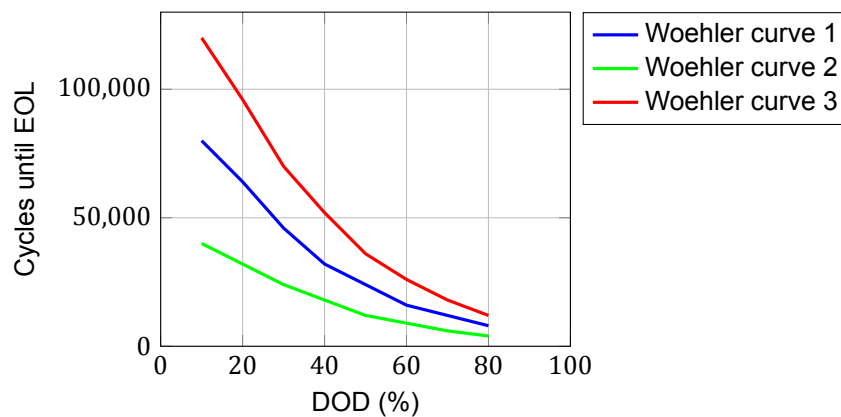


Figure 5.5: Three different Woehler curves to represent three batteries with different aging characteristics

The simulations are performed at a DOD of 10%, 20%, 30% and 40%; C-rates of 0.5 C and 1 C; and for 2, 6 and 12 operational hours per day. Table F.42, F.43 and F.44 in appendix F show the results of the simulations. Figure 5.6 shows the performed FEC at different DOD for an EOL after 10 years of operations. For all different Woehler curves the optimum lies around 20% DOD, but a DOD of 30% also provides an efficient use of the battery. This shows that independent of the aging characteristics of the battery, the optimal DOD remains similar.

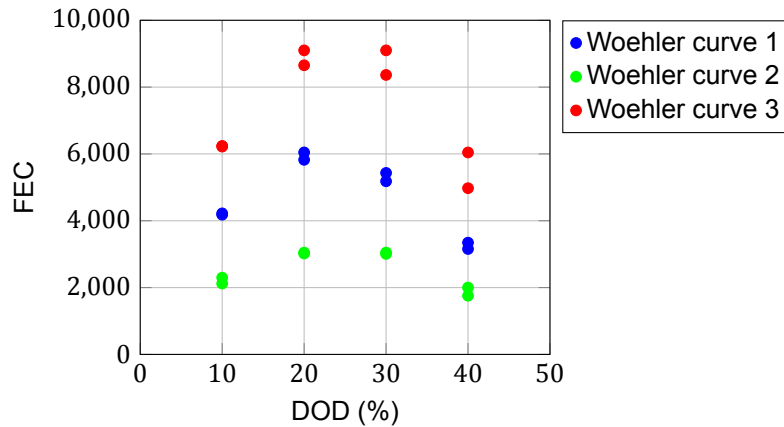


Figure 5.6: Performed FEC at EOL after 10 years with different Woehler curves

5.2.4. Charge strategy

The effect of charge strategy is investigated with three sets of simulations. The first set is to determine the effect of a resting period between charging and discharging. Ten cycles of 20% DOD at a C-rate of 1C are performed per day. The resting periods are 0, 15, 30 or 60 minutes. The second set is to determine the effect of charge C-rate. Again ten cycles of 20% DOD are performed per day, with a discharge rate of 1C and a charge rate of 0.25C, 0.5C, 0.75C or 1C. The cycles will be from 60% SOC to 40%. The third set is to investigate the strategy for overnight charging. The battery is discharged during the day and the overnight charge time is varied.

Table 5.1: Results of simulating aging model until EOL with different rest periods

20% DOD, 1C variable resting period				
Rest period	FEC	Increase	Years	Increase
0 minutes	6327	0%	8.46	0%
15 minutes	6549	3.5%	8.74	3.3%
30 minutes	6756	6.8%	9.02	6.6%
60 minutes	7192	13.7%	9.61	13.6%

Table 5.1 shows the results for simulating variable rest periods between charging and discharging the battery. The life expectancy and performed FEC increase with an increasing rest period. The change of the performed FEC and years until EOL is the percentage it differences from the result for applying no rest period. The increase of the performed FEC is slightly higher than the increase in years, which means that the effective use of the battery also increases. However, the maximum increase in efficiency is about 0.2% and therefore not significant.

Table 5.2: Results of simulating aging model until EOL with different charge rates

20% DOD, 1C discharge, variable charge rate				
Charge rate	FEC	Increase	Years	Increase
0.25 C	6337	0%	8.96	0%
0.5 C	6362	0.4%	8.64	-3.6%
0.75 C	6320	-0.3%	8.55	-4.6%
1 C	6327	-0.1%	8.46	-5.6%

The results for a variable charge rate are shown in table 5.2. The change of the performed FEC and years until EOL is the percentage it differences from the result for applying a 0.25C charge rate. The life expectancy decreases with an increasing charge rate, but the performed FEC remains similar. This shows that the effective use of the battery decreases with a higher charge rate.

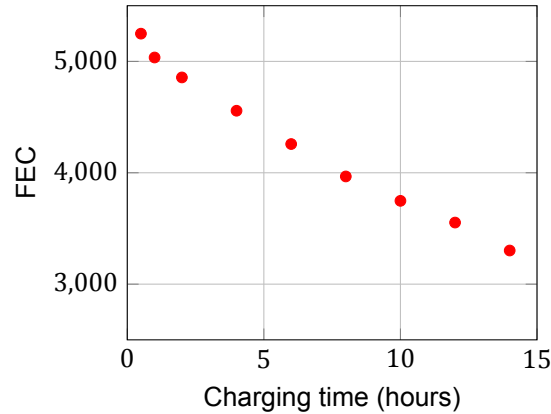


Figure 5.7: Simulation results for cycling at 50% DOD and variable overnight charge strategy

In some situations, the ship will be operated during the day on a single charge and during the night it will receive a recharge. Different charging schedules are investigated to determine the optimal strategy. The battery of 1000 kWh is discharged in 10 hours per day with a DOD of 50%, between 75% SOC and 25% SOC. The battery is charged varying from 14 hours at 40 kW up to 0.5 hours at 1050 kW. In the case of the 14 hour charge there is no resetting period between the discharge and charge. For all shorter charge times the charge is started at the latest moment. The resting period between discharge and charge is assumed to decrease the calendar aging rate by keeping the battery at low SOC levels for a longer period. Figure 5.7 shows the results of the simulations. Short charge times result in the longest life of the battery. Charging the battery fast, shortly before the operation start results in less aging than slowly charging the battery over a longer period.

5.2.5. Thermal management

The influence of the ambient temperature and the effect of the thermal management system is investigated by performing multiple simulations at ambient temperatures of 10°C, 20°C and 30°C. For these simulations the DOD is kept constant at 20%. The C-rates that are investigated are 0.5 C and 1 C and the operations of 2, 6 and 12 hours per day are performed. The simulations are performed with an engaged thermal management system and without it. Table F.45 and F.46 in appendix F show the results of these simulations. The effect of different ambient temperatures and the use of a thermal management system on the life expectancy and efficient use of the battery is shown in figure 5.8. At a constant ambient temperature of 10°C, the battery reaches EOL on average 2.4% in years later without a thermal management system. Also on average 2.7% more FEC are performed. At an ambient temperature of 20°C, the battery without thermal management system reaches EOL on average 7.7% in years earlier and performs 7.3% less FEC. At an ambient temperature of 30°C, EOL is reached 35.9% in years earlier and 36.9% less FEC are performed. This shows that for cold climates it might even be more effective to not use a thermal management system, but for moderate or hot climates it is definitely recommended to use a thermal management system.

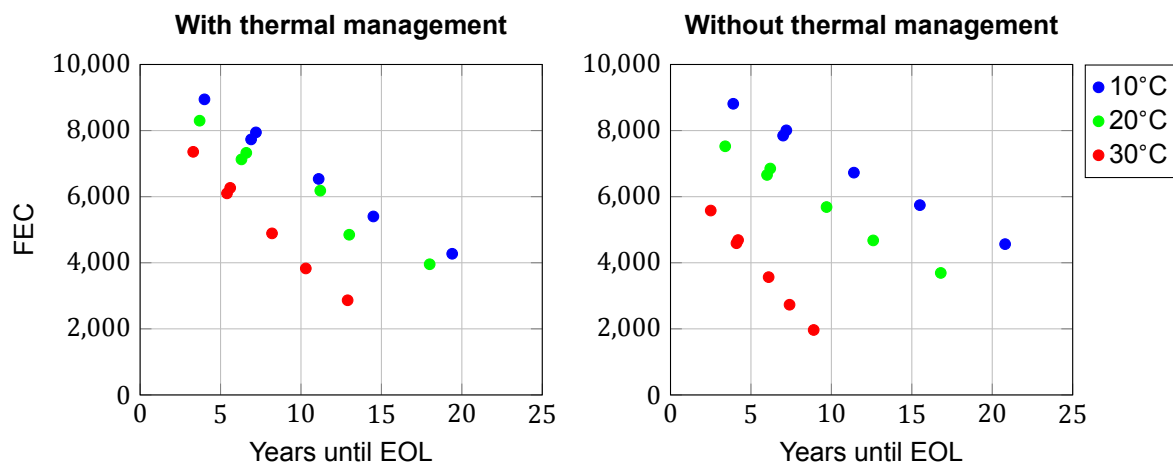


Figure 5.8: FEC and years until EOL at different ambient temperatures with thermal management system

5.2.6. Conclusions

The following conclusions are drawn from the general analysis and should be taken into account when investigating the options for battery sizes and operational strategies for full electric ships.

- Cycling the battery at a DOD of 20% results in the highest combination of life expectancy and performed FEC.
- The cycle from 50% to 30% SOC results in the least capacity loss.
- The 20% DOD is valid for different battery types.
- A resting period between a charge and discharge improves the life expectancy.
- Higher C-rates during charging decrease the life expectancy.
- A short and fast charge ages the battery less than a long and slow charge.
- Especially at higher ambient temperatures the thermal management system improves the life expectancy significantly.

5.3. Optimization method 1

The first optimization method makes use of the proposed model to simulate different combinations of battery size and operational strategy to an optimal solution. The optimization steps consists of four steps.

5.3.1. Optimization steps

The first step in the optimization process is to determine the different strategies for the operational profile of the ship. Depending on the type of ship there is a part of the operational profile that is fixed and a part that is variable. By adjusting the sailing speed on the variable parts the required energy changes which influences the required charging time.

The second step is to match different battery sizes to fit the operational profile, based on the conclusions of the general analysis. Based on the intensity of the operational profile a goal for the DOD can be set. This directly influences the C-rates on the batteries. By varying the number of battery systems the operational hours per day can be determined and resting periods can be applied to improve life expectancy.

The third step is to use the proposed model to simulate the life of the battery with the operational profiles determined in step 1 and 2. This will result in the life expectancy and the performed FEC to compare the different operational strategies for optimality.

The fourth step is to calculate the costs for the installation and possible replacements of the battery. Also the operational costs can be used for the evaluation of the different battery sizes.

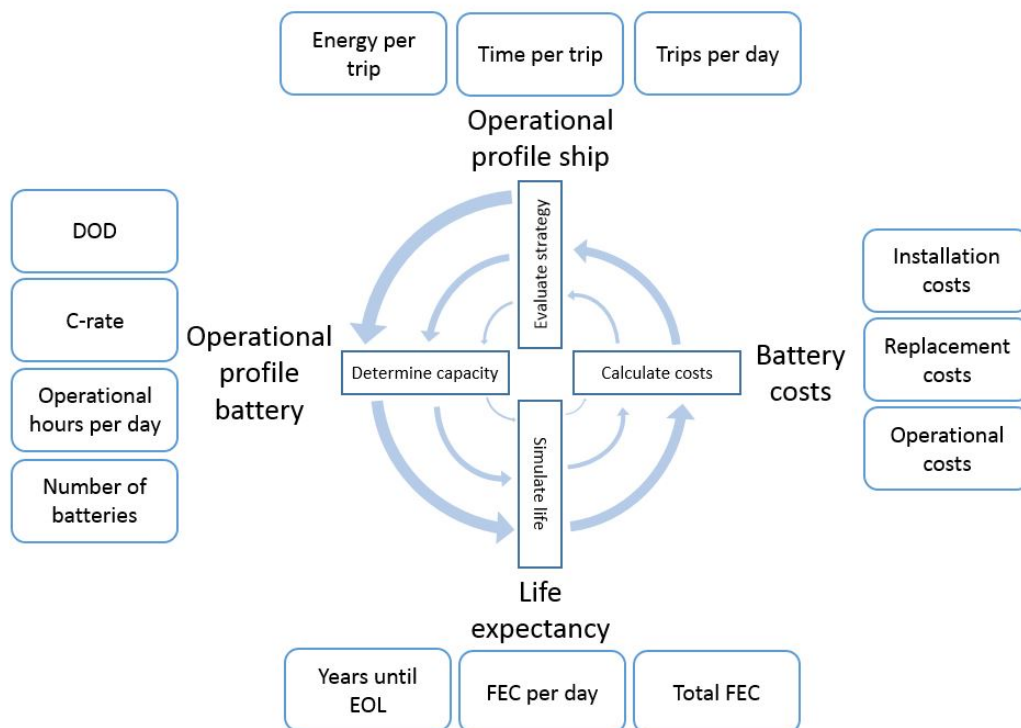


Figure 5.9: The four steps for battery optimization

5.3.2. Case study: Harbour tug

The tug that is used for the case study is the Damen ASD2810. The maximum power of 4000 kW is determined for this case study. The displacement of the ASD2810 is approximately 580 tons, of which usually 60 tons is fuel oil. If the weight of this fuel would be replaced by a battery it will be the equivalent of a 5 MWh battery. Tugs generally are very heavy, which is required for the heavy towing work that has to be performed. Therefore the effect of increasing the weight of a tug has only a small influence on the required propulsive power. This is why in this case study the effect of changing the size of the battery does not influence the power demand. The size of the battery however, can be a problem. Tugs usually don't have much free space on board to fit a large battery system. Electric motors are smaller than diesel engines and the electrical system is more flexible, this could make up for the large batteries.

Operational profile ship

Harbour tugs are used to assist large vessels entering and leaving ports. The operational area of the harbour tug is limited as well as the demand for high sailing speeds. These are the two important aspects that make batteries interesting for the propulsion of these types of ships. Depending on the type of tug, the port where the tug is located and the company it belongs to there can be large variations in the working hours and operational profiles. Usually, about 50% of the operational time the ship is on standby. The high amount of waiting time is very suitable for charging the tug. Table F.48 summarizes the different types of tasks during a job, the power that is required to perform that task and the percentage of time that task takes.[40] Based on this information three jobs are determined for the tug, see figure 5.10

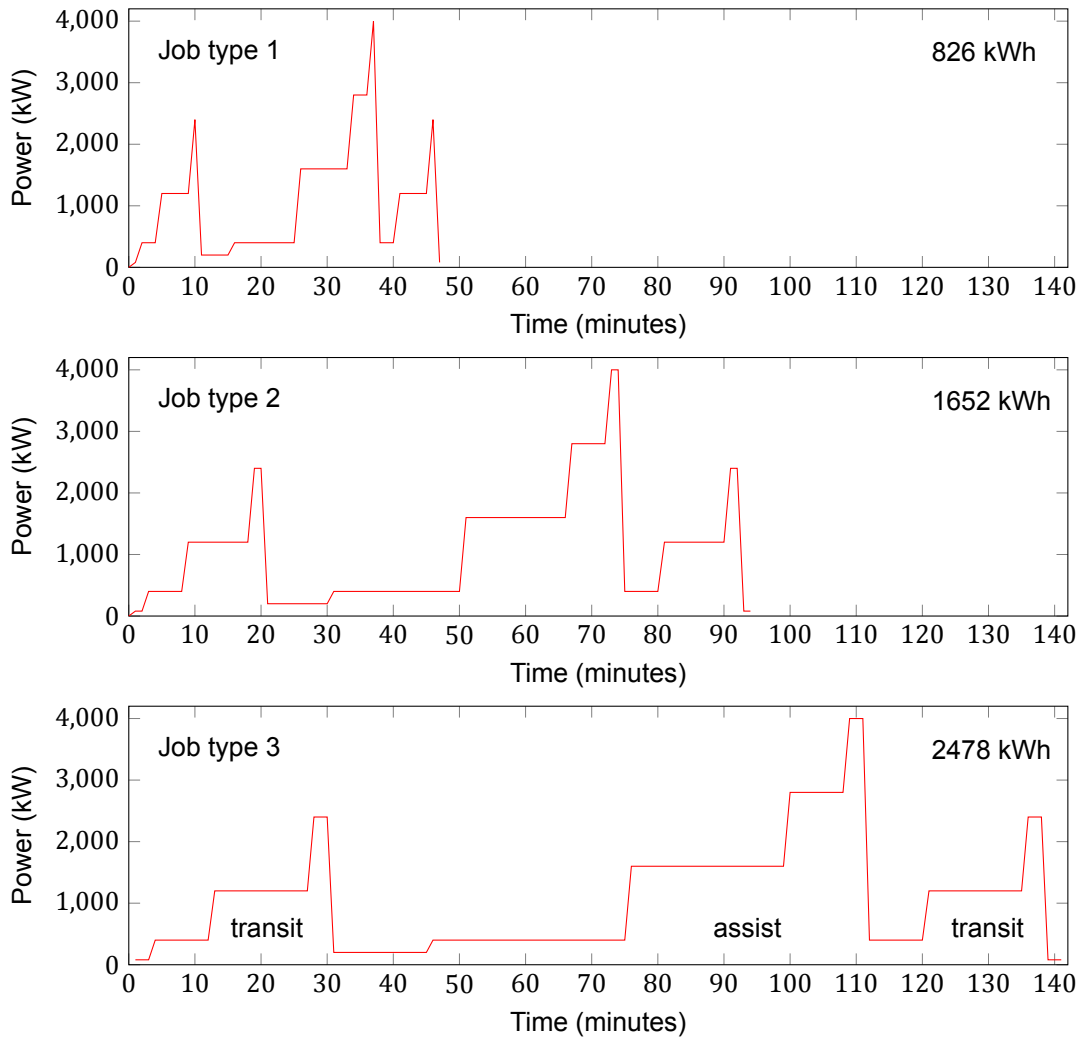


Figure 5.10: Light, medium and heavy job types for the harbour tug

There are too many variations in the operations of tugs to investigate the whole spectrum of operational profiles in this study. Therefore five operational profiles, shown in figure 5.11, are simulated to determine the effect of changing the battery capacity. Each profile represents a single day which is performed daily until the battery has reached 80% SOH. In the figures the size of the tug represents the type of job, where job type 1 is represented by the smallest tug and job type 3 by the largest tug. The figures also indicate when the charging of the battery is started. As determined in section 5.2.4 the battery is charged shortly before a job

starts to increase the life expectancy. The maximum charge power of 1.75 MW is applied. The different types of jobs require different amounts of energy and therefore different charging times. After job type 1 charging will begin 1 hour before the next job, after job type 2 charging starts 1.5 hours before the next job and after job type 3 charging starts 2 hours before the next job. The auxiliary power demand is estimated to be 40 kW from 06:00 until 22:00.



Figure 5.11: Operational profiles for harbour tug

Operational profile battery

All profiles are simulated with a battery capacity of 4.5, 5, 5.5, 6, 6.5, 7, 7.5 and 8 MWh. Figure 5.12 shows the SOC of the 4.5 MWh battery during operational profile 1. It is cycled from 80% to 20% SOC, which was determined to be the maximum size of a cycle. Therefore the minimum required capacity to perform all types of profiles is 4.5 MWh and it is assumed that increasing the battery size to more than 8 MWh will not be beneficial for the cost efficiency of the battery. There are two different strategies tested for the battery. Strategy 1 is to always charge the battery up to 80% SOC before each job. It is assumed that it is known with the crew of a tug at what time the next job starts, but not how big the job is going to be. Strategy 2 is to charge the battery up to 3.6 MWh, which is 80% of the smallest battery of 4.5 MWh. This strategy is chosen to keep the SOC as low as possible to keep the calendar aging down.

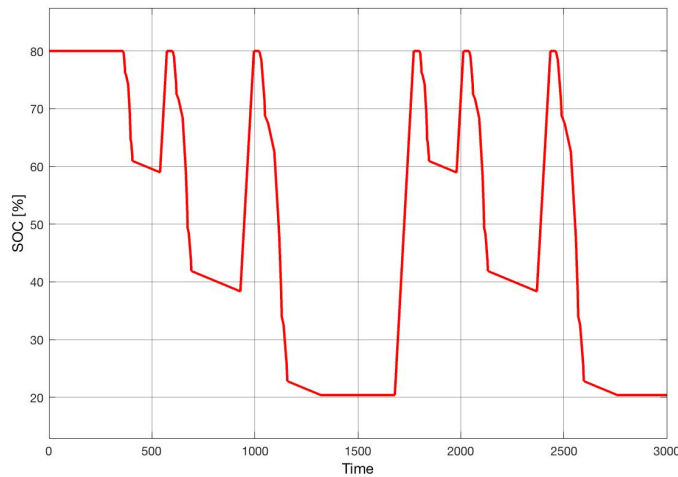


Figure 5.12: State of charge of the 4.5 MWh battery during operational profile 1

Life expectancy

The results of the simulations of the 5 different profiles with both strategies are shown in figure 5.13. The two strategies clearly result in different aging rates of the battery. By using strategy 1, charging the battery up to 80% SOC, the overall life expectancy is much lower than for strategy 2, charging the battery up to 3.6 MWh. There is also an optimum in battery size for all profiles when strategy 1 is used. With strategy 2 the life expectancy continuously increases with the increasing capacity. This decrease in life expectancy is caused by the high SOC at which the battery is kept with strategy 1. Increasing the capacity also increases the average SOC and therefore increases the calendar aging rate. In the case of profile 4, where all cycles are small, the high SOC even causes the life expectancy to drop significantly with a capacity above 6 MWh. These results show two things. Firstly, for the optimization of the battery size and strategy it is very important to determine the minimum required level of redundancy of stored energy. With too little redundancy the functionality of the tug will not be optimal. With too much redundancy the life expectancy of the battery reduces drastically. Secondly, a realistic goal for this specific case is a battery replacement after 10 years.

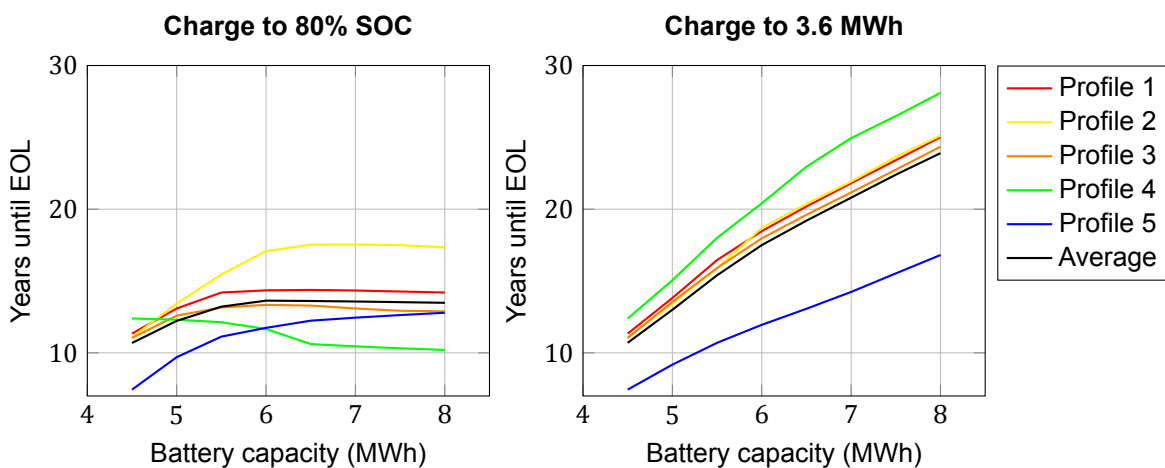


Figure 5.13: Years until EOL for different profiles and battery sizes strategy 1 and strategy 2

Costs

In tables F.52 and F.53 the costs per year for the different installed batteries and different strategies are calculated. The installation costs are estimated at €1000 per kWh with an interest of 5%. Figure 5.14 shows the annual costs for the different battery sizes and strategies. For strategy 1 a total installed capacity of 5 MWh is calculated to be the cheapest option per year. For strategy 2 the annual costs decrease with an increasing battery capacity. However, above a capacity of 6 MWh the annual costs stabilize. Considering the difficulty of estimating the required redundant energy before each job, the advised optimal battery size for this situation is at the point of the lowest average costs per year, at a capacity of 5.5 MWh.

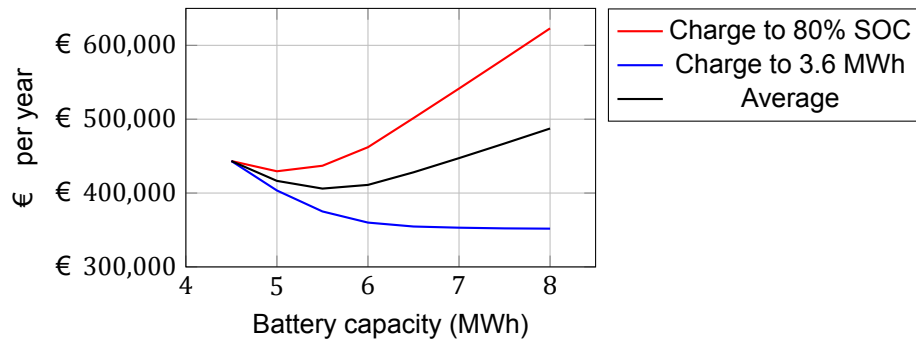


Figure 5.14: Costs in €/year for different battery sizes and for strategy 1 and 2

5.3.3. Case study: Ferry

The Damen DRPa9919 is used for the ferry case study. This ferry has a length of 100 m, breadth of 14.5 m, draught of 2.29 m, displacement of 1525 tons and a block coefficient of 0.459. The maximum propulsive power is assumed to be 1800 kW for this case. The route of the ferry is between two points with a distance of 5 kilometers. Every day between 6AM and 8PM the ferry will travel between these two points, with a departure every half hour, making a round trip in 1 hour.

Operational profile ship

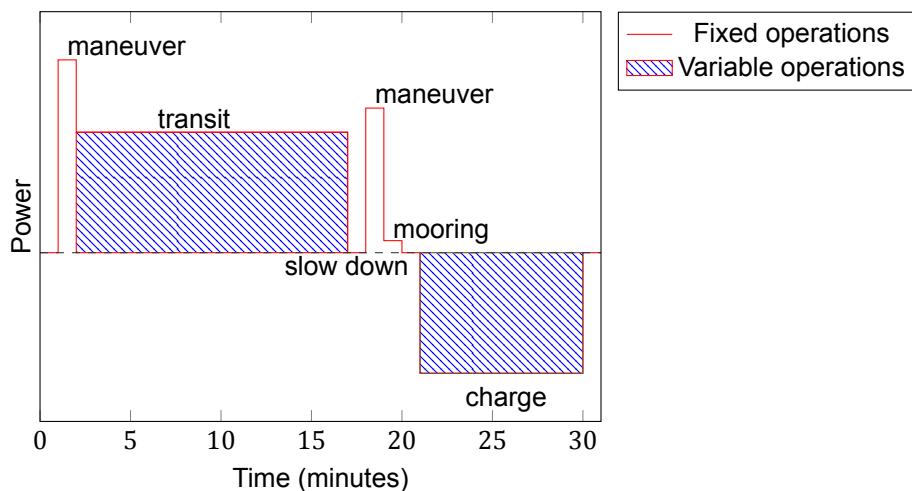


Figure 5.15: Typical profile for a single job of a ferry

Figure 5.15 shows the simplified, typical power profile for a single trip of a ferry. There are two parts (hatched in blue) that can have a variable power and duration. By adjusting the sailing speed the required charging power and time can be varied. There are 6 different operational strategies chosen to simulate, see table 5.3. In 5 of those strategies the battery is being charged at both stops. With the 6th strategy the battery is only charged at one of the stops. Because there is a minimum of 5 minutes required at each stop to unload and load the passengers, there is only one speed at which this strategy will be possible and to stay within the hourly schedule. If the ferry will go faster it will use more energy and a charge power above 1.75 MW is required to recharge the battery in the available time. If the ferry will go slower there will not be enough time to recharge the battery. The auxiliary power requirement for this type of ferry is assumed to be 80 kW.

Table 5.3: Variable operational strategies for the ferry

Operational strategies ferry						
Charge at	Speed (kts)	Power (kW)	Time (min)	Charge (kW)	Time (min)	Energy/trip
2 stops	10.1	447	16	1611	8	203 kWh
2 stops	10.8	552	15	1566	9	221 kWh
2 stops	11.6	690	14	1477	10	245 kWh
2 stops	12.5	881	13	1507	11	274 kWh
2 stops	13.5	1163	12	1591	12	316 kWh
1 stop	11.6	690	14	1750	17	245 kWh

Operational profile battery

Four different options are chosen for the operational profile of the battery, for more information see also table F.55 to F.58.

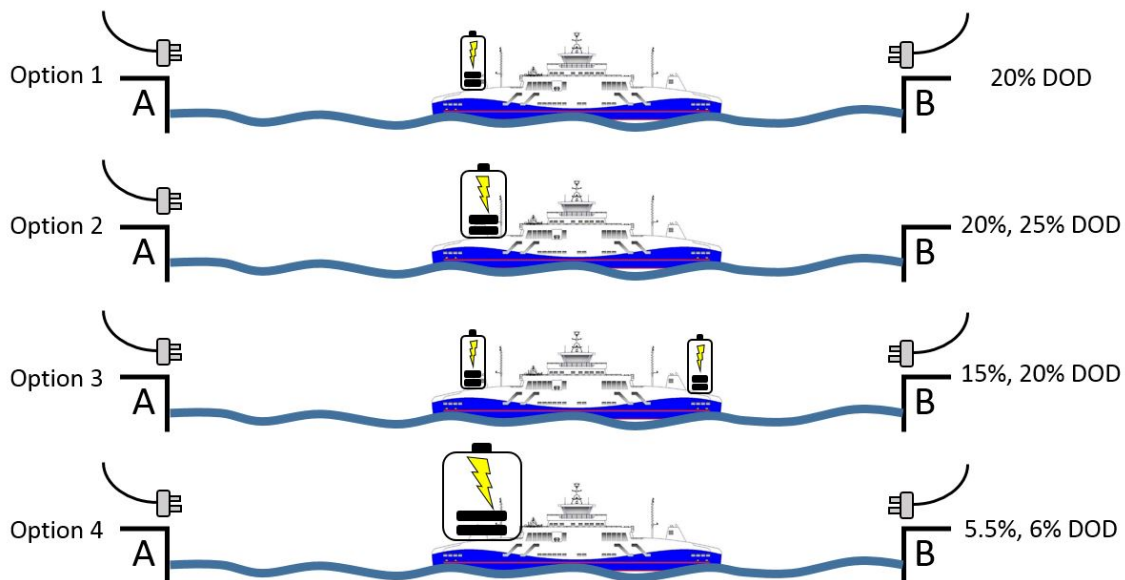


Figure 5.16: Four different options for the battery strategy of the ferry

1. For option 1 it is fixed that the battery charges after every trip at a DOD of 20%. The battery is cycled from 50% SOC to 30% SOC. The speed, charge power and battery capacity are variable. For the speed and charge power, strategy 1 to 5 are applied. The capacity of the battery is adjusted for each strategy to have a DOD of 20%.

2. For option 2 it is fixed that the battery only charges at one of the two stops. This is only possible at a speed of 11.6 knots. If the ferry is slower there is not enough time to charge the battery with the maximum charge power of 1.75 MW to the desired SOC and if the ferry is faster it uses too much energy to charge within the available time as well. The battery capacity is varied to observe the effect of a different DOD. A capacity of 2450 kWh is used to investigate a DOD of 20% and a capacity of 1960 kWh is used to investigate a DOD of 25%.
3. For option 3 two individual batteries are used, each for one trip. Battery A is charged at side A and is used to sail from A to B. Battery B is charged at side B and is used to sail from B to A. This is to provide a resting period for the batteries between discharging and discharging. This option is simulated at two fixed depths of discharge, 20% and 15%. A DOD of 20% is chosen for the expected benefits for battery life versus effective battery use. A DOD of 15% is chosen to decrease the average C-rate, which is expected to increase the life expectancy at this amount of operational hours per day. The speed, charge power and capacity is varied according to strategy 1 to 5.
4. For option 4 the battery size is increased to lower the average C-rate to approximately 0.3C. This C-rate is expected to improve the life expectancy when the battery is operational for 14 hours per day as is the case for the ferry. The battery size is increased to 3564 kWh to have a DOD of 5.5% with strategy 1, sailing at 10.1 knots. A capacity of 3745 kWh is used to cycle the battery at a DOD of 6% with strategy 3, sailing at 11.6 knots. The speed of 10.1 knots is used because it requires the smallest amount of energy for a discharge. The speed of 11.6 knots is used because it requires the lowest charging power.

Life expectancy

The results of the simulations are shown in table F.59. The different combinations of battery size and operational strategy are evaluated for their life expectancy in years, performed FEC and the energy used per year. The life expectancy of the batteries varies between 4.2 and 8.6 years. Therefore a battery replacement after 5 years is required. The smallest battery of 1014 kWh that is charged at both stops and discharged at the slowest sailing speed of 10.1 knots results in the highest number of performed FEC and the lowest energy usage per year. Therefore, this battery is chosen as the most efficient. However, the battery reaches the EOL after 4.2 years. This strategy is then used for with simulating different battery sizes to see the effect on the SOH after 5 years. Figure 5.17 shows the SOH for the different battery sizes. The SOH improves for the batteries with a larger capacity, but it is not a linear relationship. The battery still works after passing 80% SOH, but it is difficult to say what SOH is still acceptable for the ferry.

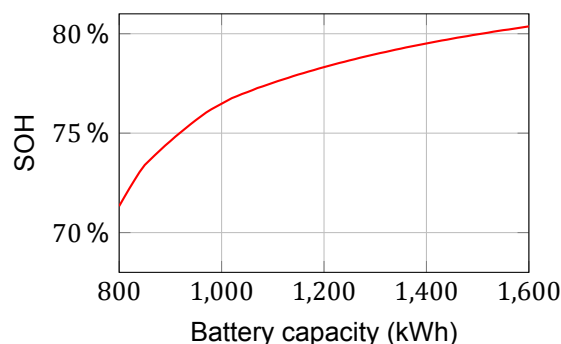


Figure 5.17: State of health after 5 years of operation at 10.1 knots

Costs

The costs are important to determine what is acceptable for the SOH after 5 years of operations. Figure 5.18 shows the relation of the total installation costs and the SOH of the battery after 5 years of cycling. In this specific situation optimality is also dependent to the risks that are taken concerning the EOL. However, the battery costs increase drastically around a SOH of 76.5%. It is assumed that this relates to the optimal battery size with a 1000 kWh capacity.

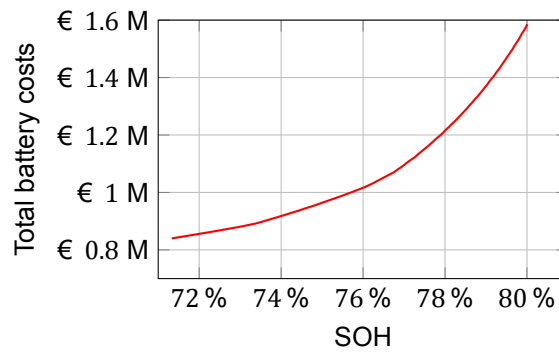


Figure 5.18: Relationship between the total installation costs and SOH after 5 years of cycling

5.4. Optimization method 2

The second optimization method uses two equations that are based on the general analysis in section 5.2.1 to calculate the optimal battery size to reach a certain life expectancy based on an average operational profile. It only focuses on the third step of the battery optimization steps discussed in section 5.3.1.

5.4.1. Optimization steps

The relation between the number of operational hours per day, average C-rate and the years until EOL is investigated first. Figure 5.19 shows the results for a DOD of 20% at different C-rates. The results can be described by a power function based on the operational hours per day, equation 5.1. These power functions are determined for all the investigated DOD's from the general analysis on the effect of DOD on life expectancy.

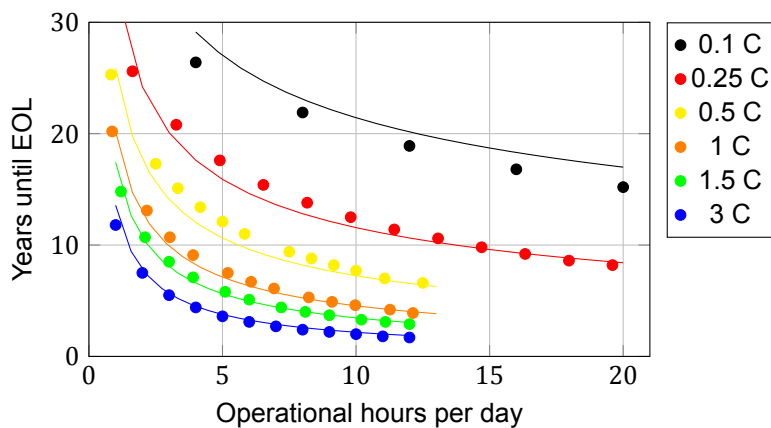


Figure 5.19: Years until EOL per C-rate and operational hours per day at 20% DOD

Parameters A and B are determined by fitting equation 5.1 to the results per DOD. With these equations it is possible to make an estimation of the life expectancy of the battery at a certain amount of operational hours per day and at different C-rates. Table 5.4 gives an overview of the parameters A and B at different values for the DOD.

$$\text{Years until EOL} = A \cdot X^{-B} \quad (X = \text{Operational hours per day}) \quad (5.1)$$

Table 5.4: Parameters for battery life expectancy equations

Parameters for equation 5.1		
DOD	A	B
10%	$19.98 \cdot \text{C-rate}^{-0.345}$	$-(0.1497 \cdot \ln(\text{C-rate}) + 0.7308)$
15%	$-9.452 \cdot \ln(\text{C-rate}) + 21.367$	$-(0.137 \cdot \ln(\text{C-rate}) + 0.6807)$
20%	$20.172 \cdot \text{C-rate}^{-0.361}$	$-(0.1357 \cdot \ln(\text{C-rate}) + 0.6472)$
25%	$-7.52 \cdot \ln(\text{C-rate}) + 19.458$	$-(0.1403 \cdot \ln(\text{C-rate}) + 0.608)$
30%	$-7.365 \cdot \ln(\text{C-rate}) + 19.034$	$-(0.1416 \cdot \ln(\text{C-rate}) + 0.6212)$
40%	$-4.504 \cdot \ln(\text{C-rate}) + 13.23$	$-(0.1524 \cdot \ln(\text{C-rate}) + 0.5157)$

How effective the battery is used during its life is partially determined by the number of performed FEC. The number of performed FEC per day can be calculated with the C-rate and operational hours per day as well, see equation 5.2.

$$\text{FEC per day} = \frac{\text{C-rate} \cdot \text{Operational hours per day}}{2} \quad (5.2)$$

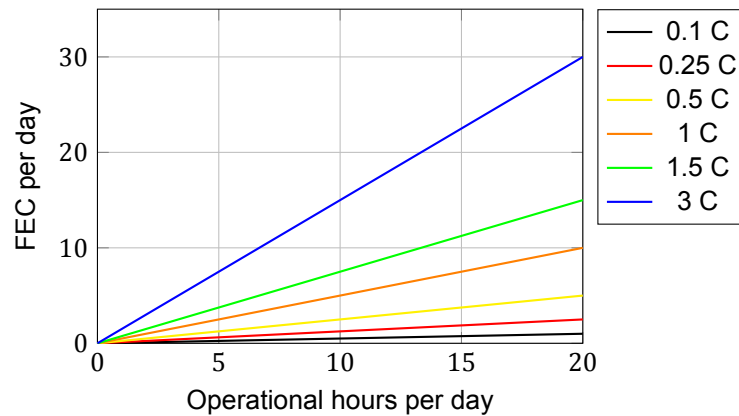


Figure 5.20: Estimation of performed FEC per day based on C-rate and operational hours per day

The two equations 5.1 and 5.2 can be used in different ways to determine the optimal battery size for a specific combination of operational hours per day, average C-rate and life expectancy. To determine the optimal battery size for the case of the tug and the ferry, the battery life and operational hours per day are fixed. Figure 5.21 shows the optimization steps that are taken.

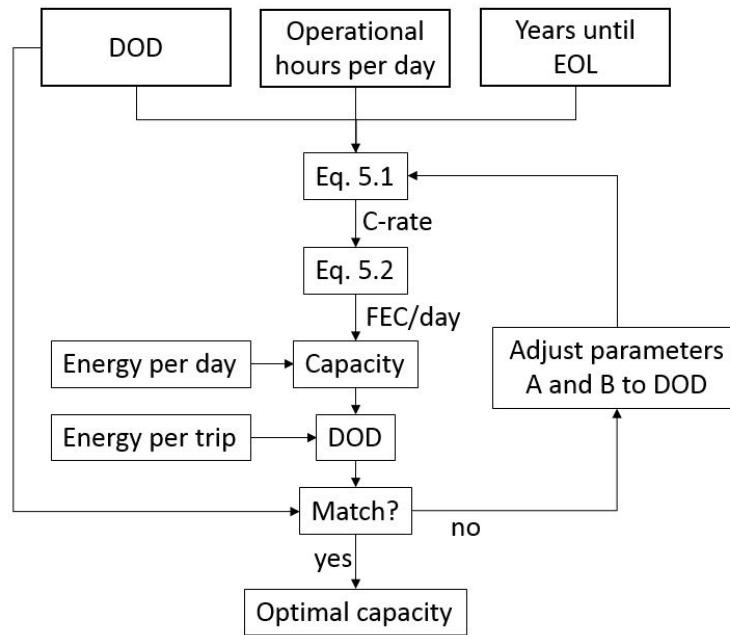


Figure 5.21: Optimization steps method 2

5.4.2. Case study: Harbour tug

Figure 5.22 shows the calculation steps in determining the optimal battery size for the harbour tug to have a ten year battery life. The first iteration results in a DOD of 40%, which does not match the used DOD of 20%. The second iteration results in a DOD of 37%, which is close to the used DOD of 40%. Therefore the capacity of 5038 kWh is determined to be the optimal battery size. This is lower compared to method 1, where the optimal battery size was determined at 5.5 MWh. This is most likely because method 2 does not take the heat generation into account during the moments of high load on the batteries.

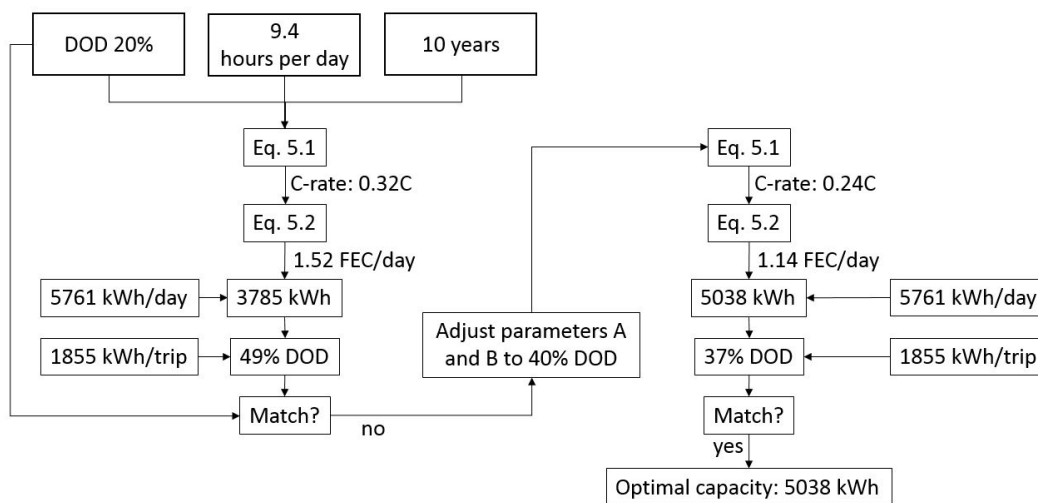


Figure 5.22: Steps to determine optimal battery size for 10 year battery life tug

5.4.3. Case study: Ferry

Figure 5.23 shows the calculation steps in determining the optimal battery size for the ferry to have a five year battery life and 14 operational hours per day. The first iteration results in a DOD of 23%, therefore the parameters for equation 5.1 are adjusted for a DOD of 25%. The second iteration results in a DOD of 18%. Apparently the optimal battery size is the average of the two calculated capacities for a DOD of 20% and 25%. This results in a capacity of 1008 kWh, which is similar as the optimal battery size calculated by method 1.

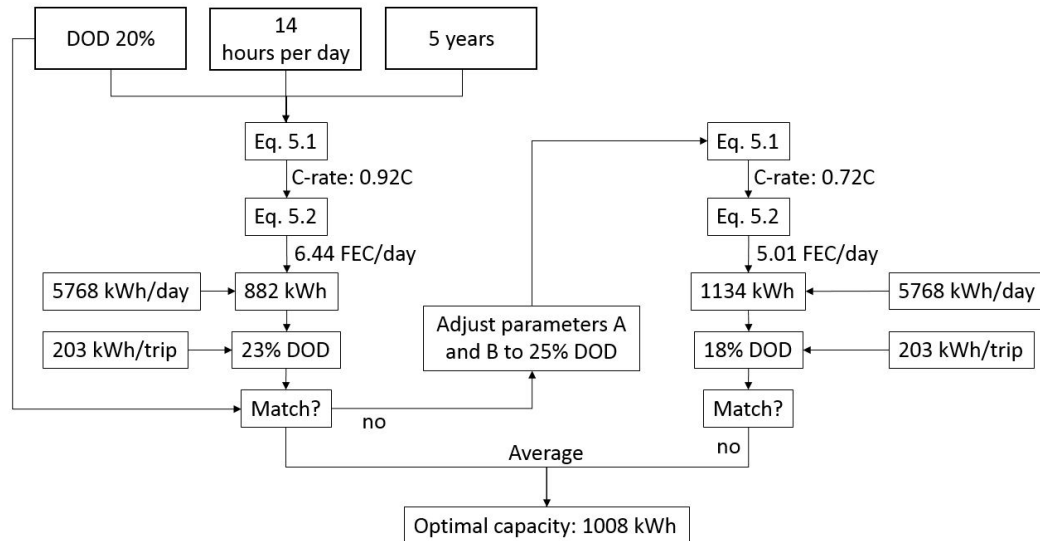


Figure 5.23: Steps to determine optimal battery size for 5 year battery life ferry

5.5. Evaluation optimization methods

Method 1, using the model to simulate different combinations of operational strategies and battery sizes, takes more time but is very useful to evaluate different operational strategies for the battery. Method 2 is much easier and faster to apply, but only uses the average operational profile. This makes method 2 less useful for ship types with a very versatile operational profile, like the tug. For the ferry, with a very constant operational profile, method 2 is a good battery size optimization tool. However, when the operational strategy needs to be determined, the model should be used to simulate various options for an accurate comparison.

6

Conclusions and recommendations

This chapter gives the conclusions and recommendations that follow from this research.

6.1. Conclusions

This research follows four steps. First the problem of selecting the appropriate battery for a full electric ship is investigated, then the aging of batteries is investigated, a model is developed to predict battery aging and finally all the findings are used to determine two methods of optimizing battery size and operational strategy for full electric ships. The conclusions in this sections are according to these same four steps.

6.1.1. Battery selection

There are 6 main selection criteria for batteries: capacity, power, longevity, costs, safety and dimensions. Depending on the requirements of the application, a trade off between functionality and redundancy has to be made to find the optimal combination of characteristics. Improving one criteria will cause others to worsen. Lithium-ion batteries are at the moment the most promising types for powering full electric ships because of the high energy density, high power density and the large amount of research that is being done to improve them. Within the lithium-ion type of batteries there are several sub-types. There is not one specific sub-type that is the best, but NMC and LFP are the most preferred for maritime use.

6.1.2. Battery aging

The aging of batteries is the loss of capacity and power over time and use. It is assumed that capacity loss is most important for full electric ships to predict and therefore power loss is not taken into account in this research. There are five main mechanisms that cause aging:

- Loss of free lithium
- Surface layer formation
- Electrode disintegration
- Material deterioration
- Contact deterioration

These mechanisms are affected in severity by four main causes:

- Temperature
- State of charge
- Depth of discharge
- Charge and discharge rates

There are two forms of aging, calendar and cycle aging. Calendar aging occurs continuously, independent of the battery being in operation or in storage. Temperature and state of charge are the conditions that affect calendar aging. Cycle aging occurs when the battery is being cycled. The depth of discharge, charge rates, discharge rates and the average state of charge are the conditions that affect cycle aging.

It is concluded for battery aging that even within a specific chemistry type, there is a large variation in aging rates per battery. There is not a standard procedure for aging measurements, which complicates the comparison between different studies.

6.1.3. Aging model

The answer to the research question: *"Can the aging of batteries be predicted based on the operational profile of a full electric ship?"*, is yes. This is proven by the proposed aging model. The model relies on three main calculations for the calendar aging, cycle aging and thermal behaviour of the battery cell

It is validated that the model is versatile to predict the aging of different types of lithium-ion batteries with only some minor adjustments to the parameters. Considering the large variations in the aging of similar cells the predictions of the proposed model have an acceptable accuracy, also compared to other models. It is verified that the proposed model can be used as a general prediction tool for the aging of batteries in full electric ships.

6.1.4. Optimal battery size and strategy

The model is used to perform a general analysis of the effects of different battery sizes and operational strategies to optimize battery life and effectiveness of use. The following is concluded from this analysis.

- A DOD of 20% leads to the highest combinations between life expectancy and effective battery use.
- The battery is cycled from approximately 50% to 30% SOC for the highest life expectancy.
- High C-rates only affect the aging rate a little and therefore are not a main concern for battery life.
- Resting periods to cool down the battery increase the life expectancy significantly.
- If the battery is charged short before the discharge, the average SOC, and therefore the calendar aging rate, is low.
- If the battery is operational for more than 5 hours per day, operating it for a longer period has only a little effect on life expectancy. Below 5 operational hours per day the life expectancy increases significantly.

The research question: *How can the combination of battery size and operational strategy for a full electric ship be optimized?*, is answered by the two developed methods of optimizing battery size and strategy considering the life expectancy and effective use of the battery. Method 1 consists of 4 steps:

- Evaluate strategy
 - Determine the operational profile of the ship
 - ◊ Energy per trip
 - ◊ Time per trip
 - ◊ Trips per day
- Determine capacity
 - Shape the operational profile of the battery
 - ◊ Operational hours per day
 - ◊ C-rate
 - ◊ DOD
 - ◊ Number of batteries
- Simulate life
 - Predict the life expectancy and effectiveness of battery use
 - ◊ Years until EOL
 - ◊ FEC per day
 - ◊ Energy per year
- Calculate costs
 - Determine the yearly costs for the battery
 - ◊ Installation costs
 - ◊ Replacement costs
 - ◊ Operational costs

Method 2 only focuses on the third step of method 1, predicting the life expectancy. Two equations to calculate the years until EOL and performed FEC are developed with the results from the general analysis. These equations use only the DOD, average C-rate and operational hours per day as input.

The two methods are used to analyze two case studies, a harbour tug and a ferry. The conclusions from these case studies are only applicable to these specific cases and should not be taken as generally true for those types of ships.

- Harbour tug
 - There is a limit for the benefits of enlarging the battery considering life expectancy, if the operational strategy is not adjusted to the battery size.
 - The battery is charged short before discharging for the highest life expectancy.
 - The optimal battery size has a capacity of approximately twice the energy demand for the largest job.
 - For a 10 year battery life a capacity of approximately 5.5 MWh is required.

- Ferry
 - The battery is discharged at a DOD of 20% for a good combination of efficiency and life expectancy.
 - If the ferry sails as slow as possible while staying within schedule, the battery is used optimal.
 - Battery replacement after 5 years is advisable.
 - A EOL deviating from the standard 80% SOH is necessary to achieve optimality in some cases.
 - For a 5 year battery life a capacity of approximately 1 MWh is required.

Optimization method 1, using the model to simulate different combinations of battery size and strategy, is more accurate, but also requires more work. It is the preferred method if the investigation of different strategies is important. Optimization method 2 is faster and is preferred for a quick determination of battery size when the average operational profile is known.

6.2. Recommendations

The work in this thesis results in some recommendations for further work on the research of battery aging, possible improvements of the model and more topics on full electric ships that should be investigated. Also the assumptions that are made are pointed out per subject.

6.2.1. Aging research

Recommended steps in further research on battery aging are:

- The effect of the temperature is different for calendar and cycle aging. It is currently assumed that the optimal temperature is around 20°C. However, there should be two optimal temperatures, one for during storage and one during cycling of the battery.
- The effect of a low SOC on calendar aging should be investigated further. In the aging tests that are used for this thesis it shows that the lowest aging rate is at the lowest SOC. However, it is assumed by some battery experts that the aging rate goes up at a lower SOC not only for cycle aging but for calendar aging as well.
- The aging behaviour after 80% SOH should be investigated further.
- The effect of C-rates is now assumed to be very little. The exact impact of high charge and discharge rates should be investigated further as well as the correlation with increasing temperatures.
- Every battery is unique in its aging behaviour. For an accurate prediction each battery should be tested before making assumptions.
- A standardized set of aging tests would make it easier to compare the tests of different batteries with each other and can help with understanding the differences per battery types.
- It is assumed that there are also other causes for battery aging, such as humidity, pressure, vibrations and impacts. However, not enough research has been performed on these causes and therefore are not taken into account in this research.

6.2.2. Battery aging model

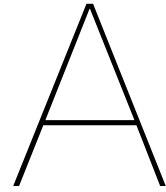
Recommended steps in the development and improvement of the proposed aging model are:

- The temperature has a very large influence on the aging of the battery. Therefore, the thermal behaviour of the battery should be modeled as accurately as possible. The proposed model uses a very basic method to simulate the generation of heat, the heat exchange between battery and surroundings and the thermal management system. Because the thermal behaviour is different for every type of battery cell, it will require in depth knowledge of the construction of the cell. It will be a challenge to develop a method which is versatile to quickly adjust to different types of batteries.
- There is a difference between the optimal temperature during cycling and during storage of the batteries which should be investigated further as recommended for the research on battery aging. This should then be applied in the model as well. The model now calculates calendar and cycle aging separately. Another, perhaps better, approach would be to combine the calculations for calendar and cycle aging, but to divide it in a calculation for storage conditions and cycle conditions.
- The temperature is assumed to be the leading cause for aging and therefore a thermal management system is added to the model. It is possible that the SOC will be more important than assumed, because the temperature is kept at more constant and lower temperatures.
- The effect of SOC on aging is in the proposed model defined as linear. The accuracy of the SOC effect can be improved by describing it with a polynomial equation. This would require more aging tests to determine if there is a general behaviour in the SOC effect for lithium-ion batteries.
- Aging consists of the capacity loss and power loss of the battery. For this thesis only the capacity loss has been taken into account, because it is assumed to be more important for full electric ships. The power loss will be related with the increase in internal resistance of the battery. This is not only influencing the aging behaviour of the battery, but also increases the heat generation during cycling. Therefore, for a more accurate model the internal resistance should be included.
- The effect of variable C-rates is assumed follow a quadratic curve and to be very small for the proposed model. More research on this topic should be performed and integrated with the internal resistance as well.
- The calendar aging rate changes related to the age of the battery. This should also be investigated and applied for the cycle aging rate.
- It is assumed that an absolute prediction error smaller than 2% in 50% of the simulations is acceptable for the general prediction method.
- The verification of the applicability of the aging model as a general prediction method is based on data from battery aging tests that lasted 3 years or shorter. It should also be verified with data from aging test that lasted 5 years and longer. Unfortunately this was not available.

6.2.3. Electric ships

For the research on fully battery powered ships the following steps are recommended:

- The model should be fitted to the battery cells that are used for maritime battery systems. Only then the optimal battery size and operational strategy for a specific ship can be determined. This will require aging tests on the specific cells as well as cooperation of the manufacturers.
- It is assumed that the installation costs for a marine battery system are €1000 per kWh and that the interests are 5%. The calculations for the costs of the battery system should be more precise for a better comparison between different battery sizes and operational strategies.
- Next to the costs for the battery system also the costs for the used electricity should be included to make an estimation of the operational costs as well.
- The difficulties and possibilities for on shore charging stations require more attention as well. The flexibility in the charging strategy is dependent on the availability of high power connections for the chargers. Adding a financial calculation to the building and utilization of the charging stations will improve the lifetime costs calculation.
- After reaching EOL the battery can be either recycled for its materials or used for a second life. The lifetime costs calculations will be complete if the after life strategies of the batteries will be investigated further.
- It is assumed that a charge power of 1.75 MW is the maximum to be realistic in most areas.



Background information

A.1. Electric ships

Battery powered ships have been around for more than 100 years, but most of them were small pleasure crafts. A small boat between 5 and 10 meters in length that carries only a handful of passengers at low speed is easy to power with batteries. But when sizes or required speed go up it becomes more of a challenge. Large battery systems in ships started out as a hybridization of the propulsion system, but recently some fully electric ships have been build that promise a bright future for zero emission shipping. This subsection provides an overview of the full electric ships that have been developed in recent years.

A.1.1. Ampere

The MF Ampere is the world's first all electric car ferry, operating between the Norwegian villages of Lavik and Oppedal. The design was a combined effort of Norled AS, Fjellstrand Shipyard, Siemens AS and Corvus Energy. The ship is a catamaran of 80 meters long and 21 meters wide. It can carry 360 passengers and 120 cars. The trip between Lavik and Oppedal is 5.6 km and takes about 20 minutes. The Ampere makes approximately 34 trips per day, with a 10 minute stop for loading and unloading at each side.



Figure A.1: The MF Ampere[26]

The ship has 8 battery packs with a combined capacity of 1040 kWh. There are 4 battery packs in a forward power station and 4 battery packs in an aft power station. Because the villages of Lavik and Oppedal are in a remote area of Norway the capacity of the local electric grid is too low to deliver the Ampere with the required power for fast charging in a direct connection. As a solution to this there are two extra battery packs, one at each side of the route. Both battery packs have a capacity of 410 kWh and are liquid cooled for extra fast discharges when the ship is connected. After the ship has left for the other side again the battery can be recharged at a slower rate from the grid. The batteries are fully charged at a slow rate overnight and after each trip they receive a burst of energy that is a little less than the energy used for the trip. Step by step the battery's charge level will go down until at the end of the day a full charge is required again. This allows the ship to keep the stops as short as 10 minutes before returning to the other side. The batteries are recharged using hydroelectric power from the grid. The operators claim to save 1,000,000 liters of diesel, 2680 metric tons of CO₂ and 37 metric tons of NO_x per year compared to the same service with a diesel powered ferry.[20]

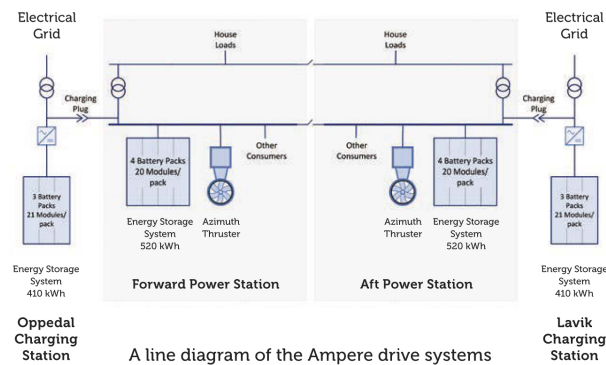


Figure A.2: Line diagram of Ampere drive systems[20]

A.1.2. BB Green

The BB Green is a prototype of a battery powered, air supported, high speed ferry. The design is a combined effort by European partners, funded by the European Commission and is built by Latitude Yachts. The BB Green has a top speed of 30 knots and a range of up to 14 nautical miles. The prototype is equipped with 200 kWh of lithium titanate batteries, offering high charging rates and a high number of cycles. The commercial version will be equipped with 400 kWh. The BB Green can carry up to 70 passengers. Due to the patented Air Supported Vessel (ASV) technology hull resistance is decreased. Propulsion is provided by two contra rotating pods for high maneuverability.[24]



Figure A.3: The BB Green[24]

A.1.3. Ar vag tredan

Ar vag tredan means "electric boat" in Breton and is a full electric ferry in Lorient, France. Although it is not a battery powered ship, it is very similar and therefore, interesting to add to this list. The electricity is stored in super capacitors, using static energy storage instead of chemical energy storage. The advantages of super capacitors over batteries are the high charge rates and the high cycle life. Disadvantages are the low energy density, high costs and poor ability to store energy over a longer period. The 22 meter long Ar vag tredan carries up to 147 passengers at a maximum speed of 10 knots. It makes trips of 10 minutes and then requires a 4 minute recharge. This operational profile is what makes the use of super capacitors in this case interesting.[21]



Figure A.4: The Ar Vag Tredan[21]

A.2. Environmental impact

The choice for a specific propulsion system to power a ship is usually based on economics. With current battery prices, fully battery powered ships are not yet an economical competitor of ships with conventional diesel powered propulsion systems. The choice for battery power must come from an environmentally driven demand. The term zero emission is preferred by most supporters of electrified transportation, but to the term zero emission can be interpreted in different ways. Usually it refers to the amount of CO₂ and NO_x that is produced. To rate fully battery powered ships on their environmental impact based on emissions, the life cycle of the batteries is investigated. Starting with the production of batteries, then the use of batteries and ending with the recycling of batteries.

A.2.1. Production of batteries

The first question that usually is asked when it comes to the environmental impact of battery production is on the possibility of material depletion when the demand for batteries increases. According to (McManus, 2012)[39] and (Gaines, 2012)[22], the world is very unlikely to run out of the materials required to produce batteries, such as lithium, even if the demand for batteries drastically increases.

The energy required to produce battery cells depends on multiple variables, such as geographical location, battery type and production process. In the life cycle assessment on lithium batteries performed in (Grenland, 2017)[25], a total energy equivalent of 200 Wh is calculated per produced Wh battery capacity. This will cover the production of batteries in most situations around the world. This is a safe estimation compared to the Tesla Gigafactory, where a total energy equivalent of 30 Wh [25] per produced Wh battery capacity is calculated to be required. The energy required to produce the batteries, relates to a specific amount of emissions produced by this used energy. To counter the produced emissions, the operational use of the batteries should result in a lower total production of emissions.

A.2.2. Energy source

The amount of produced emissions by a fully battery powered ship is dependent on the electricity that is supplied to the battery. The operating of the battery it self produces zero emissions. Depending on the location the ship is operating, the supplied energy can come from renewable sources or not, this is known as the electricity mix. In the life cycle assessment performed by (Grenland, 2017)[25] the comparison is made between the electricity mix of Norway, the European Union and a global average. The electricity mix in Norway is known to be low on emissions, for the EU it is a bit higher and the global average has the highest emission rates. In the life cycle assessment they compare the case of a fully battery powered ferry and the payback time on produced emissions in case of a different electricity mix. The payback time is calculated as the time it takes of operating the ferry using only batteries until it has produced less CO₂ and NO_x than a ferry with a conventional diesel propulsion system. This is shown in figure A.5, where first the emissions of battery production is taken into account and after that the emissions from the electricity mix, compared to the situation of the diesel powered ferry. According to the life cycle assessment by (Grenland, 2017)[25], the payback time for CO₂ emissions is 1.4 months for Norway, 2.5 months for the EU and 11.8 months globally. The payback time for NO_x is 0.3 months for Norway, 0.32 months for the EU and 0.35 months globally. This shows that the environmental impact of the production of batteries is easily overcome by the reduction in emissions by using batteries in stead of burning fossil fuels.

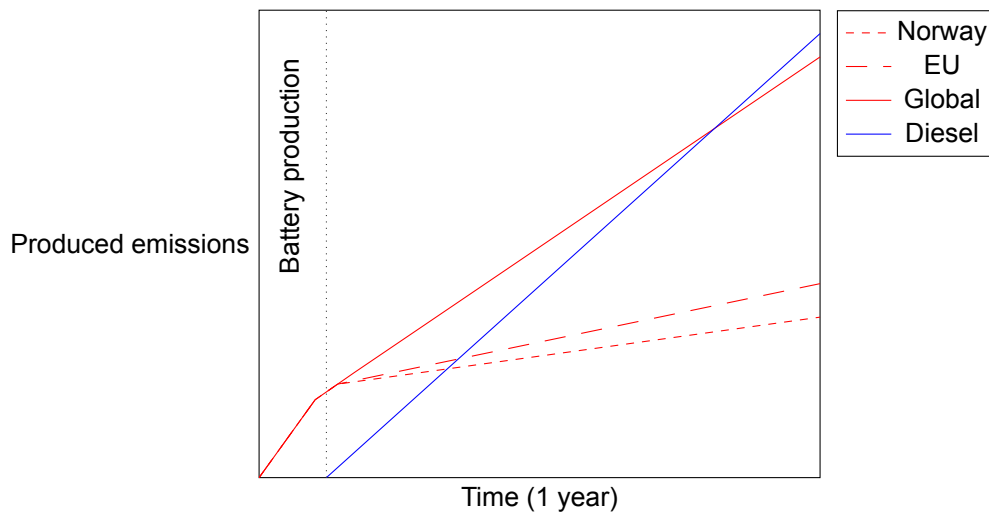


Figure A.5: Payback time on emissions fully electric vs. diesel

A.2.3. Recycling

The last step in the life cycle assessment for batteries is after reaching the end of life capacity. Usually this will be when the battery reaches a capacity of 80% of its original capacity. After this point there are two different options. The battery can be used as a second hand battery for a system with lower energy demands, or the materials in the battery are recycled.

The first option, using batteries that have reached their end of life capacity as second hand batteries is being experimented with at the moment. After reaching the end of life capacity the battery does not stop working. It still has about 80% of its original capacity. The problem with these batteries is that the batteries become more unreliable and it is difficult to say how long they will last. Using the batteries in systems that have a lower energy demand helps the batteries to stay operational longer. Also, the second hand battery cells need to have a similar remaining capacity and a lot of cell balancing is required. The selection of battery cells with a similar remaining capacity and the reassembling of the battery packs takes time and costs money. With the prices of new batteries decreasing every year, the costs for second hand batteries should be much lower to compete with new batteries. This appears to be difficult and therefore, the market for second hand batteries is not supported by everyone.[59]

The second and final option is to recycle the materials of the battery. Modern battery recycle facilities like Umicore in Belgium [61], can recover up to 95% of the materials in batteries and these can be used for the production of new batteries. This can potentially save up to 51.3% natural resources in the manufacturing of new batteries and saves up to 70% on CO₂ emissions compared to the battery production process using "virgin" materials.[1]

A.3. System boundaries

A battery can perform two types of operations, charging and discharging. Each operation is dependent on several limiting factors, determining the boundaries of the system. These boundaries are required for defining the scope of this research.

A.3.1. Charging

A connection to the electric grid is required to charge the battery. The electric grid is divided in different levels of power. In the Netherlands for instance, there are 3 main levels of grid power.[62] First is the inter-regional grid, transporting electricity at 220, 380 or 450 kV. Then the regional grid with 100 or 150 kV. The lowest power levels are at the distribution grid and are between 0.4 and 50 kV. To get a connection to the electrical grid, standard prices can vary from €4000,- for 100 kVA connection, to €300.000,- for a 5 MVA connection.[36] This is also dependent on the location and distance from the grid, which could lead to rising costs up to millions in some cases. The connection to the electrical grid will be more of an economical boundary than a technical boundary to the system. Connections up to 1.75 MVA can usually be made with the local distribution grid, for higher power connections a substation will be required to the regional grid. Another possibility will be to use existing connections. In and around ports there are connection points for ships. Using these connections are beneficial for the initial costs. However, they are usually not capable of delivering power above 25 KVA, resulting in very slow charges.

The charging schedule should also be determined considering the time of the day. The demand for electricity fluctuates heavily during the day. Figure A.6 shows the power demand in the Netherlands from November 24 at 00:00 hours until November 26 at 00:00 hours. During the nights the demand is the lowest, which causes the price for electricity to drop at those moments. Charging during the night can be beneficial if the operational profile of the ship allows it.

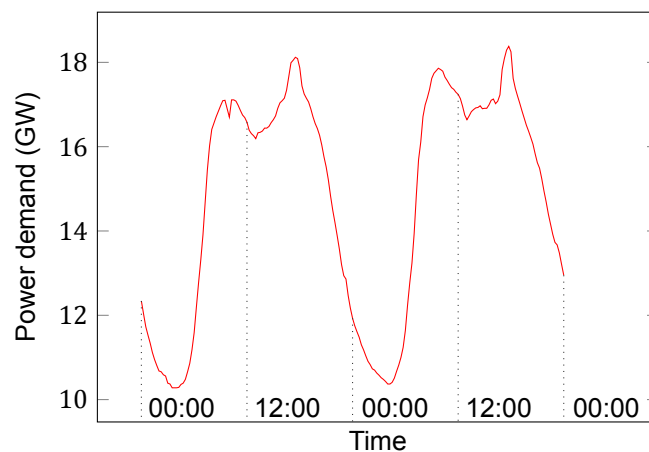


Figure A.6: Power demand in the Netherlands from November 24, 00:00 until November 26, 00:00 (2016) [58]

A.3.2. Discharging

The efficiency of discharging and charging a battery is described as the coulombic efficiency and is dependent on the temperature, SOC and C-rate. The voltage of the battery changes with the SOC and temperature. A higher SOC or higher temperature increases the voltage. For simplification of the proposed model it is assumed that the coulombic efficiency and

voltage are constant. Using real time voltage and charge throughput for the calculation of consumed power would be insignificant compared to the assumptions made for the calculation of faded capacity. Therefore, the power to and from the battery is described in kW and kWh. The power from the battery is used for propulsion and hotel loads.

When determining the optimal battery size and charging strategy for an electric ship it is important to know when the battery has to be replaced. Defining the end of life (EoL) of a battery is very arbitrary. Depending on the battery type, manufacturer, appliance or user the EoL can be at a different point in the battery's life. Most common is to determine the EoL to be the moment when the remaining capacity reaches 80% of the initial capacity. The first problem with this is that depending on the method of measuring the capacity can lead to large variations. The second problem with the 80% rule is that this doesn't mean that the battery doesn't work properly anymore. It might still be capable of performing the job perfectly. However, after reaching 80% of the original capacity the probability of increased capacity fading or even sudden battery failure does increase. Depending on the specific application and safety requirements the EoL capacity can be adjusted to fit the situation.

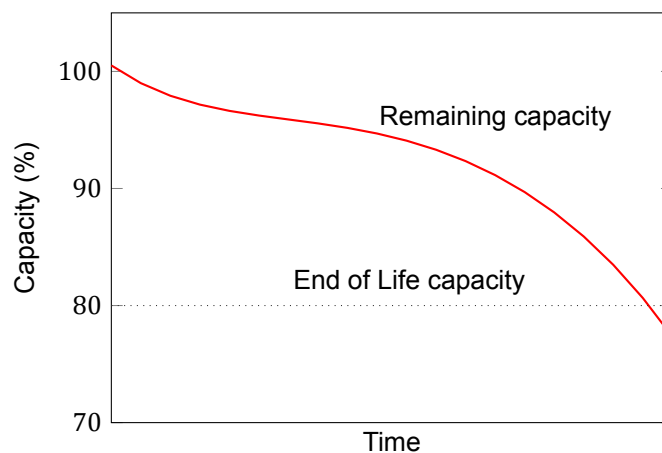


Figure A.7: Battery aging

An alternative to the predetermined 80% limit is to use the battery as long as it can perform the required operations of the specific application. Depending on the intensity of the operational profile, batteries can suffer more, or less, from aging. For an application with low and predictable loads on the battery, the EoL capacity can be decreased to for instance 70% or 60%, because of a smaller aging rate. First the operational profile needs to be determined. Safety margins need to be taken into account for in case the standard operational loads are exceeded by external influences. With the expected loads and safety margins an estimation of the aging rate can be determined. The required operational life will determine the initially required capacity. To improve the life expectancy of the battery a SOC below 10% and above 90% should be avoided. Figure A.8 shows the resulting effective use of battery capacity. The red parts at both ends are not being used to avoid high aging rates. The blue part is the determined acceptable capacity fade until reaching the EoL. The yellow part is the reserve capacity as safety margin and only the green part is effectively used for operations. The exact proportional sizes of each part of the battery's capacity differs per situation.

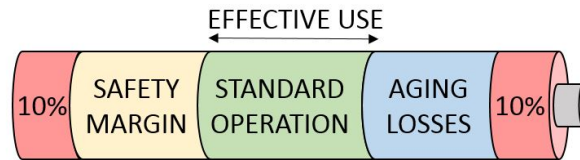


Figure A.8: Effective use of battery capacity

Another aspect that influences the determination of the EoL capacity is whether the battery is expected to have a second life or will be recycled. Depending on the possibility of battery reuse it can be an economically interesting option to sell the battery after reaching the 80% remaining capacity limit for the use in a less demanding application. For this option it can be advisable to stick to the 80% for a higher second-hand value. The feasibility of this option depends on the demand for second-hand batteries and the economical benefits compared to using the battery for a longer period before replacing it.

B

Aging test methodologies

B.1. Calendar aging

B.1.1. Keil et al.

Three different types of 18650 cylindrical cells are tested in this research, all with graphite anodes but different cathodes. A 2.8 Ah NCA cell from Panasonic, a 2.05 Ah NMC cell from Sanyo and a 1.1 Ah LFP cell from A123. The cells are stored at 3 different temperatures, 25°C, 40°C and 50°C and at 16 different SOC levels, 0, 5, 10, 20, 30, 40, 45, 50, 55, 60, 65, 70, 80, 90, 95 and 100%. The NCA and NMC cells are tested for their remaining capacity after 10 months of storage and the LFP cells after 9 months. The remaining capacity is measured at 25°C with the following method. First the cell is fully discharged at 1 A, then a resting period of at least 15 minutes is applied. After that, the cell is fully charged at 100 mA, followed by another resting period of at least 15 minutes. The cell then is fully discharged at 2 A, followed by another resting period of at least 15 minutes and a charge at 700 mA to until reaching a SOC above 50%. This method of a constant charge and discharge current is used because the cells have different capacities, but, electrodes of almost the same size. Applying the same C-rate to test the cells would induce higher stresses on the electrodes of the cells with a higher capacity, because the applied currents would be higher on the similar sized electrodes.[32]

B.1.2. MOBICUS

The MOBICUS project is a combined effort of twelve companies and research labs to perform research on the aging of lithium batteries for the use in electric vehicles. A 43 Ah NMC high energy battery is tested for calendar aging. The cells are tested at a SOC of 30 and 80% and at temperatures of 0, 25, 45 and 60°C. The remaining capacity is periodically calculated by applying a full discharge at a C-rate of 0.1C.[7]

B.1.3. Safari et al.

This research is performed on 2.3 Ah cylindrical 26650 LFP cells with graphite anodes. The cell are tested on calendar aging by storing them for a year at a temperature of 25°C or 45°C and a SOC of 50% or 100%. The remaining capacity was calculated by bringing the cells to a temperature of 25°C and applying a full charge and discharge at a very low 0.04C after 1, 3, 6, 9 and 12 months.[50]

B.1.4. Schmalstieg et al.

This research tested 2.05 Ah high energy cylindrical 18650 cells from Sanyo with NMC cathodes and graphite anodes. The cells are tested for both calendar and cycle aging. The cells are stored at a temperature of 50°C and at variable SOC levels of 0, 10, 20, 30, 50, 60, 70, 80, 85, 90 and 95% for calendar aging tests. Every test condition is used to test three cells and the average is used as result. The remaining capacity of the cells is measured at a temperature of 35°C by applying a full charge and discharge at a C-rate of 1C. After every seven weeks of storage for calendar aging and after every 100 cycles for cycle aging. A wide variety of DOD and mean SOC combinations is tested, but only the results of the test series at a DOD of 10% are known. The tests are performed at six different mean SOC levels; 10, 25, 50, 75, 90 and 95%.[55]

B.1.5. SIMCAL

A total of 6 different cells have been tested on calendar aging in the SIMCAL project. A 7 Ah NCA cylindrical cell from SAFT, a 12 Ah NMC pouch cell from Kokam, a 5.3 Ah LMO-NMC pouch cell from LGChem, an 8 Ah LFP cylindrical cell from LiFeBatt, a 15 Ah LFP cylindrical cell from LiFeBatt and a 2.3 Ah LFP cylindrical cell from A123 Systems, all with graphite anodes. Three cells were tested at nine different combinations of temperature and SOC of each battery. The used storage conditions are temperatures of 30, 45 and 60°C, and SOC levels of 30, 65 and 100%. The remaining capacity is tested after each 15 days to 2 months, depending on the aging conditions. The measurements are done at a temperature of 25°C and by a full charge and discharge at 1C.[15]

B.2. Cycle aging

B.2.1. Deshpande et al.

In this research, 2.2 Ah 28650 cylindrical LFP cells with a graphite anode from A123 Systems are tested on cycle aging. The cells are tested at temperatures of 15°C, 45°C and 60°C. Charging and discharging is done at a C-rate of 0.5C. The batteries are fully charged and subsequently discharged to 90% DOD for every cycle. The cells rested for a maximum of two days after every full charge. The tests are stopped after every 1 or 2 months to perform four different characterization tests; capacity characterization, relaxation, electrochemical impedance spectroscopy and hybrid pulse power characterization. The capacity was measured at a discharge C-rate of 0.05C.[16]

B.2.2. Liu et al.

2.2 Ah cylindrical LFP cells with graphite anodes from A123 Systems are tested on cycle aging in this research. The cells are cycled at temperatures of -30, 0, 15, 45 and 60°C. The results for the tests at -30 and 0°C are not taken into account because battery cells inside a ship are unlikely to reach these temperatures. The cells are cycled at 10, 20, 50, 80 and 90% DOD at C-rates of 0.5, 2, 6 and 10C. The remaining capacity is periodically measured with a 0.5C discharge.[38]

B.2.3. Omar et al.

This research tested 2.3 Ah cylindrical LFP cells with graphite anodes for cycle aging. Three battery cells are used for testing each condition. The average result of the three cells is taken as the end result. One part of the cells is cycled at a fixed C-rate of 1C and variable DOD

of 100, 80, 60, 40 and 20%. The other part of the cells is cycled at a fixed DOD of 100% at C-rates of 5, 10 and 15C. The temperature is kept at around 20 to 25°C. After every charge and discharge the batteries are rested for 30 minutes. After every 50 cycles the battery cells are tested for their remaining capacity by first applying a 6 hours resting period and after that a 1C full discharge.[44]

B.2.4. Peterson et al.

Four different production lots of 2.3 Ah cylindrical 26650 LFP cells from A123 Systems are tested on cycle aging in this research. The cells are cycled at a temperature of 25°C, and from being fully charged to a DOD of 34, 35, 48, 49, 57, 59, 72, 73 and 97% at a C-rate of 0.5C. After every cycle the batteries rest 5 minutes. The cells are fully charged and discharged at 0.5C with a resting period of 5 minutes between charging and discharging to calculate the capacity after every 100 cycles.[47]

B.2.5. Saxena et al.

LCO pouch cells with a nominal capacity of 1.5 Ah and graphite anodes are tested for cycle aging with this research. The cells are cycled at a temperature of 25°C at multiple combinations of DOD, mean SOC and C-rate. The C-rates that are used are 0.5C and 2C. The combinations of DOD and mean SOC are 100% DOD at 50% mean SOC, 60% DOD at 50% mean SOC, 20% DOD at 50% mean SOC, 60% DOD at 70% mean SOC and 60% DOD at 30% mean SOC. The remaining capacity is calculated by applying a full charge and discharge at 0.5C.[54]

B.2.6. Watanabe et al.

A 0.4 Ah cylindrical NCA cells is tested on cycle aging and the influence of high temperatures. The charge and discharge cycles are performed at 25°C and 60°C and at a C-rate of 1C. Two different DOD ranges are tested on both temperatures, one with a DOD of 60% and a mean SOC level of 40% SOC, and one at a DOD of 100% and a mean SOC 50%. The remaining capacity is measured every 50 cycles for the first 500 cycles. This increased to 500 cycles after performing 500 cycles and up to 2500 cycles. The capacity measurements are done by performing a full charge and discharge at a C-rate of 1C.[66]

B.2.7. Wang et al.

A 2.2 Ah LFP 26650 cylindrical cell from A123 Systems is tested on cycle aging for this research. The tests are performed at multiple combinations between temperatures of 0, 15, 25, 45 and 60°C, C-rates of 0.5, 2, 6 and 10C and DOD ranges of 10, 20, 50, 80 and 90%. Two cells are tested at each condition. The cells are fully cycled twice at a C-rate of 0.5C to calculate the remaining capacity. They are tested every 1 or 2 months for their remaining capacity, depending on the aging rates.[65]

B.2.8. Wong et al.

Three 3 Ah NCA cells are tested on the effect of high charge rates on cycle aging. All cells are cycle at a DOD of 50% at a mean SOC of 75%. One cell is cycled at a C-rate of 1C, one at 25C and one with pulses of 83C. The remaining capacity is calculated by applying a full charge and discharge at a C-rate of 1C.[67]

B.3. Calendar and cycle aging

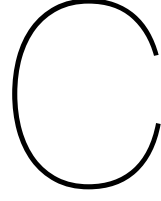
B.3.1. Ecker et al.

This concerns two different aging tests. The first test is performed on 6 Ah NMC high power pouch cells with a graphite anode. The batteries are stored at the following ten different combinations of temperature and SOC; 25°C and 80% SOC, 35°C and 20% SOC, 35°C and 50% SOC, 35°C and 100% SOC, 50°C and 20% SOC, 50°C and 50% SOC, 50°C and 80% SOC, 50°C and 100% SOC, 65°C and 50% SOC and 65°C and 100% SOC. Three cells are tested at every combination of temperature and SOC for relevant statistics. The remaining capacity is measured at a discharge rate of 1C after every 6 weeks of cycling.[17]

The second tests are performed on 2.05 Ah high energy NMC cylindrical 18650 cells with graphite anodes, the Sanyo UR18650E. The cells are tested on both calendar and cycle aging. Calendar aging is tested at 35°C and 50% SOC, 40°C and 50% SOC and 50°C and a SOC of 0, 10, 20, 30, 50, 60, 70, 80, 85, 90, 95 and 100%. Cycle aging is tested at a temperature of 35°C and a C-rate of 1C. The batteries are cycled at a DOD of 5, 10, 20, 50, 80 and 100%, around different mean SOC levels. Three cells are tested at each condition. The cells are tested on their remaining capacity after every 7 weeks of storage for calendar aging and after every 3 weeks of cycling for cycle aging. Capacity is measured at a discharge rate of 1C and a temperature of 35°C. The tests are stopped when the cells reach a remaining capacity of 70% compared to the initial capacity.[18]

B.3.2. Sarasketa et al.

High power 2.3 Ah 26650 cylindrical LFP cells with graphite anodes are tested for both calendar and cycle aging in this research. For calendar aging the cells are stored at 30°C and 70% SOC, 40°C and 30% SOC, 40°C and 70% SOC, 40°C and 90% SOC, 50°C and 70% SOC and 50°C and 90% SOC. Three cells are used to test each different condition. The remaining capacity was measured at a temperature of 25°C by performing three consecutive full charges and full discharges at 1C.[51] The same type of cells are used for the cycle aging tests. The cycles are all performed at 1C and at a DOD of 5, 10, 30, 50, 60 and 100% at a mean SOC of 50%. The remaining capacity is measured at the same conditions as for calendar aging, by performing three consecutive full charges and discharges at 25°C and a C-rate of 1C.[52]



Aging models

C.1. Li et al.

The model by Li et al. (2011)[35] is based on the degradation of LFP batteries. Five stress factors are determined, ambient temperature, end of discharge voltage (EODV), end of charge voltage (EOCV), discharge rate and charge rate. The standard levels of these stress levels are determined as well as the increased stress levels, see table C.1.

Table C.1: Overview of stress factor levels for empirical aging model by Li(2011)[35]

Levels of stress factors battery aging					
Stress level	Temperature	EODV	EOCV	Discharge rate	Charge rate
Standard	30°C	2V	3.65V	1/3C	1/3C
High	45°C	1.25V	3.95V	4C	1.5C

For each increased stress level, the standard capacity fade rate (SCFR) is determined experimentally. The SCFR is defined as the capacity loss in Ah per cycle. After determining the SCFR for each stress factor individually, the stress factors are coupled and the SCFR for combinations of two increased stress factors is determined. The SCFR for each stress factor is described by the following equations.

$$SCFR_T = \frac{b}{A_T e^{C_T/T}} \quad (C.1)$$

$$SCFR_{EODV} = \frac{b}{B_{EODV} v_{EODV}^{-D_{EODV}}} \quad (C.2)$$

$$SCFR_{EOCV} = \frac{b}{B_{EOCV} v_{EOCV}^{-D_{EOCV}}} \quad (C.3)$$

$$SCFR_{DR} = \frac{b}{B_{DR} I_{DR}^{-D_{DR}}} \quad (C.4)$$

$$SCFR_{CR} = \frac{b}{B_{CR} I_{CR}^{-D_{CR}}} \quad (C.5)$$

Here, $b = a - y_{sec}$, where a is the initial capacity and y_{sec} is the end of life capacity. The factors A and B are multiplier factor parameters and factor C and D are power factor parameters. T is the temperature in K, I is the discharge or charge C-rate and v is the end of discharge or end of charge voltage. To calculate the total capacity fade rate ($SCFR_0$), the combined stresses are corrected and coupled to form equation C.6. δ_1 to δ_{10} are coupling correction factors that are determined experimentally.

$$\begin{aligned}
SCFR_0^c = & \frac{\delta_1}{4}(SCFR_T + SCFR_{DR}) + \frac{\delta_2}{4}(SCFR_T + SCFR_{EODV}) + \frac{\delta_3}{4}(SCFR_T + SCFR_{CR}) \\
& + \frac{\delta_4}{4}(SCFR_T + SCFR_{EOCV}) + \frac{\delta_5}{4}(SCFR_{DR} + SCFR_{EODV}) + \frac{\delta_6}{4}(SCFR_{DR} + SCFR_{CR}) \\
& + \frac{\delta_7}{4}(SCFR_{DR} + SCFR_{EOCV}) + \frac{\delta_8}{4}(SCFR_{EODV} + SCFR_{CR}) + \frac{\delta_9}{4}(SCFR_{EODV} + SCFR_{EOCV}) \\
& + \frac{\delta_{10}}{4}(SCFR_{CR} + SCFR_{EOCV})
\end{aligned} \tag{C.6}$$

In the research performed by Li et al. it is claimed that the developed model has an accuracy of 15% when the cycling reaches the stable decay period. If this accuracy is achieved over the full life of the battery, and an end of life capacity of 80% of the initial capacity is retained, this would be equal to an uncertainty of 3% at the end of life. So the remaining capacity of the battery could be somewhere between 83% and 77% of the initial capacity. All the stress factors that are defined in this model correspond to the aging causes defined in chapter 3. Overcharging, over-discharging, the depth of discharge and mean SOC levels are all expressed by the coupling of the EOCV and OEDV. The effect of charging and discharging C-rates is separated and the temperature is also taken into account. The problem with this model is that all capacity fade rates are calculated per cycle. Therefore, only cycle aging can be calculated and not calendar aging. In chapter 3 is shown that calendar aging plays an important role in the overall aging of batteries and that the temperature is an important factor in that. Also, the capacity fade rates and coupling factors are only determined on a standard stress level and an elevated stress level. To calculate the aging at other conditions it is assumed that the aging behaviour of the battery is linear, although chapter 3 clearly shows the non-linearity of battery aging behaviour.

C.2. Omar et al.

In Omar et al.(2014) [44], four equations are proposed for modeling the aging of LiFePO4 batteries. Equation C.7 describes the cycle life based on the temperature (T). Equation C.8 describes the cycle life based on constant discharge current rates (I_d). Equation C.9 describes the cycle life based on the depth of discharge (DOD). Equation C.10 describes the cycle life based on constant charge current rates (I_{ch}). Parameters a to p need to be fitted for the specific battery cell. The proposed model does not describe the degradation of battery capacity or power, but predicts the number of cycles the battery performs until reaching the end of life capacity.

Figure C.1 shows the expected number of cycles that can be performed at different temperatures according to equation C.7. The parameters of the equation are fitted to the test performed on a LFP cell. The behaviour of this equation from 20°C upward shows some similarity to the theory and to the findings in chapter 3. With an increasing temperature, the aging rate increases and therefore, less cycles can be performed until reaching the end of life. However, according to figure C.1, no cycles can be performed at a temperature of 60°C or above. Although from other researches it is clear that capacity fades rapidly above 60°C, it is not likely that a battery can't perform a single cycle at that temperature. The research in chapter 3 does not include temperatures below 20°C. However, the prediction in figure C.1 is in line with the theory that at temperatures below 20°C the internal resistance of the battery increases and the aging rate increases as a result.

$$CL(T) = a \cdot T^3 - b \cdot T^2 + c \cdot T + d \tag{C.7}$$

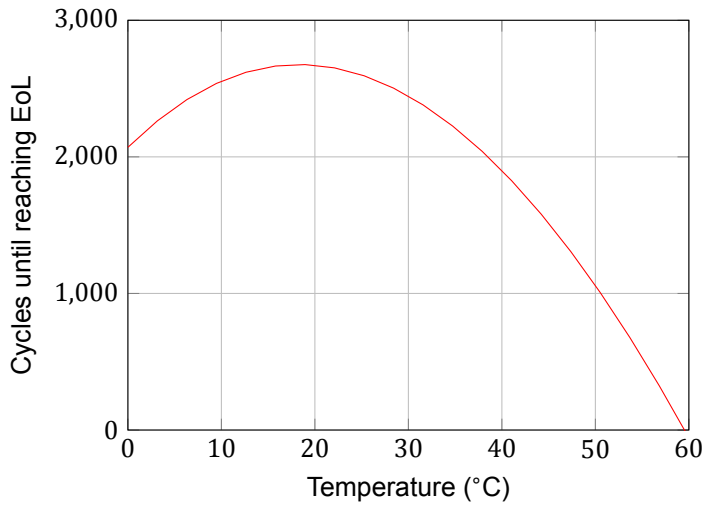


Figure C.1: Effect of temperature on cycle life according to model Omar et al.[44]

Figure C.2 shows the number of cycles predicted by equation C.8. The behaviour is fairly similar to the theory that the aging rate increases with an increasing C-rate. Remarkable is that according to this equation the increase in aging rate becomes less above 6C. This is can't be found in the theory or in any previous research.

$$CL(I_d) = e \cdot e^{(f \cdot I_d)} + g \cdot e^{(h \cdot I_d)} \tag{C.8}$$

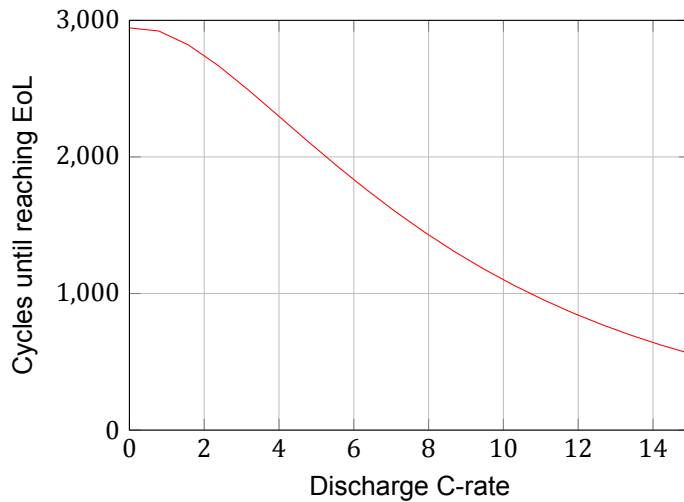


Figure C.2: Effect of discharge C-rate on cycle life according to model Omar et al.[44]

Figure C.3 shows the actual measured cycles during the aging tests with the red line. The blue dots represent the full equivalent cycles of the measured data. The blue line represents the fitted equation C.9. On average the fitted equation might show a similar trend to the development of aging in combination with the depth of discharge. However, just as with the data in chapter 3, a small DOD is not always similar to a larger number of full equivalent cycles. In this particular situation a DOD of 40% shows to have the lowest effect on the aging rate.

$$CL(DOD) = i \cdot e^{(j \cdot DOD)} + k \cdot e^{(l \cdot DOD)} \tag{C.9}$$

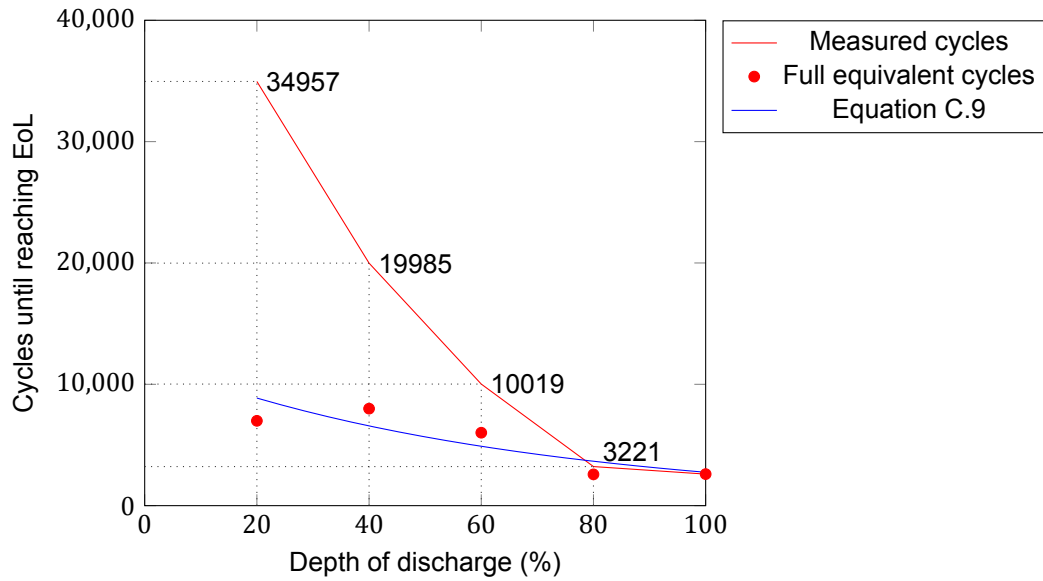


Figure C.3: Effect of depth of discharge on cycle life according to model Omar et al.[44]

Figure C.4 shows the fitted equation C.10 for the effect of the charge C-rate on the aging of the battery. The effect of the charge rate as proposed here does not show many similarities to the previous findings in chapter 3. This equation implies that above a C-rate of 6C, increasing the C-rate will have close to no effect on the aging rate. Also it implies that at a C-rate below 1C, decreasing the C-rate will exponentially decrease the aging rate. Batteries are usually charged with C-rates below 1C, such strong effects on the aging rate have not been encountered in that range.

$$CL(I_{ch}) = m \cdot e^{(n \cdot I_{ch})} + o \cdot e^{(p \cdot I_{ch})} \tag{C.10}$$

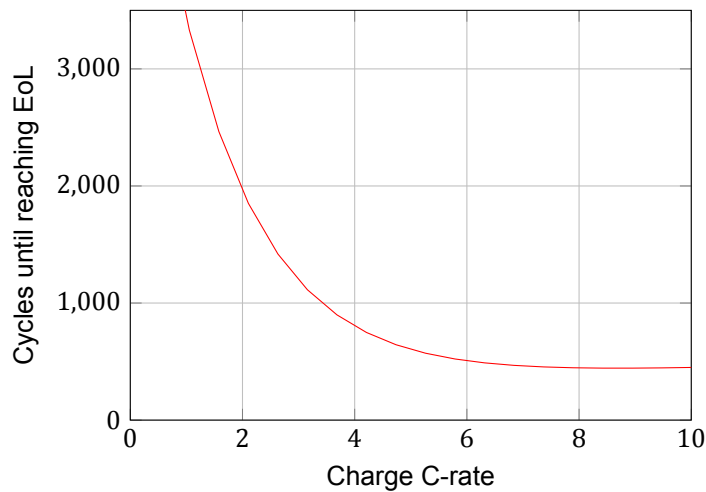


Figure C.4: Effect of charge C-rate on cycle life according to model Omar et al.[44]

The four equations proposed by Omar et al. are not linked to each other. From previous research it has been shown that the different stress factors do influence each other on the effects on the aging rate. The proposed model calculates the aging in terms of performed cycles until reaching the end of life and is calculated based on averages per cycle. Therefore, only cycle aging is taken into account and not calendar aging. Also the mean SOC levels are not taken into account for cycle aging.

C.3. Saxena et al.

The model developed by Saxena et al.(2016)[54] is based on the effects of DOD and mean SOC (μ_{SOC}) on the aging at constant temperature and C-rates. The model exists of one equation (eq.C.11) expressing the normalized discharge capacity (NDC) in percentage calculated by the performed full equivalent cycles (FEC). The parameter k_1 , k_2 , k_3 and b are fitted on test results from a LCO battery cell at a temperature of 25°C and C-rate of 0.5C.

$$NDC(\%) = 100 - k_1 \cdot \mu_{SOC} \cdot (1 + k_2 \cdot DOD + k_3 \cdot DOD^2) \cdot (FEC/100)^b \quad (C.11)$$

Where,

$$k_1 = 3.25 \quad k_2 = 3.25 \quad k_3 = -2.25 \quad b = 0.453$$

The model is based only on the capacity measurements for the first 500 performed cycles for two reasons. Firstly, the aging tests are not continued after 500 cycles for every testing condition. Secondly, because the aging rate increased significantly above 500 performed cycles at 100% DOD. This suggest a different aging mechanism to be dominant, which would need a different model.

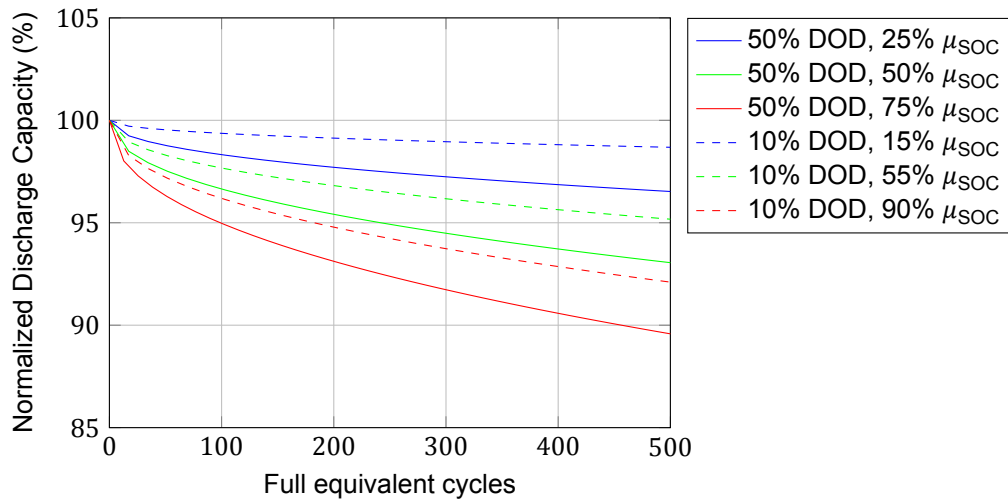


Figure C.5: Effect of DOD and mean SOC on cycle life according to model Saxena et al.[54]

Figure C.5 shows the predicted normalized discharge capacity based on equation C.11. The solid lines represent the aging at a DOD of 50%, and at a mean SOC of 25%, 50% and 75%. The dashed lines represent the aging at a DOD of 10%, and at a mean SOC of 15%, 55% and 90%. The general behaviour of the model is similar to the results in chapter 3. A higher mean SOC and a higher DOD cause the aging rate to increase. Also, the power factor b results in a similar relationship between the aging rate and performed equivalent full cycles. The power factor b is 0.453 in this situation, which is close to the 0.5 as discussed in section 3.4.3. The limitations of this model are that it is only applicable to fit to only one aging mechanism, it has to be fitted separately for each different cycling condition and it does not include calendar aging.

C.4. Schmalstieg et al.

The model by Schmalstieg et al.(2013)[55] calculates the total capacity loss based on calendar aging and cycle aging. An equation is given for the calendar aging rate α and another for the cycle aging rate β . Both aging rates are used in a single equation to calculate the remaining capacity C . The calendar aging rate is calculated based on the voltage and temperature,

equation C.12. The voltage represents the effect of state of charge and the temperature is in Kelvin. Constants k_1 to k_7 are fitted by performing aging tests on a series of battery cells.

$$\alpha = (k_1 \cdot V - k_2) \cdot 10^6 \cdot e^{-\frac{k_3}{T}} \quad (\text{C.12})$$

The cycle aging rate is calculated based on the mean Voltage and the depth of discharge, equation C.13. The mean voltage represents the mean SOC and the DOD is in percentage.

$$\beta = k_4 \cdot (\mu V - k_5)^2 + k_6 + k_7 \cdot DOD \quad (\text{C.13})$$

The total remaining capacity is calculated by equation C.14. The calendar aging rate is multiplied with the time in days to the power of 0.75. The cycle aging rate is multiplied with the square root of the charge throughput in Ah.

$$C = 1 - \alpha \cdot t^{0.75} - \beta \cdot Q^{0.5} \quad (\text{C.14})$$

Figure C.6 shows the total remaining capacity, as well as the contribution from both calendar and cycle aging, for a NMC battery cell at 3.8V, 30°C and a DOD of 50%. The battery performs one cycle per day. This model agrees with the conclusion from section 3.5.4 that the calendar aging is dominant over the cycle aging. The power factor for the effect of charge throughput is again 0.5, similar to the conclusion in section 3.4.3. However, the power factor for the effect of the storage time is 0.75. Table 3.3 shows that for the tested NMC batteries the power factors are higher compared to the other battery types (0.624 and 0.617). This might be caused by the higher temperature, or it is a characteristic of NMC batteries for calendar aging. More test results are required for a final conclusion on this matter.

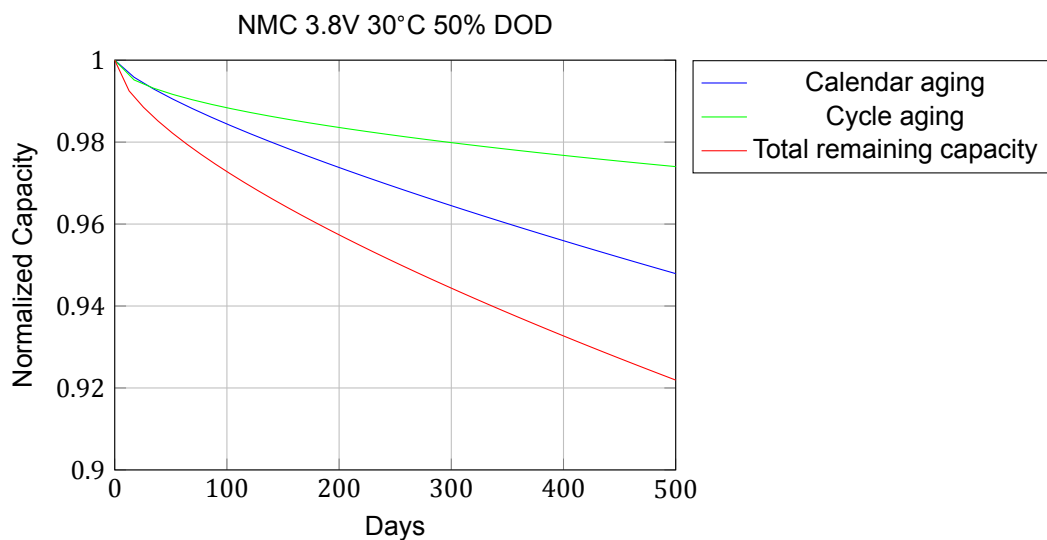


Figure C.6: Remaining capacity according to model by Schmalstieg et al.[55]

C.5. Ecker et al.

In Ecker et al.(2012) [17], a semi-empirical model is proposed based on the time (t), temperature (T) and voltage (V), eq. C.15. Where $L_{cal}(t_0, T, V)$ is the initial capacity of the battery. $F(t)$ describes the time dependency and is given by equation C.16. Here, c_a is a coefficient describing the rate of aging at reference conditions T_0 and V_0 . SEI layer formation is assumed to be the dominant aging process and therefore β is 0.5. The effect of storage temperature is given by $B(T, V)$ in equation C.17. Here, T and V are the actual temperature in °C and voltage

in V. ΔT is set at 10°C, meaning an increase in temperature of 10°C results in an increase in aging by a factor C_T . The same yields for ΔV , which is set at 0.1V, which will lead to an increase in aging by a factor C_V .

$$L_{cal}(t, T, V) = L_{cal}(t_0, T, V) \cdot (1 + B(T, V) \cdot F(t)) \quad (C.15)$$

$$F(t) = c_a \cdot t^\beta \quad (C.16)$$

$$B(T, V) = C_T \frac{T-T_0}{\Delta T} \cdot C_V \frac{V-V_0}{\Delta V} \quad (C.17)$$

This model does not predict the effect of temperature on aging correctly. A lower temperature results in a lower aging rate, independent of how low the temperature is. Sub-zero temperatures are also decreasing the aging rate, although the optimum should be around 20°C. It also is mainly suited as a static model, because the effects of temperature and voltage are always with respect to a predetermined reference condition and not to the previous state of the battery.

C.6. Magnor et al.

In the model proposed by Magnor et al.(2009)[19] an aging factor for calendar aging (eq. C.18) and for cycle aging (eq. C.19) is developed to determine the effect of battery size and operational use on the life cycle cost of the system. The calendar aging rate is dependent on the temperature, SOC and time. For this model it is required to know the reference calendar lifetime $t_{cal,ref}$ at specific conditions of T_0 and SOC. Also the maximum number of cycles ($N_{max,DOD}$) at each DOD has to be determined in advance.

$$c_{calendar} = \frac{1}{t_{cal,ref}} \cdot \int_{t_0}^{t_1} \frac{2^{\frac{T_{bat}-T_0}{\Delta T}}}{a + b \cdot \exp(c \cdot (100 - SOC))} dt \quad (C.18)$$

$$c_{cycle} = \sum_i \frac{N_{DOD}}{N_{max,DOD}} \quad (C.19)$$

After calculating the expected lifetime (L) in years for a specific operational profile, the total life cycle costs (LCC) are calculated by dividing the investment costs over the expected lifetime in years and the delivered energy per year. There are two parts of this model that are interesting. Firstly, the method to determine the cycle aging rate. This is based on information that is usually available from the battery manufacturer, a so called Woehler curve. Secondly, the calculation of the LCC to determine the effect of battery size and operational profile. However, this is only simply integrated in the model and can use improvements.

C.7. Sarasketa-Zabala et al.

The model developed by Sarasketa et al. (2016)[53] is based on a LFP 26650 cylindrical cell, but by adjusting the fitting parameters the model is also applicable to other lithium batteries. The calendar aging is dependent on the temperature and the state of charge of the battery cells. The capacity loss caused by calendar aging ($Q_{loss,cal}[\%]$) is described by equation C.20. The parameters α_1 , α_2 , β_1 and β_2 need to be fitted on the data from the aging test measurements. Also for this model the calendar aging rate has a dependency on the square root of time.

$$Q_{\text{loss,cal}}[\%] = \alpha_1 \cdot \exp(\beta_1 \cdot T^{-1}) \cdot \alpha_2 \cdot \exp(\beta_2 \cdot \text{SOC}) \cdot t^{0.5} \quad (\text{C.20})$$

The capacity loss caused by cycle aging is described by two different equations, eq.C.21 and eq.C.22, depending on the depth of discharge and charge throughput. The C-rate is not directly integrated in these equations. The assumption is made that the effect of the C-rate on battery aging is accounted for by this equation for most acceptable C-rates. The DOD and C-rate effects are dependent at most DOD levels and investigating their separate influences would require a large amount of extra experimental work.

For, $10\% \leq \text{DOD} \leq 50\%$

$$Q_{\text{loss,cyc}}[\%] = (\gamma_1 \cdot \text{DOD}^2 + \gamma_2 \cdot \text{DOD} + \gamma_3) \cdot \text{Ah}^{0.87} \quad (\text{C.21})$$

For, $\text{DOD} < 10\%$ and $\text{DOD} > 50\%$

$$Q_{\text{loss,cyc}}[\%] = (\alpha_3 \cdot \exp(\beta_3 \cdot \text{DOD}) + \alpha_4 \cdot \exp(\beta_4 \cdot \text{DOD})) \cdot \text{Ah}^{0.65} \quad (\text{C.22})$$

The fitting of the parameters is done by performing two aging tests, one for calendar aging and one for cycle aging. The least squares method is used to fit the equations to the measured data. For determining the fitting parameters for calendar aging, a test at certain combinations of temperature and state of charge is required. For the LFP 26650 cell, 5 tests are performed (Sarasketa-Zabala et al.(2014) [51]). At 30°C and 70% SOC, at 40°C and 30%, 70% and 90% SOC and at 50°C and 70% SOC. In figure D.14 the data points of the aging tests and their fitted curves are shown.

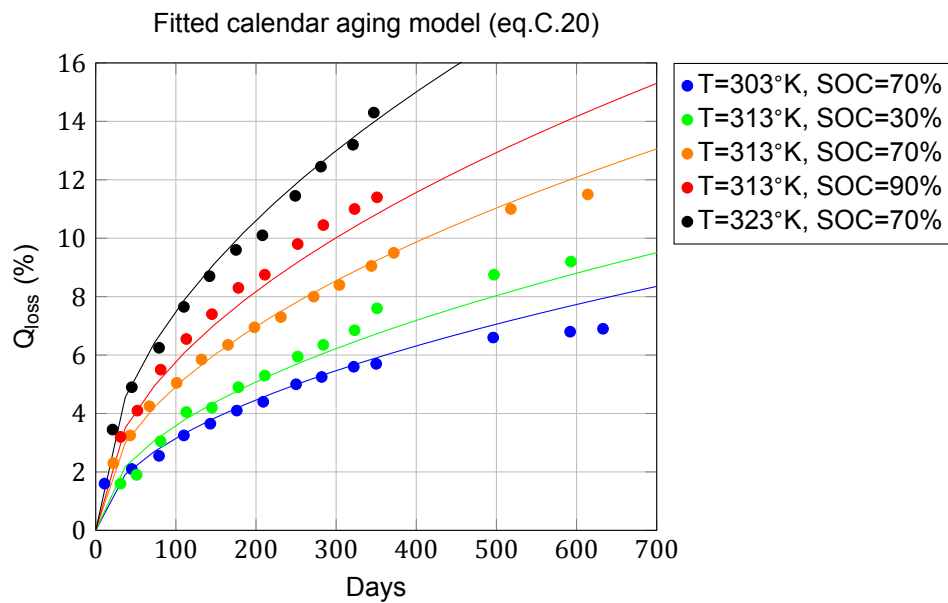


Figure C.7: Calendar aging data fitting

For determining the fitting parameters for cycle aging, a test at a C-rate of 1C and at several different depths of discharge is required. For the LFP 26650 cell, 6 tests are performed (Sarasketa-Zabala et al.(2015) [52]). For the test, each battery is cycled at 5%, 10%, 30%, 50%, 60% or 100%. In figure ?? the data points of the aging tests and their fitted curves are shown. There is a clear difference between the curves of the two equations. The equation

for a DOD between 10% and 50% has an almost linear profile. The equation for the outer DOD regions has an exponential profile. The exponential profile is closer to the conclusions from chapter 3. One possible explanation for this difference is that the tests at 30% and 50% are stopped before completing 4000 equivalent full cycles. Therefore, the aging rate did not yet have the time to reach the stable region. The measurements at 10% DOD show a very particular behaviour. The first two measurements show a very low aging and after that the aging rate jumps to a higher but stable region. Sometimes it occurs that the capacity of the battery increases during the first cycles, a sort of reversed aging. The two low measurements could be explained by this. This two reasons could explain the linear profile for these DOD ranges. Taking this in consideration, it is more likely that equation C.22 is more accurate in describing the effect of DOD on the cycle aging rate.

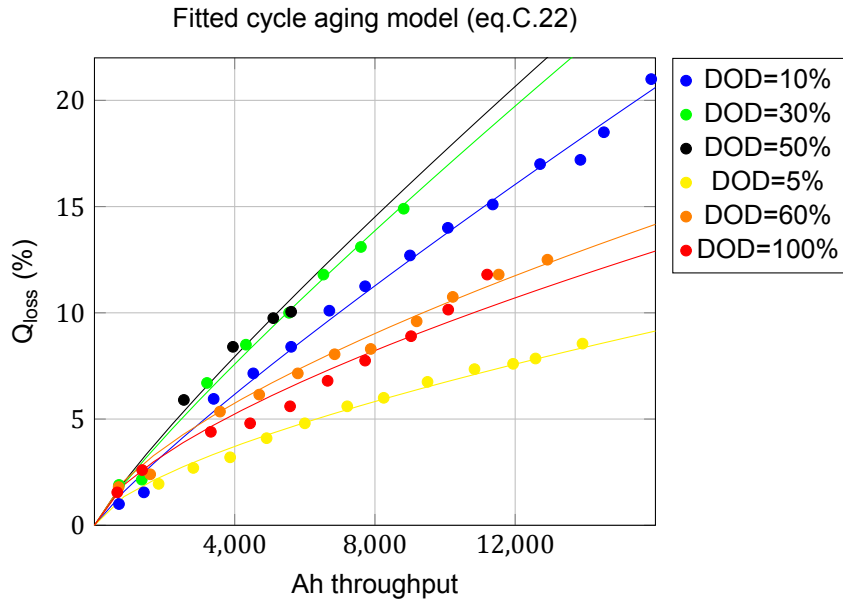


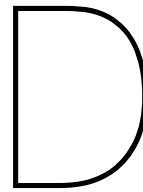
Figure C.8: Cycle aging data fitting ($10\% \leq \text{DOD} \leq 50\%$)

C.8. Wang et al.

In Wang et al.(2011) [65], equation C.23 and equation C.24 are proposed for modeling the, respectively, calendar and cycle aging of a LiFePO₄-graphite cell. These equations are based on the Arrhenius equation, $k=Ae^{-E_a/RT}$, for the temperature dependence of chemical reaction rates. Here, B is a pre-exponential factor depending on the state of charge of the battery for the calendar aging and on the charge throughput for the cycle aging. E_a is the activation energy, expressed in $\text{J}\cdot\text{mol}^{-1}$. This evaluates the dependency of aging on temperature T and R is the gas constant. Time is expressed by t for calendar aging, the charge throughput is expressed by Ah for cycle aging and z is a dimensionless constant. Multiple assumptions have been made to cancel the DOD and C-rates out of the equations. Therefore, this model is only applicable in a small DOD and C-rate ranges.

$$Q_{\text{loss}} = B(\text{SOC}) \cdot \exp\left(\frac{-E_a}{R \cdot T}\right) t^z \quad (\text{C.23})$$

$$Q_{\text{loss}} = B(\text{Ah}) \cdot \exp\left(\frac{-E_a}{R \cdot T}\right) \text{Ah}^z \quad (\text{C.24})$$



Simulink[®] model

D.1. Simulink[®]

D.1.1. Main screen

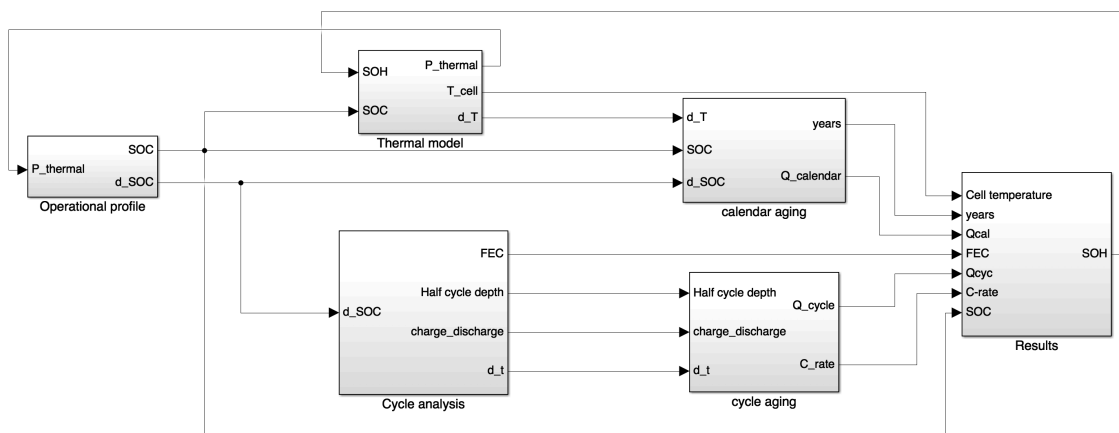


Figure D.1: Main screen of the aging model

D.1.2. Operational profile

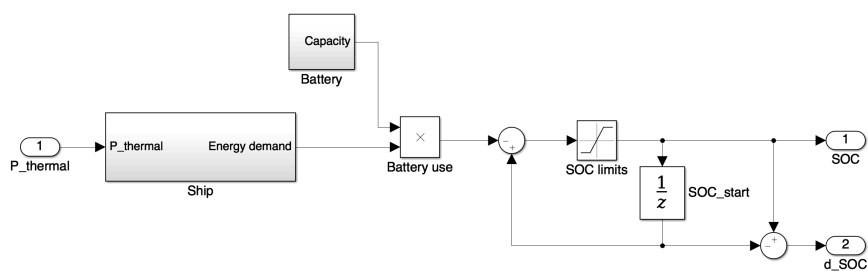


Figure D.2: Subsystem operational profile

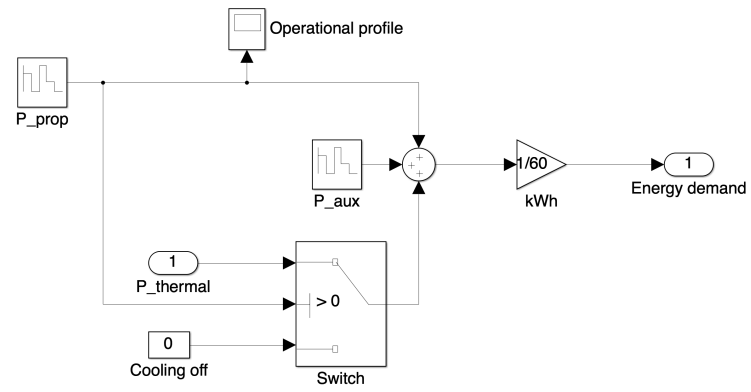


Figure D.3: Subsystem operational profile/ship

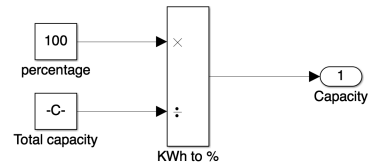


Figure D.4: Subsystem operational profile/battery

D.1.3. Thermal model

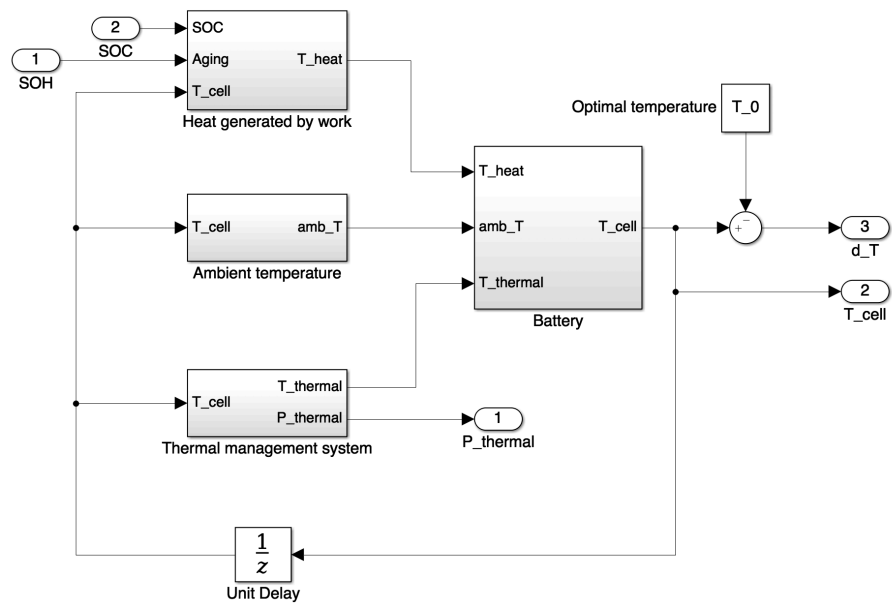


Figure D.5: Subsystem thermal model

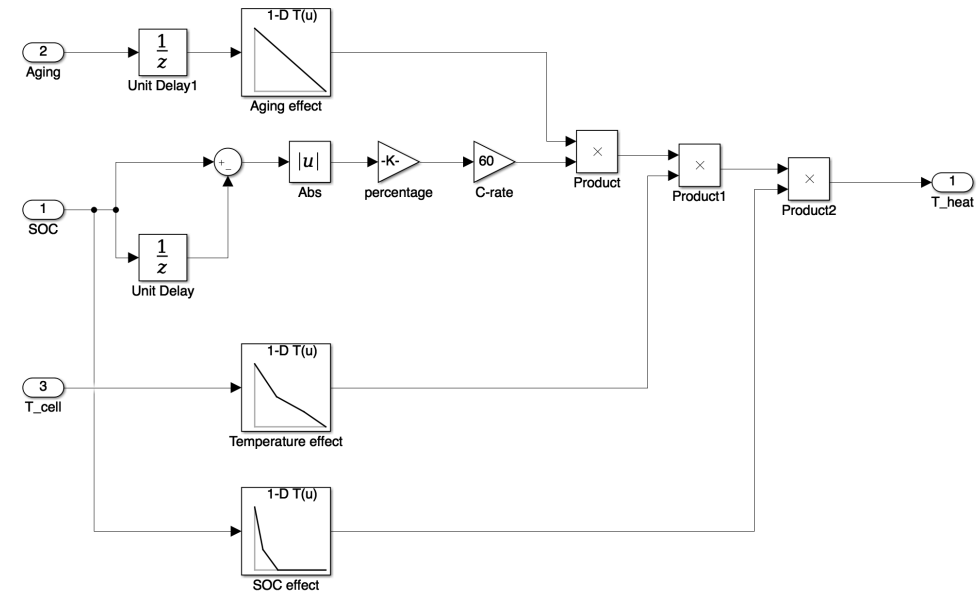


Figure D.6: Subsystem thermal model/heat generation

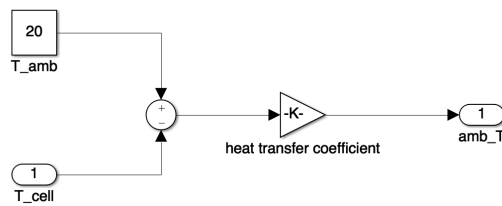


Figure D.7: Subsystem thermal model/ambient temperature

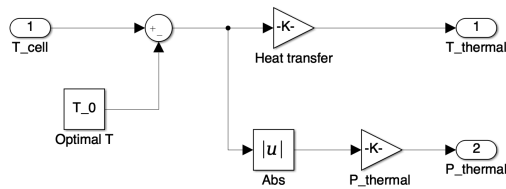


Figure D.8: Subsystem thermal model/thermal management

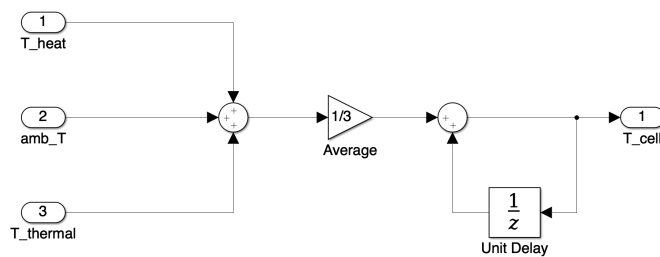


Figure D.9: Subsystem thermal model/battery

D.1.4. Cycle analysis

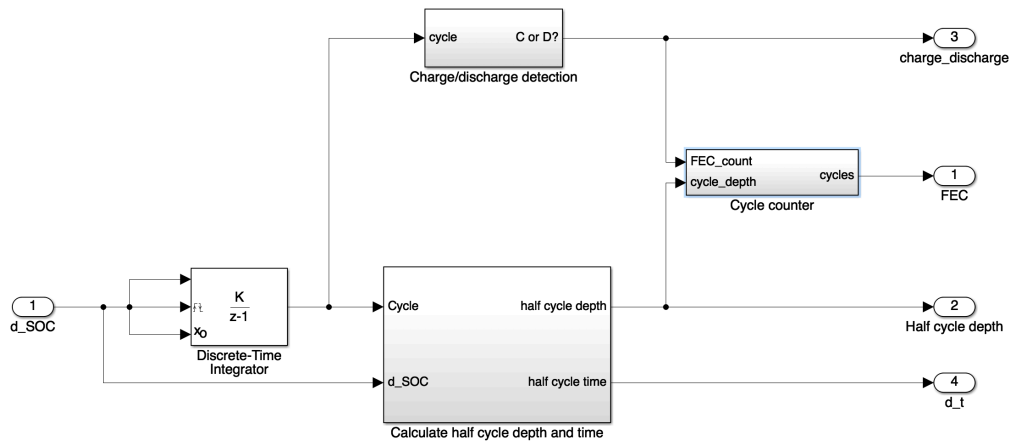


Figure D.10: Subsystem cycle analysis

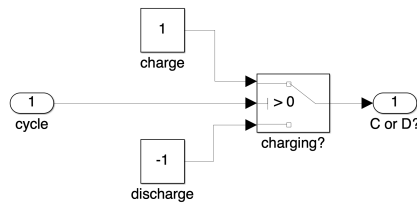


Figure D.11: Subsystem cycle analysis/Charge discharge detection

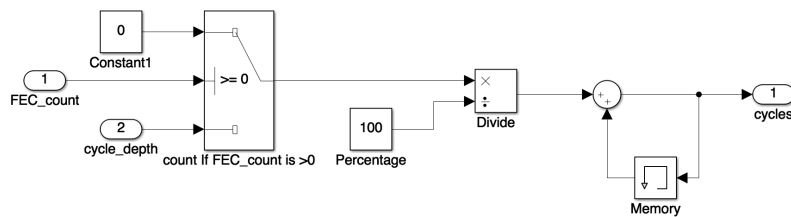


Figure D.12: Subsystem cycle analysis/Cycle counter

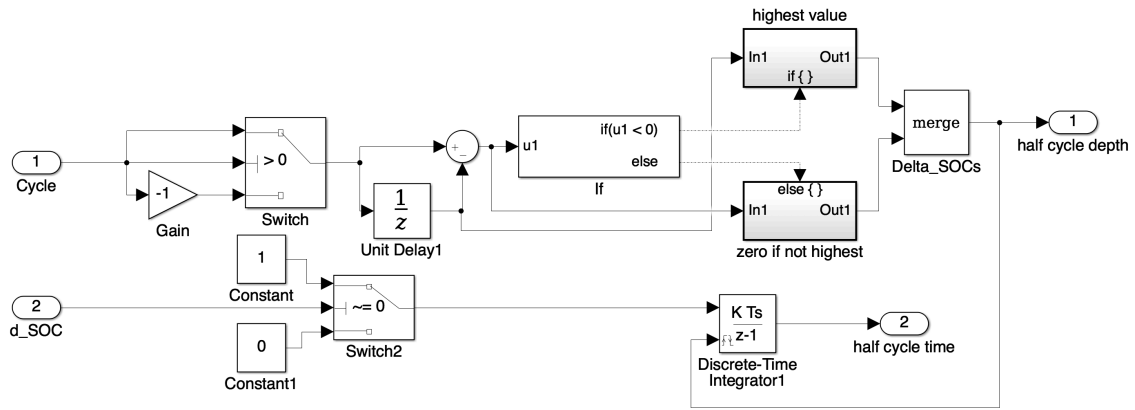


Figure D.13: Subsystem cycle analysis/Calculate half cycle depth and time

D.1.5. Calendar aging

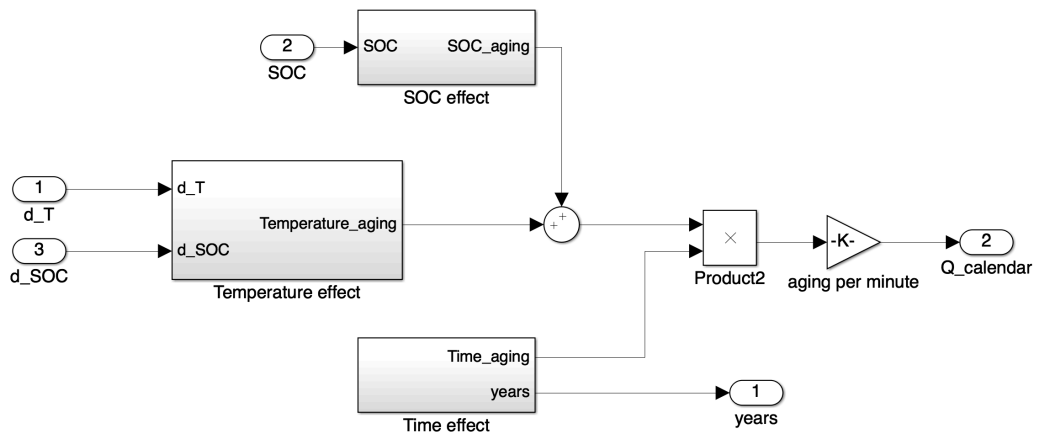


Figure D.14: Subsystem calendar aging

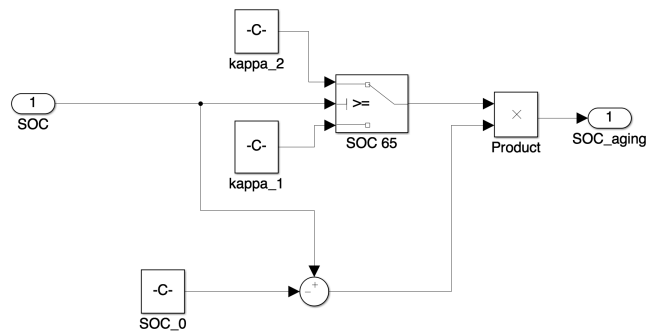


Figure D.15: Subsystem calendar aging/SOC effect

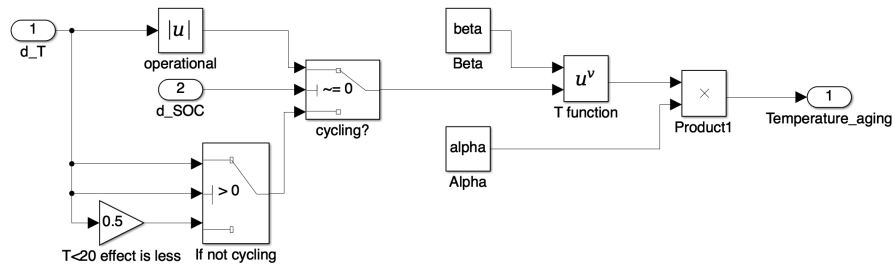


Figure D.16: Subsystem calendar aging/temperature aging

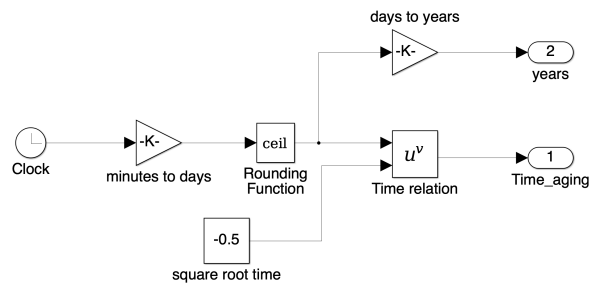


Figure D.17: Subsystem calendar aging/Time effect

D.1.6. Cycle aging

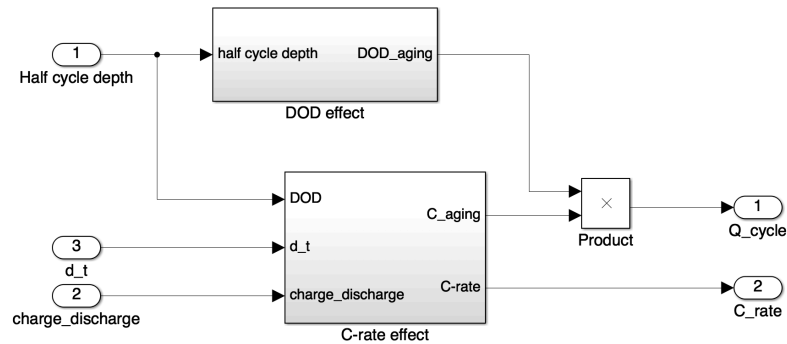


Figure D.18: Subsystem cycle aging

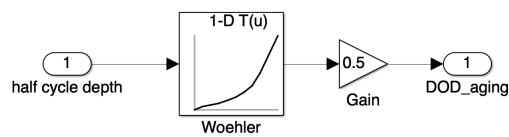


Figure D.19: Subsystem cycle aging/DOD effect

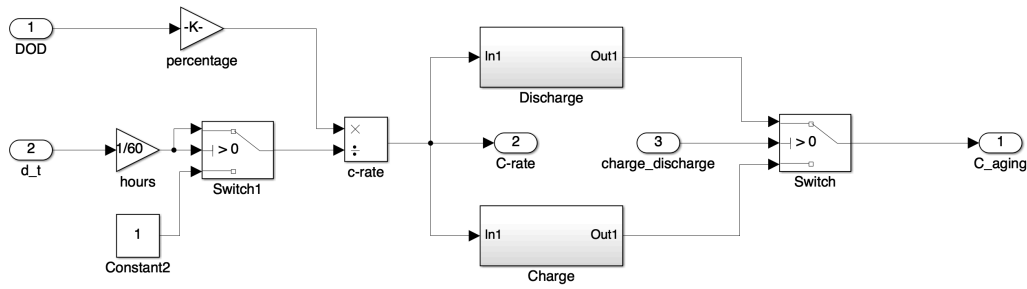


Figure D.20: Subsystem cycle aging/C-rate effect

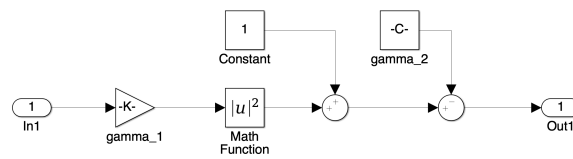


Figure D.21: Subsystem cycle aging/C-rate effect/Discharge

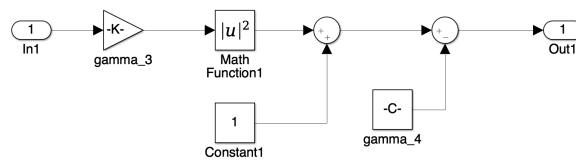


Figure D.22: Subsystem cycle aging/C-rate effect/Charge

D.1.7. Results

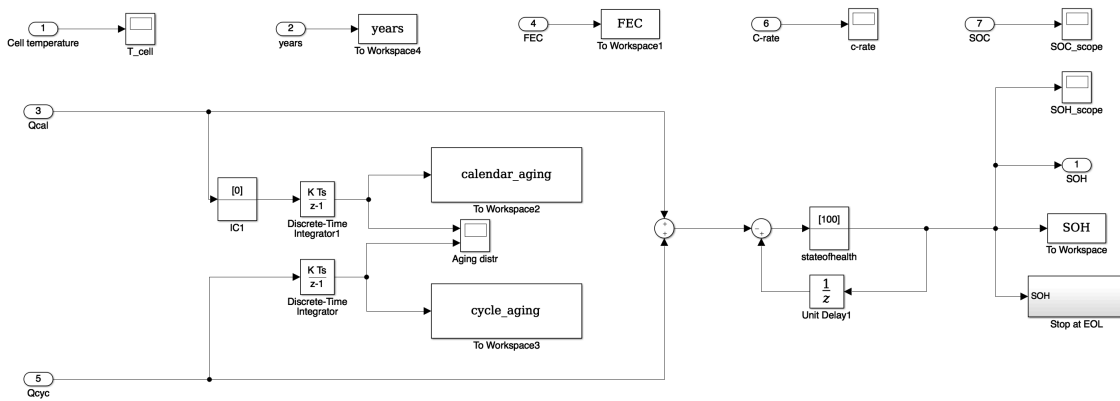


Figure D.23: Subsystem Results

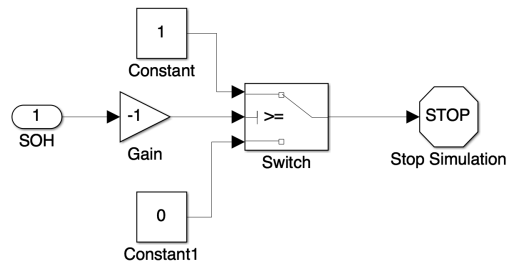
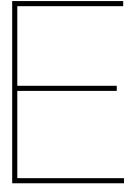


Figure D.24: Subsystem Results/EOL



Validation

Table E.1: Results of simulations set 1

Sarasketa, LFP, $\alpha_1 = 0.08086, \alpha_2 = 0.07583, \alpha_3 = 0.07834$							
#	SOC	T	Days	SOH	Sim 1	Sim 2	Sim 3
1	70%	30 °C	633	93.1%	92.85%	93.30%	93.28%
2	30%	40 °C	593	90.8%	88.08%	88.85%	88.47%
3	70%	40 °C	614	88.5%	87.28%	88.07%	87.68%
4	90%	40 °C	351	88.6%	90.12%	90.71%	90.41%
5	70%	40 °C	347	85.7%	82.89%	83.95%	83.42%

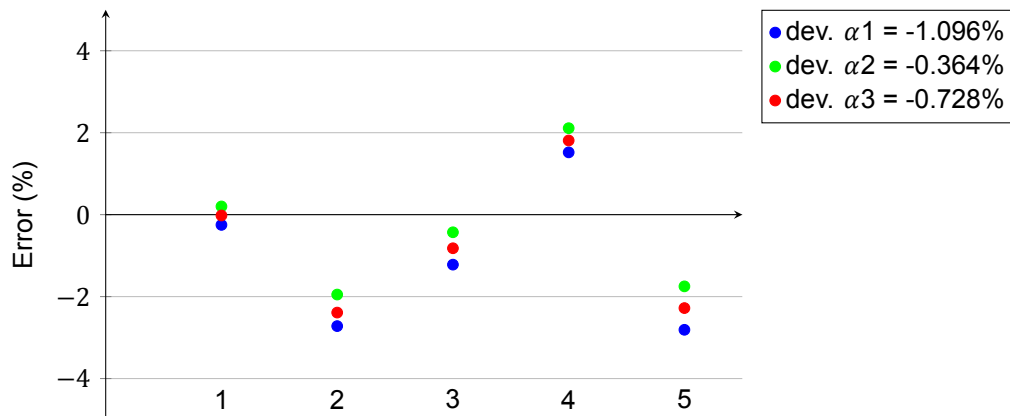


Figure E.1: Distribution of the errors of the simulation compared to Sarasketa data[51]

Table E.2: Results of simulations set 2

SIMCAL 2.3 Ah, LFP, $\alpha_1 = 0.05563, \alpha_2 = 0.08613, \alpha_3 = 0.07088$							
#	SOC	T	Days	SOH	Sim 1	Sim 2	Sim 3
1	30%	30 °C	797	96.59%	95.04%	92.01%	93.53%
2	65%	30 °C	799	94.45%	94.46%	91.42%	92.94%
3	100%	30 °C	824	91.39%	93.39%	90.31%	91.85%
4	30%	45 °C	698	85.57%	87.98%	81.09%	84.53%
5	65%	45 °C	965	78.61%	87.46%	80.59%	84.03%
6	100%	45 °C	965	75.54%	86.57%	79.69%	83.13%
7	30%	60 °C	214	84.08%	83.76%	74.69%	79.22%
8	65%	60 °C	236	73.67%	82.59%	73.05%	77.82%
9	100%	60 °C	167	77.24%	85.06%	77.01%	81.08%

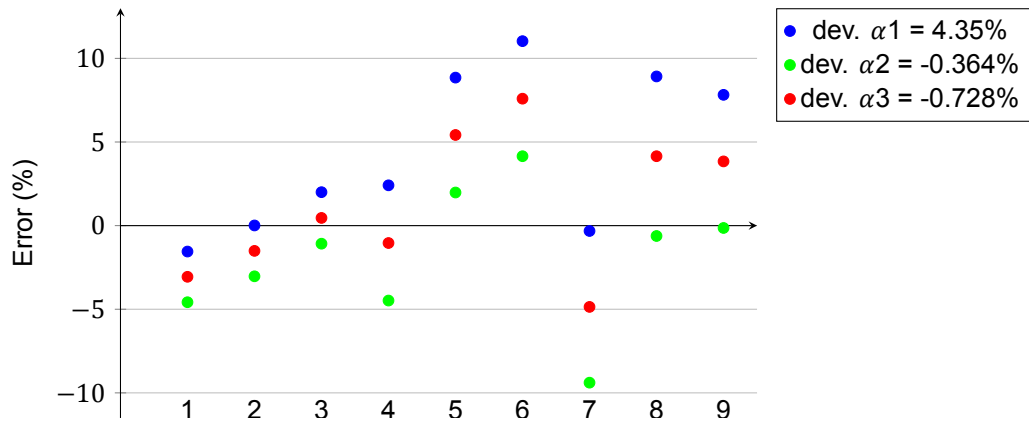


Figure E.2: Distribution of the errors of the simulation compared to SIMCAL data[15]

Table E.3: Results of simulations set 3

SIMCAL 8 Ah, LFP, $\alpha_1 = 0.01886$, $\alpha_2 = 0.07332$, $\alpha_3 = 0.04609$							
#	SOC	T	Days	SOH	Sim 1	Sim 2	Sim 3
1	30%	30 °C	797	99.63%	98.70%	93.29%	95.99%
2	65%	30 °C	795	98.83%	98.13%	92.72%	95.42%
3	100%	30 °C	823	97.14%	97.11%	91.61%	94.36%
4	30%	45 °C	710	87.75%	96.25%	83.84%	90.04%
5	65%	45 °C	707	81.52%	95.71%	83.33%	89.52%
6	100%	45 °C	707	80.06%	94.81%	82.43%	88.62%
7	30%	60 °C	582	70.53%	91.06%	63.84%	77.45%
8	65%	60 °C	579	60.32%	90.60%	63.44%	77.02%
9	100%	60 °C	554	58.31%	90.01%	63.46%	76.74%
10	100%	60 °C	61	84.40%	96.89%	88.61%	92.75%

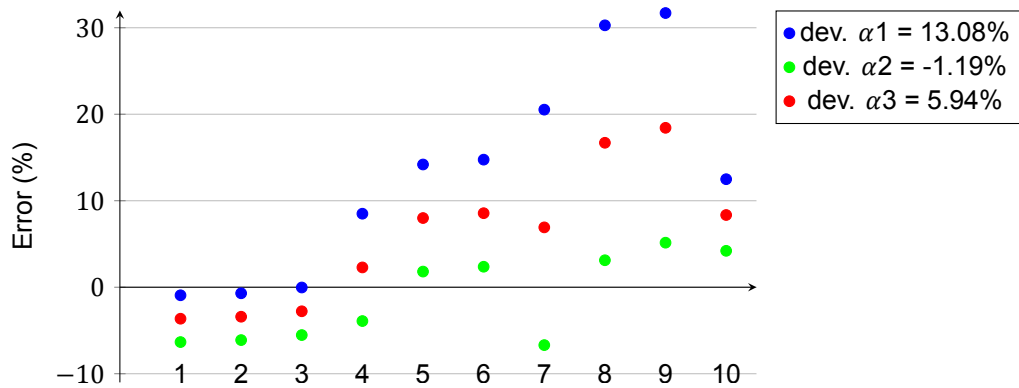


Figure E.3: Distribution of the errors of the simulation compared to SIMCAL data[15]

Table E.4: Results of simulations set 4

SIMCAL 15 Ah, LFP, $\alpha_1 = 0.05982$, $\alpha_2 = 0.09254$, $\alpha_3 = 0.07618$							
#	SOC	T	Days	SOH	Sim 1	Sim 2	Sim 3
1	30%	30 °C	799	95.48%	94.62%	91.36%	92.99%
2	65%	30 °C	798	94.15%	94.05%	90.79%	92.42%
3	100%	30 °C	794	92.82%	93.10%	89.85%	91.48%
4	30%	45 °C	706	82.71%	86.95%	79.52%	83.24%
5	65%	45 °C	702	77.79%	86.45%	79.04%	82.74%
6	100%	45 °C	705	74.34%	85.55%	78.09%	81.84%
7	30%	60 °C	560	74.07%	71.16%	55.12%	63.14%
8	65%	60 °C	82	82.98%	89.34%	83.49%	86.41%
9	65%	60 °C	477	52.79%	73.01%	58.15%	65.63%
10	100%	60 °C	55	80.72%	91.18%	86.48%	88.83%
11	100%	60 °C	387	51.20%	75.11%	61.87%	68.49%

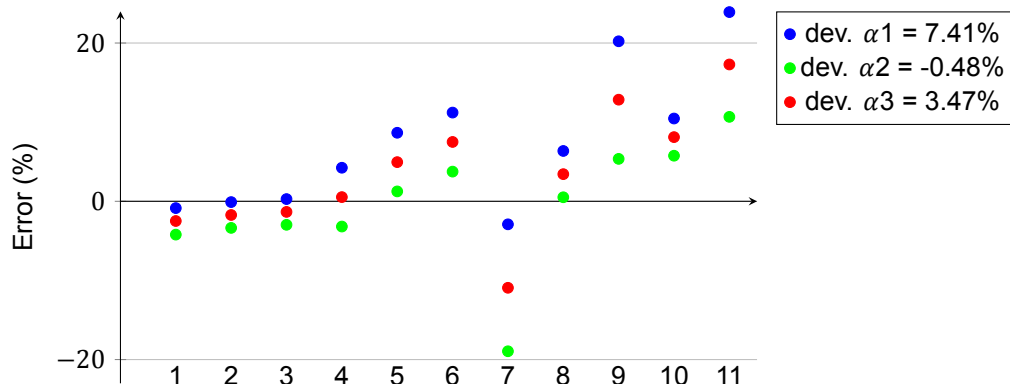


Figure E.4: Distribution of the errors of the simulation compared to SIMCAL data[15]

Table E.5: Results of simulations set 5

Keil 18650, LFP, $\alpha_1 = 0.09254$, $\alpha_2 = 0.06755$, $\alpha_3 = 0.080045$							
#	SOC	T	Days	SOH	Sim 1	Sim 2	Sim 3
1	30%	25 °C	270	97.10%	96.28%	97.33%	96.81%
2	50%	25 °C	270	97.10%	96.09%	97.15%	96.62%
3	70%	25 °C	270	96.50%	95.77%	96.83%	96.30%
4	30%	40 °C	270	93.70%	90.68%	93.25%	91.97%
5	50%	40 °C	270	93.10%	90.49%	93.06%	91.78%
6	70%	40 °C	270	92.30%	90.18%	92.75%	91.46%
7	30%	50 °C	270	89.80%	83.00%	87.64%	85.32%
8	50%	50 °C	270	88.20%	82.81%	87.46%	85.13%
9	70%	50 °C	270	88.30%	82.50%	87.14%	84.82%

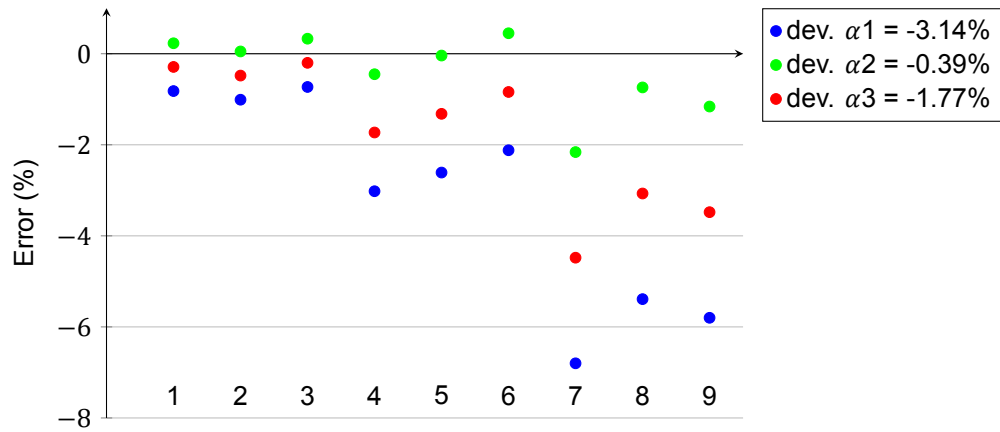


Figure E.5: Distribution of the errors of the simulation compared to Keil data[32]

Table E.6: Results of simulations set 6

Safari, LFP, $\alpha_1 = 0.06755$, $\alpha_2 = 0.07176$, $\alpha_3 = 0.069655$							
#	SOC	T	Days	SOH	Sim 1	Sim 2	Sim 3
1	50%	25 °C	365	96.70%	96.66%	96.45%	96.56%
2	100%	25 °C	365	94.70%	95.74%	95.53%	95.64%
3	50%	45 °C	365	88.40%	89.08%	88.40%	91.63%
4	100%	45 °C	365	85.70%	88.16%	87.48%	90.71%

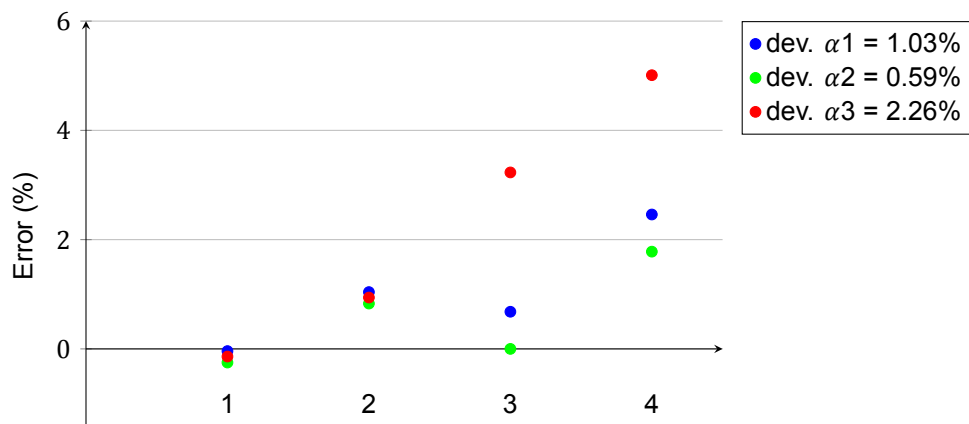


Figure E.6: Distribution of the errors of the simulation compared to Safari data[50]

Table E.7: Results of simulations set 7

Schmalstieg, NMC, $\alpha_1 = 0.07376$, $\alpha_2 = 0.07818$, $\alpha_3 = 0.07597$							
#	SOC	T	Days	SOH	Sim 1	Sim 2	Sim 3
1	10%	50 °C	1000	80%	73.81%	72.38%	73.09%
2	20%	50 °C	760	80%	77.08%	75.84%	76.46%
3	30%	50 °C	560	80%	80.28%	79.21%	79.75%
4	50%	50 °C	560	80%	80.00%	78.94%	79.47%
5	60%	50 °C	500	80%	81.01%	80.01%	80.51%
6	70%	50 °C	410	80%	82.59%	81.76%	82.17%
7	80%	50 °C	295	80%	85.16%	84.46%	84.81%
8	90%	50 °C	270	80%	85.67%	85.01%	85.34%

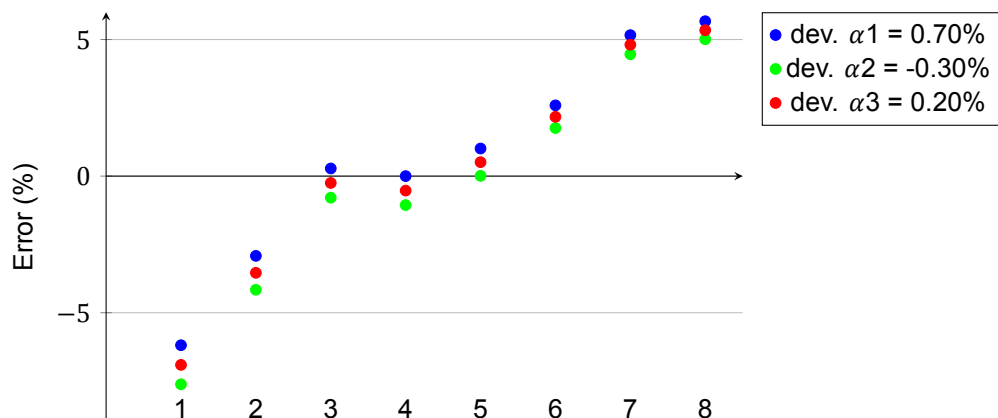


Figure E.7: Distribution of the errors of the simulation compared to Schmalstieg data[55]

Table E.8: Results of simulations set 8

Keil 18650, NMC, $\alpha_1 = 0.07818$, $\alpha_2 = 0.06336$, $\alpha_3 = 0.07077$							
#	SOC	T	Days	SOH	Sim 1	Sim 2	Sim 3
1	30%	25 °C	300	97.40%	96.71%	97.37%	97.04%
2	50%	25 °C	300	97.20%	96.51%	97.17%	96.84%
3	80%	25 °C	300	94.50%	96.01%	96.67%	96.34%
4	30%	40 °C	300	94.30%	91.71%	93.32%	92.52%
5	50%	40 °C	300	93.50%	91.51%	93.12%	92.32%
6	80%	40 °C	300	89.10%	91.01%	92.63%	91.82%
7	30%	50 °C	300	90.10%	84.86%	87.77%	86.31%
8	50%	50 °C	300	87.90%	84.66%	87.57%	86.11%
9	80%	50 °C	300	82.60%	84.16%	87.07%	85.62%

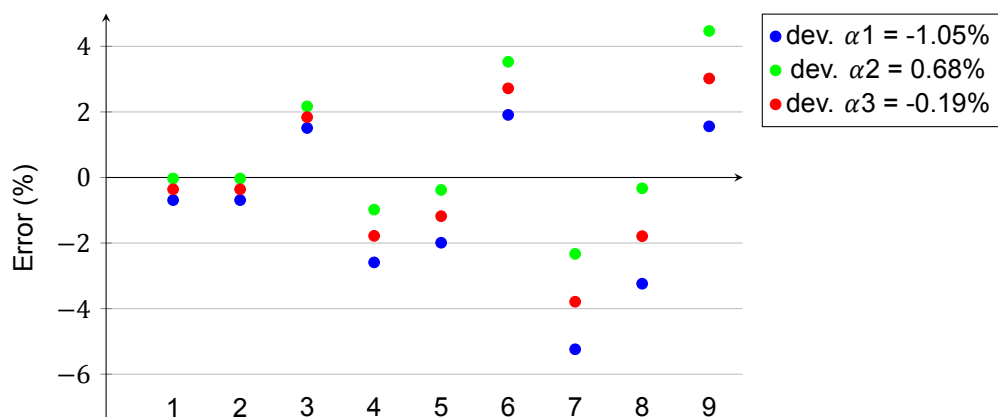


Figure E.8: Distribution of the errors of the simulation compared to Keil data[32]

Table E.9: Results of simulations set 9

MOBICUS, NMC, $\alpha_1 = 0.13$, $\alpha_2 = 0.07$, $\alpha_3 = 0.10$							
#	SOC	T	Days	SOH	Sim 1	Sim 2	Sim 3
1	30%	25 °C	164	95.14%	96.13%	98.72%	97.11%
2	30%	45 °C	161	89.50%	86.67%	95.06%	89.83%
3	80%	25 °C	238	94.86%	94.86%	98.01%	96.04%
4	80%	45 °C	86	91.45%	90.21%	96.21%	92.47%
5	80%	60 °C	70	75.60%	78.71%	91.75%	83.62%

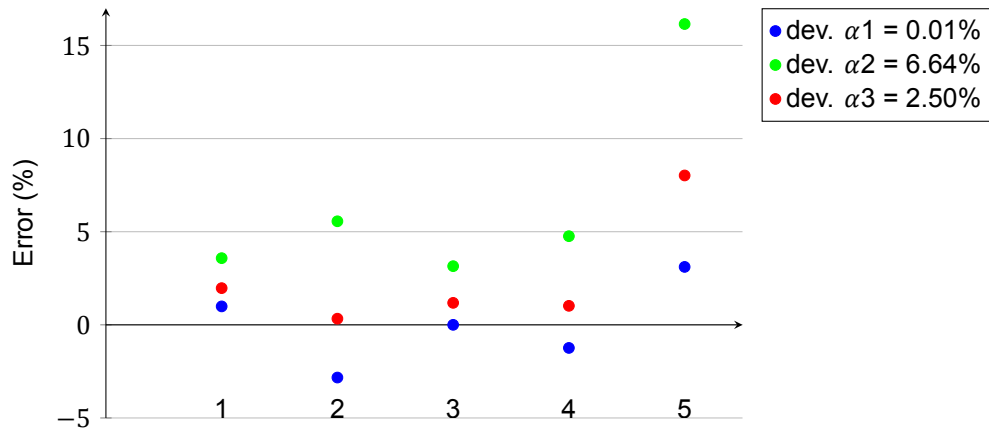


Figure E.9: Distribution of the errors of the simulation compared to MOBICUS data[7]

Table E.10: Results of simulations set 10

SIMCAL 5.3 Ah, NMC, $\alpha_1 = 0.01067$, $\alpha_2 = 0.13498$, $\alpha_3 = 0.07282$							
#	SOC	T	Days	SOH	Sim 1	Sim 2	Sim 3
1	30%	30 °C	907	93.06%	89.28%	86.27%	92.88%
2	65%	30 °C	909	88.48%	88.66%	85.65%	92.26%
3	100%	30 °C	631	67.28%	89.73%	87.24%	92.72%
4	30%	45 °C	670	83.38%	76.93%	70.68%	84.42%
5	65%	45 °C	560	72.78%	78.48%	72.78%	85.31%
6	100%	45 °C	185	70.68%	87.46%	84.26%	91.30%
7	30%	60 °C	362	71.34%	58.65%	47.59%	71.90%
8	65%	60 °C	60	77.62%	83.93%	79.68%	89.03%
9	100%	60 °C	32	79.11%	88.50%	85.49%	92.09%

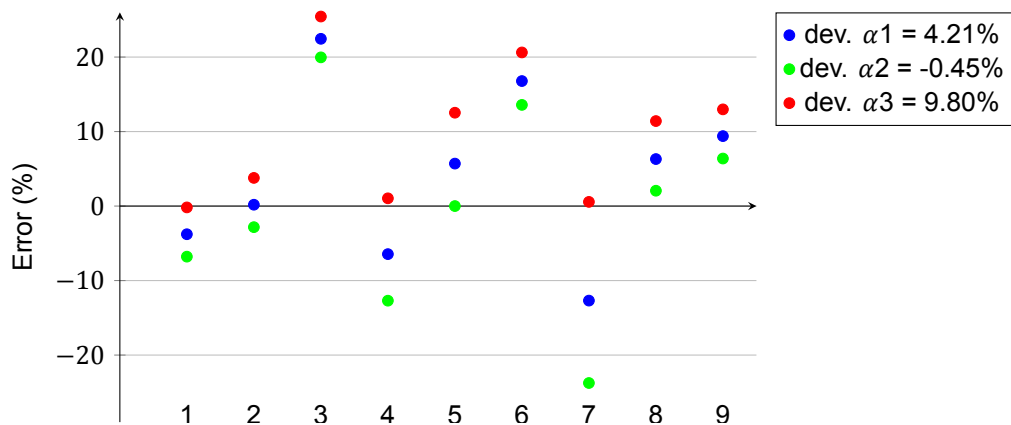


Figure E.10: Distribution of the errors of the simulation compared to SIMCAL data[15]

Table E.11: Results of simulations set 11

SIMCAL 12 Ah, NMC, $\alpha_1 = 0.08, \alpha_2 = 0.10333, \alpha_3 = 0.02641$							
#	SOC	T	Days	SOH	Sim 1	Sim 2	Sim 3
1	100%	30 °C	887	91.81%	91.59%	89.14%	96.59%
2	30%	45 °C	723	96.85%	82.70%	77.33%	94.48%
3	65%	45 °C	722	94.33%	82.53%	77.17%	93.93%
4	100%	45 °C	718	76.32%	81.67%	76.32%	93.04%
5	30%	60 °C	549	88.04%	62.14%	50.82%	87.66%
6	65%	60 °C	557	78.09%	61.70%	50.66%	87.09%
7	100%	60 °C	124	69.90%	82.18%	76.98%	93.75%

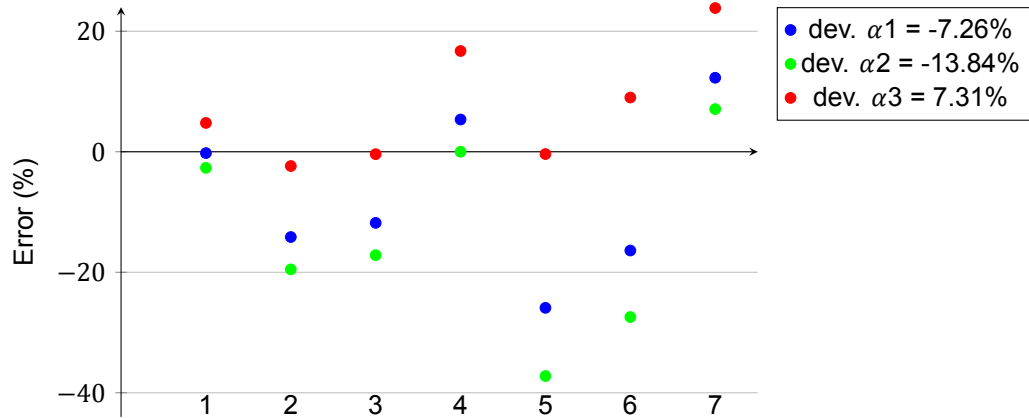


Figure E.11: Distribution of the errors of the simulation compared to SIMCAL data[15]

Table E.12: Results of simulations set 12

Ecker 18650, NMC, $\alpha_1 = 0.05859, \alpha_2 = 0.06254, \alpha_3 = 0.07$							
#	SOC	T	Days	SOH	Sim 1	Sim 2	Sim 3
1	50%	35 °C	345	95.24%	94.91%	94.59%	93.92%
2	50%	40 °C	343	92.72%	93.18%	92.72%	91.85%
3	50%	50 °C	408	84.48%	86.51%	85.60%	83.89%
4	30%	50 °C	407	85.06%	86.76%	85.85%	84.14%
5	80%	50 °C	418	76.23%	85.75%	84.83%	83.09%

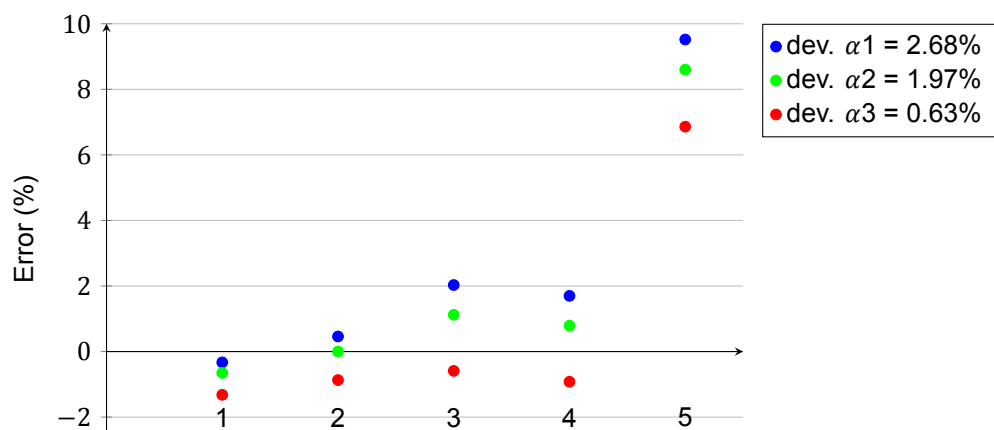


Figure E.12: Distribution of the errors of the simulation compared to Ecker data[18]

Table E.13: Results of simulations set 13

Ecker pouch, NMC, $\alpha_1 = 0.07128$, $\alpha_2 = 0.04346$, $\alpha_3 = 0.05737$							
#	SOC	T	Days	SOH	Sim 1	Sim 2	Sim 3
1	50%	35 °C	422	93.13%	93.13%	95.81%	94.47%
2	50%	50 °C	426	89.80%	83.30%	89.77%	86.49%
3	50%	65 °C	427	73.71%	59.16%	75.10%	67.13%

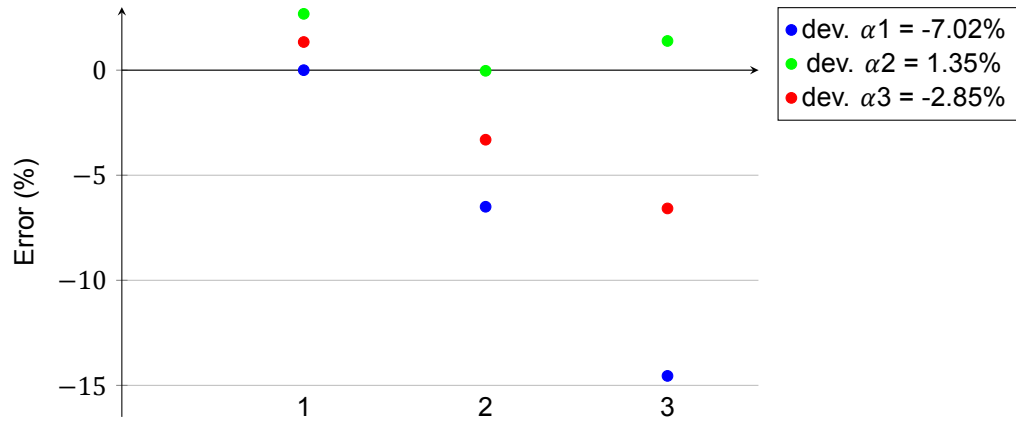


Figure E.13: Distribution of the errors of the simulation compared to Ecker data[17]

Table E.14: Results of simulations set 14

Keil, NCA, $\alpha_1 = 0.06472$, $\alpha_2 = 0.04697$, $\alpha_3 = 0.05585$							
#	SOC	T	Days	SOH	Sim 1	Sim 2	Sim 3
1	30%	25 °C	300	97.02%	97.31%	98.10%	97.71%
2	50%	25 °C	300	97.10%	97.11%	97.90%	97.51%
3	80%	25 °C	300	94.90%	96.61%	97.40%	97.01%
4	30%	40 °C	300	95.20%	93.18%	95.10%	94.14%
5	50%	40 °C	300	94.90%	92.98%	94.90%	93.94%
6	80%	40 °C	300	91.70%	92.48%	94.40%	93.44%
7	30%	50 °C	300	93.20%	87.50%	90.98%	89.24%
8	50%	50 °C	300	92.80%	87.30%	90.78%	89.04%
9	80%	50 °C	300	89.20%	86.80%	90.28%	88.54%

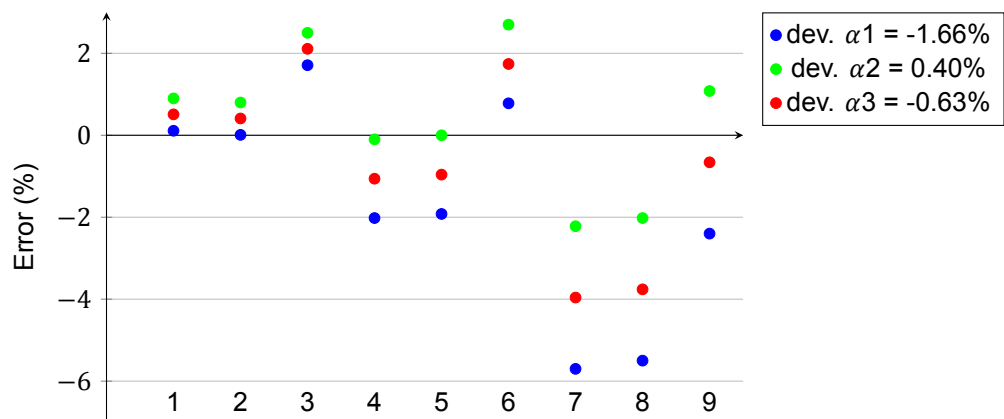


Figure E.14: Distribution of the errors of the simulation compared to Keil data[32]

Table E.15: Results of simulations set 15

SIMCAL, NCA, $\alpha_1 = 0.04238$, $\alpha_2 = 0.04632$, $\alpha_3 = 0.04$							
#	SOC	T	Days	SOH	Sim 1	Sim 2	Sim 3
1	30%	30 °C	865	97.01%	96.21%	95.80%	96.45%
2	65%	30 °C	905	95.57%	95.50%	95.08%	95.75%
3	100%	30 °C	864	92.32%	94.60%	94.19%	94.85%
4	30%	45 °C	729	91.67%	90.76%	89.85%	91.31%
5	65%	45 °C	726	89.32%	90.23%	89.32%	90.78%
6	100%	45 °C	724	86.46%	89.33%	88.42%	89.88%
7	30%	60 °C	794	83.85%	75.72%	73.41%	77.12%
8	65%	60 °C	819	78.13%	74.75%	72.39%	76.16%
9	100%	60 °C	820	67.58%	73.77%	71.42%	75.19%

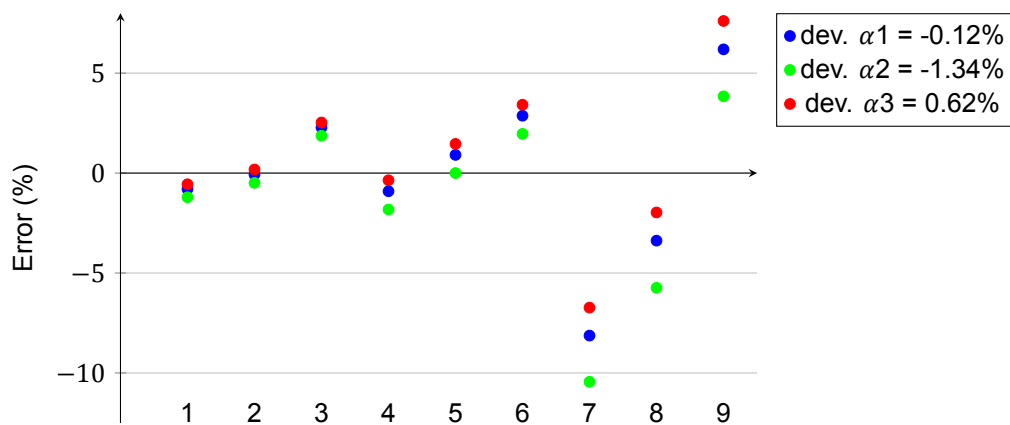
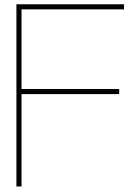


Figure E.15: Distribution of the errors of the simulation compared to SIMCAL data[15]



Results

F.1. Behavioural analysis

Table F.1: Results of simulating aging model until EOL at 5% DOD and 0.1C

5% DOD, 0.1 C				
OP Hrs/day	FEC	Years	Calendar	Cycle
1.00	747	39.7	18.16%	1.84%
2.03	1284	34.3	16.84%	3.16%
3.07	1701	30.3	15.81%	4.19%
4.10	2039	27.2	14.98%	5.02%
5.13	2321	24.8	14.28%	5.72%
6.17	2563	22.8	13.69%	6.31%
7.20	2773	21.2	13.17%	6.83%
8.23	2958	19.8	12.71%	7.29%
9.27	3123	18.5	12.31%	7.69%
10.30	3272	17.5	11.94%	8.06%
11.33	3407	16.5	11.61%	8.39%
12.37	3530	15.7	11.30%	8.70%

Table F.2: Results of simulating aging model until EOL at 5% DOD and 0.25C

5% DOD, 0.25 C				
OP Hrs/day	FEC	Years	Calendar	Cycle
1.27	1693	30.2	15.83%	4.17%
2.13	2303	24.7	14.33%	5.67%
3.00	2744	21.0	13.24%	6.76%
3.87	3085	18.4	12.40%	7.60%
5.17	3478	15.5	11.43%	8.57%
6.03	3687	14.1	10.92%	9.08%
6.90	3866	13.0	10.48%	9.52%
8.20	4093	11.6	9.92%	10.08%
9.07	4222	10.8	9.60%	10.40%
9.93	4338	10.1	9.31%	10.69%
11.23	4491	9.3	8.94%	11.06%
12.10	4582	8.8	8.71%	11.29%

Table F.3: Results of simulating aging model until EOL at 5% DOD and 0.5C

5% DOD, 0.5 C				
OP Hrs/day	FEC	Years	Calendar	Cycle
0.90	2018	27.1	15.03%	4.97%
2.07	3068	18.4	12.44%	7.56%
3.00	3563	14.8	11.22%	8.78%
3.93	3918	12.5	10.35%	9.65%
5.10	4246	10.4	9.54%	10.46%
6.03	4451	9.3	9.03%	10.97%
6.97	4620	8.3	8.62%	11.38%
8.13	4795	7.4	8.19%	11.81%
9.07	4913	6.8	7.90%	12.10%
10.00	5016	6.3	7.64%	12.36%
10.93	5108	5.9	7.42%	12.58%
12.10	5208	5.4	7.17%	12.83%

Table F.4: Results of simulating aging model until EOL at 5% DOD and 1C

5% DOD, 1 C				
OP Hrs/day	FEC	Years	Calendar	Cycle
1.03	2933	19.5	12.78%	7.22%
1.97	3776	13.4	10.70%	9.30%
3.03	4317	10.0	9.36%	10.64%
3.97	4630	8.2	8.59%	11.41%
5.03	4889	6.9	7.96%	12.04%
5.97	5062	6.0	7.53%	12.47%
7.03	5220	5.3	7.14%	12.86%
7.97	5333	4.7	6.86%	13.14%
9.03	5441	4.3	6.60%	13.40%
9.97	5520	3.9	6.40%	13.60%
11.03	5599	3.6	6.21%	13.79%
11.97	5659	3.4	6.06%	13.94%

Table F.5: Results of simulating aging model until EOL at 5% DOD and 1.5C

5% DOD, 1.5 C				
OP Hrs/day	FEC	Years	Calendar	Cycle
0.98	3226	17.3	12.05%	7.95%
1.98	4138	11.1	9.81%	10.19%
2.98	4621	8.3	8.62%	11.38%
3.98	4932	6.6	7.85%	12.15%
4.98	5152	5.5	7.31%	12.69%
5.98	5318	4.8	6.90%	13.10%
6.98	5448	4.2	6.58%	13.42%
7.98	5553	3.7	6.32%	13.68%
8.98	5639	3.4	6.11%	13.89%
9.98	5711	3.1	5.93%	14.07%
10.98	5772	2.8	5.78%	14.22%
11.98	5825	2.6	5.65%	14.35%

Table F.6: Results of simulating aging model until EOL at 5% DOD and 3C

5% DOD, 3 C				
OP Hrs/day	FEC	Years	Calendar	Cycle
1.02	3255	16.8	12.05%	7.95%
2.03	4074	10.8	10.04%	9.96%
3.03	4495	8.0	9.01%	10.99%
4.03	4757	6.4	8.38%	11.62%
5.03	4935	5.3	7.94%	12.06%
6.03	5063	4.5	7.63%	12.37%
7.03	5160	4.0	7.39%	12.61%
8.03	5233	3.5	7.21%	12.79%
9.03	5291	3.2	7.07%	12.93%
10.03	5337	2.9	6.96%	13.04%
11.03	5373	2.6	6.87%	13.13%
12.03	5402	2.4	6.80%	13.20%

Table F.7: Results of simulating aging model until EOL at 10% DOD and 0.1C

10% DOD, 0.1 C				
OP Hrs/day	FEC	Years	Calendar	Cycle
2.03	1193	32.2	17.09%	2.91%
4.07	1933	26.1	15.29%	4.71%
6.10	2462	22.2	14.00%	6.00%
8.13	2870	19.4	13.00%	7.00%
10.17	3200	17.3	12.20%	7.80%
12.20	3475	15.7	11.52%	8.48%

Table F.8: Results of simulating aging model until EOL at 10% DOD and 0.25C

10% DOD, 0.25 C				
OP Hrs/day	FEC	Years	Calendar	Cycle
0.83	1195	31.9	17.11%	2.89%
1.67	1925	25.8	15.34%	4.66%
3.33	2830	19.0	13.14%	6.86%
4.17	3143	16.9	12.38%	7.62%
5.00	3401	15.2	11.75%	8.25%
5.83	3620	13.9	11.22%	8.78%
6.67	3809	12.8	10.76%	9.24%
8.33	4121	11.1	10.00%	10.00%
9.17	4252	10.4	9.68%	10.32%
10.00	4370	9.8	9.40%	10.60%
10.83	4478	9.2	9.13%	10.87%
11.67	4576	8.8	8.90%	11.10%

Table F.9: Results of simulating aging model until EOL at 10% DOD and 0.5C

10% DOD, 0.5 C				
OP Hrs/day	FEC	Years	Calendar	Cycle
0.87	1913	25.7	15.36%	4.64%
2.17	3103	16.8	12.43%	7.57%
3.03	3564	13.8	11.30%	8.70%
3.90	3904	11.7	10.47%	9.53%
5.20	4281	9.7	9.54%	10.46%
6.07	4476	8.7	9.07%	10.93%
6.93	4640	7.9	8.66%	11.34%
8.23	4843	6.9	8.17%	11.83%
9.10	4958	6.4	7.89%	12.11%
9.97	5059	6.0	7.64%	12.36%
10.83	5149	5.6	7.42%	12.58%
12.13	5268	5.1	7.13%	12.87%

Table F.10: Results of simulating aging model until EOL at 10% DOD and 1C

10% DOD, 1 C				
OP Hrs/day	FEC	Years	Calendar	Cycle
0.93	2832	18.8	13.18%	6.82%
2.10	3943	11.7	10.49%	9.51%
3.03	4417	9.1	9.34%	10.66%
3.97	4740	7.4	8.56%	11.44%
5.13	5028	6.1	7.86%	12.14%
6.07	5202	5.3	7.43%	12.57%
7.00	5344	4.8	7.09%	12.91%
7.93	5461	4.3	6.81%	13.19%
9.10	5582	3.8	6.51%	13.49%
10.03	5663	3.5	6.32%	13.68%
10.97	5734	3.3	6.15%	13.85%
12.13	5811	3.0	5.96%	14.04%

Table F.11: Results of simulating aging model until EOL at 10% DOD and 1.5C

10% DOD, 1.5 C				
OP Hrs/day	FEC	Years	Calendar	Cycle
1.00	3372	15.1	11.83%	8.17%
2.00	4288	9.6	9.59%	10.41%
3.00	4770	7.1	8.42%	11.58%
4.00	5078	5.7	7.67%	12.33%
5.00	5296	4.7	7.13%	12.87%
6.00	5459	4.1	6.74%	13.26%
7.00	5587	3.6	6.43%	13.57%
8.00	5689	3.2	6.18%	13.82%
9.00	5774	2.9	5.97%	14.03%
10.00	5844	2.6	5.80%	14.20%
11.00	5904	2.4	5.65%	14.35%
12.00	5956	2.2	5.53%	14.47%

Table F.12: Results of simulating aging model until EOL at 10% DOD and 3C

10% DOD, 3 C				
OP Hrs/day	FEC	Years	Calendar	Cycle
1.00	3505	14.0	11.57%	8.43%
2.00	4508	7.8	9.02%	10.98%
3.00	4968	5.5	7.88%	12.12%
4.00	5233	4.2	7.23%	12.77%
5.00	5407	3.4	6.80%	13.20%
6.00	5528	2.9	6.50%	13.50%
7.00	5617	2.5	6.29%	13.71%
8.00	5684	2.2	6.12%	13.88%
9.00	5735	2.0	6.00%	14.00%
10.00	5775	1.8	5.90%	14.10%
11.00	5806	1.6	5.82%	14.18%
12.00	5831	1.5	5.76%	14.24%

Table F.13: Results of simulating aging model until EOL at 20% DOD and 0.1C

20% DOD, 0.1 C				
OP Hrs/day	FEC	Years	Calendar	Cycle
4.00	1949	26.4	16.99%	3.01%
8.00	3233	21.9	15.01%	4.99%
12.00	4194	18.9	13.53%	6.47%
16.00	4965	16.8	12.34%	7.66%
20.00	5609	15.2	11.34%	8.66%

Table F.14: Results of simulating aging model until EOL at 20% DOD and 0.25C

20% DOD, 0.25 C				
OP Hrs/day	FEC	Years	Calendar	Cycle
1.63	1902	25.6	17.07%	2.93%
3.27	3082	20.8	15.24%	4.76%
4.90	3928	17.6	13.94%	6.06%
6.53	4582	15.4	12.93%	7.07%
8.17	5110	13.8	12.11%	7.89%
9.80	5552	12.5	11.43%	8.57%
11.43	5930	11.4	10.85%	9.15%
13.07	6260	10.6	10.34%	9.66%
14.70	6552	9.8	9.89%	10.11%
16.33	6813	9.2	9.49%	10.51%
17.97	7049	8.6	9.12%	10.88%
19.60	7264	8.2	8.79%	11.21%

Table F.15: Results of simulating aging model until EOL at 20% DOD and 0.5C

20% DOD, 0.5 C				
OP Hrs/day	FEC	Years	Calendar	Cycle
0.83	1886	25.3	17.09%	2.91%
2.50	3840	17.3	14.07%	5.93%
3.33	4455	15.1	13.12%	6.88%
4.17	4947	13.4	12.37%	7.63%
5.00	5354	12.1	11.74%	8.26%
5.83	5699	11.0	11.21%	8.79%
7.50	6256	9.4	10.35%	9.65%
8.33	6489	8.8	9.99%	10.01%
9.17	6692	8.2	9.67%	10.33%
10.00	6879	7.7	9.38%	10.62%
11.07	7203	7.0	8.88%	11.12%
12.50	7346	6.6	8.66%	11.34%

Table F.16: Results of simulating aging model until EOL at 20% DOD and 1C

20% DOD, 1 C				
OP Hrs/day	FEC	Years	Calendar	Cycle
0.87	3042	20.2	15.31%	4.69%
2.17	4920	13.1	12.41%	7.59%
3.03	5637	10.7	11.30%	8.70%
3.90	6162	9.1	10.49%	9.51%
5.20	6739	7.5	9.60%	10.40%
6.07	7035	6.7	9.15%	10.85%
6.93	7282	6.1	8.76%	11.24%
8.23	7587	5.3	8.29%	11.71%
9.10	7757	4.9	8.03%	11.97%
9.97	7907	4.6	7.80%	12.20%
11.27	8100	4.2	7.50%	12.50%
12.13	8214	3.9	7.33%	12.67%

Table F.17: Results of simulating aging model until EOL at 20% DOD and 1.5C

20% DOD, 1.5 C				
OP Hrs/day	FEC	Years	Calendar	Cycle
1.20	4419	14.8	13.18%	6.82%
2.10	5600	10.7	11.36%	8.64%
3.00	6324	8.5	10.24%	9.76%
3.90	6827	7.1	9.47%	10.53%
5.10	7307	5.8	8.72%	11.28%
6.00	7579	5.1	8.31%	11.69%
7.20	7864	4.4	7.86%	12.14%
8.10	8038	4.0	7.60%	12.40%
9.00	8185	3.7	7.37%	12.63%
10.20	8350	3.3	7.11%	12.89%
11.10	8456	3.1	6.95%	13.05%
12.00	8549	2.9	6.81%	13.19%

Table F.18: Results of simulating aging model until EOL at 20% DOD and 3C

20% DOD, 3 C				
OP Hrs/day	FEC	Years	Calendar	Cycle
1.00	5272	11.8	11.86%	8.14%
2.00	6631	7.5	9.77%	10.23%
3.00	7331	5.5	8.69%	11.31%
4.00	7765	4.4	8.02%	11.98%
5.00	8064	3.6	7.56%	12.44%
6.00	8280	3.1	7.22%	12.78%
7.00	8444	2.7	6.97%	13.03%
8.00	8573	2.4	6.77%	13.23%
9.00	8674	2.2	6.61%	13.39%
10.00	8756	2.0	6.49%	13.51%
11.00	8823	1.8	6.38%	13.62%
12.00	8877	1.7	6.30%	13.70%

Table F.19: Results of simulating aging model until EOL at 30% DOD and 0.1C

30% DOD, 0.1 C				
OP Hrs/day	FEC	Years	Calendar	Cycle
6.00	2350	21.2	16.37%	3.63%
12.00	3917	17.7	13.96%	6.04%
18.00	5117	15.4	12.11%	7.89%

Table F.20: Results of simulating aging model until EOL at 30% DOD and 0.25C

30% DOD, 0.25 C				
OP Hrs/day	FEC	Years	Calendar	Cycle
2.43	2224	20.0	16.57%	3.43%
4.87	3558	16.0	14.51%	5.49%
7.30	4505	13.5	13.05%	6.95%
9.73	5236	11.8	11.92%	8.08%
12.17	5830	10.5	11.01%	8.99%
14.60	6306	9.5	10.23%	9.77%

Table F.21: Results of simulating aging model until EOL at 30% DOD and 0.5C

30% DOD, 0.5 C				
OP Hrs/day	FEC	Years	Calendar	Cycle
1.23	2190	19.7	16.62%	3.38%
2.47	3449	15.5	14.68%	5.32%
3.70	4317	13.0	13.34%	6.66%
4.93	4971	11.2	12.33%	7.67%
6.17	5490	9.9	11.53%	8.47%
7.40	5919	8.9	10.87%	9.13%
8.63	6281	8.1	10.31%	9.69%
9.87	6594	7.4	9.83%	10.17%
11.10	6868	6.9	9.40%	10.60%
12.33	7111	6.4	9.03%	10.97%
13.57	7330	6.0	8.69%	11.31%
14.80	7527	5.7	8.39%	11.61%

Table F.22: Results of simulating aging model until EOL at 30% DOD and 1C

30% DOD, 1 C				
OP Hrs/day	FEC	Years	Calendar	Cycle
1.27	3431	15.2	14.71%	5.29%
1.90	4269	12.6	13.42%	6.58%
3.17	5372	9.6	11.71%	8.29%
4.43	6094	7.7	10.60%	9.40%
5.07	6374	7.1	10.17%	9.83%
6.33	6830	6.1	9.46%	10.54%
6.97	7020	5.7	9.17%	10.83%
8.23	7342	5.0	8.67%	11.33%
8.87	7481	4.8	8.46%	11.54%
10.13	7724	4.3	8.08%	11.92%
11.40	7931	3.9	7.76%	12.24%
12.03	8024	3.8	7.62%	12.38%

Table F.23: Results of simulating aging model until EOL at 30% DOD and 1.5C

30% DOD, 1.5 C				
OP Hrs/day	FEC	Years	Calendar	Cycle
0.87	3406	15.2	14.75%	5.25%
2.17	5317	9.5	11.80%	8.20%
3.03	6018	7.7	10.72%	9.28%
3.90	6521	6.5	9.94%	10.06%
5.18	7066	5.3	9.10%	10.90%
6.07	7341	4.7	8.68%	11.32%
6.93	7569	4.2	8.32%	11.68%
8.23	7847	3.7	7.90%	12.10%
9.10	8001	3.4	7.66%	12.34%
9.97	8134	3.2	7.45%	12.55%
10.83	8252	3.0	7.27%	12.73%
12.13	8406	2.7	7.03%	12.97%

Table F.24: Results of simulating aging model until EOL at 30% DOD and 3C

30% DOD, 3 C				
OP Hrs/day	FEC	Years	Calendar	Cycle
1.17	5287	9.5	11.84%	8.16%
2.10	6443	6.5	10.06%	9.94%
3.03	7095	4.9	9.05%	10.95%
3.97	7520	4.0	8.40%	11.60%
4.90	7822	3.4	7.93%	12.07%
6.30	8139	2.7	7.44%	12.56%
7.23	8293	2.4	7.21%	12.79%
8.17	8418	2.2	7.01%	12.99%
9.10	8518	2.0	6.86%	13.14%
10.03	8602	1.8	6.73%	13.27%
10.97	8671	1.7	6.26%	13.38%

Table F.25: Results of simulating aging model until EOL at 40% DOD and 0.25C

40% DOD, 0.25 C				
OP Hrs/day	FEC	Years	Calendar	Cycle
3.23	1957	13.2	16.94%	3.06%
6.47	3323	11.2	14.80%	5.20%
9.70	4388	9.9	13.14%	6.86%
12.93	5271	8.9	11.76%	8.24%
16.17	6031	8.2	10.57%	9.43%
19.40	6704	7.6	9.52%	10.48%

Table F.26: Results of simulating aging model until EOL at 40% DOD and 0.5C

40% DOD, 0.5 C				
OP Hrs/day	FEC	Years	Calendar	Cycle
1.63	1884	12.7	17.04%	2.96%
3.27	3096	10.5	15.16%	4.84%
4.90	3990	9.0	13.77%	6.23%
6.53	4695	7.9	12.67%	7.33%
8.17	5277	7.2	11.76%	8.24%
9.80	5773	6.5	10.99%	9.01%
11.43	6205	6.0	10.32%	9.68%
13.07	6587	5.6	9.72%	10.27%
14.70	6931	5.2	9.19%	10.81%
16.33	7242	4.9	8.71%	11.29%

Table F.27: Results of simulating aging model until EOL at 40% DOD and 1C

40% DOD, 1 C				
OP Hrs/day	FEC	Years	Calendar	Cycle
0.83	1861	12.4	17.05%	2.95%
1.67	3011	10.0	15.23%	4.77%
2.50	3824	8.5	13.94%	6.06%
3.33	4444	7.4	12.96%	7.04%
4.17	4941	6.6	12.18%	7.82%
5.00	5355	6.0	11.52%	8.48%
5.83	5706	5.4	10.97%	9.03%
6.67	6011	5.0	10.49%	9.51%
7.50	6279	4.7	10.07%	9.97%
8.33	6516	4.4	9.69%	10.31%
9.17	6730	4.1	9.35%	10.65%
10.00	6925	3.9	9.04%	10.96%

Table F.28: Results of simulating aging model until EOL at 40% DOD and 1.5C

40% DOD, 1.5 C				
OP Hrs/day	FEC	Years	Calendar	Cycle
1.13	2981	10.0	15.30%	4.70%
1.70	3777	8.5	14.06%	5.94%
2.83	4858	6.5	12.36%	7.64%
3.97	5583	5.4	11.23%	8.77%
4.53	5868	4.9	10.78%	9.22%
5.67	6339	4.3	10.04%	9.96%
6.23	6535	4.0	9.74%	10.26%
7.37	6873	3.6	9.21%	10.79%
7.93	7019	3.4	8.98%	11.02%
8.50	7154	3.2	8.77%	11.23%
9.07	7278	3.1	8.57%	11.43%
9.63	7393	2.9	8.39%	11.61%

Table F.29: Results of simulating aging model until EOL at 40% DOD and 3C

40% DOD, 3 C				
OP Hrs/day	FEC	Years	Calendar	Cycle
0.90	3750	8.3	14.06%	5.94%
1.80	5170	5.8	11.93%	8.07%
2.70	5982	4.5	10.67%	9.33%
3.60	6523	3.7	9.83%	10.17%
4.50	6915	3.1	9.22%	10.78%
5.40	7215	2.7	8.75%	11.25%
6.30	7454	2.4	8.38%	11.62%
7.20	7648	2.2	8.08%	11.92%
8.10	7807	2.0	7.83%	12.17%
9.00	7944	1.8	7.62%	12.38%
9.90	8060	1.7	7.44%	12.56%
10.80	8159	1.5	7.29%	12.71%

Table F.30: Results of simulating aging model until EOL at 25% DOD and 0.1

25% DOD, 0.1 C				
OP Hrs/day	FEC	Years	Calendar	Cycle
5.03	2135	23.1	16.71%	3.29%
10.07	3551	19.2	14.52%	5.48%

Table F.31: Results of simulating aging model until EOL at 25% DOD and 0.25C

25% DOD, 0.25 C				
OP Hrs/day	FEC	Years	Calendar	Cycle
2.03	2047	22.1	16.84%	3.16%
4.07	3300	17.9	14.91%	5.09%
6.10	4194	15.1	13.53%	6.47%
8.13	4884	13.2	12.47%	7.53%
10.17	5443	11.8	11.60%	8.40%
12.20	5912	10.7	10.88%	9.12%
14.23	6316	9.8	10.26%	9.74%
16.27	6669	9.0	9.71%	10.29%

Table F.32: Results of simulating aging model until EOL at 25% DOD and 0.5C

25% DOD, 0.5 C				
OP Hrs/day	FEC	Years	Calendar	Cycle
1.03	2028	21.8	16.87%	3.13%
2.07	3229	17.5	15.02%	4.98%
3.10	4067	14.7	13.73%	6.27%
4.13	4701	12.7	12.75%	7.25%
5.17	5206	11.3	11.97%	8.03%
6.20	5624	10.2	11.32%	8.68%
7.23	5977	9.3	10.78%	9.22%
8.27	6282	8.5	10.31%	9.69%
9.30	6548	7.9	9.90%	10.10%
10.33	6785	7.4	9.53%	10.47%
11.37	6997	6.9	9.20%	10.80%
12.40	7189	6.5	8.91%	11.09%

Table F.33: Results of simulating aging model until EOL at 25% DOD and 1C

25% DOD, 1 C				
OP Hrs/day	FEC	Years	Calendar	Cycle
1.07	3228	17.2	15.02%	4.98%
2.13	4658	12.4	12.82%	7.18%
3.20	5530	9.8	11.47%	8.53%
4.27	6140	8.2	10.53%	9.47%
5.33	6598	7.0	9.82%	10.18%
6.40	6959	6.2	9.27%	10.73%
7.47	7252	5.5	8.81%	11.19%
8.53	7498	5.0	8.43%	11.47%
9.60	7707	4.6	8.11%	11.89%
10.67	7888	4.2	7.83%	12.17%
11.73	8047	3.9	7.59%	12.41%
12.80	8186	3.6	7.37%	12.63%

Table F.34: Results of simulating aging model until EOL at 25% DOD and 1.5C

25% DOD, 1.5 C				
OP Hrs/day	FEC	Years	Calendar	Cycle
0.73	3207	17.2	15.05%	4.95%
1.47	4624	12.4	12.87%	7.13%
2.20	5483	9.8	11.54%	8.46%
2.93	6077	8.2	10.63%	9.37%
3.67	6520	7.0	9.94%	10.06%
4.40	6868	6.2	9.41%	10.59%
5.13	7149	5.5	8.97%	11.03%
5.87	7383	5.0	8.61%	11.39%
6.60	7581	4.5	8.31%	11.69%
7.33	7751	4.2	8.04%	11.96%
8.07	7899	3.9	7.81%	12.19%
8.80	8029	3.6	7.61%	12.39%

Table F.35: Results of simulating aging model until EOL at 25% DOD and 3C

25% DOD, 3 C				
OP Hrs/day	FEC	Years	Calendar	Cycle
0.80	4628	12.3	12.86%	7.14%
1.60	6029	8.2	10.70%	9.30%
2.40	6791	6.1	9.52%	10.48%
3.20	7279	4.9	8.77%	11.23%
4.00	7623	4.1	8.24%	11.76%
4.80	7878	3.6	7.85%	12.15%
5.60	8076	3.1	7.54%	12.46%
6.40	8234	2.8	7.30%	12.70%
7.20	8361	2.5	7.10%	12.90%
8.00	8466	2.3	6.94%	13.06%
8.80	8555	2.1	6.80%	13.20%
9.60	8629	2.0	6.69%	13.31%

Table F.36: Results of simulating aging model until EOL at 15% DOD and 0.1C

15% DOD, 0.1 C				
OP Hrs/day	FEC	Years	Calendar	Cycle
3.03	1580	28.4	17.10%	2.90%
6.07	2593	23.4	15.25%	4.75%
9.10	3335	20.0	13.88%	6.12%
12.13	3919	17.7	12.81%	7.19%
15.17	4398	15.9	11.94%	8.06%

Table F.37: Results of simulating aging model until EOL at 15% DOD and 0.25C

15% DOD, 0.25 C				
OP Hrs/day	FEC	Years	Calendar	Cycle
1.23	1567	28.0	17.15%	2.85%
2.47	2538	22.7	15.37%	4.63%
3.70	3229	19.2	14.11%	5.89%
4.93	3760	16.8	13.14%	6.86%
6.17	4187	15.0	12.36%	7.64%
7.40	4542	13.5	11.71%	8.29%
8.63	4845	12.4	11.16%	8.84%
9.87	5107	11.4	10.68%	9.32%
11.10	5337	10.6	10.26%	9.74%
12.33	5543	9.9	9.88%	10.12%
13.57	5727	9.3	9.55%	10.45%
14.80	5895	8.8	9.24%	10.76%

Table F.38: Results of simulating aging model until EOL at 15% DOD and 0.5C

15% DOD, 0.5 C				
OP Hrs/day	FEC	Years	Calendar	Cycle
1.27	2506	22.5	15.41%	4.59%
2.53	3684	16.6	13.24%	6.76%
3.80	4425	13.3	11.88%	8.12%
5.07	4953	11.2	10.91%	9.09%
6.33	5356	9.7	10.17%	9.83%
7.60	5677	8.5	9.57%	10.43%
8.87	5941	7.7	9.09%	10.91%
10.13	6164	7.0	8.68%	11.32%
11.40	6356	6.4	8.33%	11.67%
12.67	6522	5.9	8.02%	11.98%
13.93	6669	5.5	7.75%	12.25%
15.20	6800	5.1	7.51%	12.49%

Table F.39: Results of simulating aging model until EOL at 15% DOD and 1C

15% DOD, 1 C				
OP Hrs/day	FEC	Years	Calendar	Cycle
1.00	3204	18.9	14.19%	5.81%
2.00	4450	13.2	11.92%	8.08%
3.00	5175	10.2	10.60%	9.40%
4.00	5667	8.4	9.70%	10.30%
5.00	6029	7.2	9.04%	10.96%
6.00	6310	6.2	8.53%	11.47%
7.00	6536	5.5	8.12%	11.88%
8.00	6723	5.0	7.78%	12.22%
9.00	6881	4.5	7.49%	12.51%
10.00	7016	4.2	7.24%	12.76%
11.00	7132	3.8	7.03%	12.97%
12.00	7234	3.6	6.84%	13.16%

Table F.40: Results of simulating aging model until EOL at 15% DOD and 1.5C

15% DOD, 1.5 C				
OP Hrs/day	FEC	Years	Calendar	Cycle
0.93	3690	16.5	13.27%	6.73%
1.87	4931	11.0	11.00%	9.00%
2.80	5617	8.4	9.74%	10.26%
3.73	6069	6.8	8.91%	11.09%
4.67	6394	5.7	8.32%	11.68%
5.60	6642	5.0	7.86%	12.14%
6.53	6838	4.4	7.50%	12.50%
7.47	6997	3.9	7.21%	12.79%
8.40	7130	3.6	6.97%	13.03%
9.33	7241	3.2	6.76%	13.24%
10.27	7337	3.0	6.59%	13.41%
11.20	7420	2.8	6.44%	13.56%

Table F.41: Results of simulating aging model until EOL at 15% DOD and 3C

15% DOD, 3 C				
OP Hrs/day	FEC	Years	Calendar	Cycle
0.93	4269	11.4	11.20%	8.80%
1.87	5232	7.1	9.15%	10.85%
2.80	5720	5.2	8.13%	11.87%
3.73	6016	4.1	7.51%	12.49%
4.67	6217	3.4	7.09%	12.91%
5.60	6361	2.9	6.79%	13.21%
6.53	6468	2.5	6.56%	13.44%
7.47	6550	2.2	6.39%	13.61%
8.40	6615	2.0	6.26%	13.74%
9.33	6666	1.8	6.15%	13.85%
10.27	6707	1.7	6.06%	13.94%
11.20	6739	1.5	6.00%	14.00%

F.2. Variable Woehler curves

Table F.42: Results of simulating aging model until EOL with Woehler curve 1

Woehler curve 1						
DOD	C-rate	OP Hrs/day	FEC	Years	Calendar	Cycle
10%	0.5 C	2	3085	16.8	12.46%	7.54%
10%	0.5 C	6	4547	8.2	8.88%	11.12%
10%	0.5 C	12	5322	4.8	6.98%	13.02%
10%	1 C	2	4062	10.9	10.17%	9.83%
10%	1 C	6	5325	4.8	7.12%	12.88%
10%	1 C	12	5888	2.6	5.76%	14.24%
20%	0.5 C	2	3818	17.3	14.10%	5.90%
20%	0.5 C	6	5976	10.2	10.77%	9.23%
20%	0.5 C	12	7322	6.6	8.70%	11.30%
20%	1 C	2	4889	13.1	12.43%	7.57%
20%	1 C	6	7136	6.4	8.98%	11.02%
20%	1 C	12	8279	3.7	7.22%	12.78%
30%	0.5 C	2	3432	15.6	14.71%	5.29%
30%	0.5 C	6	5475	9.9	11.55%	8.45%
30%	0.5 C	12	7090	6.4	9.06%	10.94%
30%	1 C	2	4867	10.9	12.49%	7.51%
30%	1 C	6	6808	6.1	9.50%	10.50%
30%	1 C	12	8078	3.6	7.54%	12.46%
40%	0.5 C	2	1871	12.7	17.08%	2.92%
40%	0.5 C	6	4684	8.0	12.70%	7.30%
40%	0.5 C	12	6567	5.6	9.77%	10.23%
40%	1 C	2	3809	8.5	13.98%	6.02%
40%	1 C	6	5992	5.0	10.53%	9.47%
40%	1 C	12	7384	3.3	8.33%	11.67%

Table F.43: Results of simulating aging model until EOL with Woehler curve 2

Woehler curve 2						
DOD	C-rate	OP Hrs/day	FEC	Years	Calendar	Cycle
10%	0.5 C	2	2028	11.1	10.08%	9.92%
10%	0.5 C	6	2697	4.9	6.81%	13.19%
10%	0.5 C	12	3020	2.7	5.23%	14.77%
10%	1 C	2	2492	6.7	7.94%	12.06%
10%	1 C	6	3031	2.7	5.34%	14.66%
10%	1 C	12	3257	1.5	4.24%	15.76%
20%	0.5 C	2	2673	12.1	11.77%	8.23%
20%	0.5 C	6	3743	6.4	8.49%	11.51%
20%	0.5 C	12	4340	3.9	6.66%	13.34%
20%	1 C	2	3234	8.7	10.09%	9.91%
20%	1 C	6	4276	3.8	6.92%	13.08%
20%	1 C	12	4763	2.1	5.44%	14.56%
30%	0.5 C	2	2617	11.9	12.82%	7.18%
30%	0.5 C	6	3796	6.9	9.60%	10.40%
30%	0.5 C	12	4635	4.2	7.30%	12.70%
30%	1 C	2	3460	7.7	10.51%	9.49%
30%	1 C	6	4493	4.0	7.69%	12.31%
30%	1 C	12	5120	2.3	5.97%	14.03%
40%	0.5 C	2	1572	10.7	15.64%	4.36%
40%	0.5 C	6	3352	5.7	10.72%	9.28%
40%	0.5 C	12	4360	3.7	7.92%	12.08%
40%	1 C	2	2836	6.3	12.04%	7.96%
40%	1 C	6	4050	3.4	8.62%	11.38%
40%	1 C	12	4754	2.1	6.64%	13.36%

Table F.44: Results of simulating aging model until EOL with Woehler curve 3

Woehler curve 3						
DOD	C-rate	OP Hrs/day	FEC	Years	Calendar	Cycle
10%	0.5 C	2	3786	20.6	13.82%	6.18%
10%	0.5 C	6	5992	10.9	10.21%	9.79%
10%	0.5 C	12	7242	6.6	8.17%	11.83%
10%	1 C	2	5226	14.0	11.56%	8.44%
10%	1 C	6	7230	6.5	8.32%	11.68%
10%	1 C	12	8166	3.6	6.81%	13.19%
20%	0.5 C	2	4526	20.5	15.36%	4.64%
20%	0.5 C	6	7629	13.0	12.19%	7.81%
20%	0.5 C	12	9725	8.8	10.05%	9.95%
20%	1 C	2	6035	16.2	13.83%	6.17%
20%	1 C	6	9451	8.4	10.36%	9.64%
20%	1 C	12	11309	5.0	8.47%	11.53%
30%	0.5 C	2	4117	18.7	16.12%	3.88%
30%	0.5 C	6	7172	13.0	13.25%	6.75%
30%	0.5 C	12	9862	8.9	10.72%	9.28%
30%	1 C	2	6217	13.9	14.14%	5.86%
30%	1 C	6	9371	8.4	11.17%	8.83%
30%	1 C	12	11603	5.2	9.07%	10.93%
40%	0.5 C	2	2077	14.1	18.01%	1.99%
40%	0.5 C	6	5932	10.1	14.32%	5.68%
40%	0.5 C	12	8947	7.6	11.43%	8.57%
40%	1 C	2	4660	10.4	15.49%	4.51%
40%	1 C	6	8031	6.7	12.22%	7.78%
40%	1 C	12	10402	4.6	9.93%	10.07%

F.3. Variable ambient temperature

Table F.45: Results of simulating aging model until EOL at different ambient temperatures with thermal management

Aging at variable temperatures, 20% DOD and with cooling						
Temperature	C-rate	OP Hrs/day	FEC	Years	Calendar	Cycle
10°C	0.5 C	2	4272	19.4	13.40%	6.60%
10°C	0.5 C	6	6537	11.1	9.92%	10.08%
10°C	0.5 C	12	7945	7.2	7.76%	12.24%
10°C	1 C	2	5401	14.5	11.67%	8.33%
10°C	1 C	6	7733	6.9	8.12%	11.88%
10°C	1 C	12	8945	4.0	6.27%	13.73%
20°C	0.5 C	2	3955	18.0	14.31%	5.69%
20°C	0.5 C	6	6183	11.2	11.11%	8.89%
20°C	0.5 C	12	7326	6.6	8.72%	11.28%
20°C	1 C	2	4848	13.0	12.53%	7.47%
20°C	1 C	6	7128	6.3	9.05%	10.95%
20°C	1 C	12	8299	3.7	7.26%	12.74%
30°C	0.5 C	2	2865	12.9	15.58%	4.42%
30°C	0.5 C	6	4889	8.2	12.48%	7.52%
30°C	0.5 C	12	6266	5.6	10.36%	9.64%
30°C	1 C	2	3828	10.3	14.10%	5.90%
30°C	1 C	6	6100	5.4	10.63%	9.37%
30°C	1 C	12	7357	3.3	8.71%	11.29%

Table F.46: Results of simulating aging model until EOL at different ambient temperatures without thermal management

Aging at variable temperatures, 20% DOD and without cooling						
Temperature	C-rate	OP Hrs/day	FEC	Years	Calendar	Cycle
10°C	0.5 C	2	4564	20.8	12.94%	7.06%
10°C	0.5 C	6	6727	11.4	9.63%	10.37%
10°C	0.5 C	12	8007	7.2	7.66%	12.34%
10°C	1 C	2	5744	15.5	11.14%	8.86%
10°C	1 C	6	7848	7.0	7.94%	12.06%
10°C	1 C	12	8811	3.9	6.47%	13.53%
20°C	0.5 C	2	3692	16.8	14.29%	5.71%
20°C	0.5 C	6	5686	9.7	11.23%	8.77%
20°C	0.5 C	12	6851	6.2	9.44%	10.56%
20°C	1 C	2	4676	12.6	12.79%	7.21%
20°C	1 C	6	6658	6.0	9.76%	10.24%
20°C	1 C	12	7525	3.4	8.44%	11.56%
30°C	0.5 C	2	1966	8.9	16.96%	3.04%
30°C	0.5 C	6	3565	6.1	14.50%	5.50%
30°C	0.5 C	12	4687	4.2	12.78%	7.22%
30°C	1 C	2	2730	7.4	15.79%	4.21%
30°C	1 C	6	4591	4.1	12.94%	7.06%
30°C	1 C	12	5580	2.5	11.43%	8.57%

F.4. Mean SOC

Table F.47: Results of simulating aging model until EOL at different mean SOC

Aging at variable mean SOC, 20% DOD and 1 C						
Upper SOC	Lower SOC	OP Hrs/day	FEC	Years	Calendar	Cycle
100%	80%	2	1528	4.0	16.54%	3.46%
100%	80%	6	2952	2.6	13.33%	6.67%
100%	80%	12	3973	1.7	11.03%	8.97%
90%	70%	2	1993	5.2	16.36%	3.64%
90%	70%	6	3786	3.3	13.11%	6.89%
90%	70%	12	5046	2.2	10.82%	9.18%
80%	60%	2	2677	7.0	16.00%	4.00%
80%	60%	6	4928	4.3	12.60%	7.40%
80%	60%	12	6458	2.8	10.30%	9.70%
70%	50%	2	3468	9.0	14.81%	5.19%
70%	50%	6	5877	5.1	11.18%	8.82%
70%	50%	12	7374	3.2	8.92%	11.08%
60%	40%	2	4994	13.0	12.53%	7.47%
60%	40%	6	7296	6.3	9.05%	10.95%
60%	40%	12	8482	3.7	7.26%	12.74%
50%	30%	2	5789	15.1	10.62%	9.38%
50%	30%	6	7697	6.7	7.48%	12.52%
50%	30%	12	8569	3.7	6.05%	13.95%
40%	20%	2	5650	14.7	7.78%	12.22%
40%	20%	6	6650	5.8	5.52%	14.48%
40%	20%	12	7009	3.0	4.70%	15.30%
30%	10%	2	4851	12.7	4.96%	15.04%
30%	10%	6	5091	4.4	4.04%	15.96%
30%	10%	12	5083	2.2	4.02%	15.98%
20%	0%	2	3432	9.0	2.57%	17.43%
20%	0%	6	3300	2.9	3.09%	16.91%
20%	0%	12	3152	1.4	3.82%	16.18%

F.5. Case study: Tug

Table F.48: Overview of typical power distribution per task for tugs[40]

Operational task	Power (% of max)	% of operational time
Moored idle	2%	5%
Transit - low power	10%	13%
Transit - medium power	30%	25%
Transit - high power	60%	5%
Assist - standby	5%	10%
Assist - low power	10%	20%
Assist - medium power	40%	15%
Assist - high power	70%	5%
Assist - full power	100%	2%

Table F.49: Durations and energy demand of each task in 3 different types of jobs for tugs

T = transit, A = assist	Job 1		Job 2		Job 3	
Task	min	kWh	min	kWh	min	kWh
Moored idle	1	1.33	2	2.67	3	4
T - low power	3	20	6	40	9	60
T - medium power	5	100	10	200	15	300
T - high power	1	40	2	80	3	120
A - standby	5	16.67	10	33.33	15	50
A - low power	10	66.67	20	133.33	30	200
A - medium power	8	213.33	16	426.67	24	640
A - high power	3	140	6	280	9	420
A - full power	1	66.67	2	133.33	3	200
T - low power	3	20	6	40	9	60
T - medium power	5	100	10	200	15	300
T - high power	1	40	2	80	3	120
Moored idle	1	1.33	2	2.67	3	4
Total	47 min	826 kWh	94 min	1652 kWh	141 min	2478 kWh

Table F.50: Results of the simulations for the case study on tugs strategy 1

Results for case study: tug strategy 1 (Years until EOL)						
Capacity	Profile 1	Profile 2	Profile 3	Profile 4	Profile 5	Average
4.5 MWh	11.34	11.08	11.04	12.39	7.44	10.66
5 MWh	13.09	13.43	12.59	12.31	9.70	12.22
5.5 MWh	14.20	15.46	13.16	12.13	11.13	13.22
6 MWh	14.35	17.08	13.34	11.66	11.74	13.63
6.5 MWh	14.38	17.53	13.29	10.61	12.24	13.61
7 MWh	14.34	17.54	13.09	10.45	12.45	13.57
7.5 MWh	14.27	17.50	12.93	10.32	12.63	13.53
8 MWh	14.20	17.34	12.89	10.20	12.79	13.48

Table F.51: Results of the simulations for the case study on tugs strategy 2

Results for case study: tug strategy 2 (Years until EOL)						
Capacity	Profile 1	Profile 2	Profile 3	Profile 4	Profile 5	Average
4.5 MWh	11.34	11.08	11.04	12.39	7.44	10.66
5 MWh	13.82	13.45	13.55	15.06	9.18	13.01
5.5 MWh	16.46	15.90	15.91	18.01	10.70	15.40
6 MWh	18.47	18.70	17.97	20.41	11.95	17.50
6.5 MWh	20.19	20.38	19.61	22.96	13.07	19.24
7 MWh	21.81	21.92	21.16	24.95	14.24	20.82
7.5 MWh	23.41	23.64	22.75	26.48	15.53	22.36
8 MWh	25.01	25.12	24.35	28.10	16.81	23.88

Table F.52: Costs estimations for different battery sizes for tug case study, strategy 1

Lifetime cost estimations tug strategy 1					
Capacity	Years	Installation	Interest	Total costs	Cost / year
4.5 MWh	10.66	€4,500,000	€225,000	€4,725,000	€443,329
5 MWh	12.22	€5,000,000	€250,000	€5,250,000	€429,483
5.5 MWh	13.22	€5,500,000	€275,000	€5,775,000	€436,970
6 MWh	13.63	€6,000,000	€300,000	€6,300,000	€462,080
6.5 MWh	13.61	€6,500,000	€325,000	€6,825,000	€501,470
7 MWh	13.57	€7,000,000	€350,000	€7,350,000	€541,476
7.5 MWh	13.53	€7,500,000	€375,000	€7,875,000	€582,040
8 MWh	13.48	€8,000,000	€400,000	€8,400,000	€622,961

Table F.53: Costs estimations for different battery sizes for tug case study strategy 2

Lifetime cost estimations tug strategy 2					
Capacity	Years	Installation	Interest	Total costs	Cost / year
4.5 MWh	10.66	€4,500,000	€225,000	€4,725,000	€443,329
5 MWh	13.01	€5,000,000	€250,000	€5,250,000	€403,474
5.5 MWh	15.40	€5,500,000	€275,000	€5,775,000	€375,097
6 MWh	17.50	€6,000,000	€300,000	€6,300,000	€360,000
6.5 MWh	19.24	€6,500,000	€325,000	€6,825,000	€354,693
7 MWh	20.82	€7,000,000	€350,000	€7,350,000	€353,094
7.5 MWh	22.36	€7,500,000	€375,000	€7,875,000	€352,160
8 MWh	23.88	€8,000,000	€400,000	€8,400,000	€351,788

F.6. Case study: Ferry

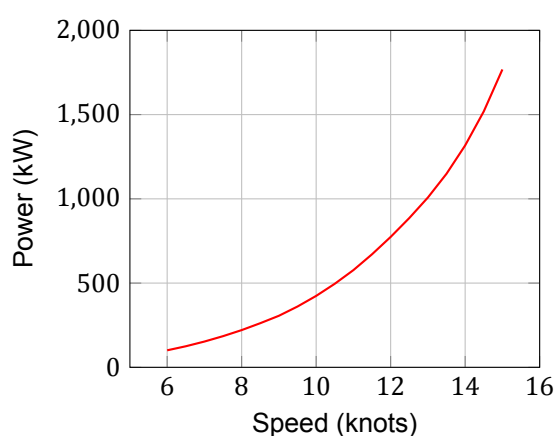


Figure F.1: Vessel speed and required power for DRPa9919 ferry

Table F.54: Overview of energy demand for the fixed part of the operational profile

Fixed part of operational schedule of the ferry			
Operational task	Time (min)	Power (kW)	Energy (kWh)
Detaching	1	0	0
Maneuvering	1	1440	24
Slow down	1	0	0
Maneuvering	1	1080	18
Mooring	1	90	1.5
Connecting	1	0	0
Auxiliary	30	80	40
Total energy			83.5 kWh

Table F.55: Variable input for operational profile option 1

Option 1, DOD 20%, charge at every stop						
#	Speed (kts)	Time (min)	Charge (kW)	Time (min)	Capacity (kWh)	avg C-rate
1	10.1	16	1611	8	1014	1.0
2	10.8	15	1566	9	1107	0.9
3	11.6	14	1477	10	1223	0.9
4	12.5	13	1506	11	1372	0.9
5	13.5	12	1591	12	1581	0.9

Table F.56: Variable input for operational profile option 2

Option 2, large battery, charge only at one stop						
#	DOD	Speed (kts)	Charge (kW)	Time (min)	Capacity (kWh)	avg C-rate
6	20%	11.6	1750	17	2450	0.55
7	25%	11.6	1750	17	1960	0.65

Table F.57: Variable input for operational profile option 3

Option 3, two battery packs, one for each trip				
#	DOD	Speed (kts)	Capacity (kWh)	avg C-rate
8	20%	10.1	2028	1.0
9	20%	10.8	2214	0.9
10	20%	11.6	2446	0.9
11	20%	12.5	2743	0.9
12	20%	13.5	3161	0.9
13	15%	10.1	2704	0.7
14	15%	10.8	2952	0.7
15	15%	11.6	3261	0.7
16	15%	12.5	3657	0.6
17	15%	13.5	4215	0.7

Table F.58: Variable input for operational profile option 4

Option 4, large battery, 0.3C average						
#	DOD	Speed (kts)	Time (min)	Charge (kW)	Time (min)	Capacity (kWh)
18	5.5%	10.1	16	1611	8	3564
19	6%	11.6	14	1477	10	3745

Table F.59: Results of the simulations for the case study on ferries

Results for case study: ferry						
#	Speed (kts)	Option	Total capacity	Years	FEC	Energy/year
1	10.1	1	1014 kWh	4.19	8611	2084 MWh
2	10.8	1	1107 kWh	4.18	8600	2278 MWh
3	11.6	1	1223 kWh	4.18	8589	2513 MWh
4	12.5	1	1372 kWh	4.17	8573	2821 MWh
5	13.5	1	1581 kWh	4.16	8557	3252 MWh
6	11.6	2	2450 kWh	7.67	7572	2419 MWh
7	11.6	2	1960 kWh	6.18	7615	2415 MWh
8	10.1	3	2028 kWh	7.42	7634	2086 MWh
9	10.8	3	2214 kWh	7.41	7623	2278 MWh
10	11.6	3	2446 kWh	7.41	7614	2513 MWh
11	12.5	3	2743 kWh	7.39	7602	2822 MWh
12	13.5	3	3161 kWh	7.38	7589	3251 MWh
13	10.1	3	2704 kWh	8.38	6463	2085 MWh
14	10.8	3	2952 kWh	8.37	6456	2277 MWh
15	11.6	3	3261 kWh	8.36	6448	2515 MWh
16	12.5	3	3657 kWh	8.35	6441	2821 MWh
17	13.5	3	4215 kWh	8.34	6432	3251 MWh
18	10.1	4	3564 kWh	8.61	5041	2087 MWh
19	11.6	4	3745 kWh	7.75	5207	2516 MWh

Bibliography

- [1]
- [2] V. Agubra and J. Fergus. Lithium ion battery anode aging mechanisms. *Materials*, 6: 1310–1325, 2013.
- [3] K. Amine, J. Liu, and I. Belharouak. High-temperature storage and cycling of c-lifepo4/graphite li-ion cells. *Electrochemistry Communications*, 7:669–673, 2005.
- [4] P. Arora, R.E. White, and M. Doyle. Capacity fade mechanisms and side reactions in lithium-ion batteries. *Journal of the Electrochemical Society*, 145:3647–3667, 1998.
- [5] A. Barre, B. Deguilhem, S. Grolleau, M. Gerard, F. Suard, and D. Riu. A review on lithium-ion battery aging mechanisms and estimations for automotive applications. *Journal of Power Sources*, 241:680–689, 2013.
- [6] J.R. Belt, C.D. Ho, C.G. Motloch, T.J. Miller, and T.Q. Duong. A capacity and power fade study of li-ion cells during life cycle testing. *Journal of Power Sources*, 123:241–246, 2003.
- [7] M. Ben-Marzouk, A. Chaumond, E. Redondo-Iglesias, M. Montaru, and S. Pelissier. Experimental protocols and first results of calendar and/or cycling aging study of lithium-ion batteries – the mobicus project. 2016.
- [8] Benning. Lionic, lithium-ion batterijen voor intern transport, May 2016.
- [9] M. Brand, S. Schuster, T. Bach, and A. Jossen. Effects of vibrations and shocks on lithium-ion cells. *Journal of Power Sources*, 288, August 2015.
- [10] P. Brodsky. Real-time modeling of battery pack temperature for thermal limit prevention in electric race vehicles. Master’s thesis, Ohio State University, 2016.
- [11] G. Bucci, T. Swamy, s. Bishop, B. Sheldon, Y. Chiang, and W. Carter. The effect of stress on battery-electrode capacity. *Journal of The Electrochemical Society*, 164:645–654, 2017.
- [12] Isidor Buchmann. *Batteries in a portable world*. Cadex Electronics Inc., fourth edition edition, 2016.
- [13] S. Byun, J. Park, W. Agyei Appiah, M. Ryou, and Y. Min Lee. The effects of humidity on the self-discharge properties of nmc and lco lithium-ion batteries during storage. *Royal society of chemistry*, 7:10915–10921, 2017.
- [14] Cleanleap. Battery cell and pack costs and characteristics, March 2017. URL http://cleanleap.com/7-electricity-transport/71-battery-cell-and-pack-costs-and-characteristics#fig_7.3.
- [15] A. Delaille, S. Grolleau, F. Duclaud, J. Bernard, and R. Revel et al. Simcal project: calendar aging results obtained on a panel of 6 commercial li-ion cells. 2013.
- [16] R. Deshpande, M. Verbrugge, Y. Cheng, J. Wang, and P. Liu. Battery cycle life prediction with coupled chemical degradation and fatigue mechanics. *Journal of the electrochemical society*, 159:1730–1738, 2012.
- [17] M. Ecker, J.B. Gerschler, J. Vogel, S. Kabitz, F. Hust, and P. Dechent. Development of a lifetime prediction model for lithium-ion batteries based on extended aging test data. *Journal of Power Sources*, 215:248–257, 2012.

- [18] M. Ecker, N. Nieto, S. Kabitz, and D. Uwe Sauer. Calendar and cycle life study of nmc-based 18650 automotive lithium-ion batteries. *Journal of Power Sources*, 248:839–851, 2014.
- [19] *Concept of a battery aging model for lithium-ion batteries considering the lifetime dependency on the operation strategy*, 2009. Electrochemical Energy Conversion and Storage Systems Group.
- [20] Corvus Energy. Ampere case study, October 2015. URL http://corvusenergy.com/wp-content/uploads/2015/09/Corvus-Energy-CASE-STUDY_Norled-Ampere_JUNE-2015.pdf.
- [21] STX France. Ar vag tredan, December 2016. URL <http://www.stxfrance.com/UK/stxfrance-reference-23-AR%20VAG%20TREDAN.awp>.
- [22] L. Gaines, editor. *Recycling of Li-ion batteries*, November 2011. Illinois Sustainable Technology Center, University of Illinois.
- [23] B. Gallant. The cost dilemma: Why are batteries so expensive?, March 2011. URL <http://miter.mit.edu/articlecost-dilemma-why-are-batteries-so-expensive/>.
- [24] BB Green. The world’s fastest electric commuter vessel, December 2016. URL <http://www.bbgreen.info/>.
- [25] *LCA study for maritime battery systems*, Januari 2017. Grenland Energy.
- [26] Tom Gulbrandsen. Ampere, January 2015. URL <https://www.flickr.com/photos/tommcnikon/15747078393>.
- [27] X. Han, M. Ouyang, L. Lu, J. Li, Y. Zheng, and Z. Li. A comparative study of commercial lithium ion battery cycle life in electric vehicle aging mechanism identification. *Journal of Power Sources*, 251:38–54, 2014.
- [28] R. Hausbrand, G. Cherkashinin, H. Ehrenberg, M. Groting, K. Albe, C. Hess, and W. Jaegermann. Fundamental degradation mechanisms of layered oxide li-ion battery cathode materials: Methodology, insights and novel approaches. *Materials Science and engineering B*, 192:3–25, 2015.
- [29] J. Hooper, J. Marco, G. Chouchelamane, C. Lyness, and J. Taylor. Vibration durability testing of nickel cobalt aluminum oxide (nca) lithium-ion 18650 battery cells. *Energies*, 9, April 2016.
- [30] *Charging optimization of battery electric vehicles including battery aging*, 2014. IEEE PES Innovative Smart Grid Technologies Europe (ISGT Europe).
- [31] M.R. Jongerden and B.R. Haverkort. Battery modeling. Technical report, University of Twente, 2008.
- [32] P. Keil, S. Schuster, J. Wilhelm, J. Travi, A. Hauser, R. Karl, and A. Jossen. Calendar aging of lithium-ion batteries. *Journal of The Electrochemical Society*, 163:1872–1880, 2016.
- [33] L. Lam. A practical circuit-based model for state of health estimation of li-ion battery cells in electric vehicles. Master’s thesis, Delft University of Technology, 2011.
- [34] F. Lambert. Electric vehicle battery cost dropped 80 percent in 6 years down to 227/kwh – tesla claims to be below 190/kwh, February 2017. URL <https://electrek.co/2017/01/30/electric-vehicle-battery-cost-dropped-80-6-years-227kwh-tesla-190kwh/amp/>.

- [35] Zhe Li, Languang Lu, Minggao Ouyang, and Yuankun Xiao. Modeling the capacity degradation of lifepo4/graphite batteries based on stress coupling analysis. *Journal of Power Sources*, 196:9757–9766, 2011.
- [36] Liander. Tarieven 2016 nieuwe elektriciteitsaansluiting voor grootverbruikers, December 2016. URL <https://www.liander.nl/grootzakelijk/aansluitingen/tarieven2016/?ref=5726>.
- [37] G. Liu, M. Ouyang, L. Lu, J. Li, and X. Han. Analysis of the heat generation of lithium-ion battery during charging and discharging considering different influencing factors. *Journal of thermal analysis and calorimetry*, 116:1001–1010, 2014.
- [38] P. Liu, J. Wang, J. Hicks-Garner, E. Sherman, S. Soukiazian, M. Verbrugge, H. Tataria, J. Musser, and P. Finamore. Aging mechanisms of lifepo4 batteries deduced by electrochemical and structural analyses. *Journal of the electrochemical society*, 157:499–507, 2010.
- [39] M.C. McManus. Environmental consequences of the use of batteries in low carbon systems: The impact of battery production. *Journal of Applied Energy*, 93:288–295, 2012.
- [40] Sadik Memis. A terminal tug's annual duty profile and fuel consumptions on high and medium speed engines, October 2014. URL <https://www.linkedin.com/pulse/20141010084248-90166035-terminal-tug-s-annual-duty-profile-and-fuel-consumptions-on-h>
- [41] P.A. Nelson, K.G. Gallagher, I. Bloom, and D.W. Deest. Modeling the performance and cost of lithium-ion batteries for electric-drive vehicles. Technical report, Argonne National Laboratory, 2012.
- [42] B. Nykvist and M. Nilsson. Rapidly falling costs of battery packs for electric vehicles. *Nature Climate Change*, 5:329–332, 2015.
- [43] Karlsruhe Institute of Technology. Jacobi's motor, July 2013. URL <https://www.eti.kit.edu/english/1382.php>.
- [44] N. Omar, M.A. Monem, Y. Firouz, J. Salminen, J. Smekens, O. Hegazy, H. Gaulous, G. Mulder, P. Van den Bossche, and T. Coosemans. Lithium iron phosphate based battery - assessment of the aging parameters and development of cycle life model. *Journal of Applied Energy*, 113:1575–1585, 2014.
- [45] M. Ouyang, D. Ren, L. Lu, J. Li, X. Feng, X. Han, and G. Liu. Overcharge-induced capacity fading analysis for large format lithium-ion batteries with $\text{LiNi}_{1/3}\text{Co}_{1/3}\text{Mn}_{1/3}\text{O}_2 + \text{LiMn}_2\text{O}_4$ composite cathode. *Journal of Power Sources*, 279:626–635, 2015.
- [46] S. Pelletier, O. Jabali, G. Laporte, and Marco Veneroni. Goods distribution with electric vehicles: Battery degradation and behaviour modeling, September 2015.
- [47] S. Peterson, J. Apt, and J.F. Whitacre. Lithium-ion battery cell degradation resulting from realistic vehicle and vehicle-to-grid utilization. *Journal of power sources*, 195:2385–2392, 2010.
- [48] H. Ploehn, P. Ramadass, and R. White. Solvent diffusion model for aging of lithium-ion battery cells. *Journal of the electrochemical society*, 151:456–462, 2004.
- [49] Qnovo. The cost components of a lithium ion battery, January 2016. URL <https://qnovo.com/82-the-cost-components-of-a-battery/>.
- [50] M. Safari and C. Delacourt. Aging of a commercial graphite/lifepo4 cell. *Journal of The Electrochemical Society*, 158:1123–1135, 2011.
- [51] E. Sarasketa-Zabala, I. Gandiaga, L.M. Rodriguez-Martinez, and I. Villarreal. Calendar ageing analysis of a lifepo4/graphite cell with dynamic model validations: Towards realistic lifetime predictions. *Journal of Power Sources*, 272:45–57, 2014.

- [52] E. Sarasketa-Zabala, I. Gandiaga, E. Martinez-Laserna, L.M. Rodriguez-Martinez, and I. Villarreal. Cycle ageing analysis of a lifepo4/graphite cell with dynamic model validations: Towards realistic lifetime predictions. *Journal of Power Sources*, 275:573–587, 2015.
- [53] E. Sarasketa-Zabala, E. Martinez-Laserna, M. Berecibar, I. Gandiaga, L.M. Rodriguez-Martinez, and I. Villarreal. Realistic lifetime prediction approach for li-ion batteries. *Journal of Applied Energy*, 162:839–852, 2016.
- [54] S. Saxena, C. Hendricks, and M. Pecht. Cycle life testing and modeling of graphite lco cells under different state of charge ranges. *Journal of power sources*, 327:394–400, 2016.
- [55] J. Schmalstieg, S. Kabitz, M. Ecker, and D. Uwe Sauer. A holistic aging model for li(nimnco)o2 based 18650 lithium-ion batteries. *Journal of Power Sources*, 257:325–334, 2014.
- [56] E. Schultz. Shipyards and ship finance, November 2016. URL https://blackboard.tudelft.nl/bbcswebdav/pid-2906377-dt-content-rid-10001891_2/courses/41165-161702/Presentation%206.2%20%28E.%20Schultz%29.pdf.
- [57] A.K. Shukla and P. Kumar. Materials for next generation lithium batteries. *Current Science*, 94:317–327, 2008.
- [58] TenneT. Belasting op elektriciteitsnet, December 2016. URL <http://www.tennet.eu/nl/elektriciteitsmarkt/data-dashboard/belasting/>.
- [59] Jos Theuns. A critical look at 2nd life battery applications, December 2016. URL <https://www.linkedin.com/pulse/critical-look-2nd-life-battery-applications-jos-theuns?trk=hp-feed-article-title-like>.
- [60] T.Kim, J. park, S. CHang, S. Choi, J. Ryu, and H. Song. The current move of lithium ion batteries towards the next phase. *Advanced energy materials*, 2:860–872, 2011.
- [61] Umicore. Battery recycling, January 2017. URL <http://www.umicore.com/en/industries/recycling/umicore-battery-recycling/>.
- [62] Frits van der Velde. Kenmerken elektriciteitsnet, December 2016. URL <https://www.vemw.nl/Elektriciteit/Netwerk%20en%20Transport/Kenmerken%20Netwerk.aspx>.
- [63] J. Vetter, P. Novak, M.R. Wagner, C. Veit, K.C. Moller, J.O. Besenhard, M. Winter, M. Wohlfahrt-Mehrens, C. Vogler, and A. Hammouche. Ageing mechanisms in lithium-ion batteries. *Journal of Power Sources*, 147:269–281, 2005.
- [64] M. Wagemaker. Hydrogen and electrical energy storage, February 2017. URL https://blackboard.tudelft.nl/bbcswebdav/pid-2922135-dt-content-rid-10131834_2/courses/41601-161703/Lecture%202%20Batteries%20February%2021%202017.pdf.
- [65] J. Wang, P. Liu, J. Hicks-Garner, E. Sherman, S. Soukiazian, M. Verbrugge, H. Tataria, J. Musser, and P. Finamore. Cycle-life model for graphite-lifepo4 cells. *Journal of Power Sources*, 196:3942–3948, 2011.
- [66] S. Watanabe, M. Kinoshita, T. Hosokawa, K. Morigaki, and K. Nakura. Capacity fade of nca cathode for lithium-ion batteries during accelerated calendar and cycle life tests (surface analysis of nca cathode after cycle life tests in restricted depth of discharge ranges). *Journal of power sources*, 258:210–217, 2014.

- [67] D. Wong, B. Shrestha, D. Wetz, and J. Heinzel. Impact of high rate discharge on the aging of lithium nickel cobalt aluminum oxide batteries. *Journal of power sources*, 280: 363–372, 2015.
- [68] E. Sarasketa Zabala. *A novel approach for lithium-ion battery selection and lifetime prediction*. PhD thesis, Mondragon University, 2014.
- [69] Y. Zheng, Y. He, K. Qian, B. Li, X. Wang, J. Li, S.W. Chiang, C. Miao, F. Kang, and J. Zhang. Deterioration of lithium iron phosphate/graphite power batteries under high-rate discharge cycling. *Electrochimica Acta*, 176:270–279, 2015.
- [70] Y. Zheng, Y. He, K. Qian, B. Li, X. Wang, J. Li, C. Miao, and F. Kang. Effects of state of charge on the degradation of lifepo4/graphite batteries during accelerated storage test. *Journal of Alloys and Compounds*, 639:406–414, 2015.

List of Figures

1.1	Main steps in approach of this research	3
2.1	Main influences on battery selection criteria	6
2.2	Different types of cell design, cylindrical (a), coin (b), prismatic (c) and pouch (d) [57]	9
2.3	Cost components for lithium-ion battery cells [49]	11
2.4	Cost determining factors for battery systems	11
2.5	Expected battery price development (Nykqvist (2015) [42])	12
2.6	Selecting a battery cell on CAPEX and OPEX	14
2.7	Battery selection process	14
3.1	Schematic representation of a lithium-ion battery	15
3.2	Battery half cell representing the five main aging mechanisms	16
3.3	Example of a resistance curve of a lithium-ion battery[31]	18
3.4	Minimum and maximum aging rate at 30% SOC	21
3.5	Effect of temperature on calendar aging	22
3.6	Effect of temperature on calendar aging	23
3.7	Minimum and maximum aging rate compared for variable SOC	24
3.8	Effect of SOC on calendar aging	25
3.9	Effect of SOC on calendar aging	26
3.10	Effect of storage time on calendar aging rate	27
3.11	Effect of depth of discharge (DOD) on cycle aging	30
3.12	Effect of C-rate on cycle aging rate for LCO	31
3.13	Effect of average SOC on cycle aging LCO	32
3.14	Effect of average SOC on cycle aging NMC	32
4.1	Effect of temperature on aging rate	37
4.2	Effect of the state of charge on aging rate	37
4.3	Woehler curve of aging data for NMC battery from figure D.19 (C)	38
4.4	Effect of C-rate on cycle aging rate	39
4.5	Schematic representation of calculation steps in Simulink	40
4.6	Schematic representation of thermal part in proposed aging model	42
4.7	Average variation of 6% in aging for similar cell type under similar testing conditions	43
4.8	$\alpha = 0.038, \beta = 1.108, \kappa_1 = 0.002, \kappa_2 = 0.003$, LFP 15 Ah cell from SIMCAL aging tests [15]	44
4.9	$\alpha = 0.077, \beta = 1.063, \kappa_1 = 0.002, \kappa_2 = 0.003$, NCA 7 Ah cell from SIMCAL aging tests [15]	45
4.10	$\alpha = 0.06, \beta = 1.092, \kappa_1 = 0.0001, \kappa_2 = 0.0211$, NMC 5.3 Ah cell from SIMCAL aging tests [15]	46
4.11	Distribution of the average errors at different values of α	48
4.12	Woehler curve for general model	49
4.13	Distribution of the absolute simulation errors at different points in time	49
4.14	Distribution of the absolute simulation errors at different SOC levels	50
4.15	Distribution of the absolute simulation errors at different temperature levels	50
4.16	Distribution of the absolute simulation errors	51
5.1	Results of general analysis simulations for performed FEC and years until EOL	54
5.2	Trend lines for FEC and years until EOL	55

5.3	Performed FEC at EOL after 10 years for different DOD at different C-rates . . .	55
5.4	Simulation results for cycling at 20% DOD and 1C with different average SOC	56
5.5	Three different Woehler curves to represent three batteries with different aging characteristics	56
5.6	Performed FEC at EOL after 10 years with different Woehler curves	57
5.7	Simulation results for cycling at 50% DOD and variable overnight charge strategy	58
5.8	FEC and years until EOL at different ambient temperatures with thermal management system	59
5.9	The four steps for battery optimization	60
5.10	Light, medium and heavy job types for the harbour tug	61
5.11	Operational profiles for harbour tug	62
5.12	State of charge of the 4.5 MWh battery during operational profile 1	63
5.13	Years until EOL for different profiles and battery sizes strategy 1 and strategy 2	63
5.14	Costs in €/year for different battery sizes and for strategy 1 and 2	64
5.15	Typical profile for a single job of a ferry	64
5.16	Four different options for the battery strategy of the ferry	65
5.17	State of health after 5 years of operation at 10.1 knots	66
5.18	Relationship between the total installation costs and SOH after 5 years of cycling	67
5.19	Years until EOL per C-rate and operational hours per day at 20% DOD	67
5.20	Estimation of performed FEC per day based on C-rate and operational hours per day	68
5.21	Optimization steps method 2	69
5.22	Steps to determine optimal battery size for 10 year battery life tug	69
5.23	Steps to determine optimal battery size for 5 year battery life ferry	70
A.1	The MF Ampere[26]	77
A.2	Line diagram of Ampere drive systems[20]	78
A.3	The BB Green[24]	79
A.4	The Ar Vag Tredan[21]	79
A.5	Payback time on emissions fully electric vs. diesel	81
A.6	Power demand in the Netherlands from November 24, 00:00 until November 26, 00:00 (2016) [58]	82
A.7	Battery aging	83
A.8	Effective use of battery capacity	84
C.1	Effect of temperature on cycle life according to model Omar et al.[44]	91
C.2	Effect of discharge C-rate on cycle life according to model Omar et al.[44]	91
C.3	Effect of depth of discharge on cycle life according to model Omar et al.[44]	92
C.4	Effect of charge C-rate on cycle life according to model Omar et al.[44]	92
C.5	Effect of DOD and mean SOC on cycle life according to model Saxena et al.[54]	93
C.6	Remaining capacity according to model by Schmalstieg et al.[55]	94
C.7	Calendar aging data fitting	96
C.8	Cycle aging data fitting (10% ≤DOD ≤50%)	97
D.1	Main screen of the aging model	99
D.2	Subsystem operational profile	99
D.3	Subsystem operational profile/ship	100
D.4	Subsystem operational profile/battery	100
D.5	Subsystem thermal model	100
D.6	Subsystem thermal model/heat generation	101
D.7	Subsystem thermal model/ambient temperature	101
D.8	Subsystem thermal model/thermal management	101
D.9	Subsystem thermal model/battery	101
D.10	Subsystem cycle analysis	102
D.11	Subsystem cycle analysis/Charge discharge detection	102
D.12	Subsystem cycle analysis/Cycle counter	102
D.13	Subsystem cycle analysis/Calculate half cycle depth and time	103

D.14	Subsystem calendar aging	103
D.15	Subsystem calendar aging/SOC effect	103
D.16	Subsystem calendar aging/temperature aging	104
D.17	Subsystem calendar aging/Time effect	104
D.18	Subsystem cycle aging	104
D.19	Subsystem cycle aging/DOD effect	104
D.20	Subsystem cycle aging/C-rate effect	105
D.21	Subsystem cycle aging/C-rate effect/Discharge	105
D.22	Subsystem cycle aging/C-rate effect/Charge	105
D.23	Subsystem Results	105
D.24	Subsystem Results/EOL	106
E.1	Distribution of the errors of the simulation compared to Sarasketa data[51]	107
E.2	Distribution of the errors of the simulation compared to SIMCAL data[15]	108
E.3	Distribution of the errors of the simulation compared to SIMCAL data[15]	108
E.4	Distribution of the errors of the simulation compared to SIMCAL data[15]	109
E.5	Distribution of the errors of the simulation compared to Keil data[32]	110
E.6	Distribution of the errors of the simulation compared to Safari data[50]	110
E.7	Distribution of the errors of the simulation compared to Schmalstieg data[55]	111
E.8	Distribution of the errors of the simulation compared to Keil data[32]	111
E.9	Distribution of the errors of the simulation compared to MOBICUS data[7]	112
E.10	Distribution of the errors of the simulation compared to SIMCAL data[15]	112
E.11	Distribution of the errors of the simulation compared to SIMCAL data[15]	113
E.12	Distribution of the errors of the simulation compared to Ecker data[18]	113
E.13	Distribution of the errors of the simulation compared to Ecker data[17]	114
E.14	Distribution of the errors of the simulation compared to Keil data[32]	114
E.15	Distribution of the errors of the simulation compared to SIMCAL data[15]	115
F.1	Vessel speed and required power for DRPa9919 ferry	136

List of Tables

2.1	Overview of characteristics per battery type[12]	8
2.2	Most common used lithium-ion battery chemistries rated for each selection criteria (1 = best option, 6 = worst option)	9
2.3	Different designs for battery cells and their main characteristics compared to each other	10
3.1	Overview of expansion rates of common electrodes	17
3.2	Overview of battery types and remaining capacity measurement conditions per test	20
3.3	Overview of fitting power functions per data set from figure D.17	28
4.1	Aging parameters included in different models	35
4.2	Simulation time and SOH for time step size of 1 second and 1 minute	43
4.3	Accuracy of proposed model compared to model by Sarasketa	47
4.4	Accuracy of proposed model compared to model by Ecker[17]	47
4.5	Parameter settings for general aging model	48
4.6	Distribution of the absolute prediction errors by the model	51
5.1	Results of simulating aging model until EOL with different rest periods	57
5.2	Results of simulating aging model until EOL with different charge rates	57
5.3	Variable operational strategies for the ferry	65
5.4	Parameters for battery life expectancy equations	68
C.1	Overview of stress factor levels for empirical aging model by Li(2011)[35]	89
E.1	Results of simulations set 1	107
E.2	Results of simulations set 2	107
E.3	Results of simulations set 3	108
E.4	Results of simulations set 4	109
E.5	Results of simulations set 5	109
E.6	Results of simulations set 6	110
E.7	Results of simulations set 7	110
E.8	Results of simulations set 8	111
E.9	Results of simulations set 9	111
E.10	Results of simulations set 10	112
E.11	Results of simulations set 11	113
E.12	Results of simulations set 12	113
E.13	Results of simulations set 13	114
E.14	Results of simulations set 14	114
E.15	Results of simulations set 15	115
F.1	Results of simulating aging model until EOL at 5% DOD and 0.1C	117
F.2	Results of simulating aging model until EOL at 5% DOD and 0.25C	117
F.3	Results of simulating aging model until EOL at 5% DOD and 0.5C	118
F.4	Results of simulating aging model until EOL at 5% DOD and 1C	118
F.5	Results of simulating aging model until EOL at 5% DOD and 1.5C	118
F.6	Results of simulating aging model until EOL at 5% DOD and 3C	119
F.7	Results of simulating aging model until EOL at 10% DOD and 0.1C	119
F.8	Results of simulating aging model until EOL at 10% DOD and 0.25C	119
F.9	Results of simulating aging model until EOL at 10% DOD and 0.5C	120

F.10	Results of simulating aging model until EOL at 10% DOD and 1C	120
F.11	Results of simulating aging model until EOL at 10% DOD and 1.5C	120
F.12	Results of simulating aging model until EOL at 10% DOD and 3C	121
F.13	Results of simulating aging model until EOL at 20% DOD and 0.1C	121
F.14	Results of simulating aging model until EOL at 20% DOD and 0.25C	121
F.15	Results of simulating aging model until EOL at 20% DOD and 0.5C	122
F.16	Results of simulating aging model until EOL at 20% DOD and 1C	122
F.17	Results of simulating aging model until EOL at 20% DOD and 1.5C	122
F.18	Results of simulating aging model until EOL at 20% DOD and 3C	123
F.19	Results of simulating aging model until EOL at 30% DOD and 0.1C	123
F.20	Results of simulating aging model until EOL at 30% DOD and 0.25C	123
F.21	Results of simulating aging model until EOL at 30% DOD and 0.5C	123
F.22	Results of simulating aging model until EOL at 30% DOD and 1C	124
F.23	Results of simulating aging model until EOL at 30% DOD and 1.5C	124
F.24	Results of simulating aging model until EOL at 30% DOD and 3C	124
F.25	Results of simulating aging model until EOL at 40% DOD and 0.25C	125
F.26	Results of simulating aging model until EOL at 40% DOD and 0.5C	125
F.27	Results of simulating aging model until EOL at 40% DOD and 1C	125
F.28	Results of simulating aging model until EOL at 40% DOD and 1.5C	126
F.29	Results of simulating aging model until EOL at 40% DOD and 3C	126
F.30	Results of simulating aging model until EOL at 25% DOD and 0.1	126
F.31	Results of simulating aging model until EOL at 25% DOD and 0.25C	126
F.32	Results of simulating aging model until EOL at 25% DOD and 0.5C	127
F.33	Results of simulating aging model until EOL at 25% DOD and 1C	127
F.34	Results of simulating aging model until EOL at 25% DOD and 1.5C	127
F.35	Results of simulating aging model until EOL at 25% DOD and 3C	128
F.36	Results of simulating aging model until EOL at 15% DOD and 0.1C	128
F.37	Results of simulating aging model until EOL at 15% DOD and 0.25C	128
F.38	Results of simulating aging model until EOL at 15% DOD and 0.5C	129
F.39	Results of simulating aging model until EOL at 15% DOD and 1C	129
F.40	Results of simulating aging model until EOL at 15% DOD and 1.5C	129
F.41	Results of simulating aging model until EOL at 15% DOD and 3C	130
F.42	Results of simulating aging model until EOL with Woehler curve 1	130
F.43	Results of simulating aging model until EOL with Woehler curve 2	131
F.44	Results of simulating aging model until EOL with Woehler curve 3	132
F.45	Results of simulating aging model until EOL at different ambient temperatures with thermal management	132
F.46	Results of simulating aging model until EOL at different ambient temperatures without thermal management	133
F.47	Results of simulating aging model until EOL at different mean SOC	134
F.48	Overview of typical power distribution per task for tugs[40]	134
F.49	Durations and energy demand of each task in 3 different types of jobs for tugs	135
F.50	Results of the simulations for the case study on tugs strategy 1	135
F.51	Results of the simulations for the case study on tugs strategy 2	135
F.52	Costs estimations for different battery sizes for tug case study, strategy 1 . . .	135
F.53	Costs estimations for different battery sizes for tug case study strategy 2	136
F.54	Overview of energy demand for the fixed part of the operational profile	136
F.55	Variable input for operational profile option 1	136
F.56	Variable input for operational profile option 2	137
F.57	Variable input for operational profile option 3	137
F.58	Variable input for operational profile option 4	137
F.59	Results of the simulations for the case study on ferries	137

List of Abbreviations

Abbreviation	Description
Ah	Ampere-hour
C-rate	Charge or discharge rate
DOD	Depth of discharge
EOL	End of life
FEC	Full equivalent cycles
HE	High energy battery
HP	High power battery
kW	kilo-Watt
kWh	kilo-Watt-hour
LCO	Lithium Cobalt Oxide battery
LFP	Lithium Iron Phosphate battery
LMO	Lithium Manganese Oxide battery
LTO	Lithium Titanate battery
MW	Mega-Watt
MWh	Mega-Watt-hour
NCA	Lithium Nickel Cobalt Aluminum battery
NMC	Lithium Nickel Manganese Cobalt Oxide battery
Q	Capacity loss in % per day
SEI	Solid Electrolyte Interphase
SOC	State of charge
SOH	State of health
μ SOC	Average state of health